

In vitro pharmacodynamics, pharmacokinetic/pharmacodynamic
modelling, *in silico* simulation and evaluation of
dosing regimens for linezolid

D i s s e r t a t i o n

zur Erlangung des akademischen Grades
doctor rerum naturalium (Dr. rer. nat.)

vorgelegt der
Naturwissenschaftlichen Fakultät I
(Biowissenschaften)
der Martin-Luther-Universität Halle-Wittenberg

von
Christian Scheerans

geb. am 17.12.1978 in Hamburg

Gutachter:

1. Prof. Dr. Charlotte Kloft
2. Prof. Dr. Michael Weiss
3. Prof. Dr. Hartmut Derendorf

Halle (Saale), 29. März 2010

*“Die interessantesten Fragen bleiben immer Fragen. Sie bergen ein Geheimnis.
Jeder Antwort muss man ein >vielleicht< hinzufügen. Nur uninteressante Fragen
haben eine endgültige Antwort.”*

- Eric-Emmanuel Schmitt -

Abstract

Infectious diseases are a leading cause of death worldwide. Concerning bacterial infections, antibiotics are essential therapeutic tools. However, the rapid development of bacterial resistance often reduces the clinical efficacy of established antibiotics. Moreover, the number of newly developed antibiotics is declining, for the last two decades. Linezolid (LZD) is a relatively new antibiotic (since 2001 in Germany, Zyvoxid[®], Pharmacia/Pfizer) approved for the treatment of gram-positive infections, e.g. infections of *Staphylococcus aureus* (*S. aureus*). However, previous investigations indicated that standard dosing of LZD, i.e. 600 mg twice daily (BID), might be insufficient for critically ill patients suffering from severe infections of *S. aureus*. This thesis aimed to develop a rational hypothesis for an optimised dosing regimen of LZD for this special patient population. The antibacterial activity of LZD against *S. aureus* was characterised via a pharmacodynamic (PD) *in vitro* model approach determining the minimum inhibitory concentration (MIC = 2 - 4 mg/L) and time-kill curves under various constant LZD exposures (static model) and *in vivo*-like LZD exposures changing over time (dynamic model). LZD was quantitatively determined via a validated high performance liquid chromatography (HPLC) assay. As descriptive PD measure, the relative bacterial reduction (RBR) was introduced as the net estimate of the antibacterial effect. Furthermore, the observed RBR of *S. aureus* under various LZD exposures was successfully analysed via pharmacokinetic/pharmacodynamic (PK/PD) modelling in Excel, using a modified indirect link model approach. Subsequently, the developed *in vitro* PK/PD model was mathematically combined with a previously developed *in vivo* (population) PK model of LZD, to investigate and evaluate the potential efficacy of twelve hypothetical dosing regimens for LZD versus (vs.) its standard dosing regimen, via deterministic and stochastic *in silico* simulations in Excel, imitating 14 days of LZD therapy. The results from both simulation approaches proposed that 600 mg LZD administered three times a day (TID) might be more efficient than its standard dosing regimen (i.e. 600 mg BID), for critically ill patients suffering from severe infections of *S. aureus* with MIC = 4 mg/L. In conclusion, to verify the clinical benefit, the developed (hypothetical) dosing recommendation for LZD should be investigated *in vivo*, i.e. in a prospective clinical trial with critically ill, septic patients showing a positive blood culture for *S. aureus*. Nonetheless, if using LZD as 600 mg TID in humans, the tolerability should be monitored very carefully.

Zusammenfassung

Infektionskrankheiten zählen weltweit zu den häufigsten Todesursachen. Zur Behandlung bakterieller Infektionen sind Antibiotika essenzielle Therapeutika. Durch die rasante Resistenzentwicklung von Bakterien verlieren jedoch viele etablierte Antibiotika zunehmend an klinischer Wirksamkeit. Darüber hinaus hat die Anzahl der neu entwickelten Antibiotika in den letzten 20 Jahren kontinuierlich abgenommen. Linezolid (LZD) ist ein relativ neues Antibiotikum (seit 2001 in Deutschland, Zyvoxid[®], Pharmacia/Pfizer), das zur Behandlung von Infektionen mit gram-positiven Bakterien, z.B. mit *Staphylokokkus aureus* (*S. aureus*), zugelassen ist. Vereinzelt vorherige Untersuchungen ergaben Hinweise, dass die Standarddosierung von LZD, d.h. 600 mg zweimal täglich (BID), bei kritisch kranken Patienten mit schwerer *S. aureus*-Infektion nur bedingt wirksam ist. Ziel dieser Doktorarbeit war die Entwicklung einer rationalen Hypothese zur optimierten Dosierung von LZD bei dieser schwer kranken Patientenpopulation. Die antibakterielle Aktivität von LZD gegen *S. aureus* wurde mit Hilfe eines pharmakodynamischen (PD) *In-vitro*-Modellansatzes charakterisiert. Hierbei wurden die minimale Hemmkonzentration (MIC = 2 – 4 mg/L) und die bakterielle Absterbekinetik unter verschiedenen konstanten LZD-Expositionen (statisches *In-vitro*-Modell) sowie sich zeitlich verändernden, d.h. *in-vivo*-ähnlichen LZD-Expositionen (dynamisches *In-vitro*-Modell), bestimmt. LZD wurde mittels eines validierten Hochdruckflüssigkeitschromatographie-(HPLC)-Verfahrens quantitativ bestimmt. Als deskriptive PD-Messgröße zur Abschätzung des antibakteriellen Nettoeffektes wurde die relative bakterielle Reduktion (RBR) eingeführt. In einer weiterführenden Analyse wurde die beobachtete RBR von *S. aureus* unter verschiedenen LZD-Expositionen mittels pharmakokinetischer/pharmakodynamischer (PK/PD) Modellierung in Excel erfolgreich mathematisch beschrieben. Hierbei wurde ein modifizierter Indirect-Link-Modellansatz angewandt. Anschließend wurde das mathematisch entwickelte *In-vitro*-PK/PD-Modell mit einem zuvor entwickelten *In-vivo*-(Populations-)PK-Modell kombiniert, um mit Hilfe von deterministischen und stochastischen *In-silico*-Simulationen in Excel die potenzielle Wirksamkeit von zwölf hypothetischen Dosierungsschemata für LZD zu untersuchen und im Vergleich zur Standarddosierung zu bewerten. Dabei wurden jeweils 14 Tage LZD-Therapie simuliert. Die Ergebnisse beider Simulationsansätze unterstützen die Hypothese, dass bei kritisch kranken Patienten, die an einer schweren *S. aureus*-Infektion (mit MIC = 4 mg/L) leiden, eine dreimal tägliche (TID) Gabe von 600 mg LZD effektiver sein könnte als die Standarddosierung (d.h. 600 mg BID). Um die aufgestellte Hypothese zu überprüfen, müsste die entwickelte Dosierungsempfehlung *in-vivo*, d.h. im Rahmen einer prospektiven klinischen Studie mit solch schwer kranken Patienten, getestet werden. Hierbei müsste jedoch unbedingt sichergestellt werden, dass die Verträglichkeit der neuen, d.h. höheren Dosierung von LZD sehr genau überwacht wird.

Table of contents

Abstract	III
Zusammenfassung	IV
Table of contents	V
Abbreviations, acronyms and symbols	XI
1 Introduction.....	1
1.1 Infectious diseases	1
1.1.1 Nosocomial infections.....	1
1.1.2 <i>Staphylococcus aureus</i>	1
1.1.3 Sepsis.....	3
1.1.4 Therapy of sepsis	4
1.2 Antibiotic therapy	4
1.2.1 Need for new antibiotics	5
1.2.2 Rational use of established antibiotics.....	6
1.2.2.1 Antibiotic ‘cycling’ and ‘mixing’	6
1.2.2.2 Rational dosing of antibiotics	6
1.2.3 ‘Appropriate’ dosing of antibiotics for septic patients	8
1.3 A rational way of finding an ‘appropriate’ dosing regimen.....	8
1.3.1 Pharmacokinetic/pharmacodynamic analysis	9
1.4 Linezolid.....	11
1.4.1 Physico-chemical properties.....	11
1.4.2 Pharmacokinetic properties	11
1.4.2.1 Absorption and distribution	11
1.4.2.2 Elimination	12
1.4.3 Pharmacodynamic properties	12
1.4.3.1 Mechanism of action and bacterial resistance	12
1.4.3.2 Antibacterial activity and susceptibility breakpoints	13
1.4.3.3 Clinical efficacy	14
1.4.3.4 Tolerability	14
1.5 Objectives	15
2 Materials and Methods	16
2.1 Materials.....	16

2.1.1	Chemicals, reagents and drugs.....	16
2.1.2	Other materials and experimental equipment.....	16
2.1.3	Scientific software.....	17
2.2	Fundamental mathematic methods	18
2.3	Bioanalysis - quantification of linezolid in broth	18
2.3.1	High performance liquid chromatography.....	18
2.3.1.1	Experimental equipment	18
2.3.1.2	Sample preparation	19
2.3.2	Method validation	19
2.3.2.1	Stock solutions.....	19
2.3.2.2	Linearity and limits of quantification	20
2.3.2.3	Stability	20
2.3.2.4	Calibration curve.....	20
2.3.2.5	(In-)Accuracy and (im-)precision.....	21
2.3.2.6	Recovery	21
2.4	Microbiology - <i>in vitro</i> pharmacodynamics of linezolid.....	21
2.4.1	Bacterial stock suspension	21
2.4.2	Preliminary investigations.....	22
2.4.2.1	<i>In vitro</i> stability of linezolid	22
2.4.2.2	Bacterial survival in different diluents.....	22
2.4.2.3	Bacterial loss during centrifugation	23
2.4.3	Static <i>in vitro</i> model	23
2.4.3.1	Bacterial inoculum	23
2.4.3.2	Linezolid exposure.....	24
2.4.3.3	Linezolid sampling	25
2.4.3.4	Bacterial sampling	25
2.4.4	Dynamic <i>in vitro</i> model	25
2.4.4.1	Bacterial inoculum	27
2.4.4.2	Linezolid exposure.....	27
2.4.4.3	Linezolid sampling	29
2.4.4.4	Bacterial sampling	29
2.4.5	Bacterial sample preparation and viable cell counts.....	29
2.4.5.1	Bacterial sample dilution and purification.....	30
2.4.5.2	Viable cell counts.....	30

2.4.6	Descriptive data analysis.....	31
2.4.6.1	<i>In silico</i> resampling (Bootstrapping).....	31
2.4.6.2	Relative bacterial reduction.....	32
2.4.6.3	Pharmacokinetic/pharmacodynamic parameters.....	33
2.5	Pharmacokinetic/pharmacodynamic modelling.....	34
2.5.1	Modelling objective and strategy.....	34
2.5.1.1	Defining data sets for model development.....	34
2.5.1.2	Model selection.....	34
2.5.1.3	Model development.....	36
2.5.1.4	Initial estimates and constraints.....	36
2.5.1.5	Curve fitting.....	36
2.5.1.6	Model comparison.....	38
2.6	<i>In silico</i> simulation and analysis.....	41
2.6.1	Objective.....	41
2.6.2	Population pharmacokinetic model for linezolid.....	41
2.6.3	Simulation methodologies and study designs.....	43
3	Results.....	46
3.1	Bioanalysis – quantification of linezolid in broth.....	46
3.1.1	Method validation.....	46
3.1.2	Measurement of linezolid samples.....	48
3.1.2.1	Linezolid samples from the static <i>in vitro</i> model.....	49
3.1.2.2	Linezolid samples from the dynamic <i>in vitro</i> model.....	50
3.2	Microbiology - <i>in vitro</i> pharmacodynamics of linezolid.....	52
3.2.1	Preliminary investigations.....	52
3.2.2	Static <i>in vitro</i> model – descriptive data analysis.....	53
3.2.2.1	Minimum inhibitory concentration and time-kill curves.....	53
3.2.2.2	Relative bacterial reduction.....	54
3.2.2.3	Phenotypic variants of <i>Staphylococcus aureus</i>	56
3.2.3	Dynamic <i>in vitro</i> model – descriptive data analysis.....	57
3.2.3.1	Time-kill curves.....	57
3.2.3.2	Relative bacterial reduction.....	59
3.2.3.3	Pharmacokinetic/pharmacodynamic parameters.....	61
3.2.3.4	Phenotypic variants of <i>Staphylococcus aureus</i>	62

3.3	Pharmacokinetic/pharmacodynamic modelling	63
3.3.1	Model development for data set I	63
3.3.1.1	‘Sigmoidal’ E_{max} model.....	63
3.3.1.2	Modified ‘sigmoidal’ E_{max} model.....	64
3.3.2	Model development for data set I+II	64
3.3.2.1	Modified ‘sigmoidal’ E_{max} model.....	64
3.3.2.2	Indirect link model.....	65
3.3.3	Model comparison	67
3.3.4	Final model.....	68
3.3.4.1	Estimated parameter values	68
3.3.4.2	Drug concentration-time courses at the ‘effect site’	69
3.3.4.3	Drug effect-time courses.....	71
3.3.4.4	Goodness of fit plots	71
3.4	<i>In silico</i> simulation and analysis.....	73
3.4.1	Deterministic simulation.....	74
3.4.2	Stochastic simulation (Monte Carlo simulation).....	77
4	Discussion	80
4.1	Bioanalysis – quantification of linezolid in broth	80
4.1.1	Comparison with the HPLC assay for plasma samples	80
4.1.2	Comparison with another HPLC assay for Mueller-Hinton broth samples	81
4.1.3	Accordance with the guideline	82
4.1.4	Future practice.....	83
4.2	Microbiology - <i>in vitro</i> pharmacodynamics of linezolid.....	83
4.2.1	Minimum inhibitory concentration	83
4.2.2	Time-kill (curve) studies.....	85
4.2.2.1	Descriptive statistics for time-kill curves	85
4.2.2.2	Relative bacterial reduction.....	86
4.2.2.3	Constant linezolid exposure.....	86
4.2.2.4	Linezolid exposure changing over time.....	88
4.3	Pharmacokinetic/pharmacodynamic modelling	93
4.3.1	Model development	94
4.3.2	Final model.....	94
4.3.3	Future model development.....	95

4.4	<i>In silico</i> simulation and analysis.....	96
4.4.1	Deterministic simulation.....	96
4.4.2	Stochastic simulation.....	97
4.4.3	Potential limitations and future investigations.....	99
5	Conclusion and perspectives.....	101
6	Bibliography.....	103
7	Appendix	116
7.1	Tables	116
7.2	Figures	118
7.3	Fundamental mathematic methods	134
7.3.1	Descriptive statistics	134
7.3.1.1	Measures of central tendency.....	134
7.3.1.2	Measures of variability, precision and accuracy.....	134
7.3.2	Inferential statistics	135
7.3.2.1	Estimation.....	135
7.3.2.2	Hypothesis testing	135
7.3.3	Correlation analysis	136
7.3.3.1	Pearson correlation coefficient.....	136
7.3.3.2	Coefficient of determination	137
7.3.4	Regression analysis	137
7.3.4.1	Models, variables, parameters and constants.....	137
7.3.4.2	Least squares method	137
7.3.4.3	Weighted least squares method	138
7.3.4.4	Simple linear regression	138
7.3.4.5	Nonlinear regression.....	139
7.3.5	Solving ordinary differential equations.....	140
7.3.5.1	Laplace transform.....	140
7.3.5.2	General partial fraction theorem	140
7.3.5.3	Fourth-order Runge-Kutta method.....	141
7.3.6	Simulation technique	142
7.3.6.1	Systems, models and simulations.....	142
7.3.6.2	<i>In silico</i> simulation.....	142

7.3.6.3	Monte Carlo method and simulation	143
7.4	Mathematic deviations	144
7.4.1	Derivation of Equation M1	144
7.4.2	Derivation of Equation R2.....	145
7.4.3	Derivation of Equation R2a.....	146
7.4.4	Derivation of Equation R3.....	147
7.4.5	Derivation of Equation R3a.....	148
7.4.6	Derivation of Equation R4.....	148
7.4.7	Derivation of Equation R4a.....	150
7.4.8	Derivation of Equation R6.....	150
7.5	VBA scripts	152
7.5.1	Pharmacokinetic/pharmacodynamic modelling	152
7.5.2	Stochastic <i>in silico</i> simulation	155
8	Publications	160
8.1	Original papers, review article and book chapter.....	160
8.2	Oral and poster presentations.....	160
9	Acknowledgements.....	163

Abbreviations, acronyms and symbols

A_{2-4}	See X_{2-4}
ACN	Acetonitrile
a_e or a_{-}	First-order rate constant of the 'time delay' term for E_{\max} in the modified 'sigmoidal' E_{\max} model (h^{-1})
AIC	Akaike's information criterion (see 2.5.1.6.2)
AIC_C	'Corrected' (second-order) Akaike's information criterion (see 2.5.1.6.3)
ANOVA	Analysis of variance (see 7.3.2.2.1)
AUC_E	Area under the drug effect-time curve ($\% \cdot h$)
$AUC_{E,\max}$	Maximal AUC_E (maximal 'response')
AUC_t	Area under the drug concentration-time curve ($\mu g \cdot h/mL$)
b	Intercept
B	Number of randomly drawn bootstraps
b_e or b_{-}	First-order rate constant of the 'time delay' term for EC_{50} in the modified 'sigmoidal' E_{\max} model (h^{-1})
BID	Twice daily (dosing regimen)
box plot	Box-and-whisker plot
BS	Bootstrapping (see 2.4.6.1)
C	Drug concentration ($\mu g/mL$)
C_0	Initial drug concentration ($\mu g/mL$)
$C_e(t)$	Drug concentration in the effect CMT ($\mu g/mL$)
$C_{e,\max}$	Maximum drug concentration in the effect CMT ($\mu g/mL$)
cfu	Colony forming units
$CI_{95\%}$	95% confidence interval (see 7.3.2.1.1)
CL	Clearance from the central CMT (L/h)
C_{LZD}	Linezolid concentration ($\mu g/mL$)
C_{\max}	Maximal observed drug concentration ($\mu g/mL$)
CMT	Compartment
$C_p(t)$	Drug concentration in the central CMT referring to plasma ($\mu g/mL$)
$C_{p,\max}$	Maximum drug concentration in the central CMT referring to plasma ($\mu g/mL$)
C_{ss}	Drug concentration at steady state ($\mu g/mL$)
CV	Coefficient of variation, % (see 7.3.1.2)
d	Number of data sets
D	Dose, administered amount of drug (mg)

Da	Dalton, a unified atomic mass unit
DD	Daily dose (mg/day)
DD ₅₀	DD producing 50% of the maximal 'response' (mg/day)
Dept.	Department
$df(t)/dt$	ODE of $f(t)$
$df(x)/dx$	ODE of $f(x)$
D _L	Loading dose (mg)
<i>E. coli</i>	<i>Escherichia coli</i>
$E(C)$	Drug effect as function of C, %
EC ₅₀	Drug concentration producing 50% of E _{max} (µg/mL)
E _{max}	Maximal drug effect, %
EMA	European Medicines Agency
E _{peak}	Maximal observed effect, %
ERI _{ss}	Effect range interval at (PD) steady state, %
ES	Effect size (see 3.4.2)
E _{ss,max}	Maximal effect at (PD) steady state, %
E _{ss,min}	Minimal effect at (PD) steady state, %
EUCAST	European Committee on Antimicrobial Susceptibility Testing
\bar{f}	Laplace transform of $f(t)$
$f(t)$	Time-dependent function
$f(x)$	Function with x as independent variable
F _{corr} and $F_{corr}(t)$	Correction factor and function (of t) for LZD samples obtained through the membrane filter unit of the dynamic <i>in vitro</i> model
FDA	Food and Drug Administration
FT	Freeze and thaw (stability)
F _x	Fraction of t _{e1/2}
g	Gram
<i>g</i>	Acceleration of gravity, ≈ 9.81 m/s ²
GC	Growth control
GOF	Goodness of fit
GPF	General partial fraction (theorem, see 7.3.5.2)
h	Hour
H or n _h	Hill coefficient of the 'sigmoidal' E _{max} model
H ₂ O	Purified water
H _{DD}	Hill coefficient of the (daily) dose-'response' curve
HPLC	High performance liquid chromatography

h_{ss}	Step size of the RK4 method
i.v.	Intravenous
IC_{50}	Drug concentration in the inhibition compartment yielding 50% of maximum clearance inhibition ($\mu\text{g}/\text{mL}$)
ICU	Intensive care unit
IDSA	Infectious Disease Society of America
IIV	Interindividual variability
<i>in silico</i>	'Performed' on a computer
<i>in vitro</i>	'Performed' in a controlled environment outside of a living organism, e.g. in a culture flask
<i>in vivo</i>	'Performed' in a living organism, e.g. animal or human
IQR	Interquartile range (see 7.3.1.2)
IQR_{median}	Median IQR
K	(Number of) estimated model parameter(s plus one)
k_0 or R_0	Infusion rate (mg/h)
k_{1-4}	Auxiliary quantities of the RK4 method
k_e	Elimination rate constant (h^{-1})
k_{eo}	Drug transfer rate constant from the effect CMT (h^{-1})
KH_2PO_4	Potassium dihydrogen phosphate
k_{ie}	Drug transfer rate constant into the effect CMT (h^{-1})
k_{ij}	Drug transfer rate constant into the inhibition compartment (h^{-1})
k_{io} or KIC	Drug transfer rate constant from the inhibition compartment (h^{-1})
K_{scale}	Scaling factor of the OBJ
L	Litre
$L(df(t)/dt)$	Laplace integral of $df(t)/dt$
LLOQ	Lower limit of quantification
log	Decadic logarithm
LS	Least squares (method, see 7.3.4.2)
LT	Long-term (stability)
LZD	Linezolid
m	Mass (g)
M	Number of roots of the denominator of the polynomial quotient for the GPF theorem
m_{av}	'Averaged' tangent slope of the RK4 method
MCM	Monte Carlo method (see 7.3.6.3)
MCS	Monte Carlo simulation (see 7.3.6.3)

MeOH	Methanol
mg	Milligram
MHB	Mueller-Hinton broth
MHBA	Mueller-Hinton blood agar
MIC	Minimum inhibitory concentration (mg/L, see 2.4.3.2.1)
min	Minute
mL	Millilitre
MRSA	Methicillin- or multi-resistant <i>S. aureus</i>
m_S	Slope
m_T	Tangent slope
m_{T1-4}	Tangent slopes of the RK4 method
n	Number of aliquots, samples or data points
n_*	See H
N	Number of simulated scenarios, via MCS
$N(C, t)$	Bacterial concentration (cfu/mL) as function of C and t
Na_2HPO_4	Disodium hydrogen phosphate
NaCl	Sodium chloride
NCA	Noncompartmental (PK) analysis
nt	Number of trapezoids
OBJ	Objective function (see 7.3.4.5)
ODE	Ordinary differential equation
P	Probability
$P(s)$	Numerator of the polynomial quotient of the GPF theorem
p.o.	Orally, oral
PBSP	Phosphate-buffered saline with peptone
PC	Partition coefficient
PD	Pharmacodynamics, pharmacodynamic (see 1.3.1)
pH	The negative decadic logarithm of the activity of dissolved hydrogen ions, which is a measure of the acidity or basicity of a solution
PK	Pharmacokinetics, pharmacokinetic (see 1.3.1)
pKa	The negative decadic logarithm of the acid dissociation constant, a quantitative measure of the strength of an acid in (aqueous) solution
PK/PD	Pharmacokinetic/pharmacodynamic (1.3.1)
P_{Ki}	Value of parameter K for the individual subject i
Q	Intercompartmental clearance (L/h)

Q(s)	Denominator of the polynomial quotient for the GPF theorem
QC	Quality control (samples, see 2.3.2.5)
QD	Once daily (dosing regimen)
QID	Four times a day (dosing regimen)
r	Correlation coefficient (see 7.3.3.1)
R	Range (see 7.3.1.2)
R0	See k_0
r^2 or R^2	Coefficient of determination (see 7.3.3.2)
RBR	Relative bacterial reduction, % (see 2.4.6.2)
RCLF	Remaining clearance fraction
RE	Relative error, % (see 7.3.1.2)
RK4	Fourth-order Runge-Kutta (method, see 7.3.5.3)
R_M	Amounts of models in a set, to be compared
rRNA	Ribosomal ribonucleic acid
s	Laplace operator
<i>S. aureus</i>	<i>Staphylococcus aureus</i>
SCV	Small colony variants (see 4.2.2.3.1)
SD	Standard deviation (see 7.3.1.2)
SIRS	Systemic inflammatory response syndrome
SSR	Squared sum of residuals (see 7.3.4.2)
SStx	Sample-set- t_x (see 2.4.6.1)
STT	Short-term temperature (stability)
t	Time (h)
T	Temperature (°C)
$t_{1/2}$	(PK) half-life (h)
TBC	Time to bacterial eradication
$t_{C \geq MIC}$	Time with drug concentration \geq MIC, measured in % of the investigated time/dosing interval
$t_{e1/2}$	Half-life of the drug in the effect CMT (h)
t_{eq}	Time of equilibrium (h)
T_i or TI	Duration of infusion (h)
TID	Three times a day (dosing regimen)
t_R	Retention time (min)
ULOQ	Upper limit of quantification
US or USA	United States (of America)
V	Volume (L), or total volume (mL) of broth in the <i>in vitro</i> model

V_{2-3}	Volume of distribution of the respective PK CMT (L)
VBA	Visual Basic for Applications
V_c	Volume of distribution of the central CMT (L)
V_e	Volume of distribution of the effect CMT (L)
vs.	Versus
V_{sub}	Substituted volume of broth (mL)
w	Akaike's weights (see 2.5.1.6.4)
W	Weighting factor (see 7.3.4.3)
WHO	World Health Organization
WSS	Weighted sum of squared residuals (see 7.3.4.3)
x	Independent variable
X_{2-4} or A_{2-4}	Drug amounts in the respective PK CMT (mg)
$X_c(t)$	Amount of drug in the central CMT referring to plasma (mg)
$X_e(t)$	Amount of drug in the effect CMT (mg)
y	Dependent variable
y'	First-order ODE
yr	Year
z_e or z_-	First-order rate constant of the 'time delay' term for H in the modified 'sigmoidal' E_{max} model (h^{-1})
α	First-order rate constant of the 'time delay' term (h^{-1})
$\Delta\text{AIC}_{C,i}$	AIC_C difference
Δd	Amount of drug removed per dilution step (mg)
η_{Ki}	Difference between the natural logarithm of P_{Ki} and θ_K .
θ_K	Population estimate of parameter K
λ_i 's	Roots of the denominator of the polynomial quotient for the GPF theorem
μg	Microgram
μL	Microlitre
ω_K	Standard deviation of η_{Ki}
ω_K^2	Variance of η_{Ki}
$^\circ\text{C}$	Degree Celsius
∞	Infinity

1 Introduction

1.1 Infectious diseases

Currently, infectious and parasitic diseases are the second leading cause of death worldwide, after cardiovascular diseases and before cancer. Moreover, in low-income countries lower respiratory infections are even the most common cause of death [2]. High-income regions, such as Germany and the United States of America (USA), particularly suffer from nosocomial infections which frequently lead to death, e.g. due to the development of septicaemia (sepsis, see 1.1.3) [3-7].

1.1.1 Nosocomial infections

Nosocomial infections are infectious diseases acquired in hospitals, secondary to the patient's original condition [8]. Patients with a weak immune system, e.g. elderly patients, easily get infected by pathogens transferred via the medical staff [9, 10]. Furthermore, bacteria like *Staphylococcus aureus* (*S. aureus*) frequently develop resistance towards several antibiotics, e.g. multi-resistant *S. aureus* (MRSA, see 1.1.2), resulting from the frequent use of antibiotics in hospitals [11, 12]. Due to multi-resistant pathogens, antibiotic therapy of bacterial nosocomial infections often fails [8, 12-14].

In Germany, the annual (2006) number of nosocomial infections is estimated as 400,000 to 600,000 with a respective mortality of 10,000 to 15,000 patients, i.e. up to 41 deaths per day [15]. Moreover, it has been shown that especially patients from intensive care units (ICUs) have a high risk of acquiring nosocomial infections. The EPIC study (1995) with over 10,000 patients from 1,417 ICUs of 17 countries in West Europe, revealed that 21% of all investigated ICU-patients suffered from ICU-acquired infections, where sepsis (see 1.1.3) was one of the four most frequent types of ICU-infections reported. Here, one third of the most frequently reported pathogens was *S. aureus*, with 60% MRSA proportion [16]. These data reveal that nosocomial infections, especially ICU-acquired infections with *S. aureus*, are a global major concern in public health.

1.1.2 *Staphylococcus aureus*

S. aureus is one of the leading pathogens causing serious infections in hospitals and in the community, worldwide [12, 17, 18]. However, despite its pathogenicity *S.*

aureus is also carried innocuously by approximately 30% of the population, usually on the moist skin in the nose, axillae and perineum [10]. It survives well on drier skin and inanimate surfaces facilitating cross-colonisation and thus infection [19].

A major problem of infections with *S. aureus* is the rapid development of resistance towards antibiotics [20], e.g. benzylpenicillin due to inactivating enzymes (penicillinase) [21]. In 1942, penicillin was introduced for the therapy of *S. aureus* infections. In 1945, the discoverer of penicillin, A. Fleming, first warned of the potential importance of the development of bacterial resistance. In 1946, already 14% of all *S. aureus* infections were resistant to penicillin (Fig. 1). This trend did not stop until the 1980s where penicillin-resistant strains of *S. aureus* had attained fractions greater than 80% both in hospitals and in the community [11, 19].

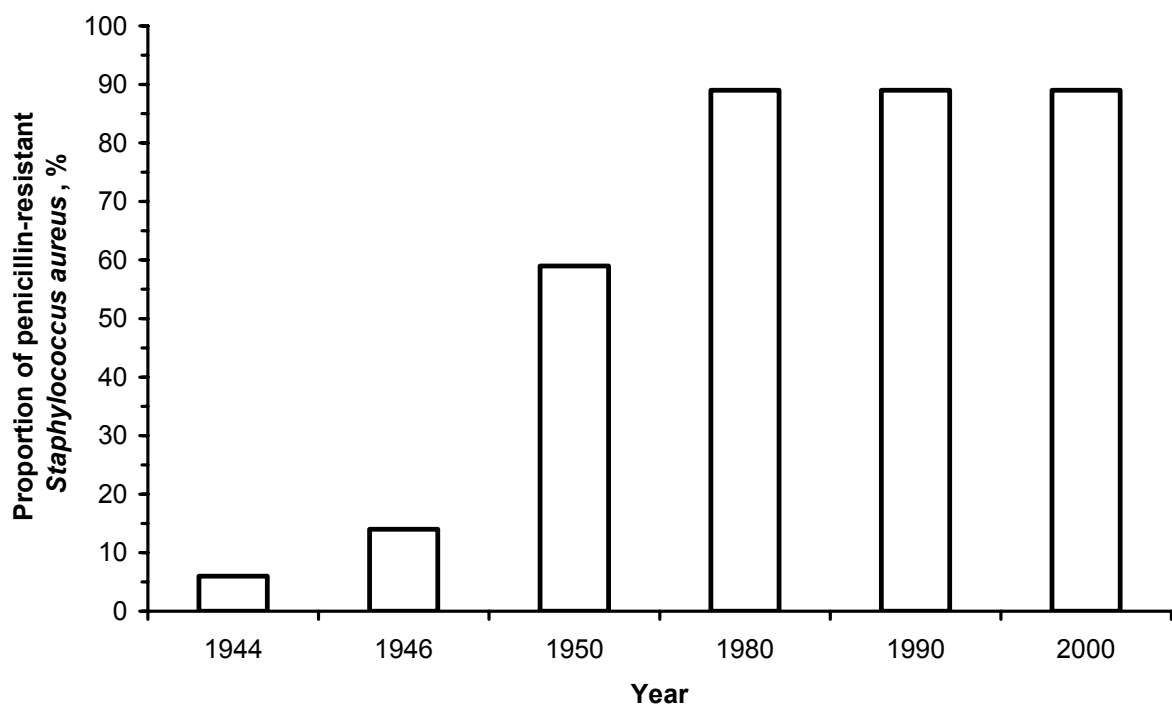


Fig. 1 The accumulation of penicillin-resistant *Staphylococcus aureus* in hospitals and the community over time, modified from [11, 19].

Furthermore, *S. aureus* rapidly developed resistance towards penicillinase-stable penicillins (e.g. methicillin) and many other antibiotics, termed as methicillin- or often multi-resistant *S. aureus* (MRSA) [10, 19]. In US ICUs, the proportion of MRSA

increased from 36% in 1992 to 64% in 2003. Currently, more patients die from MRSA infections in US hospitals than from HIV/AIDS and tuberculosis combined [22, 23].

In German hospitals, the MRSA proportion increased from 23% in 2004 to 28% in 2007 [24, 25]. Thus, regional differences exist [10]. However, the *World Health Organization* (WHO) warned that due to the increased global mobility of people, originally regional pathogens by now can easily spread all over the world [11]. Hence, an MRSA epidemic may easily lead over to a pandemic [26].

1.1.3 Sepsis

The term sepsis refers to a severe inflammatory state resulting from systemic (bacterial) infections, with three stages of severity. These are sepsis, severe sepsis and septic shock. *Sepsis* is a systemic infection accomplished by a reaction called *systemic inflammatory response syndrome* (SIRS) which represents an acute inflammatory reaction with systemic manifestations caused by numerous endogenous mediators of inflammation which are released into the bloodstream. A *severe sepsis* is present, if SIRS is combined with signs of (multi-)organ failure, and *septic shock* means severe sepsis with (multi-)organ failure and hypotension that is poorly responsive to initial fluid resuscitation [27].

Blood cultures from patients with suspected diagnosis of sepsis contained 55% gram-positive bacteria and 44% gram-negative bacteria. The frequency of pathogens is dependent on the respective patient population, e.g. for nosocomial sepsis the gram-positive bacterium *S. aureus* is a leading pathogen [6, 10, 19, 28].

In the USA, sepsis is a leading cause of death, with about 210,000 deaths annually (2002), and mortalities of 15% (sepsis), 20% (severe sepsis) and 45% (septic shock) [4]. The overall mortality in patients with this illness is estimated as approximately 40% [27] to 60% [28], and consistently high since many decades. Moreover, in the USA the incidence of sepsis has been increased fivefold, in the last 20 years [29].

In Germany, sepsis occurred in 79,000 patients and severe sepsis or septic shock in 75,000 patients (2002). Moreover, sepsis is estimated as the *third leading cause of death* in Germany, almost equal to death from acute myocardial infarction. This illness is responsible for approximately 60,000 deaths annually. Thus, about 162 patients die from sepsis every day, in this region [3, 30]. On average, patients suffering from sepsis have to stay about 16 days in the ICU and about 32 days in

hospital [29]. The direct costs for the treatment of severe sepsis are estimated as approximately 1.77 billion euros, i.e. about 30% of the budget in ICUs is used to treat severe sepsis [30].

1.1.4 Therapy of sepsis

Considering the unchanged high mortality from all stages of sepsis, any adjunctive therapy that led to improved outcomes for these critically ill patients is in high medical need. Thus, septic patients necessarily receive poly-medication, i.e. often several antibiotics, hydrocortisone, norepinephrine, acetaminophen, insulin, recombinant activated protein C and many other drugs against the bacterial infection and the severe symptoms e.g. fever, tachycardia and hypotension [4, 27, 30, 31].

Concerning the causal therapy of sepsis, clinicians advise that the early use of an 'appropriate' antibiotic therapy can reduce mortality from sepsis [4]. Poor outcomes often follow failure to institute early 'aggressive' antibiotic therapy, i.e. within 6 h of suspected diagnosis of sepsis. Once severe lactic acidosis with decompensated metabolic acidosis becomes established, especially in conjunction with multi-organ failure, septic shock is likely to be irreversible and fatal [27]. However, even if the antibiotic therapy is started early, the appearance of bacterial resistance towards the chosen antibiotic(s) can reduce clinical efficacy [18]. Thus, parallel to antibiotic therapy individual susceptibility testing of blood cultures is essential for a successful therapy of sepsis [4].

1.2 Antibiotic therapy

Antibiotics target structures that are 'specific' to bacteria, e.g. cell wall formation, intermediary metabolism, membrane functions, gene replication, transcription, and various steps involved in protein synthesis. Bacteria develop *resistance* to antibiotics through spontaneous mutation and through the transfer of genes between strains and species of bacteria [11]. All known resistance mechanisms against antibiotics are based on one of three 'simple' strategies. These are inactivation of the antibiotic, prevention of the antibiotic from reaching its target, and the alteration of the target, rendering it insensitive to the antibiotic. A combination of these various resistance strategies can often be encountered within a single bacterial species [32].

1.2.1 Need for new antibiotics

The selection and spread of bacterial resistance have been facilitated by either over-prescribing or inappropriate dosing regimens of antibiotics [11, 24, 33-36]. Thus, due to the development of bacterial resistance, originally highly potent antibiotics may lose their clinical efficacy [37, 38]. The remaining therapeutic options for highly resistant pathogens are sometimes so extremely limited that clinicians are forced to use older, previously discarded drugs, e.g. colistin, that are associated with significant toxicity and for which there is a lack of robust data to guide the selection of an 'appropriate' dosing regimen and duration of therapy [17]. Hence, novel therapeutic strategies with new antibiotics are needed, that are clinically efficient against multi-resistant pathogens [11]. However, a decreasing trend is found for the pipeline of novel therapeutics against multi-resistant bacteria (Fig. 2). Whereas 16 antibacterial agents have been approved in the USA in-between 1983 and 1987, the respective amount was reduced to only 5 in-between 2003 and 2007 [13].

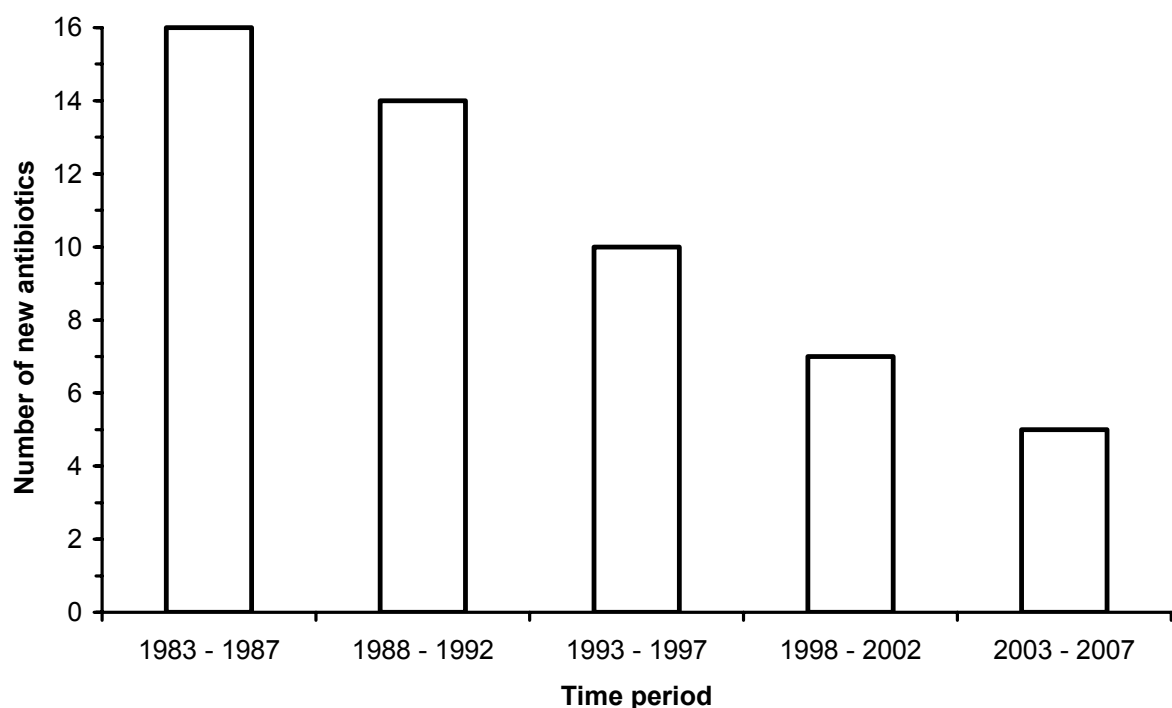


Fig. 2 Number of new antibiotics approved in the United States of America, per 5-year period, data from [13, 17].

Hence, the *Infectious Disease Society of America* (IDSA) proposed legislative and other federal actions to this emerging public health problem in its July 2004 report “Bad Bugs, No Drugs” [18]. Nevertheless, as shown by a recent IDSA report, the need of new antibiotics against problematic pathogens is still present [17].

1.2.2 Rational use of established antibiotics

Considering the currently ‘lean’ pipeline of novel therapeutics against multi-resistant bacteria, alternative strategies must be applied. Therefore, the rational use of established antibiotics that are available for therapy, is a fundamental task aiming to maintain or even to optimise their clinical efficacy [34]. Different strategies for a rational use of established antibiotics have been suggested, as described in the following.

1.2.2.1 Antibiotic ‘cycling’ and ‘mixing’

Antibiotic ‘cycling’, in which two or more antibiotic classes are used alternately, was considered to be a leading candidate in the search for treatment strategies that can slow the evolution and spread of bacterial resistance towards antibiotics [39]. However, there is little substantive evidence about the clinical success of antibiotic ‘cycling’. Bergstrom et al. predicted, via an ecological theory, that antibiotic ‘cycling’ is unlikely to be effective and may even hinder resistance control [40]. These theoretical results correspond with the limited success reported from clinical trial using antibiotic ‘cycling’ [41].

As alternative antibiotic-use strategy, antibiotic ‘*mixing*’ was suggested, in which each treated patient receives one of several drug classes used simultaneously in the hospital [38, 42]. The theoretical analysis from Bergstrom et al. revealed that the heterogeneous antibiotic use via antibiotic ‘mixing’ reduces the spread of resistance [40]. Nevertheless, in clinical practice, the overall success of antibiotic ‘mixing’ might be limited due to the currently limited choice of therapeutic alternatives.

1.2.2.2 Rational dosing of antibiotics

‘Appropriate’ dosing of antibiotics can help preventing or at least reducing the development of bacterial resistance. Complex interactions between an administered antibiotic, the infected patient, and the pathogenic bacteria, essentially determine the success of an antibiotic therapy. In clinical praxis, the complexity of these interactions

is usually reflected by a high variability in the *dose-response relation* (Fig. 3), which may result in both therapeutic failure and emergence of resistant bacterial strains. Therefore, to minimise the dose-response variability for antibiotics, rational dosing regimens must be applied [33-35].

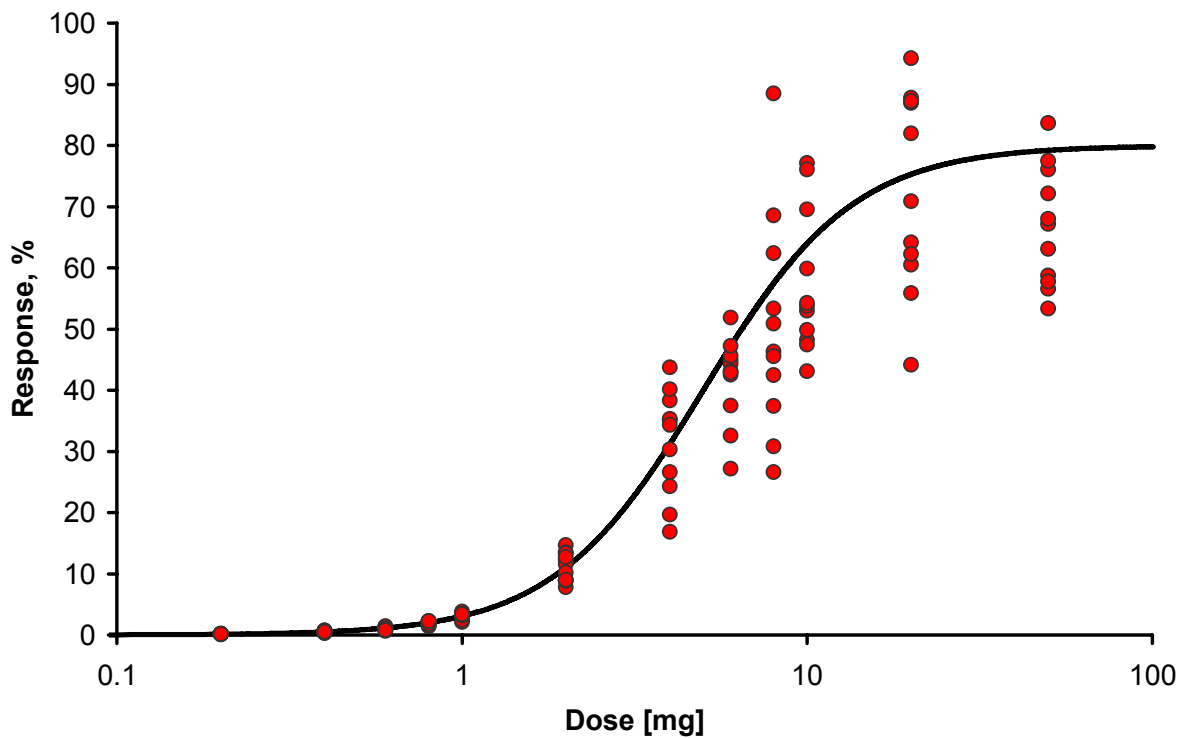


Fig. 3 Dose-response relation of a hypothetical antibiotic, showing high variability of the data from virtual individual patients (red data points), and the averaged (black) curve.

As an example, for *aminoglycosides* like gentamicin, the overall clinical success has been increased via optimising its dosing regimen after its approval. The results from a meta-analysis, comparing multiple daily vs. extended-interval dosing, revealed that for many indications, once daily dosing of the common daily dose of aminoglycosides is an attractive alternative to conventional multiple daily dosing [43]. Accordingly, the guidelines for dosing of aminoglycosides have been adjusted [14, 28]. This example illustrates that dosing regimen optimisation for established antibiotics can help increasing the overall clinical success of antibiotic therapy.

1.2.3 'Appropriate' dosing of antibiotics for septic patients

The population of patients suffering from sepsis show several differences in (patho-) physiology towards patients with other diseases and healthy people, respectively. Due to the appearance of SIRS, severe changes in systemic and organ blood flow, enzyme activity and interstitial fluid can be assumed [27]. These changes are essentially determining the drug disposition in the patient [35], i.e. drug distribution in the body fluids and drug elimination [44], of an therapeutically administered antibiotic [45].

Moreover, due to the necessary poly-medication for septic patients (see 1.1.4), several *drug-drug interactions* can occur in the patient, e.g. inhibition or induction of drug metabolism or competing bindings to plasma proteins. As a result, the drug disposition of an administered antibiotic can be significantly affected by the co-medication, depending on the respective drugs [45, 46]. Hence, the complex and severe course of disease for septic patients and the respectively administered co-medication reveal potential individual differences, causing variability in drug disposition, which is meaningful for the clinical success of the causal antibiotic therapy of sepsis. Despite using the same dosing regimen of an antibiotic for each critically ill patient, the interindividual variability (IIV) can cause differences in the antibiotic concentration-time course in plasma which may result in different clinical outcomes [35, 45, 47, 48]. Because, too low antibiotic concentrations in the patient's body fluids facilitate bacterial growth, and thus increase morbidity [49], whereas too high, i.e. toxic antibiotic concentrations cause serious adverse effects which might force the clinician to stop or change the antibiotic therapy [34].

This consideration reveals that the dosing regimen of (some) antibiotics, administered to critically ill patients suffering from sepsis, might need to be adjusted, i.e. patient-individualised or more general population-optimised, in order to provide maximal clinical success for the therapy of this severe illness [35].

1.3 A rational way of finding an 'appropriate' dosing regimen

For rational dosing of antibiotics, the key characteristics of the drug, the pathogenic bacteria and the infected patient have to be taken into account. Thus, the dosing regimen of an antibiotic should be designed with reference to the interactions between the administered drug and the infected patient, i.e. the *pharmacokinetics*

(PK), and the interactions between the drug and the pathogenic bacteria, i.e. the *pharmacodynamics* (PD) [33-35]. Due to the complexity of these interactions both areas often have been investigated separately. However, in a subsequent step these results can be combined in an integrated pharmacokinetic/pharmacodynamic (PK/PD) analysis [50].

1.3.1 Pharmacokinetic/pharmacodynamic analysis

PK is the quantitative study of the time course of drug *invasion* into the body, e.g. absorption from the intestine, *distribution*, and *elimination*, i.e. metabolism and excretion. Drug distribution and elimination are frequently summarised as drug *disposition*. As a main outcome, PK studies firstly measure the concentration-time course of an administered drug, sampled in body fluid(s), e.g. in plasma. Afterwards, PK analysis is used to describe the single processes, e.g. drug distribution and elimination, essentially determining the drug concentration-time course [44].

PD is the quantitative study of the *drug action(s)* as biochemical (primary) effect(s), e.g. the inhibition of an enzyme, the respectively resulting *drug effect(s)* as a (secondary) change in physiological function(s), which may determine the therapeutic response, i.e. the *clinical efficacy*, e.g. a decreased mortality [47]. In the more recent literature, drug action(s) and drug effect(s) are summarised as *biomarkers*: “a characteristic that is objectively measured and evaluated as an indicator of normal biological processes, pathogenic processes or pharmacologic responses to a therapeutic intervention” [51]. Furthermore, biomarkers that are predictive for the clinical efficacy (or more general clinical outcome) are termed surrogate markers or *surrogate endpoints* [51-54]. Using surrogate endpoints in early studies can sometimes make further studies with clinical endpoint unnecessary [55].

Pharmacometrics is the science of developing and applying mathematic and statistical methods to characterise, understand, and predict the PK and PD behaviour of the considered drug [54]. Moreover, combined PK/PD analysis is used to interpret and extrapolate the temporal relation between (simultaneously) sampled drug concentrations and biomarker(s) magnitudes/concentrations. Hence, PK/PD analysis provides an understanding of the *dosing-exposure-effect-efficacy relation* (Fig. 4), which can be used to predict, i.e. to estimate, the most rational dosing regimen of the considered drug, e.g. for an individual patient or a (special) subgroup of patients [1, 47, 50, 54, 56, 57].

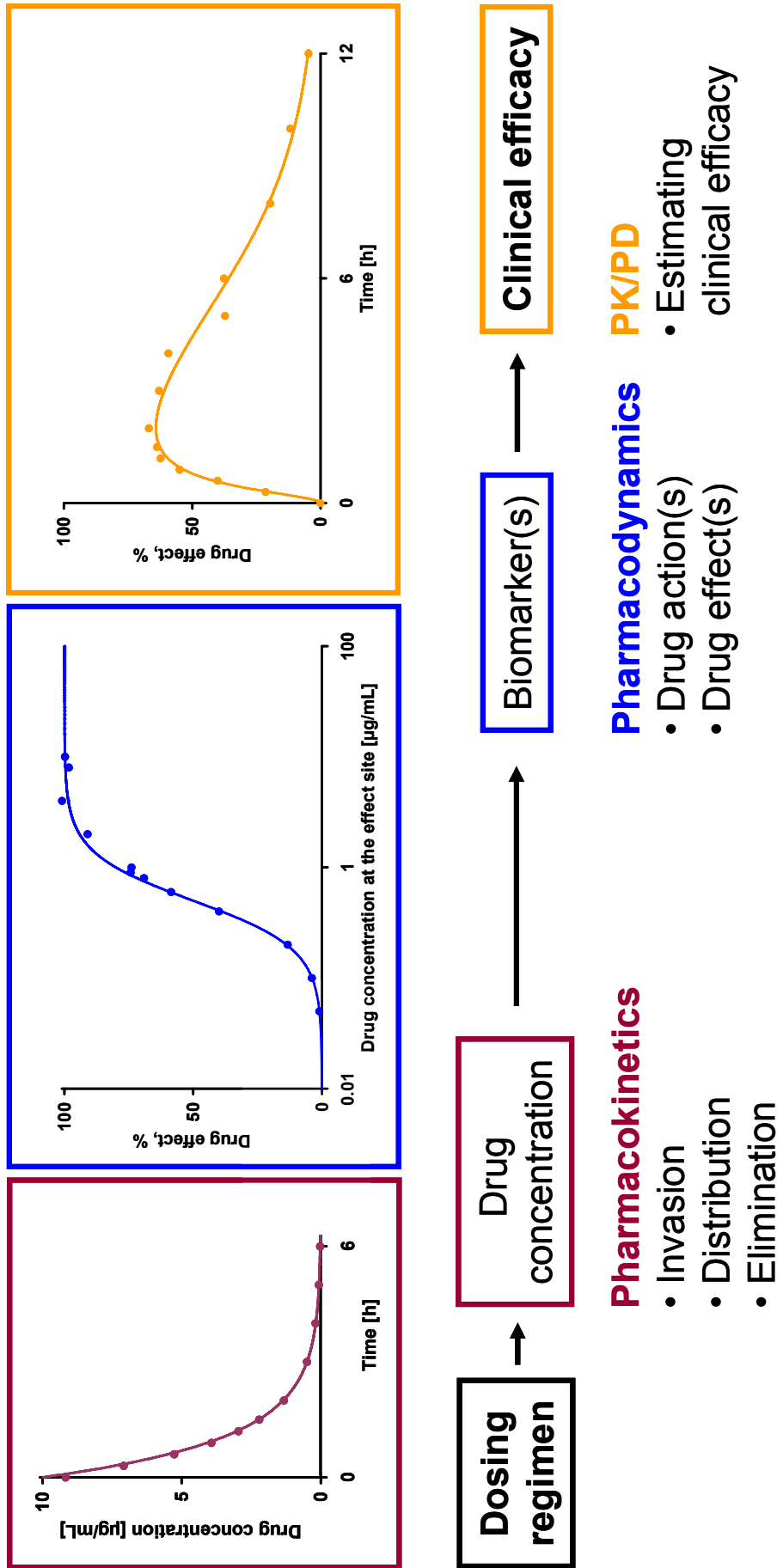


Fig. 4 Dosing-exposure-effect-efficacy relation described via simultaneous pharmacokinetic/pharmacodynamic analysis to find the most rational dosing regimen of the considered drug, e.g. for an individual patient or a special subgroup of patients, modified from [1].

1.4 Linezolid

Linezolid (LZD) is the first (2000 in USA and 2001 in Germany, Zyvoxid[®], Pharmacia/Pfizer) member of oxazolidinones, approved for the treatment of severe skin and soft skin infections, nosocomial and community-acquired pneumonia caused by gram-positive bacteria, e.g. enterococci and *S. aureus* including MRSA. Its standard dosing regimen is 600 mg twice daily (BID) administered intravenously (i.v.) or orally (p.o.) for 10 to 14 days.

1.4.1 Physico-chemical properties

The chemical name is (S)-N-[[3-[3-Fluoro-4-(4-morpholinyl)phenyl]-2-oxo-5-oxazolidinyl]-methyl]-acetamide (Fig. 5), with a molecular weight of 337.35 Da. LZD is a white to off-white, crystalline powder that changes its crystal form at 155 °C and melts at 170 °C. The logarithm of the n-octanol-water partition coefficient (log PC = 0.55) reveals an amphiphilic character [58]. The aqueous solubility of LZD at room temperature is \approx 2.9 - 3.2 mg/mL in water, in which the compound dissolves relatively slowly [59]. For pH = 5 – 9, the solubility is independent of pH, and increases for pH < 3. LZD is a weak base (pKa = 1.8). Therefore, the compound is expected to be unionised in the physiological pH range (i.e. pH \approx 7.35 – 7.45) [58].

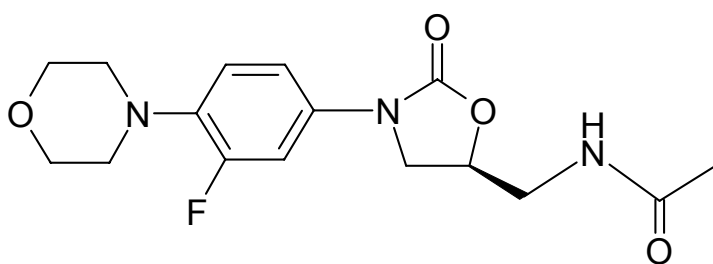


Fig. 5 Chemical structure of linezolid, brand name: Zyvoxid[®], chemical name: (S)-N-[[3-[3-Fluoro-4-(4-morpholinyl)phenyl]-2-oxo-5-oxazolidinyl]-methyl]-acetamide.

1.4.2 Pharmacokinetic properties

1.4.2.1 Absorption and distribution

After oral administration, LZD is rapidly absorbed with a bioavailability of almost 100%, which is not significantly affected by food [60]. However, the rate of LZD absorption is decreased by food intake [61].

The binding of LZD to plasma proteins is approximately 31%, which is independent from the respective LZD concentration [62]. The volume of distribution at steady state condition is approximately 40 to 50 L, comparable to the average total body water (i.e. ≈ 42 L for a 70 kg person [52]). As shown in a recent microdialysis study, LZD penetrates rapidly into the interstitial space fluid of subcutaneous adipose and skeletal muscle tissue in healthy volunteers [63]. For critically ill, septic patients, LZD showed on average good distribution into tissue fluids, but with high IIV. In addition, these patients showed a 37% higher volume of distribution (≈ 63 L) at steady state, compared to healthy volunteers (≈ 46 L) [64].

1.4.2.2 Elimination

For patients with normal renal function, 30% of LZD appears unchanged in the urine, whereas no unchanged LZD appears in faeces. LZD is primarily metabolised by oxidation at the morpholine ring to form two known inactive carboxylic acid metabolites [62]. The elimination half-life of LZD is averaged as 5 – 7 h [60], and the total clearance in healthy volunteers is about 8 L/h [63]. However, critically ill patients suffering from severe sepsis showed an 88% higher clearance (≈ 15 L/h), compared to healthy volunteers [65]. Furthermore, a population PK analysis revealed nonlinear PK for LZD, i.e. the clearance was inhibited over time to 76% of its original value, dependent on the LZD concentration in an empirical inhibition compartment [66].

LZD is not a substrate, inhibitor or inducer of any known isoform of cytochrome P450 [58, 62]. *In vitro* studies with human liver microsomes showed that LZD oxidation is partially dependent upon microsomal proteins and nicotinamide adenine dinucleotide phosphate [67].

1.4.3 Pharmacodynamic properties

1.4.3.1 Mechanism of action and bacterial resistance

The antibacterial activity of oxazolidinones was originally discovered by DuPont Pharmaceuticals in the late 1980s. However, the first molecules of this group were unsuitable for pharmaceutical development [68]. LZD acts through the inhibition of the initiation complex of bacterial protein synthesis [69]. The domain V of the 23S ribosomal ribonucleic acid (rRNA), i.e. a component of the ribosomal peptidyl transferase centre, was suggested as the main ribosomal binding site [70, 71].

Relevant pathogen bacteria provide several copies of the 23S rRNA in the bacterial genome, e.g. enterococci and *S. aureus* possess four to five and five to six copies, respectively [58, 72-74].

For the development of bacterial resistance towards LZD, mutations in several copies must be present to obtain a significant proportion of 'resistant' ribosomes [32, 70, 71, 73-76]. Moreover, the spontaneous *in vitro* mutation frequency of relevant pathogens is low, e.g. $< 8 \cdot 10^{-11}$ for *S. aureus* [77]. Due to the '*multiple target strategy*' and the low rate of *in vitro* mutation of relevant pathogens, bacterial resistance towards LZD is extremely difficult to select *in vitro*. As a result, no resistance towards LZD was found in the many *in vitro* surveys performed before licensing [58].

Despite the difficulty of *in vitro* selection of resistant bacterial strains, 15 cases of emergent resistance in enterococci were encountered in phase III clinical trial before licensing [58]. Moreover, several subsequent cases of resistance in *enterococci* have been reported from different regions of the world [76, 78-82]. As demonstrated in an animal model with enterococci infected mice, the probability of bacterial resistance towards LZD *in vivo* increases with duration of LZD exposure [74].

The first case of a clinically isolated *S. aureus* strain (MRSA) with resistance towards LZD has been obtained 2001 in the USA from a dialysis patient who had received LZD for four weeks [83]. In Germany, the first case of clinically isolated *S. aureus* strains with resistance towards LZD was reported in 2004, and few subsequent cases were announced [10, 84].

Gram-negative bacteria, e.g. *Escherichia coli* (*E. coli*), show an inherent resistance toward LZD, due to multi-drug resistant efflux pumps, type AcrAB pump [85], preventing the intracellular accumulation of LZD [86]. A variety of non-antibiotic molecules have been shown to be active as efflux pump inhibitors. These inhibitors might potentially serve as an 'adjuvant' to extend the antibacterial activity of LZD towards gram-negative bacteria like *E. coli*. However, most investigated inhibitors are not useful for therapy due to their toxicity or poor biological stability [87].

1.4.3.2 Antibacterial activity and susceptibility breakpoints

The antibacterial activity of LZD against staphylococci and enterococci is *bacteriostatic* with some persistent antibiotic effects [88]. The *European Committee on Antimicrobial Susceptibility Testing* (EUCAST) determined *minimum inhibitory*

concentration (MIC) breakpoints for the p.o. and i.v. use of LZD 600 mg BID, based on its PK and PD properties. The non-species-related breakpoints for sensitive and resistant strains were $\text{MIC} \leq 2 \text{ mg/L}$ and $> 4 \text{ mg/L}$, respectively. For staphylococci and enterococci, the averaged susceptible breakpoint was given as $\text{MIC} \leq 4 \text{ mg/L}$ [89].

1.4.3.3 Clinical efficacy

LZD demonstrated good clinical efficacy in a compassionate use programme with patients suffering from gram-positive bacterial infections, without an apparent alternative therapeutic option [58, 62]. However, a recent (2008) retrospective sub-analysis using clinical data of a compassionate use trial, found relevant differences in the clinical success rate at the end of LZD therapy (600 mg BID) and the respective time to bacterial eradication (TBE), between MRSA strains with $\text{MIC} \leq 2 \text{ mg/L}$ and $\text{MIC} = 4 \text{ mg/L}$. The clinical success rates were 92% ($\text{MIC} \leq 2 \text{ mg/L}$) vs. 79% ($\text{MIC} = 4 \text{ mg/L}$), and the median (with interquartile range) TBEs were 4 (3 to 25) days for $\text{MIC} \leq 2 \text{ mg/L}$ vs. 22.5 (6 to > 56) days for $\text{MIC} = 4 \text{ mg/L}$. Thus, diminished clinical efficacy can be expected for the standard dosing regimen of LZD in case of 'susceptible' isolates of *S. aureus* with $\text{MIC} = 4 \text{ mg/L}$ [90].

1.4.3.4 Tolerability

Clinical trials have shown that the standard dosing regimen of LZD (600 mg BID) is generally well tolerated. In adults, the most frequent adverse drug effects were diarrhoea, headache, nausea and vomiting, which were mild to moderate in intensity. However, long-term administration of LZD, i.e. \geq two weeks, increased the probability of serious adverse drug effect, e.g. thrombocytopenia [60, 62, 91]. It has been shown that LZD may inhibit the mitochondrial protein synthesis in human cells, which is linked to the clinical adverse events of LZD [92].

Moreover, LZD is a weak, reversible monoamine oxidase inhibitor [58], i.e. patients should avoid food containing high concentrations of tyramine, and patients taking adrenergic or serotonergic agents should be advised caution [91].

1.5 Objectives

In clinical practice, LZD has often been used as a *reserve antibiotic* for gram-positive bacterial infections, which is utilised when standard antibiotic therapies have failed to be effective, due to the development of bacterial resistance [62, 93-95]. Guidelines for antibiotic therapy explicitly recommend the use of LZD for (nosocomial) infections caused by multi-resistant gram-positive bacteria like MRSA [14, 28, 96, 97]. Hence, in order to successfully treat such problematic bacterial infections, it is especially important that LZD will be used with the most 'appropriate' dosing regimen.

This thesis aimed to develop a rational hypothesis for an optimised dosing regimen of LZD for critically ill patients suffering from severe infections of *S. aureus* susceptible to LZD, based on PK/PD analysis. This overall objective was pursued via the following steps:

- *Bioanalysis*: Validation and use of an high performance liquid chromatography (HPLC) assay for the quantitative determination of LZD in broth.
- *Microbiology*: Establishment and use of a static and dynamic PD *in vitro* model to characterise the antibacterial activity of LZD towards a penicillin-resistant strain of *S. aureus* under various LZD exposure profiles.
- *Pharmacokinetic/pharmacodynamic modelling*: Development of a mathematic PK/PD model for LZD that describes its antibacterial activity against the investigated strain of *S. aureus*.
- *In silico simulation and analysis*: Use of the developed PK/PD model via deterministic and stochastic *in silico* simulations to investigate and evaluate the potential efficacy of twelve different hypothetical dosing regimens for LZD vs. its standard dosing regimen.

This work is partially based on methods and results previously developed at the Dept. of Clinical Pharmacy [66, 98].

2 Materials and Methods

2.1 Materials

2.1.1 Chemicals, reagents and drugs

Acetonitrile, Rotisolv [®] HPLC gradient grade	Carl Roth GmbH, Karlsruhe, Germany
Disodium hydrogen phosphate	Merck KGaA, Darmstadt, Germany
Linezolid, purity 100%	Pharmacia/Pfizer, Kalamazoo/New York, USA
Methanol, Rotisolv [®] HPLC gradient grade	Carl Roth GmbH, Karlsruhe, Germany
Milli-Q water, purified by Milli-Q [™] Plus water purification system	See 2.1.2
Mueller-Hinton broth	Oxoid GmbH, Wesel, Germany
Peptone, from meat, peptic	Merck KGaA, Darmstadt, Germany
Phosphate-buffered saline with peptone	See 2.4.5.1
Potassium dihydrogen phosphate	Merck KGaA, Darmstadt, Germany
Sodium chloride	Merck KGaA, Darmstadt, Germany

2.1.2 Other materials and experimental equipment

Bunsen burner, Labogaz [®] 206	Camping Gaz GmbH, Hungen-Inheiden, Germany
Cannulae, Sterikan, Gr. 1, 0.90 × 40 mm	B. Braun, Melsungen, Germany
Canted neck culture flasks with vented caps, 70 mL	Nunc, Roskilde, Denmark
Casein-peptone soya-meal-peptone agar with 5% sheep blood	Oxoid GmbH, Wesel, Germany
Centrifuge tubes with flat caps, 15 mL and 50 mL	Corning, New York, USA
Centrifuge, 5417 R	Eppendorf, Hamburg, Germany
Culture tubes, DURAN [®] , with Kapsenberg caps, 20 mL	Schott AG, Mainz, Germany
Deep-freezer, type 6483, T = -70 °C	Gesellschaft fuer Labortechnik mbH, Burgwedel, Germany
Digital analytical balance R180 D- [*] D1	Sartorius AG, Goettingen, Germany
Disposable plastic pipettes, 10 mL x 0.1	Nunc, Roskilde, Denmark
Drigalski-spreaders, glass	Carl Roth GmbH, Karlsruhe, Germany
Drill bit, Craftomat HSS, 1 mm	Bahag AG, Mannheim, Germany

Electric screw driver, Trovex [®] Tras 48	Abraham Diederichs OHG, Wuppertal, Germany
Freezer, No-frost-system, T = -26 °C	Liebherr, Lienz, Germany
HPLC system	See 2.3.1.1
Incubation hood, Certomat [®] HK	B. Braun, Melsungen, Germany
Incubator	Heraeus, Hanau/Frankfurt, Germany
Latex slide agglutination test, Staphylect Plus	Oxoid GmbH, Wesel, Germany
Membrane filter units, Minisart [®] , pore Ø = 0.2 µm	Sartorius AG, Goettingen, Germany
Membrane filters, pore Ø = 0.2 µm	Sartorius AG, Goettingen, Germany
Micro tubes with screw caps, 2 mL	Sarstedt, Nuernbrecht, Germany
Mili-Q [™] Plus water purification system	Milipore, Bedford, USA
Mueller-Hinton blood agar with 5% sheep blood	Oxoid GmbH, Wesel, Germany
Multipette [®] with 2.5 mL and 5 mL tips	Eppendorf, Hamburg, Germany
Orbital benchtop shaker, Certomat [®] M	B. Braun, Melsungen, Germany
Pasteur-pipettes, glass	Carl Roth GmbH, Karlsruhe, Germany
Pipette controller, accu-jet [®]	Brand GmbH, Wertheim, Germany
Pipette tips	Eppendorf, Hamburg, Germany
Plastic tubes with push caps, 4 mL	Sarstedt, Nuernbrecht, Germany
Safe lock vials, 0.5 mL and 1.5 mL	Eppendorf, Hamburg, Germany
Seed Vac [®] Plus SC110A	Savant, Farmingdale, USA
Semi-automatic colony counter	Schuett, Goettingen, Germany
<i>Staphylococcus aureus</i> , ATCC 29213	American Type Culture Collection
Syringes, Injekt 2 mL Luer	B. Braun, Melsungen, Germany
Turbidity meter, DensiCheck	bioMérieux, Nuertingen, Germany
Ultrasonic bath, Sonorex RK100 H	Bendelin electronic, Berlin, Germany
Vacuum filtration device, 1 L	Sartorius AG, Goettingen, Germany
Pipettes, Reference [®] , 0.5-1000 µL	Eppendorf, Hamburg, Germany
Vibrofix [®] VF1 Electronic	IKA Jahnke & Kunkel, Staufen, Germany

2.1.3 Scientific software

Excel, version 2003	Microsoft Corporation, Bellevue/Washington, USA
SPSS, version 15	SPSS Inc., Chicago/Illinois, USA
KromaSystem [®] 2000, version 1.83	Kontron Biotech, Neufahrn, Germany

2.2 Fundamental mathematic methods

Several mathematic methods were utilised as scientific tool for the description, evaluation and interpretation of the experimental data. The fundamental mathematic methods used are mentioned in the respective sections and explained in the Appendix (see 7.3).

2.3 Bioanalysis - quantification of linezolid in broth

The quantification of LZD in Mueller-Hinton broth (MHB) samples, obtained from the PD *in vitro* models (see 2.4), was performed by high performance liquid chromatography (HPLC) with UV detection. The utilised HPLC assay was validated before its application, as described below (see 2.3.2).

2.3.1 High performance liquid chromatography

HPLC is a column chromatography technique, frequently used to identify and quantify drugs in biological matrices. The utilised HPLC system contained of a *stationary phase* (column) with chromatographic packing material (reversed phase C-18), a *pump* which transports the liquid *mobile phase*, containing 80/20 (V/V) Milli-Q water (H₂O)/acetonitrile (ACN), at an isocratic flow rate of 1 mL/min through the system, and an UV detector that quantifies the absorption at 251 nm, over time. The detected peaks for LZD in the chromatograms were digitally integrated to calculate the respective peak areas. The chromatographical separation process, and thus the *retention time* (t_R) of LZD was determined by the physical interactions between the drug and the chosen mobile and stationary phase, respectively [99].

2.3.1.1 Experimental equipment

All HPLC experiments were performed with the same software controlled HPLC system containing the following components:

pump:	HPLC pump 420 and 422 (Kontron Biotech, Neufahrn, Germany)
autosampler:	HPLC autosampler SA 360 (Kontron Biotech, Neufahrn, Germany)
column:	Sphere-Image 80-5 ODS2, RP-18, 5 μ m, 125 x 4 mm with pre-column (Knauer, Berlin, Germany)

UV detector:	HPLC detector 430 (Kontron Biotech, Neufahrn, Germany)
control unit:	HPLC multport (Kontron Biotech, Neufahrn, Germany)
control and integration software:	KromaSystem [®] 2000 (see 2.1.3)

2.3.1.2 Sample preparation

The sample preparation for LZD in MHB was based on a method for LZD plasma samples, previously developed at the Dept. of Clinical Pharmacy [98]: 200 μ L ACN were added to 50 μ L of each MHB sample and mixed. After 10 min of resting at room temperature, the mixtures were centrifuged at 10,000 $\cdot g$ for 5 min and subsequently, 200 μ L of the supernatants were evaporated at medium heat (45 $^{\circ}$ C) to dryness via Speed Vac[®], within 1 h. Finally, the dried sample preparations were redissolved in 50 μ L 80/20 (V/V) H₂O/ACN, mixed and placed in the rack of the autosampler. For each sample, a volume of 20 μ L was injected into the HPLC system, using a 20 μ L sample loop.

2.3.2 Method validation

The HPLC method (based on [98]) was validated for the matrix MHB, according to the Food and Drug Administration (FDA) guideline for bioanalytical method validation [100]. For the *pre-study* validation process, *linearity* between the intended lower and upper *limit of quantification*, *stability*, (in-)accuracy, (im-)precision, and analytical *recovery* of LZD in MHB were determined.

2.3.2.1 Stock solutions

Two aqueous LZD stock solutions were prepared, one for testing the linearity and preparing the *calibration curve* (see 2.3.2.4), and another one for the *quality control* samples for the determination of (in-)accuracy and (im-)precision (see 2.3.2.5), and samples for stability testing (see 2.3.2.3) and the determination of the analytical recovery (see 2.3.2.6). Each solution contained a nominal LZD concentration of (C_{LZD}) \approx 1 mg/mL, considering the known aqueous solubility of LZD (see 1.4.1).

2.3.2.2 Linearity and limits of quantification

Based on the aqueous LZD stock solution (see 2.3.2.1), six spiked MHB samples were freshly prepared with nominal $C_{LZD} = 0.2, 0.5, 1.0, 5.0, 20.0$ and $30.0 \mu\text{g/mL}$. The *linearity* of these six dilutions was explored in triplicates, via an unweighted linear regression (see 7.3.4.4) and the coefficient of determination r^2 (see 7.3.3.2) using Excel. Based on previous work [98], the intended *lower* and *upper* limit of quantification (LLOQ, ULOQ) were chosen as $0.2 \mu\text{g/mL}$ and $30.0 \mu\text{g/mL}$.

2.3.2.3 Stability

The stability of stored *aqueous* LZD stock and working solutions and *prepared* LZD samples in the HPLC autosampler had already been determined at the Dept. of Clinical Pharmacy, using the same sample preparation method and the very same HPLC equipment [98].

For the *freeze and thaw* (FT) stability and *short-term temperature* (STT) stability of LZD in MHB, quadruplicates of the intended LLOQ ($0.2 \mu\text{g/mL}$) and ULOQ ($30.0 \mu\text{g/mL}$) were explored and compared with freshly prepared samples. The FT stability investigation was performed with three FT cycles at the intended sample storage temperature of $-26 \text{ }^\circ\text{C}$ for 24 h per cycle. In-between the three freezing periods, the stability samples were completely thawed unassisted at room temperature ($24 \text{ }^\circ\text{C}$) and subsequently refrozen. For the STT stability test, the samples were thawed at room temperature, kept at this temperature for 4 and 24 h, respectively, and subsequently analysed together with freshly prepared samples.

Additionally, the *long-term* (LT) stability of LZD in MHB was investigated, using triplicates of LZD spiked MHB samples with nominal $C_{LZD} = 0.5, 10.0$ and $25.0 \mu\text{g/mL}$. The samples were stored at $-26 \text{ }^\circ\text{C}$ and analysed afterwards together with the very last sample set at the end of the HPLC project. All stock and working solutions were stored at $-70 \text{ }^\circ\text{C}$.

2.3.2.4 Calibration curve

For each HPLC run, a six point calibration curve was utilized with nominal $C_{LZD} = 0.2, 0.5, 1.0, 5.0, 20.0$ and $30.0 \mu\text{g/mL}$ including the LLOQ and ULOQ. Due to the *heteroscedasticity* of the data, a *weighted* linear regression (see 7.3.4.4) was used via Excel. The *weighting factor* was set to $1/(C_{LZD})^2$, i.e. one divided by the squared

respective nominal LZD concentration. The linearity of the weighted regression line was monitored by the weighted correlation coefficient r (see 7.3.3.1 and 4.1.3) [101].

2.3.2.5 (In-)Accuracy and (im-)precision

For the within- and between-day (in-)accuracy and (im-)precision, quintuplicates of four separately prepared LZD *quality control* (QC) samples, i.e. LZD spiked MHB samples, with nominal $C_{LZD} = 0.2, 0.5, 10.0$ and $25.0 \mu\text{g/mL}$ including the LLOQ, were analysed on three different days. The relative error (RE) and the coefficient of variation (CV) served as statistical measures of inaccuracy and imprecision, respectively (see 7.3.1.2). A one-way ANOVA (see 7.3.2.2.1) was performed for the between day comparison. Furthermore, for the *in-study* validation process the inaccuracy and imprecision were monitored for all HPLC runs by means of three duplicates of separately prepared QC samples with nominal $C_{LZD} = 0.5, 10.0$ and $25.0 \mu\text{g/mL}$.

2.3.2.6 Recovery

The analytical recovery of LZD in MHB was calculated by the comparison of peak areas between quintuplicates of LZD spiked MHB samples at three different concentrations (nominal $C_{LZD} = 0.5, 10.0$ and $25.0 \mu\text{g/mL}$) and quintuplicates of three diluted aqueous LZD solutions at the same nominal concentrations.

2.4 Microbiology - *in vitro* pharmacodynamics of linezolid

A PD *in vitro* approach was utilised to characterise the antibacterial activity of LZD towards a penicillin-resistant strain of *S. aureus*. The antibacterial activity was investigated in dependency of time (t) and the respective LZD exposure, via a *static* and a *dynamic in vitro* model (see 2.4.3 and 2.4.4). The bacterial growth/survival was quantified on agar as *colony forming units* (cfu). The static model was used to determine the bacterial growth and death under *constant* LZD exposures, whereas the dynamic model was chosen to investigate *in vivo*-like, i.e. *changing* LZD exposures.

2.4.1 Bacterial stock suspension

The utilised strain of *S. aureus* (ATCC 29213) was obtained by the Institute of Microbiology und Hygiene, Charité Campus Benjamin Franklin in Berlin, Germany.

A pure culture of *S. aureus* was plated on casein-peptone soya-meal-peptone agar with 5% sheep blood and incubated at 36 °C for 24 h. Thereafter, single colonies were selected from the agar plate and suspended in 3.0 mL of 0.45% saline (m/m). The turbidity of the bacterial stock suspension was adjusted to a McFarland index of ≈ 0.50 to produce a bacterial concentration of about $1 \cdot 10^8$ cfu/mL [102].

2.4.2 Preliminary investigations

Prior to the main experiments, several preliminary experiments were performed to qualify the chosen settings of the *in vitro* system. The most important preliminary experiments are described below or briefly mentioned in the respective sections (see 2.4.4.3 and 2.4.5.1.1).

2.4.2.1 *In vitro* stability of linezolid

The stability of LZD in the (static) *in vitro* system, i.e. in MHB at 36 °C, was investigated *with* and *without* bacteria over 48 h. Three previously inoculated culture flasks (with bacteria, see 2.4.3.1) and three non-inoculated culture flasks (without bacteria) were incubated continuously shaking with 62 min^{-1} at 36 °C for 2 h. A 1 mg/mL LZD stock solution was prepared with Milli-Q water and diluted with MHB in two working solutions. Subsequently, 1 mL of the respective working solution was added in triplicates to the pre-incubated culture flasks to obtain nominal $C_{\text{LZD}} = 0.5 \text{ }\mu\text{g/mL}$ and $10.0 \text{ }\mu\text{g/mL}$, respectively. LZD samples (1 mL) were taken at $t = 0, 3, 6, 12, 24$ and 48 h post LZD administration, from each cell culture flask. Afterwards, the samples were centrifuged ($610 \cdot g$ for 10 min) to remove the bacteria. The supernatant fluids (800 μL) were immediately frozen at $-26 \text{ }^\circ\text{C}$ and subsequently analysed by HPLC. For data analysis, the *relative stability* was calculated by the percentaged ratio of the respective LZD concentration measured at $t = 0, 3, 6, 12, 24$ and 48 h, and the LZD concentrations measured at $t = 0$ h.

2.4.2.2 Bacterial survival in different diluents

The survival of *S. aureus* was studied (without LZD) in the utilised dilution medium *phosphate-buffered saline with peptone* (PBSP, see 2.4.5.1), and for comparison in unbuffered 0.85% saline (m/m), during 48 h. The prepared bacterial stock suspension (see 2.4.1) was diluted with both diluents in two bacterial working suspensions containing $\approx 1 \cdot 10^4$ cfu/mL and $1 \cdot 10^5$ cfu/mL, respectively. Immediately after the

dilution process and every 10 min up to 1 h, bacterial samples of 50 μL or 100 μL were taken and plated in quadruplicates on Mueller-Hinton blood agar (MHBA) plates. Inoculated agar plates were incubated at 36 °C for 24 h. Afterwards, the colony forming units were counted (see 2.4.5.2) to calculate the respective bacterial concentrations. For statistical inference, a one-way ANOVA (see 7.3.2.2.1) was performed, using the respective log-transformed bacterial concentrations.

2.4.2.3 Bacterial loss during centrifugation

The potential bacterial loss during the centrifugation step of the bacterial sample preparation (see 2.4.5.1.2), was quantitatively investigated. The prepared bacterial stock suspension (see 2.4.1) was diluted with PBSP (see 2.4.5.1) via serially decimal dilution in four bacterial working suspensions containing $\approx 1 \cdot 10^5 - 1 \cdot 10^2$ cfu/mL. Bacterial samples (10 – 100 μL) were taken in two steps. The first set was *directly* plated in quintuplicates on MHBA plates. The second set of bacterial samples were prepared via the *centrifugation* method (see 2.4.5.1.2) and subsequently plated in quintuplicates on MHBA plates. All inoculated MHBA plates were incubated at 36 °C for 24 h. Thereafter, the colony forming units were counted (see 2.4.5.2), the respective bacterial concentrations were calculated, and a one-way ANOVA (see 7.3.2.2.1) was performed for statistical inference, using the respective log-transformed data.

2.4.3 Static *in vitro* model

Bacteria were exposed to seven different *constant* LZD concentrations for 24 h. In addition, a *growth control* (GC) without antibiotic was simultaneously applied as positive control for bacterial growth in the static *in vitro* model. The bacterial survival was quantified by monitoring the respective bacterial concentrations $N(C,t)$ for a given drug concentration C at time t , measured in *colony forming units per millilitre* (cfu/mL). These experiments were repeated three times on different days. The working principle is illustrated in Fig. 6.

2.4.3.1 Bacterial inoculum

The bacterial stock suspension was 60-fold diluted with PBSP (see 2.4.5.1). Subsequently, eight 70 mL canted neck cell culture flasks with vented caps were filled with 17 mL of MHB and 2 mL of the diluted bacteria suspension, for

simultaneously obtaining an initial inoculum of $\approx 1.7 \cdot 10^5$ cfu/mL in each culture flask. The inoculated culture flasks were immediately incubated continuously shaking with 62 min^{-1} at $36 \text{ }^\circ\text{C}$ for 2 h to induce bacterial growth up to $\approx 1 \cdot 10^6$ cfu/mL.

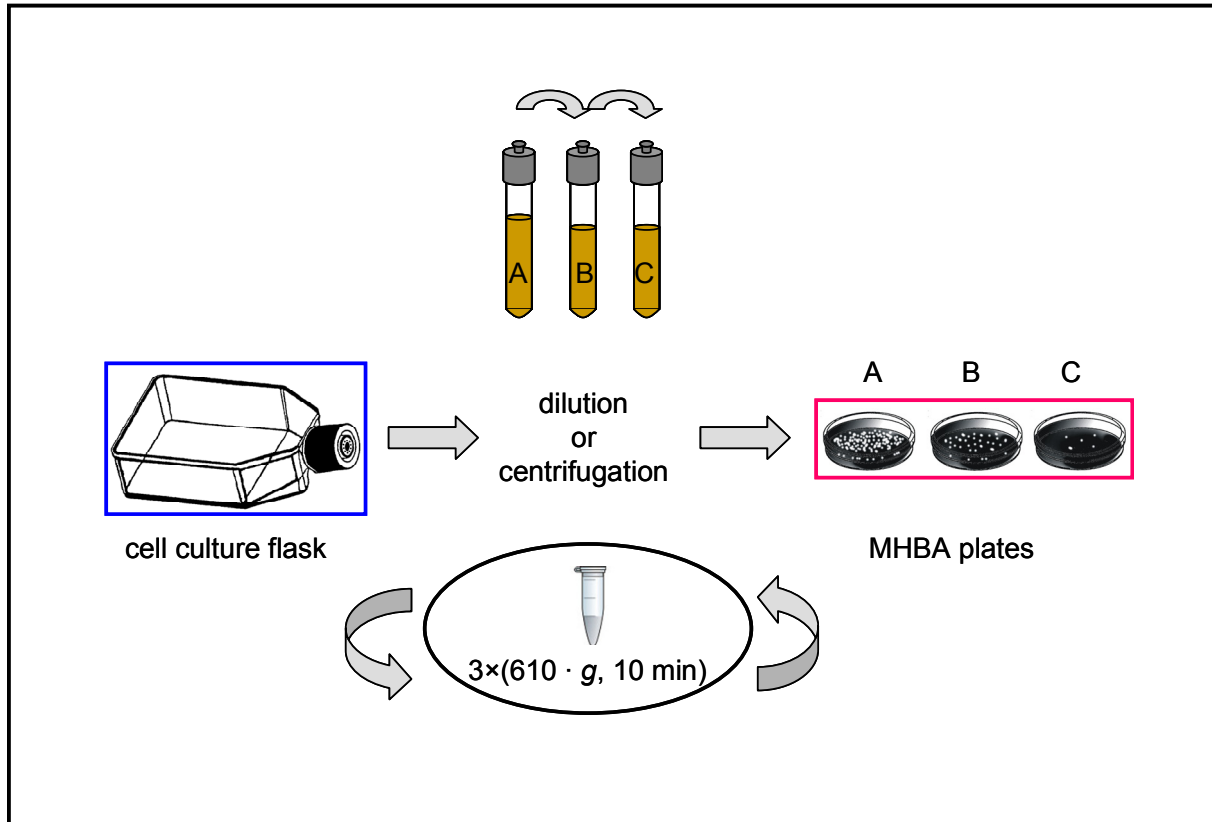


Fig. 6 Schematic work flow of the static *in vitro* model with MHBA = Mueller-Hinton blood agar, for a detailed description of the methods used see text.

2.4.3.2 Linezolid exposure

A stock solution containing 1 mg/mL LZD was prepared with Milli-Q water and diluted with MHB in seven working solutions of different LZD concentrations. Afterwards, 1 mL of the respective working solution was added to the pre-incubated culture flasks to obtain final nominal concentrations of $C_{\text{LZD}} = 0.5, 1.0, 2.0, 4.0, 8.0, 16.0$ and $32.0 \text{ } \mu\text{g/mL}$. In addition, one culture flask served as GC, i.e. 1 mL MHB was added instead of LZD working solution. All LZD exposed culture flasks, including the GC, were immediately re-incubated continuously shaking at $36 \text{ }^\circ\text{C}$ for 24 h.

2.4.3.2.1 Minimum inhibitory concentration

The minimum inhibitory concentration (MIC) conventionally refers to the lowest antibiotic concentration that inhibits visible growth of bacteria that have been grown in broth in the presence of antibiotics at 36 °C for 18 - 24 h, using an inoculum of $\approx 10^5 - 10^6$ cfu/mL [103]. Thus, each LZD exposed culture flask was visually observed at $t = 18$ and 24 h to determine the MIC of LZD for the utilised strain of *S. aureus*.

2.4.3.3 Linezolid sampling

Two LZD samples (1 mL each) were taken from each cell culture flask. One was taken directly after the addition of LZD to the system. The other was taken at the end of the experiment. To remove the bacteria, samples were centrifuged ($610 \cdot g$ for 10 min) and the respective supernatant fluid (800 μ L) was immediately frozen at -24 °C. Afterwards, all LZD samples were analysed by HPLC and the respective LZD concentrations were calculated.

2.4.3.4 Bacterial sampling

Bacterial samples of 10 μ L, 50 μ L or respectively 100 μ L were taken simultaneously from all eight culture flasks of one experiment at $t = 0, 1, 2, 4, 6, 8, 10, 12, 16, 20$ and 24 h of constant LZD exposure. The samples were immediately prepared (see 2.4.5.1), plated on MHBA plates and incubated at 36 °C for 24 h. Subsequently, visual colony counting was performed (see 2.4.5.2).

2.4.4 Dynamic *in vitro* model

Bacteria were exposed to LZD concentrations changing over time. The respective antibiotic exposure was chosen to simulate *unbound* LZD concentration-time profiles, similar to those observed in humans after intravenous (i.v.) administrations of LZD [64]. In total, four different LZD concentration-time profiles were investigated, three for single dose i.v. bolus injections and one for i.v. bolus injection plus continuous infusion (Fig. 7, Tab. 1). For the three simulated i.v. bolus injections, the initial LZD concentrations (C_0) were chosen as 5.0, 10.0 and 15.0 μ g/mL. For the continuous i.v. infusion with initial i.v. bolus injection, the respective LZD exposure was chosen as $C_0 = 17.0$ μ g/mL, which was kept constant as steady state drug concentration (C_{ss}) for the simulated duration of infusion (T_i) of 6 h (see 4.2.2.3).

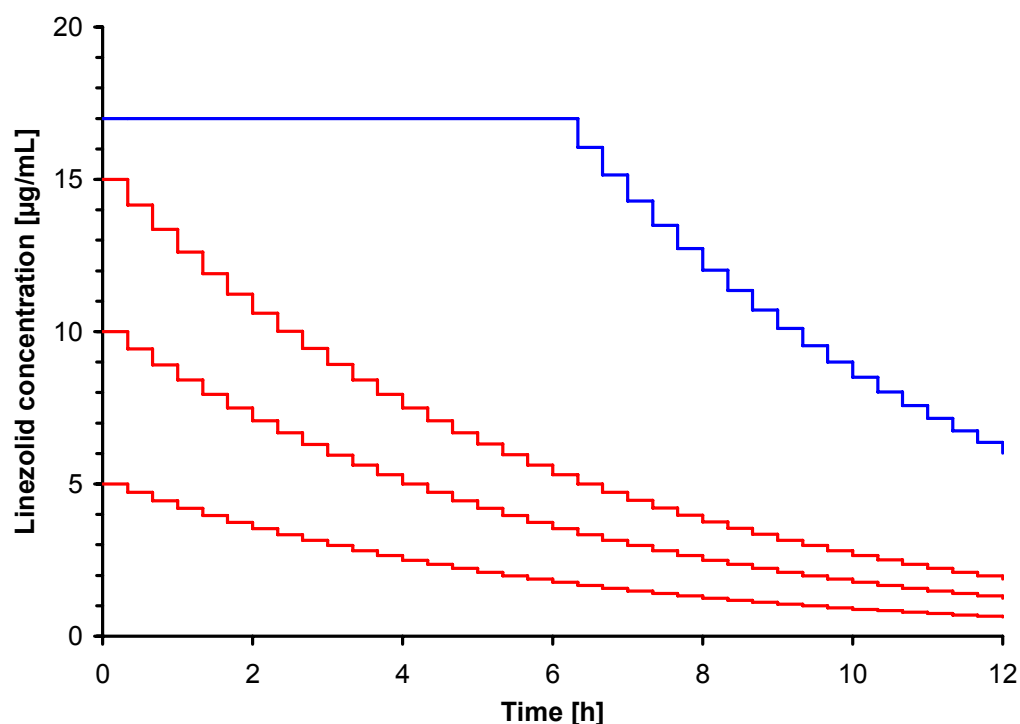


Fig. 7 Theoretical linezolid (LZD) concentration-time profiles simulated in the dynamic *in vitro* model, imitating three intravenous (*i.v.*) bolus injections with initial LZD concentrations (C_0) of 5.0, 10.0 and 15.0 $\mu\text{g/mL}$, respectively (red lines), and an *i.v.* bolus injection with $C_0 = 17.0 \mu\text{g/mL}$ plus continuous infusion over 6 h (blue line).

Tab. 1 Pharmacokinetic parameters with nominal values for the *in vitro* simulated linezolid (LZD) concentration-time profiles, with C_0 = initial LZD concentration at $t = 0$ h, $t_{1/2}$ = half-life, T_i = duration of infusion, and C_{ss} = LZD concentration at steady state.

<i>In vitro</i> simulated route of drug administration	Pharmacokinetic parameters		
	C_0 [$\mu\text{g/mL}$]	$t_{1/2}$ [h]	T_i [h]
<i>i.v.</i> bolus injection	5.0	4	-
<i>i.v.</i> bolus injection	10.0	4	-
<i>i.v.</i> bolus injection	15.0	4	-
<i>i.v.</i> bolus injection with continuous infusion	17.0 (= C_{ss})	4	6

The simulation of drug elimination was performed by a *stepwise substitution* method (see 2.4.4.2.1) [104], for a period of 12 h post LZD administration. For each experiment, two LZD concentration-time profiles were simultaneously investigated. Additionally, a GC without antibiotic was applied as positive control for bacterial

growth in the dynamic *in vitro* model. These experiments were repeated four times on different days.

2.4.4.1 Bacterial inoculum

For each experiment, three inoculated cell culture flasks were prepared as previously described for the static *in vitro* model (see 2.4.3.1).

2.4.4.2 Linezolid exposure

A LZD stock solution containing 1 mg/mL was prepared with Milli-Q water and diluted with MHB in two working solutions of different LZD concentrations. Afterwards, 1 mL of the respective working solution was added to the pre-incubated culture flasks to obtain a final volume of 20 mL with nominal concentrations of $C_{\text{LZD}} = 10.0$ and $15.0 \mu\text{g/mL}$ or 5.0 and $17.0 \mu\text{g/mL}$, respectively. For each experiment, the third culture flask served as GC, i.e. 1 mL MHB was added instead of LZD working solution. The two LZD exposed culture flasks and the GC were immediately re-incubated continuously shaking at 36°C for 12 h.

2.4.4.2.1 Stepwise substitution method

For the three imitated i.v. bolus injections, the initial LZD concentrations in the culture flasks were diluted in a stepwise manner by fresh, *antibiotic-free* broth to mimic exponentially descending LZD concentration-time profiles, according to the PK characteristics of LZD (see 2.4.4.2.2). In contrast, for imitating the continuous i.v. infusion with initial i.v. bolus injection, LZD dilution started with a delay at $t = 6$ h, to maintain the initial LZD concentration as steady state concentration for the first six hours.

During the respective elimination phase, MHB containing LZD in the *in vitro* system was withdrawn through a cannula and a membrane filter unit via a 2 mL syringe and subsequently replaced by the same volume of fresh, LZD-free MHB pre-warmed at 36°C (Fig. 8). The membrane filter (pore $\varnothing = 0.2 \mu\text{m}$) allowed the passage of LZD, but was impermeable for bacteria to prevent bacterial loss during the stepwise dilution of LZD. The functional efficiency of the filter unit was assured via the *bobble-point-test* method, at the end of each experiment [105]. In-between the dilution steps, the respective LZD concentrations remained constant (Fig. 7). The substitution process was applied to the LZD exposed culture flasks and the culture flask

containing the GC. Before and after each dilution step, all cell culture flasks were incubated continuously shaking with 62 min^{-1} at $36 \text{ }^\circ\text{C}$. The Substitution process was executed every 20 min up to 12 h, and the replaced volume was chosen as 1.1 mL according to the following PK characteristics of LZD.



Fig. 8 A set of three dynamic *in vitro* models, containing a 70 mL canted neck cell culture flask filled with 20 mL broth containing a defined bacterial inoculum, a cannula firmly inserted in the flask wall, a membrane filter unit, and a 2 mL syringe; respectively. For a more detailed description see text.

2.4.4.2.2 Pharmacokinetic characteristics of linezolid

The PK of LZD was described in a simplified manner by a one compartment model (Fig. 9) [44], with an intended half-life ($t_{1/2}$) of $\ln(2)/k_e \approx 4 \text{ h}$ [63-65], where k_e refers to the first-order elimination rate constant. In the dynamic *in vitro* model, the simulated $t_{1/2}$ was influenced by the total volume (V) of broth in the *in vitro* model, the substituted volume (V_{sub}) and the time interval between the single dilution steps Δt_{dil} . For practical reasons, V and Δt_{dil} were chosen as 20 mL and 20 min, respectively. The resulting V_{sub} was calculated as 1.1 mL via eq. M1 [106]. The derivation of eq. M1 can be found in the Appendix (see 7.4.1).

$$V_{\text{sub}} = V \cdot \left(1 - e^{-\ln(2) \cdot \frac{\Delta t_{\text{dil}}}{t_{1/2}}} \right)$$

eq. M1

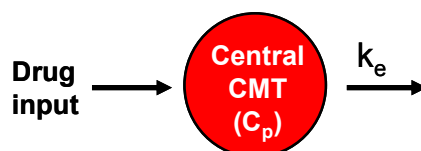


Fig. 9 Schematic depiction of the pharmacokinetic one compartment (CMT) model imitating the pharmacokinetics of linezolid (LZD) in the dynamic *in vitro* model, with C_p = LZD concentration in the central CMT and k_e = first-order elimination rate constant.

2.4.4.3 Linezolid sampling

LZD samples (1.1 mL) were obtained from the volume of broth that was periodically removed by the substitution process. Bacteria-free samples were taken at $t = 20, 40$ and 80 min and from $t = 2$ h every hour up to $t = 12$ h, and directly frozen at -26 °C. Afterwards, all LZD samples were analysed by HPLC and the respective LZD concentrations were calculated.

Prior to the main experiments using the dynamic *in vitro* model, a *preliminary investigation* without bacteria was performed, imitating i.v. bolus injections with nominal $C_0 = 5.0, 10.0$ and 15.0 µg/mL. The aim of this investigation was to determine, if the LZD samples taken through the membrane filter unit were biased compared to LZD samples taken directly through the flask neck. For practical reasons, direct LZD sampling through the flask neck was not accomplishable in the main experiments with bacteria. Thus, it was necessary to assure the ‘quality’ of LZD samples taken through the membrane filter unit.

2.4.4.4 Bacterial sampling

Bacterial samples of 10 µL or respectively 50 µL were taken simultaneously from all culture flasks at $t = 0, 40$ and 80 min and $2, 3, 4, 6, 8, 10$ and 12 h after the initial LZD administration.

2.4.5 Bacterial sample preparation and viable cell counts

Bacterial samples were immediately prepared (see 2.4.5.1) and plated on MHBA plates. Inoculated agar plates were incubated at 36 °C for 24 h, and subsequently viable cell counts (see 2.4.5.2) were determined on each plate.

2.4.5.1 Bacterial sample dilution and purification

Bacterial sample preparation was performed via a serial dilution or centrifugation method (see 2.4.3, Fig. 6 middle part) to assure appropriate *dilution* of bacteria for visual colony counting on agar (see 2.4.5.2) and bacterial sample *purification* to avoid the *antibiotic carry-over effect*, i.e. artefacts due to growth-inhibiting amounts of LZD on the agar plates, causing bias. For both methods, PBSP (composition see 7.1, Tab. 13) served as dilution medium [107].

2.4.5.1.1 Dilution method

Bacterial samples were diluted two to three times via serially decimal dilution with PBSP in 20 mL culture tubes. Afterwards, 100 μL of each dilution was plated in duplicates on MHBA plates and subsequently incubated at 36 °C for 24 h. The respective final extent of dilution was empirically found in *preliminary investigations* and varied between $\approx 5 \cdot 10^{-4}$ and $1 \cdot 10^{-7}$.

2.4.5.1.2 Centrifugation method

Centrifugation was utilised for the purification of samples with low bacterial concentrations ($< 2 \cdot 10^4$ cfu/mL), where serial dilution was not accomplishable. In this process, 100 μL or respectively 50 μL of the bacterial sample was added to 1.5 mL safe-lock tubes filled with 1400 μL or respectively 1450 μL PBSP, and centrifuged ($610 \cdot g$ for 10 min). Subsequently, 1300 μL of the supernatant was removed and discarded. Three cycles of centrifugation were performed with a total LZD dilution factor of $\approx 1 \cdot 10^{-3}$. Thereafter, 50 μL and 100 μL or respectively 200 μL of the remaining residue were plated on MHBA plates and incubated at 36 °C for 24 h.

2.4.5.2 Viable cell counts

Viable cell counts were determined via visual colony counting on MHBA plates by means of a semi-automatic colony counter using plates with 10 to 1,000 colonies. Thus, the LLOQ of viable cell counting was given as $1 \cdot 10^2$ cfu/mL. Based on the measured colony counts the respective bacterial concentrations were calculated.

To detect bacterial contaminants, colonies with atypical morphology, e.g. those exhibiting different size or colour, were subjected to the *latex slide agglutination test* (Staphytest Plus). This test identifies *S. aureus* by the detection of the *clumping*

factor, *protein A* and certain *polysaccharides* [108]. If the test was negative, these colonies were plated on agar and incubated at 36 °C for another 24 h. Subcultures were again visually examined and investigated via the agglutination test.

2.4.6 Descriptive data analysis

For the measured bacterial concentrations from the static and dynamic *in vitro* model respectively, geometric means and $CI_{95\%}$ were numerically estimated by means of *bootstrapping* (see 2.4.6.1), as measure of central tendency and its precision. The calculated statistical summary parameters were plotted against time, and *bacteriostatic* and *bactericidal* concentrations were identified (see 2.4.6.1.2). Furthermore, the *net* estimate of the antibacterial effect was defined and calculated (see 2.4.6.2).

2.4.6.1 *In silico* resampling (Bootstrapping)

Bootstrapping (BS) is a numeric technique widely-used to obtain estimates of summary statistics. This technique is based on iterative random sampling from the original data set (resampling) with replacement, via digital computing power (*in silico*) [109-111]. For the present work, BS was performed with Excel using standard spreadsheet functions:

The two sample sets obtained from the static and dynamic *in vitro* model, were classified in eleven partial sample sets for each investigated (initial) LZD concentration, according to the respective sampling time points (t_x). Each partial sample set containing 12 - 16 data points (n), which originated from 3 – 4 experiments each with 4 colony counts, was digitally defined as “sample-set- t_x ” (SSt_x) with $t_x = 0, 1, 2, 4, 6, 8, 10, 12, 16, 20$ and 24 h for the static *in vitro* model and respectively $t_x = 0, 20, 40, 80$ min, 2, 3, 4, 6, 8, 10 and 12 h for the dynamic *in vitro* model. Subsequently, (re-)samples (exact n) were randomly drawn with replacement from the respective SSt_x to produce resampled data sets [110]. The random resampling process was performed by the spreadsheet function:

$$= INDEX(SSt_x, ROWS(SSt_x)*RAND()+1, COLUMNS(SSt_x)*Rand()+1) \quad [112].$$

The sub function *RAND()* refers to a *pseudo-random number generator* (see 7.3.6.3) that produces random numbers between 0 and 1 [113-115]. For each resampled data set, the geometric mean was calculated. The resampling process was automatically repeated one thousand times ($B = 1,000$) per SSt_x by means of the *data table*

function [116], to generate an empirical distribution of geometric means for each SSt_x [109]. From these distributions, the median, 2.5% and 97.5% percentiles were calculated as numeric estimations of the geometric mean of the population and the respective 95% confidence interval ($CI_{95\%}$, see 7.3.2.1.1) for each SSt_x [110].

2.4.6.1.1 Time-kill curves

The bootstrap estimates (geometric mean and $CI_{95\%}$) of the bacterial concentrations were used to provide conventional *time-kill curves*, i.e. bacterial concentration-time courses [33], for all investigated constant LZD concentrations, LZD concentration-time courses, and the respective GCs.

2.4.6.1.2 Bacteriostatic and bactericidal activities

In addition, for the static *in vitro* model the *bactericidal* and *bacteriostatic* activities were calculated as the difference between the log-transformed bacterial concentration at $t = 0$ h and $t = 24$ h of constant LZD exposure, defined as reduction of bacteria of ≥ 3 log units or < 3 log units, respectively [103].

2.4.6.2 Relative bacterial reduction

For the *net* estimate of the antibacterial effect of LZD, the relative bacterial reduction (RBR) was calculated as ‘*baseline-normalised*’ drug effect [117]. The RBR was defined as the percentaged ratio of the difference between the measured drug effect $DE(C,t)$ and the observed baseline effect $BE(t)$ [118, 119], to the respective absolute value of $BE(t)$, i.e. $|BE(t)|$ (eq. M2). For a certain antibiotic concentration (C), $DE(C,t)$ was set equal to the negative decadic logarithm of the respective concentration of viable bacteria $N(C,t)$ at time point t , i.e. $DE(C,t) = -\log(N(C,t))$. $BE(t)$ was set equal to the negative decadic logarithm of the concentration of viable bacteria of the GC at t , i.e. $BE(t) = -\log(N(C=0,t))$ [120].

$$RBR, \% = \left(\frac{DE(C,t) - BE(t)}{|BE(t)|} \right) \cdot 100 = \left(\frac{\log\left(\frac{N(C=0,t)}{N(C,t)}\right)}{\log(N(C=0,t))} \right) \cdot 100 \quad \text{eq. M2}$$

If e.g. for a given antibiotic concentration at a given exposure time, the bacterial concentrations were measured as $N(C,t) = 1 \cdot 10^2$ cfu/mL and $N(C=0,t) = 1 \cdot 10^{10}$ cfu/mL, respectively, the RBR will be calculated as 80%. RBE = 100%, as

extreme example, implies total bacterial eradication. Thus, the RBR quantifies the *net* antibacterial effect in a descriptive percentage measure with reference towards the situation without antibiotic exposure.

2.4.6.3 Pharmacokinetic/pharmacodynamic parameters

2.4.6.3.1 Pharmacokinetic parameters

For the LZD concentration-time profiles investigated in the dynamic *in vitro* model, a noncompartmental analysis (NCA) was performed via Excel. Here, the maximal observed LZD concentration (C_{\max}) and the *area und the LZD concentration-time curve* (AUC_t) were used as NCA parameters. The integral parameter was calculated for the time interval $t = 0 - 12\text{h}$, i.e. $AUC_{12\text{h}}$, via the linear *trapezoidal rule* [44].

2.4.6.3.2 Pharmacodynamic parameter and outcome

The MIC (see 2.4.3.2.1) of LZD against *S. aureus*, measured at 24 h in the static *in vitro* model, served as PD parameter for the calculation of the PK/PD indices (see 2.4.6.3.3). However, as main *in vitro* PD outcome the *area under the effect-time curve* ($AUC_{E(t)}$), a cumulative measure of the overall drug effect [57], was applied for the RBR-time courses obtained from the dynamic *in vitro* model. The PD outcome was calculated for the time interval $t = 0 - 12\text{h}$, i.e. $AUC_{E(12\text{h})}$, via the linear trapezoidal rule in Excel [44].

2.4.6.3.3 Pharmacokinetic/pharmacodynamic indices

For descriptive PK/PD analysis, the relation of PK and PD of LZD was determined by calculating the following PK/PD indices [121, 122]:

- C_{\max}/MIC
- $AUC_{12\text{h}}/\text{MIC}$
- $t_{C \geq \text{MIC}}$

The first two PK/PD indices refer to the NCA (PK) and PD parameters. The latter PK/PD index ($t_{C \geq \text{MIC}}$) refers to the time with the LZD concentration $\geq \text{MIC}$, measured in % of the investigated time interval of 12 h. The calculated PK/PD indices were analysed together with the *in vitro* PD outcome $AUC_{E(12\text{h})}$, via correlation analysis (see 7.3.3) in Excel.

2.5 Pharmacokinetic/pharmacodynamic modelling

PK/PD modelling investigates the drug effect as function of drug concentration and time, e.g. via curve fitting. Curve fitting implies the use of (nonlinear) regression analysis to find an appropriate mathematic function (and a parameter value set) which best fits the data points of the experimentally obtained data set and possibly other constraints (see 7.3.4.5). In this thesis, PK/PD modelling was applied via curve fitting in Excel (see 2.5.1.5).

2.5.1 Modelling objective and strategy

PK/PD modelling was utilised to characterise the RBR (see 2.4.6.2) of *S. aureus*, for various LZD exposure profiles measured in the static and dynamic PD *in vitro* model, over time. Afterwards, the developed PK/PD model was aimed to be used for predicting future scenarios that were not experimentally investigated, via *in silico* simulation (see 2.6). To accomplish these aims, the following modelling strategy was used, containing five main steps:

- Defining data sets for model development (see 2.5.1.1)
- Model selection (see 2.5.1.2) and development (see 2.5.1.3)
- Finding initial estimates and constraints (see 2.5.1.4)
- Curve fitting (see 2.5.1.5)
- Model comparison (see 2.5.1.6)

2.5.1.1 Defining data sets for model development

During the model development, the developed PK/PD models were first fitted to the RBR data set obtained from the static *in vitro* model (*data set I*, with $n = 88$). Subsequently, the best model was selected (see 2.5.1.6) and fitted to the data set containing both the RBR of LZD from the static and dynamic *in vitro* model (*data set I+II*, with $n = 128$). Hence, data set II, obtained from the dynamic *in vitro* model, was not used separately for PK/PD modelling.

2.5.1.2 Model selection

For the basic characterisation of the structural relation between the antibacterial effect *in vitro*, i.e. the RBR, and the LZD exposure, the 'sigmoidal' E_{max} model was

chosen (eq. M3). This (structural) model describes the (equilibrium) relationship between the measured drug concentration C and the drug effect $E(C)$ [1, 47, 50, 57, 119].

$$E(C) = \frac{E_{\max} \cdot C^H}{EC_{50}^H + C^H} \quad \text{eq. M3}$$

Here, the respective drug concentration-effect curve is simply determined by the three model parameters E_{\max} , EC_{50} and H . E_{\max} is a descriptive measure of the *maximal effect*, whereas EC_{50} implies the *drug concentration producing 50% of E_{\max}* . If two drugs are compared, E_{\max} and EC_{50} are denominated as their *intrinsic efficacy* and *potency*, respectively.

The *steepness* of the drug concentration-effect curve is determined by the *Hill coefficient* H . Thus, the 'shape' of the drug concentration-effect curve is importantly affected by this parameter (Fig. 10). As an example, for $H \leq 1$ *hyperbolic* curves and for $H > 1$ *sigmoidal* curves are found. When $H = 1$, a 16-fold change in drug concentration is required to step from $E(C) = 20\%$ to 80% of E_{\max} . In contrast, for $H = 2$ only a fourfold change is needed, and for $H > 5$ even a small change in drug concentration may produce almost the maximal effect from no detectable effect [47].

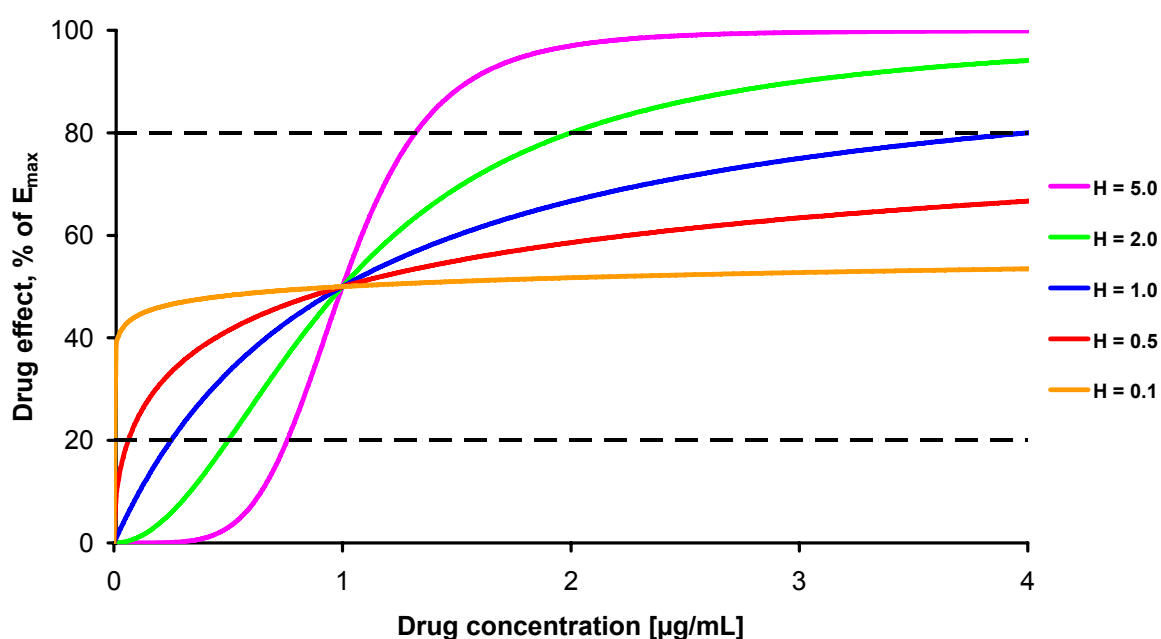


Fig. 10 Theoretical drug concentration-(C)-effect (E) curves of the 'sigmoidal' E_{\max} model with $E_{\max} = 100\%$, $EC_{50} = 1.0 \mu\text{g/mL}$ and $H = 0.1, 0.5, 1.0, 2.0$ and 5.0 , the black dashed lines refer to $E(C) = 20\%$ and 80% of E_{\max} , respectively.

2.5.1.3 Model development

During the modelling process, the 'sigmoidal' E_{\max} model was adapted to different *nested models* to account for the observed time dependency of the RBR for LZD. Two models are called '*nested*' if one of these models is the simpler case of the other [117]. Additionally, during the model development process the concentration term in the 'sigmoidal' E_{\max} model was replaced by linear ordinary differential equations (ODEs) which were algebraically solved via *Laplace transform* (see 7.3.5.1). Subsequently, the derived PK/PD models were compared to choose the best model as final model (see 2.5.1.6).

2.5.1.4 Initial estimates and constraints

For curve fitting via Solver (see 2.5.1.5), initial estimates (see 7.3.4.5.1) were needed for each parameter. The initial values of the parameters E_{\max} , EC_{50} and H were graphically estimated from the plotted RBR data set. These parameters obtained narrow lower and upper limits as rational constraints (see 7.3.4.5.1). For further parameters which were additionally implemented in the PK/PD model during the model development, various initial estimates were used to avoid local minima in the objective function (OBJ, see 7.3.4.5). For these model parameters, the lower and upper limits were set at one tenth and the tenfold of the chosen initial estimates, respectively. Moreover, it was aimed that the chosen parameter constraints did not decisively influence the calculated $CI_{95\%}$ (see 2.5.1.5.2). Furthermore, model parameters which were exactly or good known from prior knowledge, e.g. k_e from the experimental settings (see 2.4.4.2.2), were fixed as *constants*.

2.5.1.5 Curve fitting

Curve fitting was performed via Excel's *Solver* function. Solver is an Excel add-in that serves as numeric general-purpose optimisation tool, developed by *Frontline systems* (<http://www.solver.com>). Solver can iteratively vary one or more freely definable *changing cells* to make a selected *target cell* have a certain value or a minimum or maximum value, accounting for previously defined constraints. Thus, Solver uses iterative numeric methods for optimising nonlinear problems, e.g. nonlinear regression analysis (see 7.3.4.5), as utilised for curve fitting here. All PK/PD model parameters were defined as changing cells and the target cell served as OBJ.

2.5.1.5.1 Solver settings

Solver offers different options to adapt the iterative approximation process to the current problem to be solved. For example, two different optimisation algorithms are selectable: the *Newton's method* and the *Generalized Reduced Gradient (GRG2)* algorithm (see 7.3.4.5.1). For the present work, the following options were changed compared to the default setting (listed in 7.5.1):

- Search = *conjugate gradient method* (GRG2 algorithm)
- Estimates = quadratic method
- Scaling = automatic scaling

These settings were selected based on recommendations from the literature: The GRG2 algorithm requires less computer memory compared to the default (Newton) method. The quadratic method is recommended for highly nonlinear problems as investigated here. The use of automatic scaling has been mentioned to be beneficial if there is a huge difference in magnitude between the model parameters. For the developed PK/PD model, such differences were present [114, 115, 123, 124]. The selected solver options were previously tested for sufficiency via an evaluation data set taken from D. Bourne's textbook [125]. Moreover, three different *Solver reports* were used during the model development process [115]:

- The *Answer report*, which contains initial and final values of the adjusted parameters and the OBJ as well as the defined constraints and which of these restrictions were actually binding.
- The nonlinear *Sensitivity report*, which tells how much the value of the OBJ would change, if the value of a parameter was increased by one, or the respective right-hand side value of the constraints (i.e. the upper limit) was increased by one.
- The *Limits report*, which describes how the value of the OBJ changes as each parameter is maximised and minimised to its limits, while all other values are kept constant and while still satisfying the problem's constraints.

2.5.1.5.2 Confidence intervals

As measure of precision of the parameter estimates, the respective $CI_{95\%}$ were numerically calculated by means of BS using the 2.5% and 97.5% percentiles from one thousand fitted resamples ($B = 1,000$). BS was performed via Excel's

spreadsheet functions, similarly as previously described (see 2.4.6.1). Each resampled data set was automatically fitted by the Solver function, via macros written in *Visual Basic for Applications* (VBA). The utilised VBA script can be found in the Appendix (see 7.5.1).

2.5.1.5.3 Correlation matrix

The *correlation matrix* was applied using the correlation coefficient r (see 7.3.3.1), calculated via Excel's spreadsheet function to determine the parameter relations to avoid over-parameterisation. If two parameters showed r -values ≥ 0.9 or ≤ -0.9 , the relation was specified as high correlation, i.e. the respective data set did not define the model unambiguously [117]. In this case, the respective model was judged as over-parameterised, and thus the model was rejected or simplified, respectively.

2.5.1.5.4 Objective function

For modelling data set I (see 2.5.1.1), the OBJ was obtained from the sum of squared residuals (SSR, see 7.3.4.2) multiplied by the *scaling factor* $K_{scale} = 10^{11}$, according to the recommendations of Frontline Systems [114]. In contrast, for modelling the combined data set (I+II) a '*weighting*' scheme was utilised for the OBJ (eq. M4).

$$OBJ = \left[\sum_{j=1}^{j=d} (SSR_j \cdot n_j) \right] \cdot K_{scale} \quad \text{eq. M4}$$

Here, the OBJ was calculated as the sum of the products of the SSR and the respective number of data points ($n_1 = 88$, $n_2 = 40$) for the two data sets ($d = 2$), multiplied by the chosen scaling factor (K_{scale}). Thus, the OBJ was 'weighted' by n in order to 'stress' the larger (partial) data set.

2.5.1.6 Model comparison

To compare and evaluate the developed key PK/PD models, graphical and parametric methods were applied. Both statistical criteria had to be satisfied for model selection. Furthermore, the $CI_{95\%}$ of the estimated parameter values were inspected as model selection criterion, i.e. if the $CI_{95\%}$ included zero or values $> 100\%$ of the estimated parameter value, the respective model was rejected or modified, respectively.

2.5.1.6.1 Goodness of fit plots

Graphical analysis was utilised to assess the goodness of fit (GOF) for the respective model. The following GOF plots were investigated:

- Predicted RBR vs. observed RBR plot
- Residuals vs. observed RBR plot
- Residuals vs. predicted RBR plot
- Residuals vs. LZD concentration plot
- Residuals vs. time plot

Residuals were defined as observed value minus the respective predicted value. Data spreading more randomly and uniformly narrow around the line of identity (for predicted vs. observed) or around zero (for residual plots) were judged as superior [125].

2.5.1.6.2 Akaike's Information Criterion

The Akaike's Information Criterion (AIC) is a parametric method for comparing nested or non-nested models, based on a combination of the maximum likelihood theory, the information theory and the concept of the entropy of information [126]. The goodness of fit of any mathematic model to a data set can be summarised by the AIC. For nonlinear regression analysis using the SSR as OBJ (see 7.3.4.5), the AIC is calculated by eq. M5.

$$AIC = n \cdot \ln\left(\frac{SSR}{n}\right) + 2 \cdot K \quad \text{eq. M5}$$

In this equation, n is the number of data points and K is the number of model parameters fit by the regression analysis plus one (because the SSR is also an estimated parameter). For comparing models, simply the respective AIC values have to be compared. The model with the lowest AIC value is the most likely one. Thus, it is not the absolute size of the AIC values of the models of interest that is important for model comparison, but the differences between the AIC values. The AIC is known to be very useful in selecting the best model in a set of models. However, if all models considered are insufficient, the AIC will still select one of these as the 'best' model, which might be poor in an absolute sense. Thus, the most effort has to be

made in finding reasonable models to be compared, as accomplished for the current problem.

2.5.1.6.3 'Corrected' Akaike's Information Criterion

Another potential limitation of the AIC is that it may perform poorly if there are too many parameters in relation to the size of the sample set. For this reason, Sugiura derived a *second-order* variant of the AIC, containing a small-sample bias adjustment, that he called c-AIC (here AIC_C , eq. M6) [127].

$$AIC_C = AIC + \frac{2 \cdot K \cdot (K + 1)}{n - K - 1} \quad \text{eq. M6}$$

If the sample size n is large, the second (correction) term will be very small and the correction is negligible. In contrast, for smaller n , e.g. with $n/K < 40$, the correction term will matter and will be relevant for model comparison. However, the AIC_C can only be calculated if the difference $n - K$ is ≥ 2 , with K including the SSR. Thus, unless n is large with respect to the number of estimated parameters, the use of AIC_C is recommended [117, 128], as applied for this work. For example, the ratio n/K was 22 using the 'sigmoidal E_{\max} model (with $K = 4$, see 2.5.1.2) for modelling data set I ($n = 88$, see 2.5.1.1).

2.5.1.6.4 Akaike's weights

As mentioned before, for comparing models of a set derived from the same data set, the model with the lower AIC_C value is the model more likely (to be 'correct'). Unfortunately, this rule does not tell how much more likely. To better interpret the AIC_C values, the probability of choosing the 'best' model can be estimated by calculating the *Akaike's weights* (w_i) via eq. M7 [128],

$$w_i = \frac{e^{\left(-\frac{1}{2} \cdot \Delta AIC_{C,i}\right)}}{\sum_{r=1}^{R_M} e^{\left(-\frac{1}{2} \cdot \Delta AIC_{C,r}\right)}} \quad \text{eq. M7}$$

where ΔAIC_C is the respective difference between the AIC_C value of the considered model and the lowest observed AIC_C value of all considered models, and R_M is the total amount of models of the model set. Here, a given w_i is considered as the *weight of evidence* in favour of model i being the actual 'best' model, assuming that one of the considered models must be the 'best' of that set of models. Hence, given that

there are only R_M models and one of them must be the ‘best’ in this set, it is convenient to *normalise* the relative likelihoods to sum to one. Thus, the relative probability (P_i) of model i being the ‘best’ model can be calculated via eq. M8 [117],

$$P_i = \frac{e^{\left(-\frac{1}{2} \cdot \Delta AIC_{C,i}\right)}}{1 + e^{\left(-\frac{1}{2} \cdot \Delta AIC_{C,i}\right)}} \quad \text{eq. M8}$$

as applied for model comparison in this thesis. The respective probabilistic ‘superiority’ of the ‘best’ model can then be calculated as $1 - P_i$.

2.6 *In silico* simulation and analysis

2.6.1 Objective

The developed *in vitro* PK/PD model for LZD was combined with an *in vivo* population PK model of LZD, previously developed at the Dept. of Clinical Pharmacy [66], for investigating *in silico* various hypothetical dosing regimens for LZD, via *deterministic* and *stochastic* simulations (see 7.3.6) using Excel. The investigated dosing regimes were evaluated concerning their potential as optimised dosing regimen of LZD for critically ill patients suffering from severe infections of *S. aureus* susceptible to LZD.

2.6.2 Population pharmacokinetic model for linezolid

Population PK is the study of PK in the population of interest. Instead of modelling the data from each individual separately, the data from all individuals are modelled simultaneously. To account for the different levels of variability (e.g. between-subjects and within-subjects) *nonlinear mixed effects models* are used [129, 130].

At the Dept. of Clinical Pharmacy, a population PK model for unbound LZD concentration-time courses in plasma was developed, referring to clinical data from 10 healthy volunteers and 24 critically ill, septic patients [66]. These individuals received 600 mg LZD administered BID as tablet or as i.v. short-term (30 min) infusion, respectively. For the purpose of the present *in silico* simulation, the mentioned population PK model was combined with the developed PK/PD model, to account for interindividual (PK) variability (IIV). The considered population PK model (Fig. 11) was adapted to the conditions of the current simulation study, for i.v. administration.

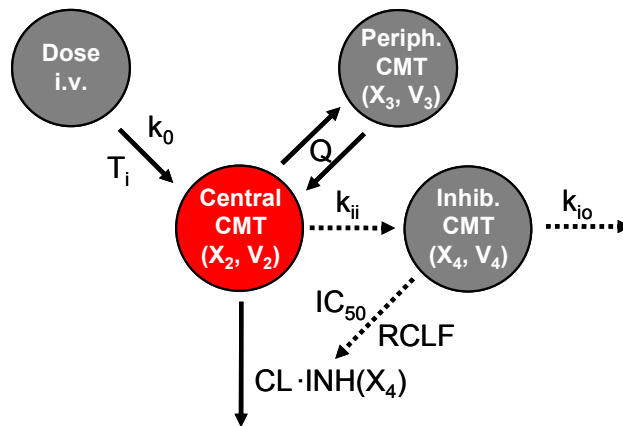


Fig. 11 Schematic depiction of the utilised (population) pharmacokinetic model for the unbound LZD concentration-time course in plasma after intravenous (i.v.) infusion, containing two (central and peripheral) compartments (CMTs) and a hypothetical inhibition CMT [66], parameters are described in the text.

The nonlinear PK model for LZD contained a *central* (including plasma) and *peripheral* compartment (CMT), where X_2 and X_3 are the respective amounts of LZD in these CMTs with V_2 and V_3 as volumes of distribution, k_0 and T_i refer to the rate and duration of infusion, respectively, and Q represents the intercompartmental clearance. The parameter CL refers to the linear clearance from the central CMT, which was partially inhibited over time by multiplying with the inhibition function:

$$INH(X_4) = RCLF + (1 - RCLF) \cdot [1 - (X_4(t)/(IC_{50} + X_4(t)))],$$

where $RCLF$ represents the remaining, i.e. non-inhibitable clearance fraction, $X_4(t)$ is the amount of LZD in a hypothetical inhibition CMT at time point t , k_{ii} and k_{io} are the rate constants into and from the inhibition CMT, respectively, and IC_{50} refers to the LZD concentration in the inhibition CMT that produces 50% of maximum clearance inhibition. The respective parameter values are shown in Tab. 2.

The following (nonlinear) system of coupled ODEs was derived from the (population) PK model to describe the change in drug amount per time for each CMT:

$$dX_2(t)/dt = k_0 + (Q/V_3) \cdot X_3(t) - (Q/V_2) \cdot X_2(t) - (CL \cdot INH/V_2) \cdot X_2(t)$$

$$dX_3(t)/dt = (Q/V_2) \cdot X_2(t) - (Q/V_3) \cdot X_3(t)$$

$$dX_4(t)/dt = k_{io} \cdot [(X_2(t)/V_2) - X_4(t)]$$

Tab. 2 Parameter (K) values of the utilised population pharmacokinetic model describing unbound linezolid concentrations in plasma after intravenous infusion [66], with θ_K = population estimate, IIV = interindividual variability, ω_K^2 = variance, and CV = coefficient of variation.

Model parameter (K)	Population estimate (θ_K)	IIV (ω_K^2 ; CV, %)
CL [L/h]	11.1	41.7
V_2 [L]	20.0	40.1
V_3 [L]	28.9	34.8
Q [L/h]	75.0	-
RCLF	0.764	-
IC ₅₀ [$\mu\text{g/mL}$]	0.1	-
k_{io} [h^{-1}]	0.0019	-

In case of the stochastic *in silico* simulation (see 2.6.3), IIV was applied for the parameters CL, V_2 and V_3 , using an *exponential variability* model [129]:

$$P_{Ki} = \theta_K \cdot e^{\eta_{Ki}},$$

where P_{Ki} denotes the *individual value* of the considered parameter K for the individual i , θ_K is the *population estimate* of a considered parameter K , and η_{Ki} is the *difference* between the natural logarithm of P_{Ki} and θ_K , which is symmetrically distributed with mean zero and variance ω_K^2 .

2.6.3 Simulation methodologies and study designs

Twelve hypothetical dosing regimens for LZD and its standard dosing regimen (Tab. 3) were investigated by means of deterministic and stochastic *in silico* simulations (see 7.3.6) [131]. Here, the above mentioned *in vivo* (population) PK model and the developed *in vitro* PK/PD model were combined as *in vivo/in vitro* PK/PD model for LZD, without (via deterministic simulation) and with (via stochastic simulation) taking into account the PK IIV of the patient population. Both types of *in silico* simulation were applied in Excel via VBA macros. An exemplarily VBA script for the stochastic simulation can be found in the Appendix (see 7.5.2).

For each investigated dosing regimen (Tab. 3), a treatment with LZD of 14 days was simulated. The nonlinear system of coupled ODEs from the population PK model was numerically solved by means of the *fourth-order Runge-Kutta* (RK4) method (see

7.3.5.3) [114, 115], using a step size of $dt = 1$ min. Multiple dosing was implemented by using the *principle of superposition* [44, 132, 133].

Tab. 3 Twelve hypothetical intravenous dosing regimens and the standard dosing regimen (italics, bold type) for LZD, utilised for the in silico simulations, with T_i = duration of infusion and k_0 = infusion rate.

Daily dose [mg/day]	Dosing interval [h]	T_i [h]	k_0 [mg/h]	Dosing regimen
600	24	0.5	1200	1 × 600 mg
1200	24	1	1200	1 × 1200 mg
1200	12	0.5	1200	2 × 600 mg
1200	8	0.333	1200	3 × 400 mg
1200	6	0.25	1200	4 × 300 mg
1800	24	1.5	1200	1 × 1800 mg
1800	12	0.75	1200	2 × 900 mg
1800	8	0.5	1200	3 × 600 mg
1800	6	0.375	1200	4 × 450 mg
2400	24	2	1200	1 × 2400 mg
2400	12	1	1200	2 × 1200 mg
2400	8	0.667	1200	3 × 800 mg
2400	6	0.5	1200	4 × 600 mg

The main outcome for all PK/PD simulations was the integral parameter $AUC_{E(t)}$ (see 2.4.6.3.2), as the area under the simulated drug effect-time course with the drug effect (E) equal to the RBR (see 2.4.6.2), obtained for $t = 14$ days, i.e. $AUC_{E(14 \text{ days})}$. This integral parameter was calculated via the linear trapezoidal rule (eq. M9) [44], with nt equals the number of trapezoids into which the effect-time curve was divided, using a time interval of $\Delta t = 1$ min.

$$AUC_{E(t_{nt})} = \int_{t_0}^{t_{nt}} E \cdot dt \approx \sum_{i=0}^{i=nt-1} \frac{(E_i + E_{i+1})}{2} \cdot \Delta t \quad \text{eq. M9}$$

The stochastic simulation was performed via the *Monte Carlo method* (MCM, 7.3.6.3), further called Monte Carlo simulation (MCS), imitating one thousand ($N = 1,000$) virtual '*in silico* patients' for each investigated dosing regimen (Tab. 3). To account for PK IIV on CL , V_2 and V_3 , the respective normally distributed probability density function of η_K was implemented via the spreadsheet function:

$$= \text{NORMINV}(\text{RAND}(), 0, \omega_{\kappa}),$$

where the sub function *RAND()* refers to a *pseudo-random number generator* (see 7.3.6.3), and ω_{κ} is the standard deviation of η_{κ} [113-115]. The randomly drawn values of these three parameters were monitored (i.e. saved) for each '*in silico* patient'. The respectively measured parameter distributions were used to subsequently compare the 'conditions' of the different simulated dosing regimens, via the *Kruskal-Wallis* test (see 7.3.2.2.2). Additionally, to avoid unintentional artefact during the MCS a numeric *indicator* was used for monitoring LZD concentrations below zero.

The distributions of measured $\text{AUC}_{\text{E}(14 \text{ days})}$ values, for the investigated dosing regimens of LZD, were analysed via the *effect size* (see 3.4.2) [134].

3 Results

3.1 Bioanalysis – quantification of linezolid in broth

3.1.1 Method validation

The bioanalytical method validation of the HPLC assay for quantifying LZD in MHB was successfully completed. The *retention time* (t_R) of LZD was determined as $t_R = 4.4$ min (Fig. 12), a high degree of analytical *linearity* ($r^2 = 0.9996$) was found for the interval between the LLOQ and ULOQ (Fig. 13), and the average analytical *recovery* was determined as 96.6% with low variability (CV = 6.2%).

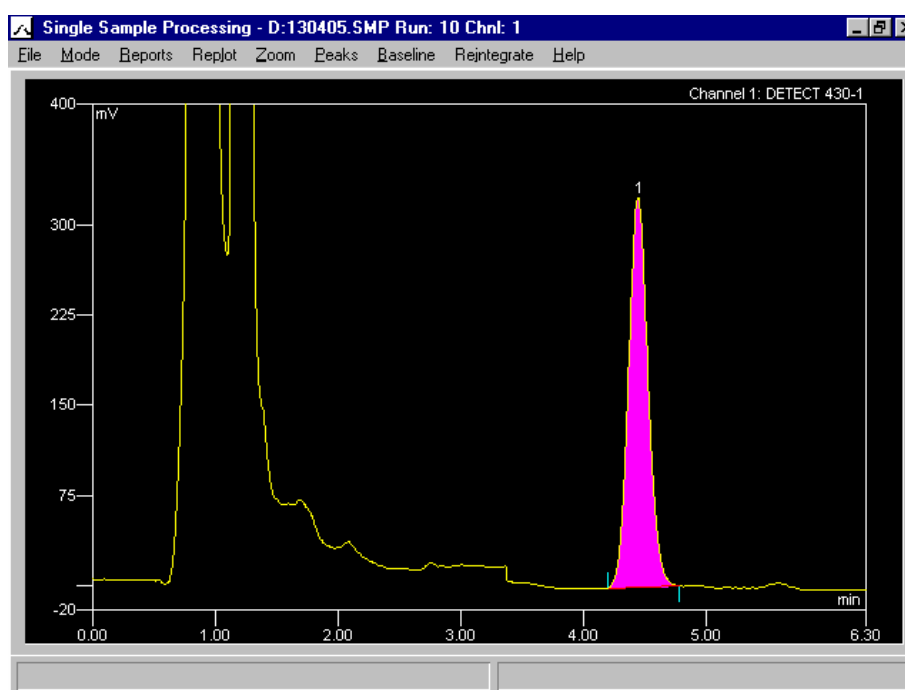


Fig. 12 Chromatogram of a prepared Mueller-Hinton broth sample of a higher linezolid (LZD) concentration (screenshot from KromaSystem[®] 2000), where the LZD peak is marked in pink.

The results from the *stability* investigations for LZD were summarised by the mean and the respective standard deviation (SD) (Tab. 4). For the FT and STT stability tests, the average stability for LZD was 99.1% - 106.5% for the LLOQ and 93.4% - 102.8% for the ULOQ, with an acceptable amount of variation ($SD \leq 9.5\%$). The LT stability samples were investigated after a *storage time* of ≈ 3.5 yr at -26 °C. This investigation showed an average stability of 93.1% - 102.5% for the concentration interval between the LLOQ and ULOQ, with a low amount of variation ($SD \leq 3.9\%$).

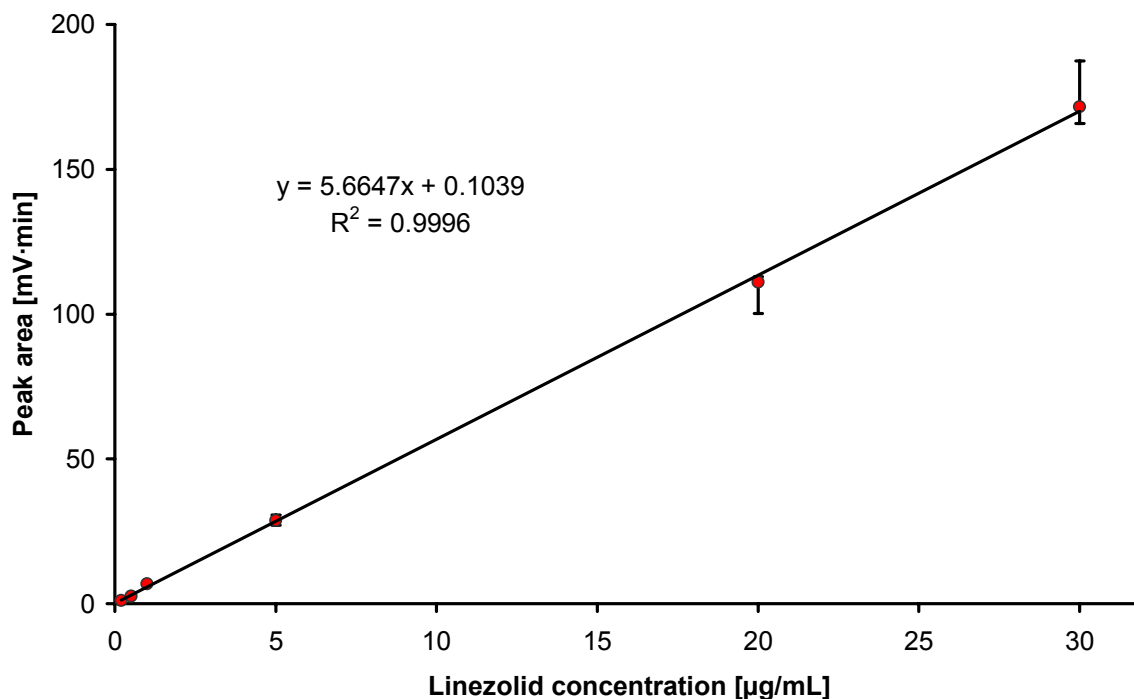


Fig. 13 Test for linearity between the peak area of the chromatograms and the respective linezolid concentration, showing the linear regression model using the median \pm range of three aliquots, with R^2 = coefficient of determination.

Tab. 4 Summary statistics of stability tests for linezolid (LZD), with C_{LZD} = LZD concentration, FT = freeze and thaw, STT = short-term temperature, LT = long term, LLOQ and ULOQ = lower and upper limit of quantification, n = number of aliquots, and SD = standard deviation.

C_{LZD} nominal [$\mu\text{g/mL}$]	FT stability for 3 cycles, % ($n = 4$)	STT stability for 4 h, % ($n = 4$)	STT stability for 24 h, % ($n = 4$)	LT stability for ≈ 3.5 yr ($n = 3$)
	<i>mean \pm SD</i>	<i>mean \pm SD</i>	<i>mean \pm SD</i>	<i>mean \pm SD</i>
0.2 (= LLOQ)	99.1 \pm 2.6	106.5 \pm 9.5	102.8 \pm 0.7	-
0.5	-	-	-	93.1 \pm 1.4
10.0	-	-	-	100.4 \pm 3.9
25.0	-	-	-	102.5 \pm 0.9
30 (= ULOQ)	93.4 \pm 1.1	102.8 \pm 3.6	101.9 \pm 3.8	-

The results for the determination of *inaccuracy* and *imprecision* were summarised by the RE and CV, respectively (Tab. 5). The *within-day* and *between-day* imprecision showed a similar range of 2.4% - 4.7% and 3.0% - 5.3%, respectively. The inaccuracy ranged between +2.3% - +7.0% (*within-day*) and -1.2% - +3.1%

(*between-day*). The one-way ANOVA ($\alpha = 0.05$, $n = 3 \times 5$) for the *between-day* comparison provided p -values ≥ 0.05 for all investigated LZD concentrations. Thus, no statistically significant differences were found during the *pre-study* validation.

Moreover, the *quality control* approach, monitoring the concentration interval between the LLOQ and ULOQ, revealed the *in-study* inaccuracy with RE = -9.8% - +10.2% and the *in-study* imprecision with CV = 0.1% - 9.6%. The respective weighted calibration curves provided weighted r -values ≥ 0.998 . Overall, the investigated *pre-* and *in-study* parameters were in accordance with the demands of the FDA guideline for bioanalytical method validation [100].

Tab. 5 Summary statistics for inaccuracy and imprecision investigations for linezolid (LZD), with C_{LZD} = LZD concentration, LLOQ = lower limit of quantification, n = number of aliquots, RE = relative error, CV = coefficient of variation, and ANOVA = analysis of variance.

Inaccuracy and imprecision:	C_{LZD} nominal [µg/mL]	Measure of imprecision: CV, %	Measure of inaccuracy: RE, %	ANOVA
within-day ($n = 5$)	0.2 (= LLOQ)	3.03	+2.30	-
	0.5	4.74	+0.64	-
	10.0	3.48	+3.89	-
	25.0	2.35	+6.96	-
between-day ($n = 3 \times 5$)	0.2 (= LLOQ)	5.30	-1.20	$p = 0.05$
	0.5	3.80	+0.03	$p = 0.39$
	10.0	3.00	+3.07	$p = 0.28$
	25.0	5.30	+3.10	$p = 0.13$

3.1.2 Measurement of linezolid samples

The LZD samples from the static and dynamic *in vitro* model were successfully analysed by the validated HPLC assay. LZD samples with concentrations > ULOQ ($\approx 4\%$) were diluted 1+1 with H₂O during sample preparation, according to the preparation method for LZD plasma samples, developed at the Dept. of Clinical Pharmacy [98].

3.1.2.1 Linezolid samples from the static *in vitro* model

3.1.2.1.1 Preliminary stability investigation

The results from the preliminary *stability* investigation of LZD inside the static *in vitro* system were summarised by the medians and ranges of the calculated *relative stability* (see 7.2, Fig. 28). For both investigated LZD concentrations (nominal $C_{LZD} = 0.5 \mu\text{g/mL}$ and $10.0 \mu\text{g/mL}$) the relative stability was determined as 92.5% - 110.2% (*with* bacteria) and 86.4% - 106.2% (*without* bacteria), over 48 h. Thus, LZD was considered as stable in the utilised *in vitro* system.

3.1.2.1.2 Main experiments

For the *main* experiments with the static *in vitro* model, mean LZD concentrations of all three experiments were calculated (Tab. 6). The measured LZD concentrations differed only slightly from the respective nominal LZD concentrations (RE = +2.3% - +6.7%) and showed only a low amount of variability (CV = 0.04% - 4.2%). Within the same *in vitro* experiment, the LZD concentrations measured at $t = 0$ h and 24 h showed relative differences of -9.7% - +10.2% (median = -0.5%) referring to the respective LZD concentration at $t = 0$ h. Hence, the constant LZD exposure in the static *in vitro* model was considered as reproducible.

Tab. 6 Measured linezolid (LZD) concentrations from the static *in vitro* model, with C_{LZD} = LZD concentration, n = number of aliquots, CV = coefficient of variation, and RE = relative error.

C_{LZD} nominal [$\mu\text{g/mL}$]	C_{LZD} measured ($n = 3$)		
	mean [$\mu\text{g/mL}$]	CV, %	RE, %
0.5	0.5	4.23	4.44
1.0	1.0	3.34	2.29
2.0	2.1	3.16	4.05
4.0	4.2	1.66	3.96
8.0	8.5	0.04	6.10
16.0	17.1	0.44	6.74
32.0	33.3	2.40	4.01

3.1.2.2 Linezolid samples from the dynamic *in vitro* model

3.1.2.2.1 Preliminary investigation

The preliminary investigation using the dynamic *in vitro* model (without bacteria) showed that LZD samples taken through the membrane filter unit were biased compared to samples taken directly through the flask neck. The LZD concentrations of the ‘filter’ samples were always lower compared to samples taken directly, for all three investigated concentration-time courses. In contrast, the directly taken samples provided optimal exponentially decreasing LZD concentration-time courses (see 7.2, Fig. 29). Thus, it was necessary to calculate an empirical correction factor/function (F_{corr}) for the ‘filter’ samples of the main experiments. The observed differences between the respective LZD concentration-time profiles of the two sample types seemed to be proportional to the parameter C_0 , i.e. the initial LZD concentration at $t = 0$ h. Hence, the measured differences were *normalised* by C_0 , i.e. divided by the respective C_0 value [117]. Subsequently, a mathematic correction was applied for the normalised differences. Here, the first three data points (i.e. at $t = 0, 0.67$ and 1.33 h) were corrected by individual factors of $F_{\text{corr}} = 0.889, 0.301$ and 0.131 , respectively, whereas for the rest of the data points (i.e. for $t = 2 - 12$ h) a time-dependent mono-exponential correction function was used:

$$F_{\text{corr}}(t) = 0.301 \cdot e^{-0.131 \text{ 1/h} \cdot t},$$

which was fitted via Excel’s log-linear regression tool. The curve fitting for the normalised differences provided $r^2 = 0.889$ and a symmetrically distributed goodness of fit plot (see 7.2, Fig. 30).

3.1.2.2.2 Main experiments

The analysed LZD samples from the *main* experiments, using the dynamic *in vitro* model, were summarised by the respective median LZD concentrations which were corrected by F_{corr} and $F_{\text{corr}}(t)$ (Fig. 14). Thereafter, the PK parameters C_0 and $t_{1/2}$ were calculated from the corrected LZD concentration-time courses (Tab. 7), and compared with the expected values (see 2.4.4, Tab. 1). The curve fitting was applied via Excel’s log-linear regression tool. Here, the calculated parameter values of C_0 showed only little deviations from the expected values of $C_0 = 5.0, 10.0, 15.0$ and $17.0 \mu\text{g/mL}$ (RE = $-4.6\% - +2.1\%$). In contrast, the values for the parameter $t_{1/2}$

showed relative large deviation (RE = +26.3 - +37.9%) from the expected values of $t_{1/2} = 4$ h.

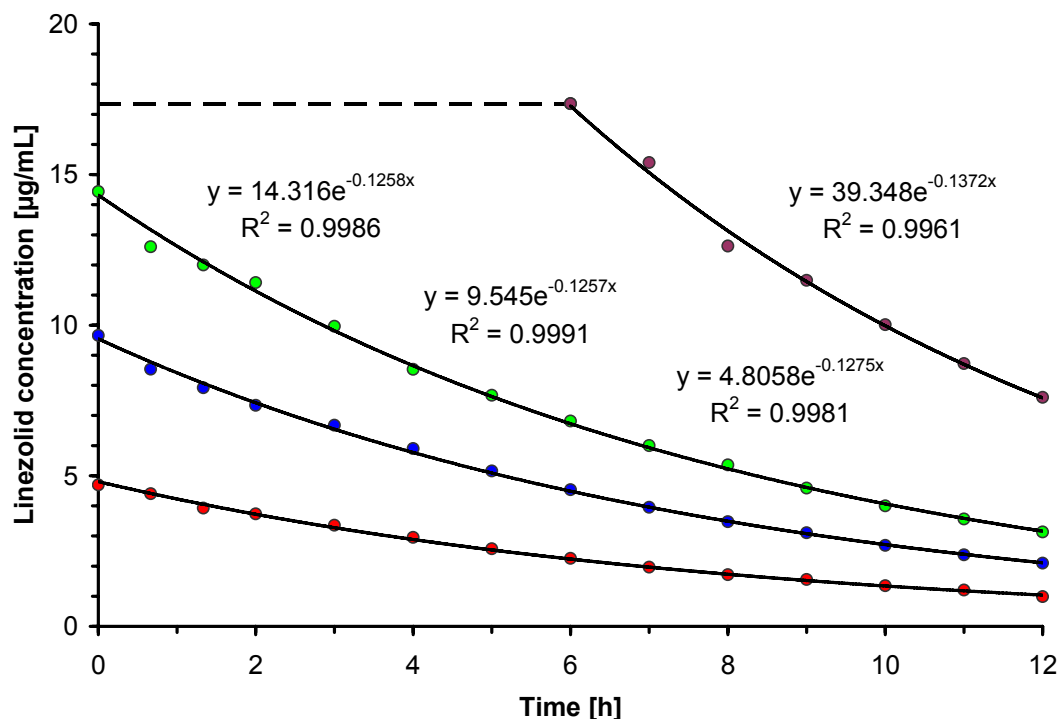


Fig. 14 Corrected linezolid (LZD) concentration-time courses obtained from the main experiments using the dynamic *in vitro* model, imitating three intravenous (*i.v.*) bolus injections (green, blue and red data points) and an *i.v.* bolus injection plus 6 h continuous infusion (purple data points, with a dashed black line during steady state), using log-linear regression (black solid lines), showing the respective regression model equations with y = LZD concentration, x = time, and R^2 = coefficient of determination.

Tab. 7 Calculated pharmacokinetic parameters for the *in vitro* simulated linezolid (LZD) concentration-time profiles, with C_0 = initial LZD concentration at $t = 0$ h, $t_{1/2}$ = half-life, T_i = duration of infusion and C_{SS} = LZD steady state concentration.

<i>In vitro</i> simulated route of drug administration	Pharmacokinetic parameters		
	C_0 [µg/mL]	$t_{1/2}$ [h]	T_i [h]
<i>i.v.</i> bolus injection	4.8	5.4	-
<i>i.v.</i> bolus injection	9.5	5.5	-
<i>i.v.</i> bolus injection	14.3	5.5	-
<i>i.v.</i> bolus injection with continuous infusion	17.3 (= C_{SS})	5.1	6.0

3.2 Microbiology - *in vitro* pharmacodynamics of linezolid

3.2.1 Preliminary investigations

The results for the *stability* of LZD within the static *in vitro* model are presented in the HPLC measurement section (see 3.1.2.1.1). The *bacterial survival* of *S. aureus* in the two investigated diluents PBSP and 0.85% saline is summarised in Fig. 31 (see 7.2). The percentaged bacterial survival rates (median with range) in *PBSP* were calculated as 100.1% (99.3% – 101.3%) after 30 min and 101.1% (100.6% - 101.6%) after 1 h, with 100% at $t = 0$ h. For comparison, the maximum required duration for bacterial sample preparation during the main experiment was ≤ 45 min. Hence, the *S. aureus* strain used here was stable in the utilised dilution fluid. In contrast, the survival rates in *0.85% saline* were decreased to 99.3% (98.1% - 101.2%) after 30 min and 97.5% (96.2% - 100.1%) after 1 h, with 100% at $t = 0$ h. Moreover, when using only saline as diluent, the colonies on agar were often unsymmetrically distributed, causing difficulties in visual colony counting. For comparing the bacterial survival of *S. aureus* in the two investigated diluents, the one-way ANOVA ($\alpha = 0.05$, $n = 2 \times 55$) provided a p -value = $1.921 \cdot 10^{-8}$, i.e. < 0.05 . Thus, the observed difference between the two diluents was statistically significant.

In addition, the potential *bacterial loss* during sample preparation via the centrifugation method was investigated in comparison to direct plating. Here, a slight trend was graphically detected (see 7.2, Fig. 32). For low bacterial concentrations ($\approx 1 \cdot 10^2$ cfu/mL = LLOQ), the centrifugation method obtained slightly higher, i.e. 'better' results, whereas this method provided slightly underdetermined results for high bacterial concentrations ($\approx 1 \cdot 10^5$ cfu/mL). Hence, in the main experiments the centrifugation method was only utilised for bacterial samples with $1 \cdot 10^2$ - $2 \cdot 10^4$ cfu/mL. Moreover, the average ratio of the geometric means of the bacterial concentrations, for both methods, was calculated as 1.0, i.e. on average both methods showed equal results. Furthermore, the one-way ANOVA ($\alpha = 0.05$) using the log-transformed bacterial concentrations ($n = 19$ vs. 20), provided a p -value = 0.513, i.e. > 0.05 . Thus, no statistically significant difference was found between these two methods. Overall, the results from these preliminary investigations confirmed the methodology used in this *in vitro* study.

3.2.2 Static *in vitro* model – descriptive data analysis

3.2.2.1 Minimum inhibitory concentration and time-kill curves

The *MIC* of LZD at 18 h and 24 h was determined as 2 mg/L and 4 mg/L, respectively, in all experiments.

The *time-kill curves* (Fig. 15) revealed that $C_{LZD} \geq 17.1 \mu\text{g/mL}$ were *bactericidal*, $C_{LZD} = 4.2 - 8.5 \mu\text{g/mL}$ were *bacteriostatic* and at $C_{LZD} \leq 2.1 \mu\text{g/mL}$ bacterial growth was observed. Moreover, different phases were found: Initially, the GC showed exponential growth (*log phase*) up to 4 - 6 h and subsequently changed into the *stationary phase*. For $C_{LZD} \geq 4.2 \mu\text{g/mL}$, a *lag phase* of ≈ 1 h followed by a *killing phase* up to 4 - 6 h, were observed. At the end of the killing phase, bacteria changed into a *persisting phase* with very little or no killing and without significant (re-)growth. In contrast, at $C_{LZD} \leq 2.1 \mu\text{g/mL}$, no relevant killing (phase) was found. Nevertheless, these LZD concentrations significantly reduced the exponential bacterial growth (*prolongated log phase*) compared to the GC.

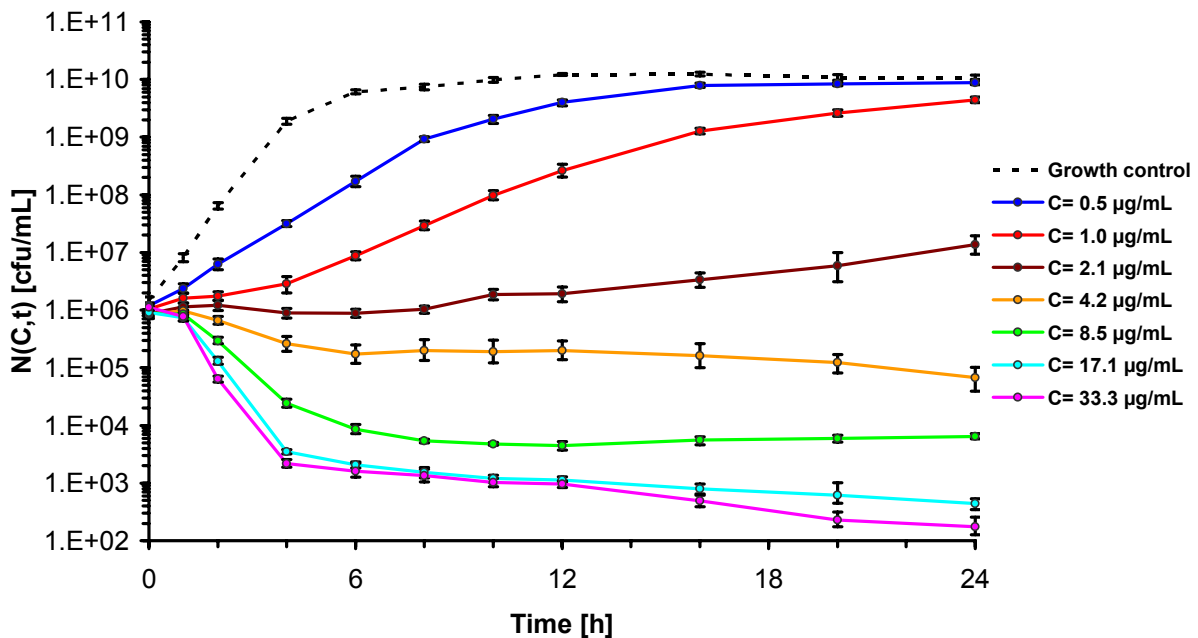


Fig. 15 Time-kill curves for the static *in vitro* model: *In vitro* survival and growth of *S. aureus* (ATCC 29213) for 7 different constant linezolid concentrations (C) and growth control, data points of the interpolated curves represent the geometric means of the bacterial concentrations ($N(C,t)$), and the error bars refer to the corresponding $CI_{95\%}$.

3.2.2.2 Relative bacterial reduction

To investigate the net antibacterial effect of LZD, the RBR for *S. aureus* was calculated and plotted against the LZD concentration and LZD exposure time:

The LZD *concentration-effect* relationship was illustrated for ten different time points (Fig. 16 a). These curves showed a *hysteresis loop* [48, 135, 136], indicating a distinctive increase of the effect over time, particularly for $C_{LZD} \geq 4.2 \mu\text{g/mL}$. Here, the time-dependent increase of the effect predominantly occurred during the first 6 h of LZD exposure. Moreover, these curves revealed that $C_{LZD} \approx 17 \mu\text{g/mL}$ was sufficient to provide almost the maximum effect. There was no relevant increase of the effect at higher LZD concentrations. Nevertheless, the maximum RBR of 78% was found for $C_{LZD} = 33.3 \mu\text{g/mL}$ at 24 h.

Furthermore, the *steepness* of the LZD concentration-effect curves was continuously increasing over time (see also 3.3.4). Up to 6 h, *hyperbolic* curves were observed, whereas *sigmoidal* curves with increasing steepness were noticed for $t \geq 8$ h. As a result of the increasing steepness, the effect of $C_{LZD} \leq 2.1 \mu\text{g/mL}$ was at first increasing within the first 4 - 6 h, but subsequently decreasing. In addition, for $t \geq 6$ h an *intersection* of the interpolated concentration-effect curves was found at $C_{LZD} = 3.5 \mu\text{g/mL}$ and RBR = 44%, i.e. about the half of the maximum observed effect (Fig. 16 b). This intersection indicated the lowest LZD concentration that provided no decrease of the effect up to 24 h, i.e. it maintained the antibacterial effect that has been reached within the first 6 h.

Moreover, for investigating the *effect-time* relationship, the RBR was plotted against the exposure time of LZD, for the seven investigated LZD concentrations (Fig. 17). Here, slightly *sigmoidal* effect-time courses were observed for $C_{LZD} \geq 4.2 \mu\text{g/mL}$, reaching the *plateau* at ≈ 6 h. In contrast, for LZD concentrations of $\leq 2.1 \mu\text{g/mL}$ the effect-time courses showed an initial increase in the effect with a maximum at 4 - 6 h, but decreased thereafter. However, a LZD concentration of $2.1 \mu\text{g/mL}$ provided a *plateau-like phase* between 6 h and 12 h, before the effect finally decreased. Thus, for all investigated LZD concentrations, a '*temporal dissociation*' of 4 - 6 h was found between the drug administration and reaching the maximum or plateau phase of the effect, respectively.

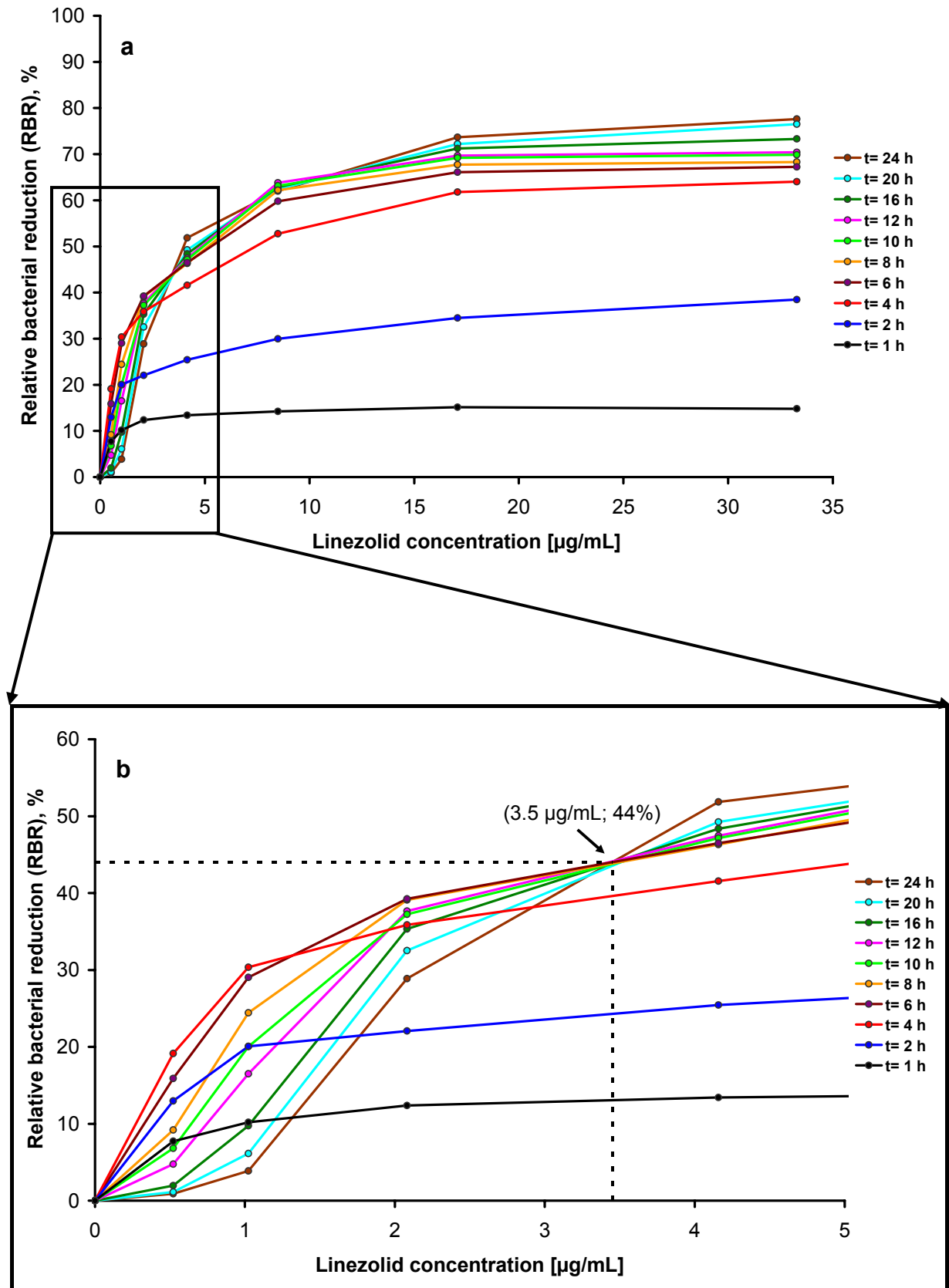


Fig. 16 Relative bacterial reduction (RBR) of *S. aureus* (ATCC 29213) vs. linezolid (LZD) concentration for different LZD exposure times (t): (a) for all investigated LZD concentrations and (b) a cut-out of lower LZD concentrations: the arrow and the black dashed lines indicate the intersection mentioned in the text.

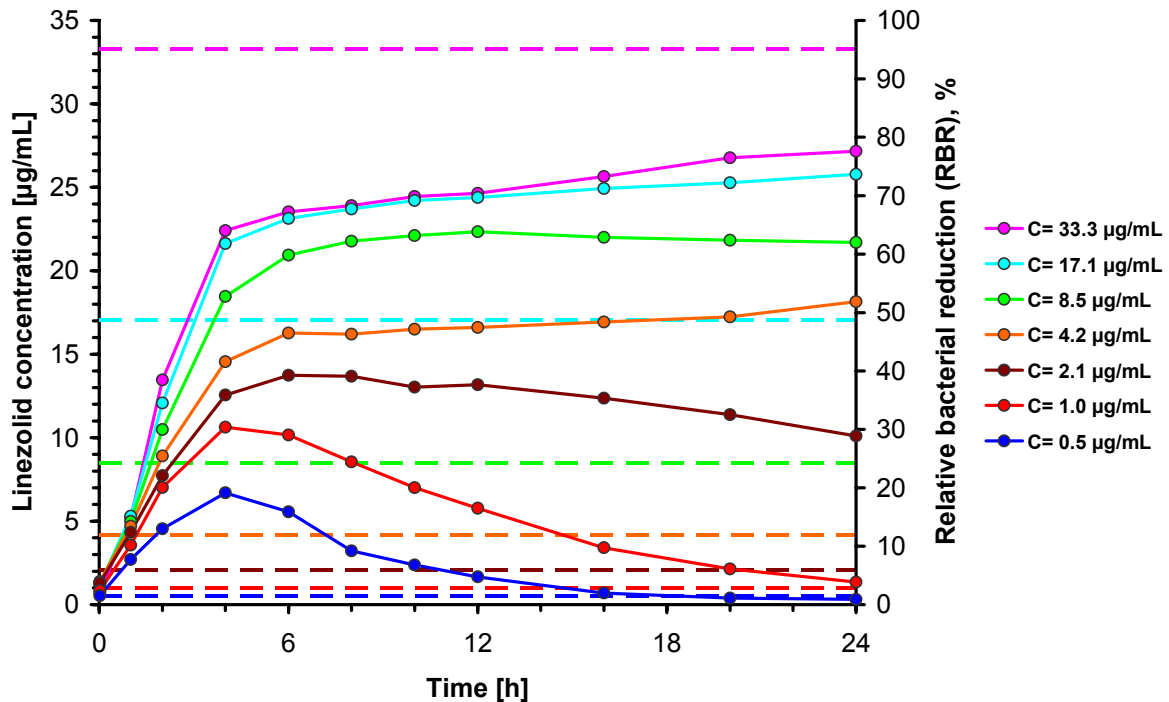


Fig. 17 Relative bacterial reduction (RBR) of *S. aureus* (ATCC 29213) vs. linezolid (LZD) exposure time for seven different LZD concentrations (C), additionally showing the measured LZD concentrations (dashed lines in the respective same colour as the RBR-time course).

3.2.2.3 Phenotypic variants of *Staphylococcus aureus*

During the 'static' *in vitro* experiments, varying colony morphologies were observed on MHBA plates. At $C_{LZD} \leq 4.2 \mu\text{g/mL}$, colonies showing beta-haemolysis, i.e. a zone of clearing in the blood agar in the area surrounding a colony [20], and similar size as the GC were found, for all investigated time points. However, at $C_{LZD} \geq 8.5 \mu\text{g/mL}$, colony size and appearance of beta-haemolysis changed over time: At the beginning, the colony size and the haemolysis zone were equal to the GC. However, within the killing phase, three different colony *morphotypes* with and without haemolysis zones were observed: normally growing, smaller and tiny colonies (Fig. 18). During the following persisting phase, predominately small and tiny colonies with reduced or without haemolysis zones and low pigmentation were found. The amount of the tiny colonies slightly increased, if the incubation time was extended to 48 h. Most of the small and tiny colony variants provided a negative latex slide agglutination test. However, when these colonies were subcultured on agar at 36 °C for another 24 h they exhibited normal colony morphology, haemolysis and a positive agglutination test.

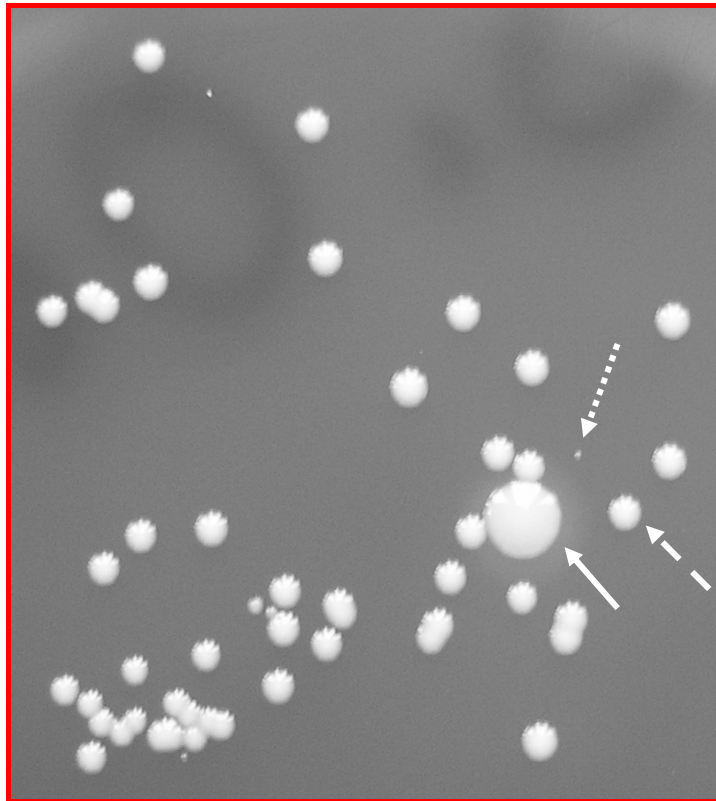


Fig. 18 Three different colony morphotypes of *S. aureus* (ATCC 29213) observed at linezolid concentrations $\geq 8.5 \mu\text{g/mL}$ during the killing phase. Bacteria were grown on Mueller-Hinton blood agar at 36°C for 24 h: normal colony ($\text{---}\rightarrow$), smaller colony ($\text{- -}\rightarrow$), and tiny colony with low pigmentation ($\text{.....}\rightarrow$).

3.2.3 Dynamic *in vitro* model – descriptive data analysis

3.2.3.1 Time-kill curves

The time-kill curves (Fig. 19) revealed the antibacterial activity of the four investigated LZD concentration-time profiles, against *S. aureus*: For all LZD exposure profiles, a *lag phase* of ≈ 1 h followed by a *killing phase* up to 4 - 6 h were observed. In case of $C_0 = 4.8 \mu\text{g/mL}$, the bacterial killing was below one log unit, whereas the other profiles with $C_0 \geq 9.5 \mu\text{g/mL}$ provided bacterial killing of $> 2 - < 3$ log units. However, none of the investigated LZD profiles provided a reduction of ≥ 3 log units. During the killing phase, the slope of the respective time-kill curves was increasing with increasing values of C_0 . Thus, a LZD concentration-dependency of bacterial killing was found here.

At the end of the killing phase, a *persisting phase* followed with no further killing and no or only limited (re-)growth. Considering the three LZD profiles imitating i.v. bolus injections, the tendency for (re-)growth was also dependent on the respective value

of C_0 : For $C_0 = 14.3 \mu\text{g/mL}$ no evidence for (re-)growth was found, whereas $C_0 = 9.5 \mu\text{g/mL}$ showed a certain tendency for (re-)growth at $t = 8 - 12 \text{ h}$. In case of $C_0 = 4.8 \mu\text{g/mL}$, the bacterial concentration measured at $t = 12 \text{ h}$ was approximately equal to the inoculum. However, for both latter mentioned LZD profiles, the increase in bacterial concentration was below one log unit.

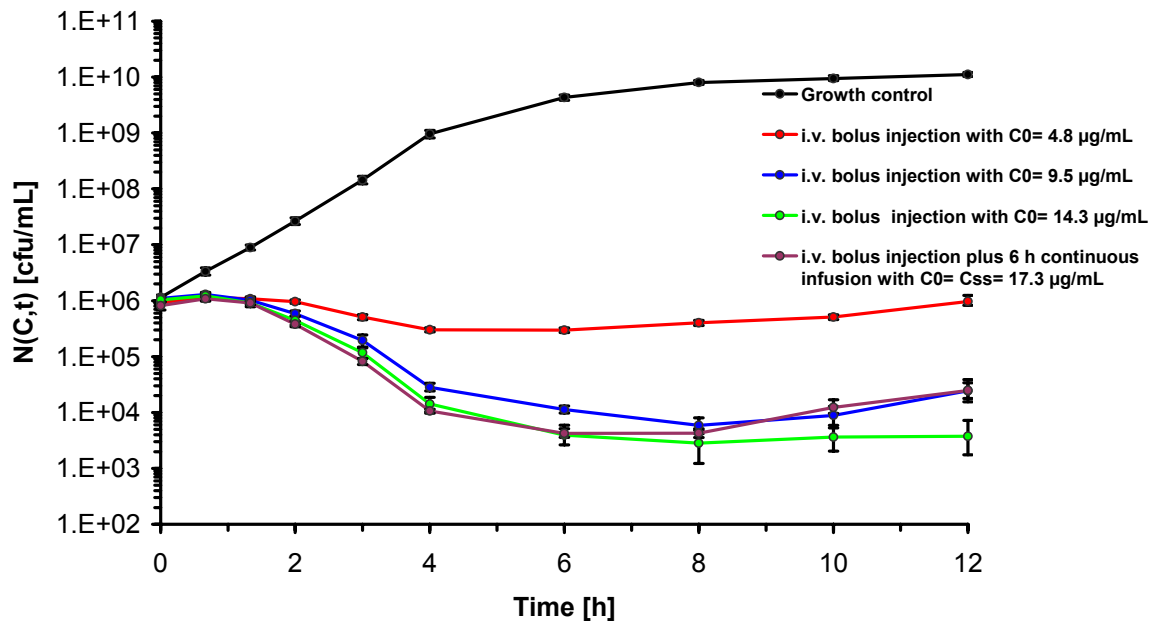


Fig. 19 Time-kill curves for the dynamic in vitro model: In vitro survival and growth of *S. aureus* (ATCC 29213) for four different linezolid (LZD) concentration-time profiles and growth control, showing the geometric means of the bacterial concentrations ($N(C,t)$), error bars referring to the corresponding $CI_{95\%}$, with C_0 = initial LZD concentration and C_{ss} = steady state LZD concentration.

In contrast, the LZD exposure profile imitating an i.v. bolus injection plus 6 h continuous infusion with $C_0 = C_{ss} = 17.3 \mu\text{g/mL}$, showed an unexpected 'high' tendency for (re-)growth. Despite its high antibacterial activity during the killing phase, the measured bacterial concentration at $t = 12 \text{ h}$ was the same as found for the LZD exposure profile with $C_0 = 9.5 \mu\text{g/mL}$. In case of $C_0 = C_{ss} = 17.3 \mu\text{g/mL}$, (re-)growth started at $t = 6 - 8 \text{ h}$, i.e. directly after starting the stepwise dilution of medium. However, the observed increase in bacterial concentration was also below one log unit. Overall, the four investigated LZD concentration-time profiles achieved *bacteriostatic* activity concerning the investigated 12 h interval.

For comparing the growth conditions, i.e. the bacterial growth without LZD exposure, in the static and dynamic *in vitro* model, the bacterial concentrations $N(C=0,t)$ of the respective GCs were directly compared for seven different time points (see 7.2, Fig. 33). At $t = 0$ and $t = 8 - 12$ h the respective $CI_{95\%}$ crosses the line of identity. Thus, for these time points no difference was found between the two *in vitro* models. However, for the time interval $t = 2 - 6$ h, i.e. during the log phase, little deviations were found. Here, the bacterial concentrations from the dynamic *in vitro* model were slightly lower. Nevertheless, the one way ANOVA ($\alpha = 0.05$), using the log-transformed average bacterial concentrations ($n = 2 \times 7$), provided a p -value = 0.867, i.e. > 0.05 . Thus, the graphically observed difference was not statistically significant.

3.2.3.2 Relative bacterial reduction

To determine the net antibacterial effect of the four investigated LZD concentration-time profiles, the RBR for *S. aureus* was calculated and plotted vs. LZD exposure time (Fig. 20). Here, slightly sigmoidal shaped effect-time courses were observed, reaching the *plateau* at ≈ 6 h.

Considering the three LZD profiles imitating i.v. bolus injections (Fig. 20 a), the plateau phase was stable in case of $C_0 = 14.3 \mu\text{g/mL}$, whereas for $C_0 \leq 9.5 \mu\text{g/mL}$ the effect slightly decreased between $t = 8 - 12$ h. After 12 h, the respectively performed RBR was 64.4% for $C_0 = 14.3 \mu\text{g/mL}$, 56.3% in case of $C_0 = 9.5 \mu\text{g/mL}$ and 40.4% for $C_0 = 4.8 \mu\text{g/mL}$. Thus, the latter mentioned profile provided a final effect $< 50\%$. Furthermore, when comparing the observed effect-time courses with the respective LZD exposure-time profiles (dashed curves in Fig. 20 a), ‘*countermoving*’ profiles were observed, i.e. while the LZD concentration was decreasing, the respective effect was increasing. Thus, in contrast to the results from the static *in vitro* model (see 3.2.2.2, Fig. 17), the ‘*dissociation*’ between the time courses of the measured LZD concentration and the respectively observed effect, was found throughout the total investigated time period of 12 h.

In case of the LZD exposure profile imitating an i.v. bolus injection plus continuous infusion with $C_0 = C_{ss} = 17.3 \mu\text{g/mL}$ (Fig. 20 b), a by trend ‘*instable*’ plateau phase was found, due to the previously mentioned unexpected tendency for (re-)growth (see 3.2.3.1). After 12 h, the observed RBR was 56.2%, similar as for the i.v. bolus injection with $C_0 = 9.5 \mu\text{g/mL}$.

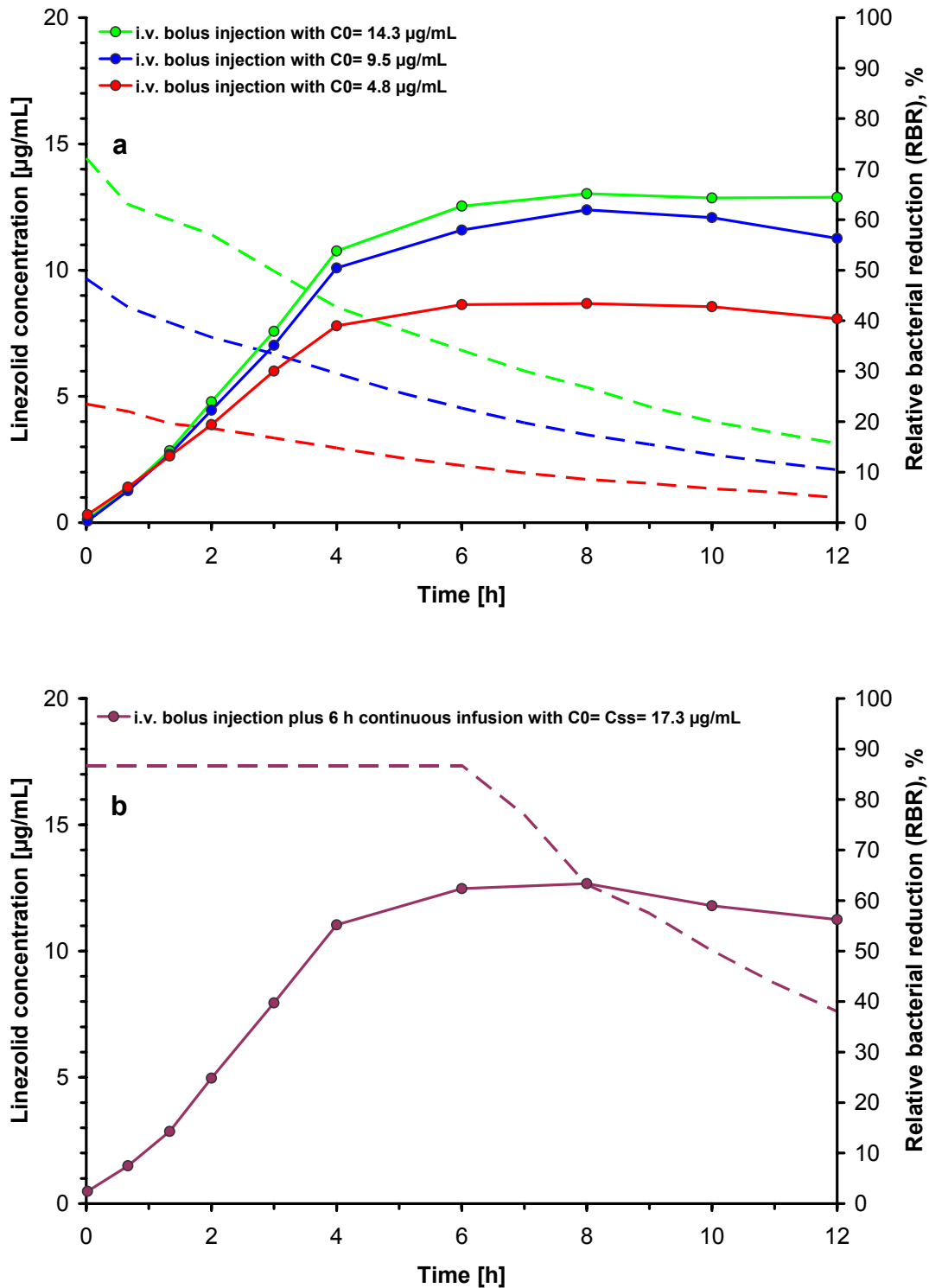


Fig. 20 Relative bacterial reduction (RBR) of *S. aureus* (ATCC 29213) vs. linezolid (LZD) exposure time for (a) the three imitated intravenous (i.v.) bolus injections, and (b) the i.v. bolus injection plus 6 h continuous infusion, additionally showing the measured LZD concentration-time profiles (dashed curves in the respective same colour as the RBR-time course), with C_0 = initial LZD concentration and C_{ss} = steady state LZD concentration.

In addition, the RBR from all four ‘dynamic’ LZD exposure profiles were plotted vs. the respective LZD concentrations in Fig. 21. In this plot, each curve represents the LZD concentration-effect relationship at different time points. These curves showed a *hysteresis loop*, similar as observed from the static *in vitro* model (see 3.2.2.2), revealing a distinctive increase of the effect over time. This time-dependent increase of the effect predominantly occurred during the first 6 h of LZD exposure.

Moreover, for $t = 10 - 12$ h the terminal part of the LZD concentration-effect curves crossed the curves from the two previous time points ($t = 6 - 8$ h). These overlaps were caused by the (two terminal) data points from the LZD exposure profile imitating an i.v. bolus injection plus continuous infusion with $C_0 = C_{ss} = 17.3 \mu\text{g/mL}$, which showed an unexpected tendency for (re-)growth (see 3.2.3.1).

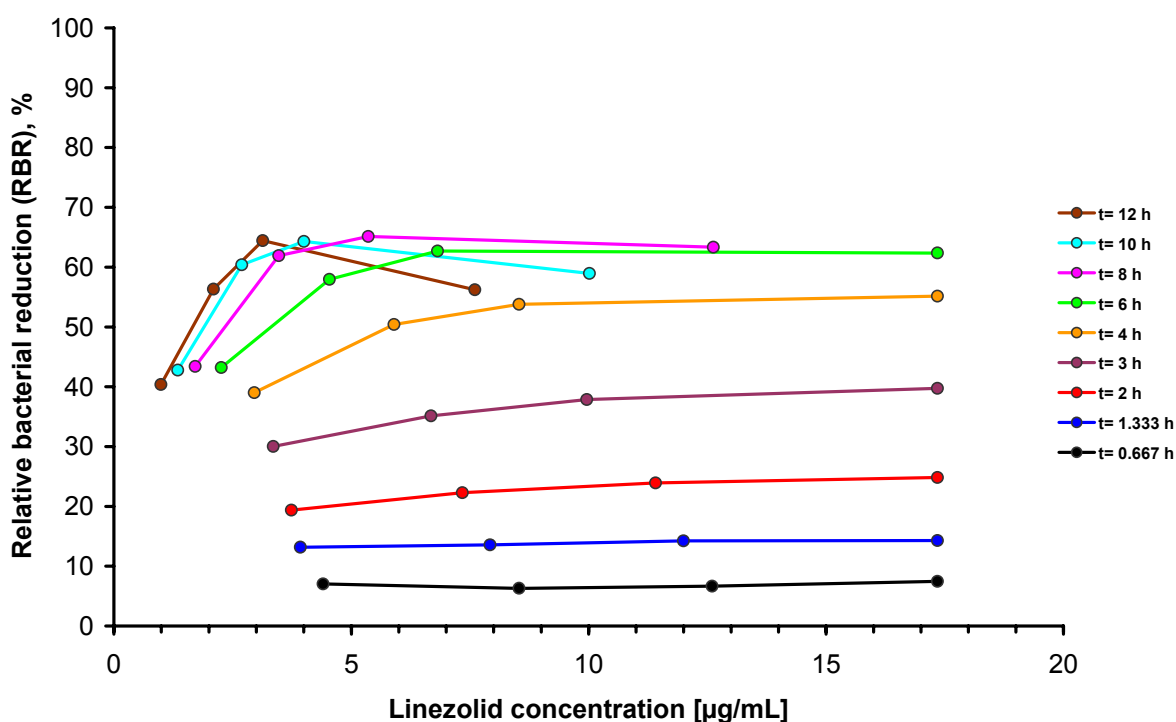


Fig. 21 Relative bacterial reduction (RBR) of *S. aureus* (ATCC 29213) vs. linezolid (LZD) concentration for different LZD exposure times (t), obtained from the dynamic *in vitro* model.

3.2.3.3 Pharmacokinetic/pharmacodynamic parameters

As *in vitro* PD outcome, the area under the respective RBR effect-time curve after 12 h ($\text{AUC}_{E(12h)}$) was calculated and presented (Tab. 8) together with the three PK/PD indices, i.e. $C_{\text{max}}/\text{MIC}$, $\text{AUC}_{12h}/\text{MIC}$ and $t_{C \geq \text{MIC}}$.

Tab. 8 Descriptive pharmacokinetic/pharmacodynamic (PK/PD) analysis for the four investigated linezolid (LZD) concentration-time profiles, with C_0 = initial LZD concentration at $t = 0$ h, C_{SS} = LZD steady state concentration, C_{max} = maximal LZD concentration, MIC = minimum inhibitory concentration (at 24 h), AUC_{12h} = area under the LZD concentration-time curve after 12 h, $t_{C \geq MIC}$ = time with the LZD concentration \geq MIC, and the *in vitro* pharmacodynamic (PD) outcome $AUC_{E(12h)}$ = area under the effect-time curve after 12 h.

<i>In vitro</i> simulated route of drug administration	PK/PD indices			<i>In vitro</i> PD outcome
	C_{max}/MIC [-]	AUC_{12h}/MIC [h]	$t_{C \geq MIC}$ %	$AUC_{E(12h)}$ [% · h]
i.v. bolus injection ($C_0 = 4.8 \mu\text{g/mL}$)	1.2	7.4	12.0	417.8
i.v. bolus injection ($C_0 = 9.5 \mu\text{g/mL}$)	2.4	14.8	57.7	559.5
i.v. bolus injection ($C_0 = 14.3 \mu\text{g/mL}$)	3.6	22.2	84.5	601.3
i.v. bolus injection with 6 h continuous infusion ($C_0 = C_{ss} = 17.3 \mu\text{g/mL}$)	4.3	43.6	100	584.0

Considering the results from the three i.v. bolus injections, the correlation analysis showed a high degree of (log-linear) correlation between $AUC_{E(12h)}$ and $\log(C_{max}/MIC)$ ($r^2 = 0.9755$), $\log(AUC_{12h}/MIC)$ ($r^2 = 0.9764$), and $\log(t_{C \geq MIC})$ ($r^2 = 0.9989$), respectively (see 7.2, Fig. 34). Moreover, the respectively administered LZD dose (D) showed a perfect (linear) correlation with the AUC_{12h} ($r^2 = 1.000$), as expected for a linear one CMT model [132].

When including the i.v. bolus injection plus continuous infusion, the log-linear correlation analysis provided $r^2 = 0.8941$ for C_{max}/MIC , $r^2 = 0.7061$ for AUC_{12h}/MIC , and $r^2 = 0.9742$ in case of $t_{C \geq MIC}$ (see 7.2, Fig. 35). Thus, overall the PK/PD index $t_{C \geq MIC}$ showed the highest degree of linear correlation with the *in vitro* PD outcome $AUC_{E(12h)}$. Furthermore, the respective correlation between D and the AUC_{12h} was also very high with $r^2 = 0.9963$, as expected.

3.2.3.4 Phenotypic variants of *Staphylococcus aureus*

During the ‘dynamic’ *in vitro* experiments also different colony morphotypes of *S. aureus* were observed on MHBA plates. Regarding the three imitated i.v. bolus injections, for $C_0 = 4.8 \mu\text{g/mL}$, colonies showing beta-haemolysis and similar size as the GC were found. However, for $C_0 \geq 9.5 \mu\text{g/mL}$, colony size and appearance of

beta-haemolysis changed over time: During the lag phase, the colony size and the haemolysis zone were equal to the GC. However, at $t = 2 - 3$ h, a mixture of different colony *morphotypes* with and without haemolysis zones occurred, similar as previously mentioned for the static *in vitro* model (see 3.2.2.3). Thereafter, the fraction of small and tiny colonies was dominant, up to 12 h.

In case of the LZD exposure profile imitating an i.v. bolus injection plus continuous infusion with $C_0 = C_{ss} = 17.3 \mu\text{g/mL}$, also a mixture of these three colony *morphotypes* occurred at $t = 2 - 3$ h. However, here the fraction of small and tiny colonies was increasing up to $t = 6$ h, and subsequently disappeared completely. Thus, between $t = 8 - 12$ h, only normally growing colonies were observed.

3.3 Pharmacokinetic/pharmacodynamic modelling

Based on the 'sigmoidal' E_{\max} model (see 2.5.1.2) as *structural* model, a *final* PK/PD model (see 3.3.4) was successfully developed to mathematically characterise the net antibacterial effect of LZD, i.e. the RBR (see 2.4.6.2) of *S. aureus* investigated under various LZD exposure profiles in the static and dynamic PD *in vitro* model.

3.3.1 Model development for data set I

3.3.1.1 'Sigmoidal' E_{\max} model

Firstly, the parameters of the structural model were fitted to *data set I* containing only the data obtained from the static *in vitro* model, with $C = C_p$ referring the constant LZD concentration in MHB, i.e. in the central CMT. For this *direct link* model approach [50], the measured LZD concentration in the central CMT was directly linked to the LZD concentration at the 'effect site', assuming that the equilibrium between both concentrations was rapidly achieved.

The structural model enabled to approximately describe the LZD concentration-effect relation observed at $t = 6 - 24$ h. However, due to the lack of the inclusion of 'time' in this model, the observed time dependency of the effect at $t = 0 - 6$ h, i.e. the hysteresis loop in the LZD concentration-effect course (see 3.2.2.2, Fig. 16) and the 'temporal dissociation' between the time course of LZD concentration and its effect (see 3.2.2.2, Fig. 17), was unconsidered with this first model approach.

3.3.1.2 Modified 'sigmoidal' E_{\max} model

The next step was the implementation of a mathematic term that incorporates 'time' (t) in the structural model, leading to time-varying PD model parameters. This was accomplished via multiplication of each PD model parameter by the empirical first-order 'time delay' term: $(1 - e^{-\alpha \cdot t})$ [104, 137-141], where α refers to a first-order rate constant that determined the magnitude of 'time delay' of the respective PD model parameter. Thus, during the model development, each PD model parameter of the structural model, i.e. E_{\max} , EC_{50} and H , was adapted by an individual 'time delay' term with $\alpha = a_e$, b_e and z_e , respectively (eq. R1 and R1a-c).

$$E(t) = \frac{E_{\max}(t) \cdot C_p^{H(t)}}{EC_{50}(t)^{H(t)} + C_p^{H(t)}} \quad \text{eq. R1}$$

$$E_{\max}(t) = E_{\max} \cdot (1 - e^{-a_e \cdot t}) \quad \text{eq. R1a}$$

$$EC_{50}(t) = EC_{50} \cdot (1 - e^{-b_e \cdot t}) \quad \text{eq. R1b}$$

$$H(t) = H \cdot (1 - e^{-z_e \cdot t}) \quad \text{eq. R1c}$$

Due to the implementation of the three 'time delay' terms, the value of AIC_C was 2.5-fold reduced in comparison to the structural model (see 3.3.3). Using Akaike's weights for directly comparing the newly developed model with the structural model, the probabilistic 'superiority' of being the relative 'best' model was calculated as $1 - P_i = 100\%$ in favour of the modified 'sigmoidal' E_{\max} model. Thus, the incorporated 'time delay' on the intrinsic activity (E_{\max}), potency (EC_{50}) and steepness (H) of the effect-time course successfully improved the goodness of fit concerning data set I.

3.3.2 Model development for data set I+II

3.3.2.1 Modified 'sigmoidal' E_{\max} model

Fitting the modified 'sigmoidal' E_{\max} model to *data set I+II* containing both the data obtained from the static and dynamic *in vitro* model, provided insufficient results concerning the three investigated i.v. bolus injections in terms of *underestimation* of the effect for $t = 8 - 12$ h. Here, asymmetrically and widely distributed residual plots with residuals up to 22% were found. The inappropriate prediction of the drug effect (i.e. the RBR) can be explained when inspecting Fig. 20 a (see 3.2.3.2):

Comparing the experimentally measured LZD exposure-time profiles imitating i.v. bolus injections with the respectively observed effect-time courses, highly ‘countermoving’ profiles were observed, i.e. while the LZD concentration was decreasing, the respective effect was increasing. This observation caused problems in fitting the PD parameters of the modified ‘sigmoidal’ E_{\max} model to data set I+II. Hence, further modifications were needed for finding a mathematic model that appropriately fits to the combined data set.

3.3.2.2 Indirect link model

To account for the mentioned ‘countermoving’ profiles of the LZD concentration-time courses and the respective effect-time courses, the developed modified ‘sigmoidal’ E_{\max} model was extended by using an *indirect link* model approach. Here, a hypothetical *effect compartment* (Fig. 22) was implemented as *indirect link* between the measured LZD exposure profiles and the respectively observed effect described by the modified ‘sigmoidal’ E_{\max} model.

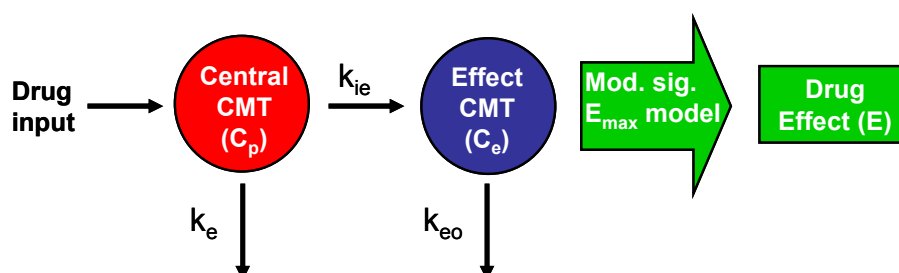


Fig. 22 Schematic depiction of the developed pharmacokinetic/pharmacodynamic model containing a hypothetical effect compartment (CMT) as indirect link between the pharmacokinetic model and the pharmacodynamic model (i.e. the modified ‘sigmoidal’ E_{\max} model), parameters are described in the text.

The hypothetical effect CMT was linked to the PK model (see 2.4.4.2, Fig. 9) which described the LZD exposure profiles investigated in the static and dynamic *in vitro* model. The implementation of the effect CMT did not affect the mass balance of the respective PK model, and only described the assumed LZD concentration-time course at the ‘effect site’ [47, 56]. The ‘hypothetical’ drug transfer into the effect CMT was assumed to follow a first-order process, described by the rate constant k_{ie} . However, as the transferred mass into the effect CMT was negligible compared to the PK model, the magnitude of k_{ie} was also negligible. Hence, the equilibration process

between the central CMT and the effect CMT was determined only by the first-order rate constant k_{eo} that described the ‘hypothetical’ drug transfer (i.e. elimination) out of the effect CMT. The latter transfer process was not directed into the central CMT, and thus did not influence the LZD concentration in the central CMT (C_p). The LZD concentration in the effect CMT (C_e) was determined by the initial LZD concentration (C_0) or the LZD concentration at steady state (C_{ss}), respectively, and the rate constants k_e and k_{eo} describing the drug elimination from the central CMT and the effect CMT, respectively [1, 50].

3.3.2.2.1 Drug concentration at the ‘effect site’

For *data set I* obtained from the static *in vitro* model with $C_p = C_0 = \text{constant}$ and thus $k_e = 0$, the respectively assumed LZD concentration at the ‘effect site’ was calculated via eq. R2.

$$C_e(t) = C_0 \cdot (1 - e^{-k_{eo} \cdot t}) \quad \text{eq. R2}$$

Here, the parameter k_{eo} was related to the *equilibrium time* (t_{eq}), which described the time interval until $C_e(t)$ approximately reached (97% of) C_0 (eq. R2a) [47].

$$t_{eq} \approx 5 \cdot \frac{\ln(2)}{k_{eo}} \quad \text{eq. R2a}$$

In case of the three i.v. bolus injections imitated in the dynamic *in vitro* model, $C_e(t)$ was calculated via eq. R3 [1, 50, 57].

$$C_e(t) = \frac{C_0 \cdot k_{eo}}{(k_{eo} - k_e)} \cdot (e^{-k_e \cdot t} - e^{-k_{eo} \cdot t}) \quad \text{eq. R3}$$

Here, the parameters k_e and k_{eo} determined the time point $t_{e,max}$ when the maximum of $C_e(t)$ was reached (eq. R3a) [47, 57].

$$t_{e,max} = \frac{\ln\left(\frac{k_{eo}}{k_e}\right)}{(k_{eo} - k_e)} \quad \text{eq. R3a}$$

Concerning the i.v. bolus injection plus continuous infusion (with $C_0 = C_{ss}$) imitated in the dynamic *in vitro* model, eq. R4 and R4a were applied to calculate $C_e(t)$ and $t_{e,max}$.

$$C_e(t) = \frac{C_{ss}}{(k_{eo} - k_e)} \cdot [k_{eo} \cdot (e^{k_e \cdot T_i} - 1) \cdot e^{-k_e \cdot t} - k_e \cdot (e^{k_{eo} \cdot T_i} - 1) \cdot e^{-k_{eo} \cdot t} + k_{eo} \cdot (e^{-k_e \cdot t} - e^{-k_{eo} \cdot t})] \quad \text{eq. R4}$$

$$t_{e,max} = \frac{\ln\left(e^{k_{eo} \cdot T_i} - 1 + \frac{k_{eo}}{k_e}\right) - k_e \cdot T_i}{(k_{eo} - k_e)} \quad \text{eq. R4a}$$

Eq. R2 – 4a were derived via Laplace transform (see 7.3.5.1) and the GPF theorem (see 7.3.5.2), which can be found in the Appendix (see 7.4).

3.3.2.2.2 Drug effect

The observed drug effect $E(t)$ was described by the *modified 'sigmoidal' E_{max} model* using $C_e(t)$, i.e. the assumed LZD concentration at the 'effect site', as independent variable (eq. R5) instead of the (measured) LZD concentration in the central CMT.

$$E(t) = \frac{E_{max}(t) \cdot C_e(t)^{H(t)}}{EC_{50}(t)^{H(t)} + C_e(t)^{H(t)}} \quad \text{eq. R5}$$

The sub functions $E_{max}(t)$, $EC_{50}(t)$ and $H(t)$ are described by eq. R1a-c (see 3.3.1.2).

3.3.3 Model comparison

For comparing the three (developed) nested models, i.e. the (structural) 'sigmoidal' E_{max} model (see 3.3.1.1), the modified 'sigmoidal' E_{max} model (see 3.3.1.2) and the indirect link model (see 3.3.2.2), utilised for modelling *data set I*, the respective AIC_C values were calculated (see 7.1, Tab. 14). Here, the *indirect link model* provided the lowest AIC_C value, and thus this model represented the 'best' model investigated for data set I.

Furthermore, Akaike's weights were applied for estimating the probability (P_i) of being the 'best' model (see 7.1, Tab. 14). The respective probabilistic 'superiority' ($1 - P_i$) of the 'best' model, i.e. concerning the indirect link model, was calculated as 100% (compared to the structural model) and 97.1% (compared to the modified 'sigmoidal' E_{max} model), respectively. Hence, the likelihood of being the 'best' model investigated for data set I was $\geq 97.1\%$ in favour of the indirect link model.

For modelling *data set I+II*, the AIC_C values for the three investigated nested model approaches are presented in Tab. 15 (see 7.1). Here, the indirect link model also showed the lowest AIC_C value and thus represents the 'best' model investigated for data set I+II. Using Akaike's weights provided a probabilistic 'superiority' for the indirect link model of 100%, compared to both the structural model and the modified

'sigmoidal' E_{\max} model. Thus, overall the indirect link model was selected as *final* PK/PD model.

3.3.4 Final model

3.3.4.1 Estimated parameter values

For both data sets, the estimated parameter values of the final PK/PD model, i.e. the *indirect link model* (see 3.3.2.2), are presented in Tab. 9. The calculated $CI_{95\%}$ revealed that the parameter estimates of E_{\max} , H, a_e and z_e did not differ concerning modelling data set I and data set I+II. However, the parameter estimates of EC_{50} , b_e and k_{eo} showed significant differences between the modelling of the two data sets.

Tab. 9 Estimated parameter values of the final pharmacokinetic/pharmacodynamic model, showing the estimated values and the respective 95% confidence intervals ($CI_{95\%}$) for modelling data set I and data set I+II, $CI_{95\%}$ that are not overlapping are signed (*), model parameters are described in 3.3.2.2.

Model parameter	For data set I (n= 88)		For data set I+II (n= 128)	
	Estimate	$CI_{95\%}$	Estimate	$CI_{95\%}$
E_{\max} , %	74.389	71.738 – 77.526	73.586	69.453 – 79.158
EC_{50} [$\mu\text{g/mL}$]	3.084	2.750 – 3.417*	5.994	5.069 – 6.963*
H [-]	1.888	1.630 – 2.147	1.975	1.484 – 2.223
k_{eo} [h^{-1}]	0.387	0.362 – 0.621*	0.113	0.094 – 0.168*
a_e [h^{-1}]	0.448	0.424 – 0.504	0.430	0.411 – 0.502
b_e [h^{-1}]	0.118	0.117 – 0.187*	0.026	0.024 – 0.039*
z_e [h^{-1}]	0.136	0.110 – 0.161	0.131	0.110 – 0.193

As data set I+II contained all experimental data, these parameter values were used for the *in silico* simulation (see 3.4). Here, the estimated value for E_{\max} was below 100%, as expected for a predominantly bacteriostatic acting antibiotic (see 4.2.2.3). For EC_{50} , the estimated value was 1.5 - 3-fold higher as the MIC_{24h} and MIC_{18h} , respectively (see 3.2.2.1). In case of the 'steepness' parameter H, the estimated value was approximately equal to 2, resulting from the sigmoidal shaped LZD concentration-effect curves for $t \geq 8$ h observed in the static *in vitro* model (see 3.2.2.2, Fig. 16). The estimated values for the three first-order rate constants a_e , b_e and z_e clearly showed different magnitudes, with $a_e > z_e > b_e$. The resulting time

courses of the three sub functions $E_{max}(t)$, $EC_{50}(t)$ and $H(t)$ are presented in Fig. 36 (see 7.2). All three curves showed a hyperbolic shape, as expected from the underlying mathematic equations (see 3.3.2.2.2), reaching their plateau values (i.e. E_{max} , EC_{50} and H , see Tab. 9) after about 8.1 h, 5.6 days, and 26.5 h for $E_{max}(t)$, $EC_{50}(t)$ and $H(t)$, respectively.

The estimated value for the parameter k_{e0} was of similar magnitude as the value of z_e . As seen from the correlation matrix (see 7.1, Tab. 16) for modelling the combined data set (I+II), these two parameters showed the 'highest' correlation with $r = 0.725$. Overall, the correlation matrix provided r -values ranging from -0.663 to 0.725, which revealed that there were no highly correlated relations between the parameters of the final PK/PD model. Hence, the combined data set (I+II) defined the final PK/PD model unambiguously, i.e. this model was not over-parameterised [117].

3.3.4.2 Drug concentration-time courses at the 'effect site'

The model-predicted LZD concentration-time courses at the 'effect site' ($C_e(t)$) are shown in Fig. 23 together with the respective LZD concentration-time profiles measured in the central CMT ($C_p(t)$). For the constant LZD exposure profiles investigated in the static *in vitro* model (Fig. 23 a), the time courses of $C_e(t)$ (see 3.3.2.2.1, eq. R2) were hyperbolically increasing, drawing near the respective constant LZD concentration in the central CMT with $C_p(t) = C_0$. The *equilibrium time* t_{eq} , where $C_e(t_{eq}) \approx C_p(t_{eq})$, was calculated as ≈ 30 h, and was irrespective of the magnitude of C_0 (see 3.3.2.2.1, eq. R2a).

In case of the three imitated i.v. bolus injection profiles with $C_0 = 4.8, 9.5$ and $14.3 \mu\text{g/mL}$ (Fig. 23 b), $C_p(t)$ and $C_e(t)$ showed 'countermoving' profiles during the first eight hours. The respective maximum of $C_e(t)$ ($C_{e,max}$) was reached at $t_{e,max} = 8.3$ h, with $C_e(t_{e,max}) = C_p(t_{e,max}) = 1.7, 3.3$ and $5.0 \mu\text{g/mL}$, respectively. As expected from eq. R3a (see 3.3.2.2.1), the value of $t_{e,max}$ was independent of C_0 , i.e. the respective initial LZD concentration in the central CMT. After reaching $C_{e,max}$, the LZD concentration-time courses in both CMTs were decreasing.

For the i.v. bolus injection plus 6 h continuous infusion with $C_0 = C_{ss} = 17.3 \mu\text{g/mL}$ (Fig. 23 b), the time course of $C_e(t)$ was firstly increasing, whereas $C_p(t)$ kept constant for the first six hours. At $t = t_{e,max} = 9.9$ h, the time course of $C_e(t)$ reached $C_{e,max}$, with $C_e(t_{e,max}) = C_p(t_{e,max}) = 10.2 \mu\text{g/mL}$, and subsequently started to decrease. Thus,

$C_{e,max}$ occurred about two hours later compared to the three single dose i.v. bolus injections, but in case of the continuous infusion $C_{e,max}$ was about 2 - 6-fold higher.

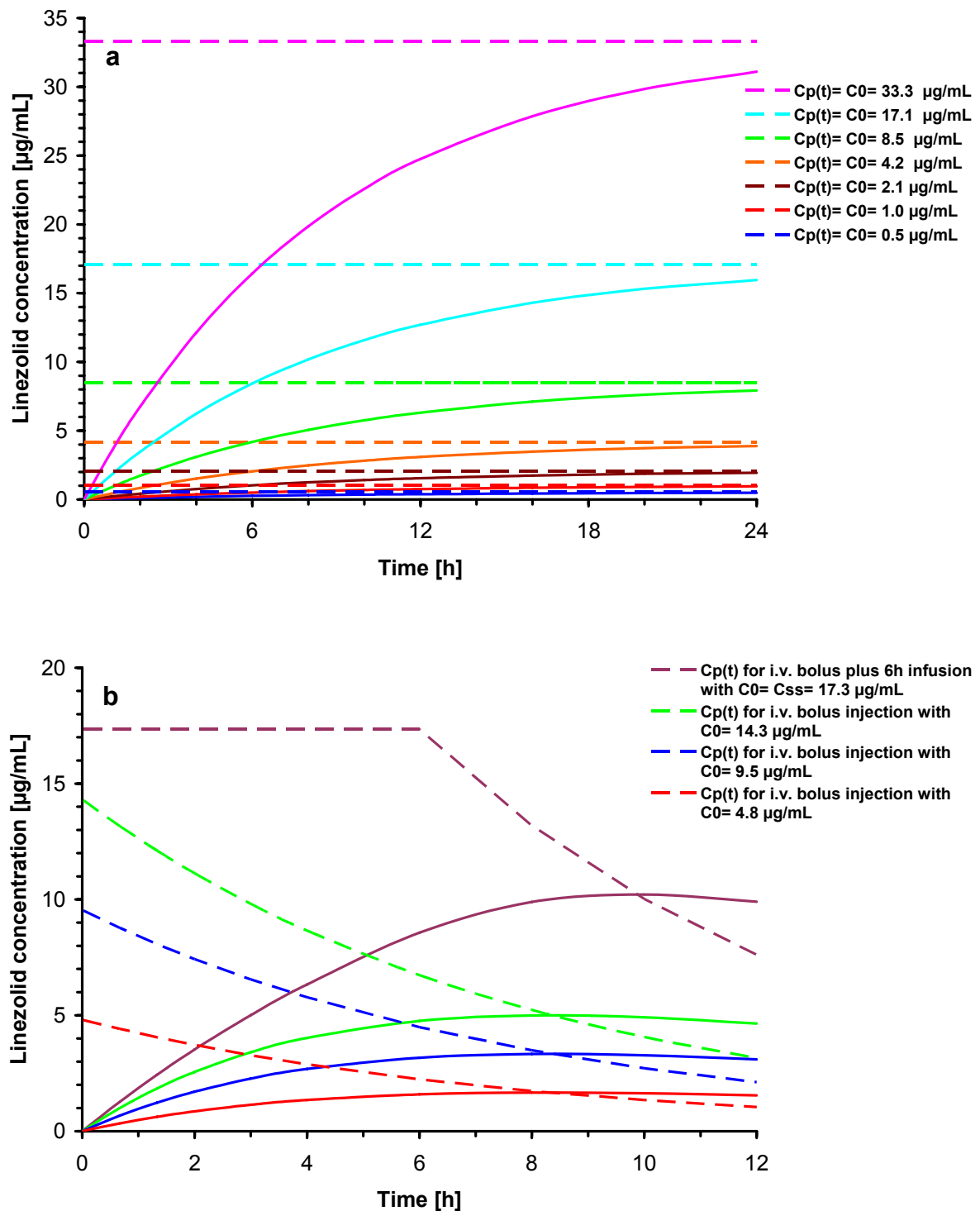


Fig. 23 Linezolid (LZD) concentration-time courses $C_p(t)$ (measured) in the central compartment (CMT, dashed lines/curves) and (simulated) LZD concentration-time courses in the effect CMT ($C_e(t)$, solid curves in the respective same colour) of the final pharmacokinetic/pharmacodynamic model, for data set I+II obtained from (a) the static and (b) dynamic in vitro model.

3.3.4.3 Drug effect-time courses

The model-predicted effect-time courses are presented in Fig. 24 together with the experimentally obtained data points from both *in vitro* model approaches.

In case of the data from the static *in vitro* model (Fig. 24 a), the effect of all investigated LZD concentrations was individually predicted by the (final) indirect link model, for the total time interval of 24 h. Overall, the observed effect-time courses resulting from the constant LZD exposure profiles, were well described by the final PK/PD model.

For the data obtained from the dynamic *in vitro* model (Fig. 24 b), the effect of the four imitated i.v. LZD administrations was also individually predicted, for the investigated time interval of 12 h. The effect-time courses from the *in vivo*-like LZD exposure profiles were well predicted by the final PK/PD model, however, the model-predicted effect-time courses partly differed from the experimental data, as described in the following section.

3.3.4.4 Goodness of fit plots

The GOF for the final model was graphically evaluated. Plotting the model-predicted RBR vs. the observed RBR from the combined data set (I+II), provided data points distributed close-by the line of identity (see 7.2, Fig. 37), with a high magnitude of linear correlation ($r^2 = 0.9787$), as desired for mathematic modelling (see 2.5.1.6.1).

Furthermore, the residuals plotted vs. the observed and predicted RBR (see 7.2, Fig. 38 a and b), and vs. the LZD exposure time and the measured LZD concentration (see 7.2, Fig. 38 c and d), were randomly distributed around zero, as desired (see 2.5.1.6.1), with a partial exception: Two residual plots (Fig. 38 b and c) showed a slight *U-pattern* [125], resulting from a tendency of underestimation at $t = 0$ h and 4 h, combined with a slight overestimation from $t = 40$ min to 3 h (Fig. 24). Overall, the residuals ranged from -12.9% to +9.2% and the 5% and 95% percentiles were calculated as -6.9% and +4.7%, respectively. Thus, the majority of residuals showed magnitudes below $\pm 7\%$. In total, the mathematic modelling of the combined data set (I+II) was judged as successful in case of the (final) the indirect link model.

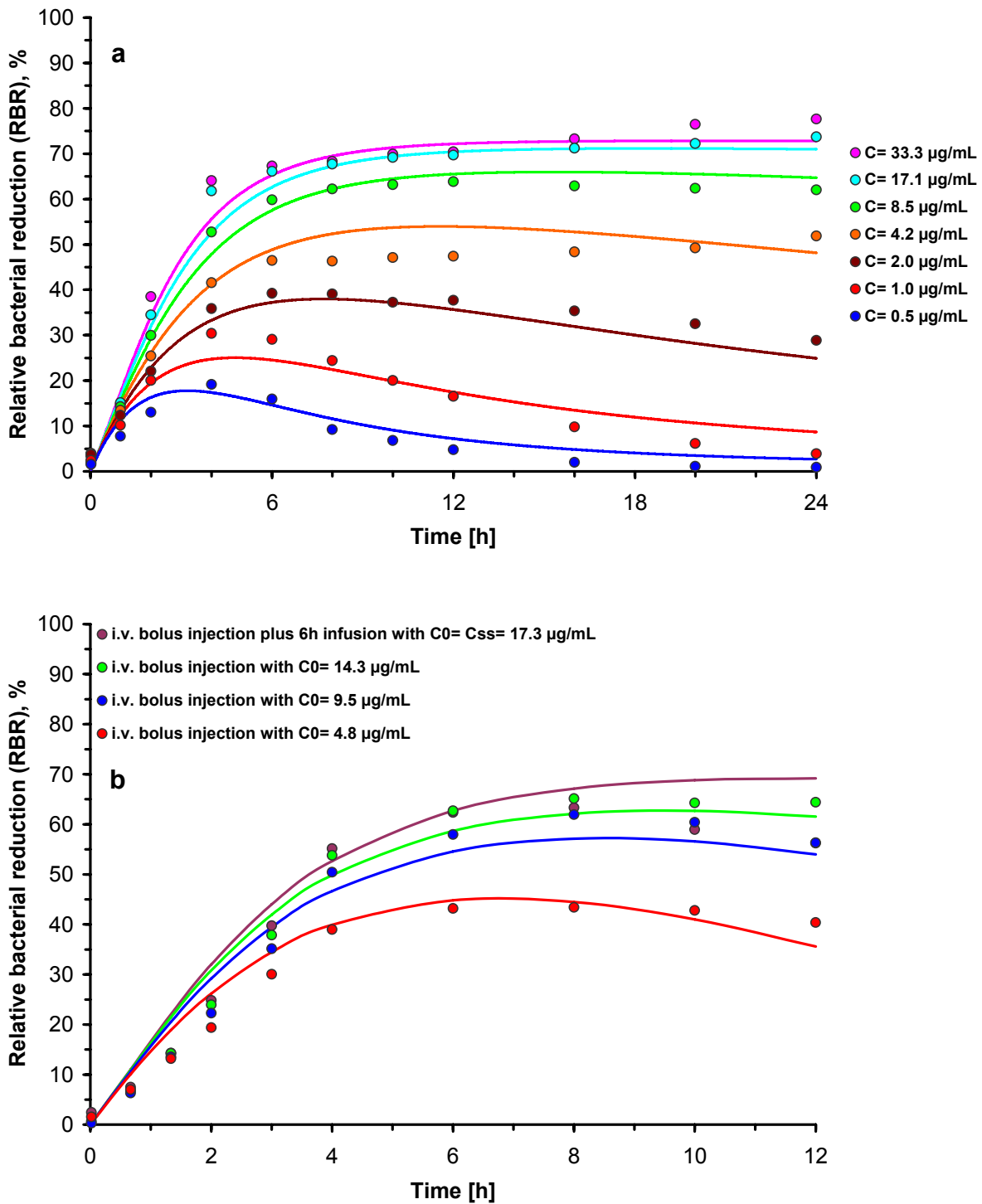


Fig. 24 Relative bacterial reduction (RBR) of *S. aureus* (ATCC 29213) vs. linezolid (LZD) exposure time for different LZD exposure profiles, showing the observed data (points) obtained from (a) the static and (b) dynamic in vitro model, and the respective (final) pharmacokinetic/pharmacodynamic model-predicted data (curves), with C = constant LZD concentration, C_0 = initial LZD concentration and C_{ss} = steady state LZD concentration.

3.4 *In silico* simulation and analysis

The developed final *in vitro* PK/PD model (see 3.3.4) for LZD was successfully combined with the previously developed (see 2.6.2) *in vivo* (population) PK model of LZD (Fig. 25). The combined (*in vivo/in vitro*) PK/PD model allowed the *in silico* investigation of thirteen dosing regimens for LZD, including twelve hypothetical dosing regimens and the standard dosing regimen of LZD (see 2.6.3, Tab. 3), via *deterministic* and *stochastic* simulations. Here, the effect CMT of the *in vitro* PK/PD model was mathematically linked to the central CMT of the *in vivo* PK model [50], via an ordinary differential equation (ODE) shown in eq. R6 [47, 56],

$$\frac{dC_e(t)}{dt} = k_{eo} \cdot (C_p(t) - C_e(t)) \quad \text{eq. R6}$$

where $C_e(t)$ and $C_p(t)$ refer to the LZD concentration in the effect CMT (i.e. at the 'effect site') and in the central CMT (i.e. in plasma), respectively, and k_{eo} is the elimination rate constant from the effect CMT. The mathematic derivation of eq. R6 can be found in the Appendix (see 7.4.8).

For the current *in silico* simulations, the ODE of eq. R6 was numerically solved as coupled system of ODEs including the ODEs of the PK model (see 2.6.2), by means of the *fourth-order Runge-Kutta* (RK4) method (see 7.3.5.3) [114, 115], using a step size of $dt = 1$ min.

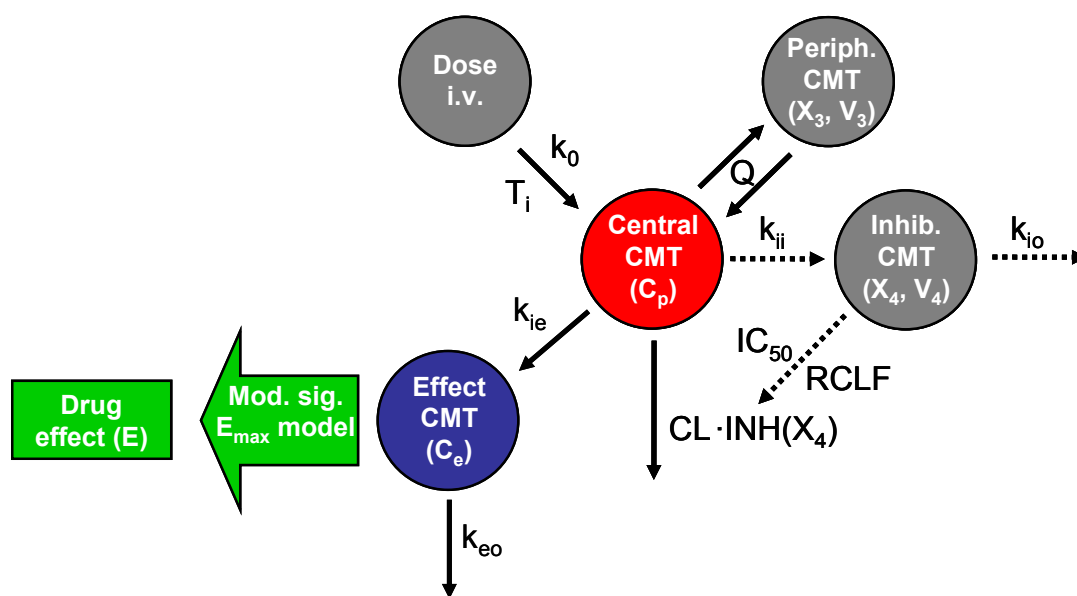


Fig. 25 Schematic depiction of the pharmacokinetic/pharmacodynamic model utilised for the *in silico* simulation, parameters are described in the text.

3.4.1 Deterministic simulation

For the deterministic *in silico* simulation, treatments with LZD of 14 days were successfully simulated using twelve hypothetical dosing regimens and the standard dosing regimen of LZD (see 2.6.3, Tab. 3), *without* taking into account the PK IIV of the patient population. Instead, the population estimates (θ_K) of the PK parameters were utilised (see 2.6.2, Tab. 2). The simulated (unbound) LZD concentration-time courses in plasma and at the ‘effect site’, and the resulting effect-time courses are presented (see 7.2) together for the respective daily LZD dose of 600 mg/day (Fig. 39), 1200 mg/day (Fig. 40), 1800 mg/day (Fig. 41) and 2400 mg/day (Fig. 42). The respective values of the *maximal* LZD concentration in plasma ($C_{p\ ss,max}$) and at the ‘effect site’ ($C_{e\ ss,max}$) at (PK) steady state, the *maximal* observed effect (E_{peak}), the *fluctuation* of the effect at (PD) steady state expressed as the *maximal* ($E_{ss,max}$) and *minimal* ($E_{ss,min}$) effects, and the area under the effect-time course after 14 days of LZD therapy ($AUC_{E(14\ days)}$), are summarised in Tab. 10.

Tab. 10 Results of the deterministic *in silico* simulation investigating twelve hypothetical dosing regimens and the standard dosing regimen (*italics, bold type*) for linezolid (LZD), showing the respective values of the maximal LZD concentration in plasma ($C_{p\ ss,max}$) and at the ‘effect site’ ($C_{e\ ss,max}$) at pharmacokinetic steady state, the maximal observed effect (E_{peak}), the maximal ($E_{ss,max}$) and minimal ($E_{ss,min}$) effects at pharmacodynamic steady state, and the area under the effect-time course after 14 days of LZD therapy ($AUC_{E(14\ days)}$).

Daily dose [mg/day]	Dosing regimen	$C_{p\ ss,max}$ [$\mu\text{g/mL}$]	$C_{e\ ss,max}$ [$\mu\text{g/mL}$]	E_{peak} %	$E_{ss,max}$ %	$E_{ss,min}$ %	$AUC_{E(14\ days)}$ [% · h]
600	1 × 600 mg	16.7	4.0	55.3	25.0	4.4	6024
1200	1 × 1200 mg	27.2	8.3	64.5	49.1	13.6	12622
1200	2 × 600 mg	18.3	6.7	59.8	41.2	29.7	13330
1200	3 × 400 mg	15.0	6.1	57.0	37.5	33.0	12940
1200	4 × 300 mg	14.0	6.3	57.2	39.3	36.7	13683
1800	1 × 1800 mg	36.5	12.7	68.1	60.2	24.5	16694
1800	2 × 900 mg	24.4	9.9	66.4	54.3	44.4	17631
1800	3 × 600 mg	20.6	9.4	64.9	52.9	48.4	17766
1800	4 × 450 mg	18.4	9.2	64.0	52.0	49.8	17650
2400	1 × 2400 mg	45.1	16.7	70.0	65.3	35.2	19137
2400	2 × 1200 mg	30.0	13.0	69.1	61.0	53.8	20012
2400	3 × 800 mg	25.0	12.0	68.0	59.5	56.7	19924
2400	4 × 600 mg	23.1	12.3	67.9	59.9	58.8	20153

The ratio of the observed maximal LZD concentrations in plasma and at the 'effect site' were found as $C_{p\ ss,max}/C_{e\ ss,max} \approx 2 - 4$ (Tab. 10). The respective LZD concentration-time courses reached the (PK) steady state within the first two days (see 7.2, Fig. 39 a - Fig. 42 a). Within this time interval, the maximal observed effects occurred, ranging from $E_{peak} = 55.3\%$ for 600 mg once daily (QD) to $E_{peak} = 70.0\%$ for 2400 mg QD (see 7.2, Fig. 39 b - Fig. 42 b). After reaching the maximum, the effect-time courses slightly decreased, and at $t \approx 5 - 6$ days they reached their (PD) steady state. The time to reach the (PD) steady state was determined by the small value of the PD parameter b_e , i.e. $\approx 5 \cdot (\ln(2)/b_e) = 5.6$ days, and thus by the time course of $EC_{50}(t)$ (see 3.3.4.1). Hence, for all investigated dosing regimens, the steady state of the effect-time course occurred about 3 – 4 days delayed compared to the respective LZD concentration-time course.

The magnitude of fluctuation of the effect-time courses during the (PD) steady state was dependent on the administered fraction of the daily LZD dose. Here, the *effect range interval* ($ERI_{ss} = E_{ss,max} - E_{ss,min}$) during (PD) steady state showed values of $ERI_{ss} = 20.6\% - 35.7\%$ for QD dosing regimens, $ERI_{ss} = 7.2\% - 11.5\%$ for twice daily (BID) dosing regimens, $ERI_{ss} = 2.8\% - 4.5\%$ for three times a day (TID) dosing regimens, and $ERI_{ss} = 1.1\% - 2.6\%$ in case of four times a day (QID) dosing regimens. Hence, for TID and QID dosing regimens the fluctuation at (PD) steady state was below 5%.

For the main outcome $AUC_{E(14\ days)}$, i.e. the measure of 'response', a (sigmoidal) relation was observed towards the administered daily dose (DD) of LZD (Fig. 26). The observed dose-'response' relation was analysed via curve fitting in Excel, based on the 'sigmoidal' E_{max} model (see 2.5.1.2, eq. M3), with DD and $AUC_{E(14\ days)}$ as independent and dependent variable, respectively, and three model parameters describing the *maximal* 'response' ($AUC_{E,max} = 24746\ \% \cdot h$), the DD producing 50% of the maximal 'response' ($DD_{50} = 1120\ mg/day$) and the *steepness* ($H_{DD} = 1.824$) of the dose-'response' curve (eq. R7).

$$AUC_{E(14\ days)}(DD) = \frac{AUC_{E,max} \cdot DD^{H_{DD}}}{DD_{50}^{H_{DD}} + DD^{H_{DD}}} \quad \text{eq. R7}$$

The model-predicted $AUC_{E(14\ days)}$ plotted vs. the observed $AUC_{E(14\ days)}$, provided data points distributed close-by the line of identity (see 7.2, Fig. 43), with a high

magnitude of linear correlation ($r^2 = 0.9900$), as desired for mathematic modelling (see 2.5.1.6.1).

The dose-‘response’ relation in Fig. 26 revealed that 600 mg/day showed about 25% of the maximal ‘response’, and 1200 mg/day (standard daily dose of LZD) was approximately equal to the estimated value of DD_{50} , i.e. this dose produced (only) about 50% of the maximal ‘response’. Hence, the standard daily dose of LZD seemed to be improvable. Increasing the standard daily dose of LZD by 1/2 (i.e. 1800 mg/day) provided a 20% increase in the ‘response’, whereas doubling the standard daily dose of LZD (i.e. 2400 mg/day) only showed a 30% increase in ‘response’. Thus, the (highly) linear relation between the administered daily dose of LZD and the respectively observed value of $AUC_{E(14\text{ days})}$, was limited up to 1800 mg/day (with $r^2 = 0.9569$).

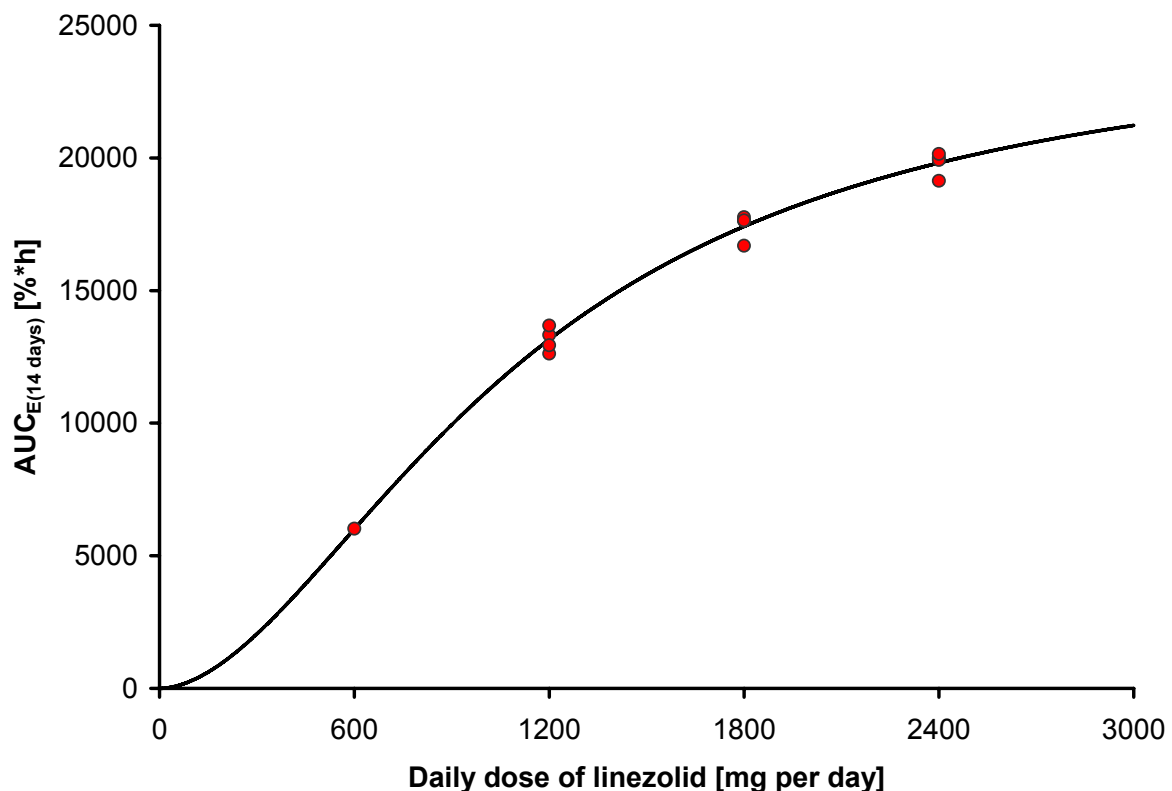


Fig. 26 Dose-‘response’ relation for the deterministic *in silico* simulation, showing the observed area under the effect-time course after 14 days of linezolid therapy ($AUC_{E(14\text{ days})}$, red data points) for different daily doses of linezolid, and the model-predicted dose-‘response’ curve (black solid line).

3.4.2 Stochastic simulation (Monte Carlo simulation)

For the MCS, in total 13,000 virtual '*in silico* patients', i.e. 1,000 for each dosing regimen (see 2.6.3, Tab. 3), were successfully investigated taking into account the interindividual variability (IIV) in the PK parameters of the patient population (see 2.6.2, Tab. 2). Each '*in silico* patient' represented an individual of a virtual population receiving a treatment with LZD for 14 days.

The respective distribution of individual PK parameter values of CL , V_2 and V_3 were monitored and are presented as *box-and-whisker plots* (box plots) in Fig. 44 (see 7.2), showing the respective interquartile range (IQR) as box containing the median as bisecting line, and the 5% and 95% percentiles as whiskers (see 7.3.1). Here, all distributions looked 'skewed' towards higher values, as expected for the utilised exponential variability model. The median values of the three PK parameters were very similar to the respective value of θ_K , i.e. the population estimate (see 2.6.2, Tab. 2), with RE = -2.0% - +4.2% for CL , RE = -2.5% - +2.1% for V_2 , and RE = -1.6% - +1.9% for V_3 . Moreover, the thirteen distributions per PK parameter looked very similarly, as desired for MCS. The Kruskal-Wallis test with $n = 13 \times 1,000$ provided *p-values* > 0.05 , i.e. $p = 0.076$, 0.898 and 0.573 for CL , V_2 and V_3 , respectively. Thus, concerning the simulated PK IIV no statistically significant differences were found between the different dosing regimens. Furthermore, the utilised numeric indicator, for monitoring LZD concentrations below zero, did not find any artefact.

The distributions of measured values of $AUC_{E(14 \text{ days})}$, for all thirteen investigated dosing regimens of LZD, are presented as box plots in Fig. 27. Comparing the median values of these $AUC_{E(14 \text{ days})}$ distributions with the respective results from the deterministic simulation (see 3.4.1, Tab. 10) using the population estimates, the deviations were small (RE = -2.3 - +1.7%). Thus, the chosen magnitude of virtual '*in silico* patients', i.e. $N = 1,000$ per dosing regimen, was judged as sufficiently representative to imitate the desired patient population.

For the respective same daily dose (Fig. 27, boxes in the respective same colour), comparable distributions of $AUC_{E(14 \text{ days})}$ values were observed. However, for 1200 – 2400 mg/day the QD dosing regimes provided distributions with slightly lower IQRs and medians. In contrast, for BID, TID and QID dosing regimens of the respective same daily dose of LZD, very similar distributions were found.

When comparing the shape of the box plots of different daily doses of LZD (see 7.2, Fig. 45, and Fig. 27, boxes in the respective same colour), differences between the distributions were found. Whereas the box plots for 1200 mg/day were very symmetrically distributed, the plots of the other daily LZD doses looked 'skewed' towards higher values (for 600 mg/day) or lower values (for ≥ 1800 mg/day). Moreover, the median values of $AUC_{E(14 \text{ days})}$ distributions showed a similar (sigmoidal) relation towards the administered daily dose of LZD (see 7.2, Fig. 45), as found for the deterministic simulation (see 3.4.1, Fig. 26). However, the individually observed $AUC_{E(14 \text{ days})}$ values from the MCS were widely scattered around the model-predicted dose-'response' curve for the deterministic *in silico* simulation (see 7.2, Fig. 46). Thus, the simulated IIV in PK caused high IIV in the observed dose-'response' relation of the virtual patient population.

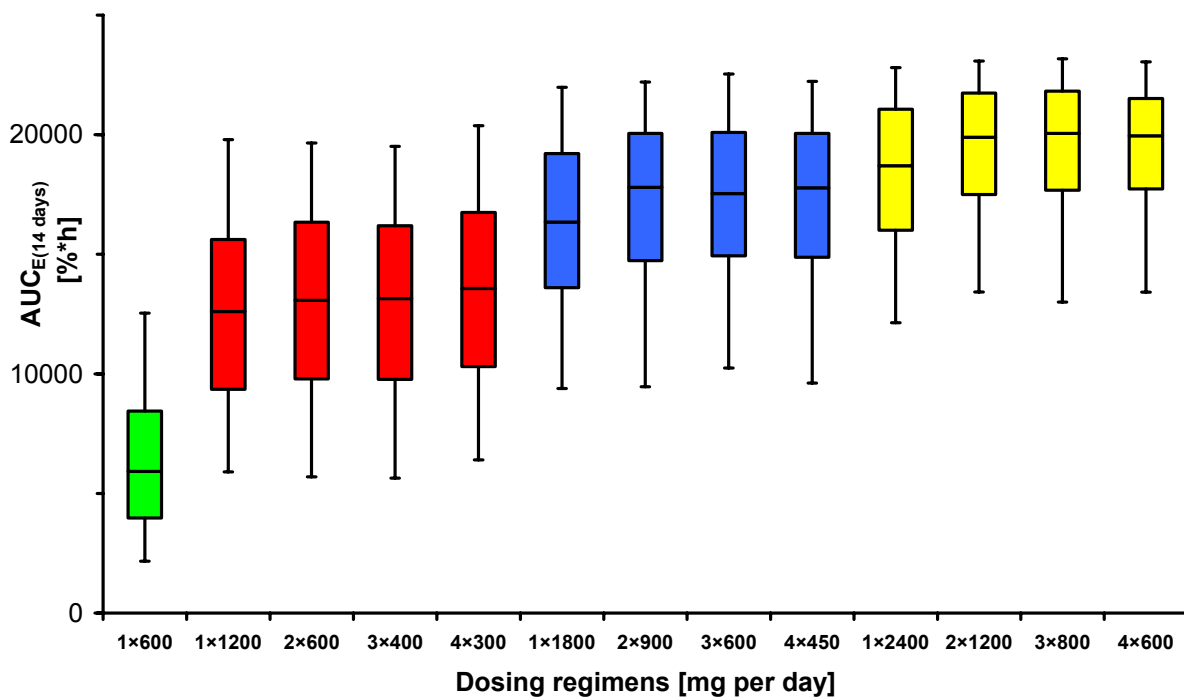


Fig. 27 Box-and-whisker plots for the Monte Carlo simulation, showing the respectively observed area under the effect-time course after 14 days of linezolid therapy ($AUC_{E(14 \text{ days})}$) of one thousand virtual 'in silico patients' for each simulated dosing regimen, the colours represent the different daily doses, the box refers to the 25% and 75% percentiles, the bisecting line of the box is equal to the median, and the whiskers represent the 5% and 95% percentiles.

For quantifying the difference between the distributions of $AUC_{E(14 \text{ days})}$ values resulting from different daily doses of LZD, the *effect size* (ES) was utilised. In case of normally distributed data, the ES of two means is generally measured in standard deviation (SD) units, where $ES \geq 0.8$ SD units is defined as large effect [134, 142]. For practical reasons (see 4.4.2), the ES of two medians was used instead (eq. R8),

$$ES = \frac{\text{median}_1 - \text{median}_2}{IQR_{\text{median}}} \quad \text{eq. R8}$$

where median_1 and median_2 refer to the respective median values of $AUC_{E(14 \text{ days})}$ of two daily LZD doses to be compared. The parameter IQR_{median} is the overall median of the interquartile ranges from all investigated dosing regimens, which is equal to the ‘average box size’, i.e. the ES was expressed in ‘*box units*’. As one ‘box unit’ generally represents 50% of the underlying population, $ES \geq 0.6$ ‘box units’ was judged as relevant difference, which is analogously equal to $ES \geq 0.8$ SD units (see 4.4.2).

Comparing the daily LZD dose of 1200 mg/day vs. 1800 mg/day and 2400 mg/day, the ESs were calculated as 0.877 and 1.314 ‘box units’, respectively. In contrast, for comparing 1800 mg/day vs. 2400 mg/day, the ES was only 0.437 ‘box units’. Hence, 1800 mg/day and 2400 mg/day showed relevant difference compared towards 1200 mg/day. However, the difference between 1800 mg/day and 2400 mg/day was below the relevant threshold.

4 Discussion

In this section, the results of the current thesis are discussed and compared with results from the literature. Moreover, for appropriate interpretation the limitations of the utilised *in vitro* and *in silico* methodologies are described.

4.1 Bioanalysis – quantification of linezolid in broth

For the quantitative determination of LZD in MHB samples, a validated HPLC assay was successfully developed. An important requirement for this assay was a relative small sample volume, because of the limited volume of broth inside the *in vitro* models and the loss of sample volume during sample preparation. An additional requirement was LLOQ < 0.5 µg/mL LZD to accurately determine at least three LZD concentrations of the geometric dilution series below the MIC (= 4 mg/L), i.e. nominal $C_{LZD} = 2.0, 1.0$ and 0.5 µg/mL. Both requirements were successfully realised in the validated HPLC assay with a sample volume of 50 µL and the LLOQ = 0.2 µg/mL.

4.1.1 Comparison with the HPLC assay for plasma samples

The validated HPLC assay for LZD samples in MHB was based on an HPLC assay for LZD samples in human plasma, previously developed at the Dept. of Clinical Pharmacy [98, 143]. Comparing the validation parameters of these two assays provided comparable results concerning the magnitude of linearity (r^2), LLOQ, FT stability, STT stability, LT stability, and within- and between-day inaccuracy and imprecision, respectively (Tab. 11). Certain differences (MHB - plasma) were found for the retention time of LZD ($\Delta = -0.6$ min), the analytical recovery ($\Delta = -12.3\%$), and the respectively utilised ULOQ with 30.0 µg/mL (in MHB) vs. 20.0 µg/mL (in plasma). The difference in retention time might be caused by differently composed mobile phases, i.e. H₂O/ACN 80/20 (V/V) for MHB samples vs. sodium acetate buffer/ACN 80/20 (V/V) for plasma samples, e.g. due to the higher ionic strength of buffer. Concerning the analytical recovery, the value reported for plasma samples was quite high ($\approx 109\%$). In contrast, Adembri et al. reported a value of only 92% recovery for LZD in plasma [144]. Assuming that reasonable values should not exceed the 100% threshold, the value found here for MHB samples ($\approx 97\%$) appears logical and reveals complete recovery of LZD from MHB samples. Moreover, Gunderson et al. and Cha et al. reported the analytical recovery of LZD as 95% for plasma and MHB samples [145, 146]. In addition, both groups used calibration curves with LZD

concentrations ranging from 0.5 – 30.0 µg/mL, i.e. they reported the same ULOQ as found for this work.

Tab. 11 Comparison of validation parameters of the HPLC assays for linezolid in Mueller-Hinton broth and human plasma (data from Buerger et al. [98, 143]), with LLOQ and ULOQ = lower and upper limit of quantification, r^2 = coefficient of determination, CV = coefficient of variation, FT = freeze and thaw, STT = short-term temperature, and LT = long term.

Validation parameter	HPLC assay for linezolid	
	in Mueller-Hinton broth	in human plasma
Retention time [min]	4.4	5.0
LLOQ – ULOQ [µg/mL]	0.2 - 30.0	0.2 - 20.0
Linearity, r^2	0.9996	0.9980
Analytical recovery, %	96.6 (CV = 6.2%)	108.9 (CV = 3.2%)
FT stability, %	96.3	101.3
STT stability (4 h), %	104.7	100.8
STT stability (24 h), %	102.4	95.4
LT stability, %	98.7 (for 3.5 yr)	105.0 (for 1.17 yr)
Within-day inaccuracy, %	+2.3 - +7.0	-0.3 - +2.6
Within-day imprecision, %	2.4 - 4.7	2.1 - 4.9
Between-day inaccuracy, %	-1.2 - +3.1	-2.7 - +3.4
Between-day imprecision, %	3.0 - 5.3	4.3 - 6.1

4.1.2 Comparison with another HPLC assay for Mueller-Hinton broth samples

A French group developed an HPLC assay for LZD in MHB samples using on-line extraction and very similar settings as used for the present work, e.g. sample volume and mobile phase [147]. This online extraction method was developed for directly analysing samples obtained from an automated PD *in vitro* model, using a 15 min run time. This assay was limited to LZD concentrations of 0.4 - 20.0 µg/mL, and for low concentrations the analytical recovery was only 88% and the within- and between-day inaccuracy were higher with values of about 10% and 12%, respectively. Thus, using online extraction might be practical for direct application in combination with an automated PD *in vitro* model, but at the expense of accuracy. Furthermore, at first glance on-line extraction seems to be time saving, however a 15 min run time per sample means only four samples per hour, i.e. 96 samples will take 24 h. In contrast,

the HPLC method presented in this work allowed using a 5 min run time per sample. Analysing 96 samples, inclusive three to four hours of total sample preparation time, took maximal 12 h, i.e. only the half duration compared to the online extraction assay. Hence, the 'manual' HPLC assay turns out to be the faster and more accurate method.

4.1.3 Accordance with the guideline

The validation parameters of the present HPLC assay were in accordance with the demands of the FDA guideline for bioanalytical method validation [100]. However, one methodical aspect has to be discussed: The utilised six point calibration curve for LZD was analysed via weighted linear regression which is generally accepted by the guideline. Nevertheless, the FDA advises to justify the selection of weighting, as done in the following.

The weighted linear regression was applied for the calibration curve of LZD, due to the identified *heteroscedasticity* of the data (see 3.1.1, Fig. 13) as frequently met for analytical data. Heteroscedasticity means that larger deviations are found at larger concentrations of the analyte. A larger deviation tends to influence the (unweighted) regression line more than smaller deviations associated with smaller concentrations of the analyte. As a result, the accuracy of the lower end of the calibration curve is reduced which might reduce the overall performance of the analytical assay. Using an appropriate weighting scheme is a rational approach to counteract heteroscedastic data, as explained in the Appendix (see 7.3.4.3). Generally, the inverse of the respective variance of a data point from the calibration curve refers to the most appropriate weighting factor. However, in laboratory routine the calculation of the variance from each point of the calibration curve is impractical, taking into account the fact that it requires several measurements for the same calibration point and the necessity that a fresh calibration curve should be used for each HPLC run. The weighting factor $1/x^2$ is a practical, frequently used and mathematic most appropriate approximation of the inverse of variance [101]. Hence, the weighting factor $1/(C_{LZD})^2$, i.e. one divided by the squared *nominal* LZD concentration, was applied in this work to improve the accuracy of the calibration curve for lower LZD concentrations.

4.1.4 Future practice

A potential limitation of presented HPLC method is the missing data about the specificity for LZD in presence of other drugs, e.g. other antibiotics. For its wide application, e.g. to LZD samples from *in vitro* models containing several antibiotics, the specificity for LZD should be determined in presence of the respective other drugs, before application of the HPLC assay. As shown by Buerger et al. and Ba et al., using the same or very similar mobile phase and column, ampicillin/sulbactam, cefotiam, flucloxacillin and many other drugs did not interfere with the LZD peak in the HPLC chromatogram [98, 147]. For the current work, no other drugs were present. Thus, the specificity for LZD was considered as less importance for this work.

4.2 Microbiology - *in vitro* pharmacodynamics of linezolid

The present *in vitro* study comprehensively characterised the antibacterial *in vitro* activity of LZD against a penicillin-resistant *S. aureus* strain (ATCC 29213), via MIC and time-kill (curve) studies performed in a static and dynamic PD *in vitro* model.

4.2.1 Minimum inhibitory concentration

In humans, interactions between the antibiotic and the pathogenic bacteria are difficult to access. *In vitro* studies represent a reasonable surrogate [148]. The most commonly used procedure is the determination of the MIC [149], which refers to the lowest (constant) antibiotic concentration that inhibits visible growth of bacteria for 18 – 24 h (see 2.4.3.2.1) [103, 150].

In the present *in vitro* study, the MIC of LZD determined at 18 h and 24 h provided different values of 2 mg/L and 4 mg/L, respectively. The observed MIC range was comparable with MIC values previously reported for the same ATCC strain of *S. aureus* (Tab. 12). Overall, the MIC values obtained here and reported in the literature showed a relative wide range, e.g. 0.25 – 4 mg/L in the recent PEG resistance study. The lack of precision of the conventional MIC might be caused by the variety of different experimental techniques, e.g. micro- and macro-dilution or Epsilon-test (E-test, AB Biodisk, Solna, Sweden), and variable incubation times, inocula and growth media [103, 150, 151]. The low precision of the MIC should be considered when interpreting MIC data in clinical and laboratory practice.

Tab. 12 Minimum inhibitory concentration (MIC) of linezolid for *Staphylococcus aureus* (ATCC 29213) obtained from the literature, showing the MIC range and the respective 90% percentile ($MIC_{90\%}$), with n = number of data points.

MIC range [mg/L]	$MIC_{90\%}$ [mg/L]	Year / Reference
-	4	1996 / Zurenko et al. [77]
-	4	1996 / Brickner et al. [152]
-	2	1998 / Wise et al. [153]
-	2	2005 / Jacqueline et al. [154]
0.25 – 4 (for $n = 123$)	4	2007 / PEG [25]

As mentioned in the introduction section (see 1.4.3.2), for European microbiology laboratories the EUCAST defines MIC breakpoints that intend to predict the clinical outcome of antibiotic therapy in terms of ‘susceptible’ or ‘resistant’ towards the considered antibiotic [155]. These breakpoints are based on both clinical observations and theoretical target attainment rates of calculated PK/PD indices including the MIC as the only PD parameter [121, 122]. The application of MIC-breakpoints in clinical and laboratory routine is surely very practical. However, the apparent simplicity of the MIC concept has led to a frequent misconception that the MIC represents an effect/no effect-threshold [104, 149, 156]. In reality, bacterial growth and death under antibiotic exposure is very complex and depends on many factors, e.g. exposure time, that are not adequately considered by the concept of MIC.

As shown in the present time-kill (curve) study for LZD, drug concentrations below the $MIC_{90\%}$ (= 4 mg/L) provided antibacterial effects of remarkable magnitude, e.g. for 2.1 $\mu\text{g/mL}$ up to $\approx 50\%$ of the observed maximal effect within the first 6 h (see 3.2.2.2, Fig. 17). This kind of additional information should be considered when using PK/PD approaches for predicting clinical outcome of antibiotic therapy and particularly for evaluating dosing regimens of antibiotics.

Taking into account the mentioned lack of precision for the MIC determination and the inadequate implementation of ‘time’ in the conventional concept of MIC, the MIC is a very limited indicator for antibacterial activity [149]. As a result, an antibiotic therapy that is only or mainly guided by a MIC-based PK/PD approach might lead to suboptimal clinical outcome. Considering the scientific work for the evaluation of antibiotic therapy in the 30 years, the MIC-based approaches were most frequently

utilised [34, 149]. With respect, this might be an important reason why optimal dosing regimens for antibiotics are still not well defined even though some antibiotics have been available for clinical use for about 60 years, as stated by the *European Medicines Agency* (EMA) [157]. Nonetheless, for comparing the current *in vitro* results with the literature, MIC-based PK/PD indices were calculated and discussed in section 4.2.2.4.5.

4.2.2 Time-kill (curve) studies

In time-kill (curve) studies, the bacterial growth and death under antibiotic exposure is monitored over time. These studies allow investigating constant (via static models) or changing (via dynamic models) antibiotic exposures to bacteria, and thus reveal a deeper insight in the interactions between the antibiotic and the bacterial strain under study, in comparison to the MIC. However, despite its potential superiority the time-kill curve approach has not (yet) complemented or replaced the MIC-based PK/PD approaches. A reason for this might be the higher experimental effort, the lack of standardised experimental conditions/procedures or the often very complex data analysis, such as PK/PD modelling that generally requires specific, more sophisticated mathematic expertise and software [149].

The present work intended to provide reasonable support for the implementation of the time-kill curve approach at ordinary microbiology laboratories. Hence, the utilised materials and methods, e.g. economic *in vitro* models and descriptive data analysis via Excel, were consciously chosen for reasons of feasibility in laboratory praxis, and qualified via several preliminary investigations.

4.2.2.1 Descriptive statistics for time-kill curves

Frequently, time-kill curves are summaries by the arithmetic means and error bars referring to the respective standard deviations. However, bacterial growth, as an observation on multiplying processes, is considered to be log-normally distributed [158]. Thus, as recommended by Olsen [159], in the present work the geometric mean and the respective $CI_{95\%}$ were applied via BS. The BS method, first introduced from Efron [160], is generally known as a reasonable numeric approach to estimate the location parameter of the population and its $CI_{95\%}$ as measure of precision [109, 161]. For reasons of practical feasibility, BS was implemented in Excel using only standard spreadsheet functions, as described in detail in section 2.4.6.1.

4.2.2.2 Relative bacterial reduction

Additional to the graphical 'standard' time-kill curve analysis, the RBR was introduced as rational approach that gives the net estimate for the antibacterial effect (see 2.4.6.2). The fundamental idea of combining the killing curve with the simultaneously measured growth curve in a time-dependent function, originated from an integral approach introduced by Frisov et al. in 1990 [120]. However, the dimension of this function, which refers to both bacterial growing and killing, was unsuitable for interpretation. Thus, the combined growth/kill function was additionally normalised by the growth curve to receive a descriptive percentaged measure which is more suitable for interpretation of time-kill studies.

4.2.2.3 Constant linezolid exposure

The performed time-kill studies with constant LZD exposures revealed a predominantly bacteriostatic activity of LZD against *S. aureus*. This result corresponds with previously published time-kill studies [153, 162-165]. Furthermore, it was found that a LZD concentration of $\approx 17 \mu\text{g/mL}$ is sufficient to approximately reach the maximal effect within the first 6 h of LZD exposure (see 3.2.2.2, Fig. 16 a and Fig. 17). Higher LZD concentrations did not relevantly increase the effect. In contrast, LZD concentrations of $\geq 3.5 \mu\text{g/mL}$ were necessary to prevent bacterial (re-)growth. Thus, a LZD concentration of $3.5 \mu\text{g/mL}$ might be the 'exact' value of the MIC (see 4.2.1).

Based on the descriptive results from the static *in vitro* model, a 6 h continuous i.v. infusion plus initial i.v. bolus injection with immediate (unbound) steady state LZD concentration of $C_{\text{ss}} \approx 17 \mu\text{g/mL}$ in plasma, was investigated in the dynamic *in vitro* model (see 4.2.2.4).

4.2.2.3.1 Bacterial persistence

The presented time-kill curves identified a persisting phase, beginning after about 6 h, where the prior bacterial killing seemed to stop (see 3.2.2.1, Fig. 15). Even a LZD concentration $> 30 \mu\text{g/mL}$ was not sufficient to eradicate *S. aureus*. The persistence of *S. aureus* under high LZD exposure indicated the development of *phenotypic tolerance*, i.e. the ability of bacteria to evade bacteria killing by antibiotics at the price of non-proliferation [166, 167]. As reported by Keren et al., phenotypic tolerance of bacteria against antibiotics is generally ignored by the concept of MIC

and often neglected in time-kill studies. However, it is known that persisting bacteria cells ('persisters') can substantially reduce the success of antibiotic therapy [168]. Furthermore, it has been hypothesised from an *in silico* simulation that bacterial tolerance can increase the incidence of (inherited) bacterial resistance against antibiotics [169].

To the author's knowledge, the development of phenotypic tolerance of *S. aureus* against LZD has hardly been explored, yet. Krut et al. reported that LZD can induce a state of intracellular persistence of viable *S. aureus*, investigated in infected murine cell lines. They concluded that the clinical use of LZD (and several other bacteriostatic antibiotics) may create a niche of invasive intracellular *S. aureus*, which may play an important role for persistence and recurrence of infection. Instead of using LZD, they recommended the use of bactericidal acting rifampicin for the treatment of invasive *S. aureus* infections [170].

A further indication for the development of 'persisters' under LZD exposure were the phenotypic changes of *S. aureus* observed under high LZD exposures (i.e. $C_{LZD} \geq 8.5 \mu\text{g/mL}$). Here, the colony sizes and beta-haemolysis differed from growth control (see 3.2.2.3, Fig. 18). These differences were reversible when these colonies were subcultured. It has been previously reported that *S. aureus* can develop a particular phenotype called *small colony variants* (SCV). They represent a slowly growing subpopulation with atypical colony morphology and biochemical characteristics such as nonpigmentation and nonhaemolytic on blood agar. SCV may not become visible before 48 h of incubation and may reach only 1/10 of the size of a regular *S. aureus* colony [171]. The tiny colonies observed under high LZD exposures very much resembled the SCV phenotype.

SCV of *S. aureus* are considered of being of high clinical importance. They have been associated with persistent and relapsing bacterial infections. SCV have been shown to be more 'resistant' to many antibiotics than the parental phenotype [172]. Proctor et al. called this 'novel' type of antibiotic resistance as *phenotypic resistance* [173]. Defects in the respiratory chain regulation might cause the expression of the SCV phenotype [174]. It has been presumed that regulatory proteins are involved in the development of SCV [175]. Hence, antibiotics that interfere with the protein biosynthesis, such as LZD, might preferentially induce the SCV phenotype. As an example, gentamicin induced a rapid phenotypic switch from the parental to the SCV

phenotype rapidly reverting to the parental phenotype, if bacteria were exposed to antibiotic-free medium [176]. Rapid phenotypic switching might explain the different *S. aureus* phenotypes found in the present study. It may also explain the observed phenotypic tolerance towards LZD exposure mentioned above in this subsection.

To the author's knowledge, LZD induced phenotypic switching to staphylococcal SCV has not been described, yet. As recommended by Levin et al. and Lewis [166, 169], future PD *in vitro* studies should focus on the molecular basis of the development and origin of phenotypic tolerance/resistance against antibiotics in more detail to successfully develop an 'anti-persister' therapy.

4.2.2.4 Linezolid exposure changing over time

Growth and killing of *S. aureus* were successfully investigated under various LZD exposure profiles (see 3.2.3.2, Fig. 20) similar to those observed in critically ill, septic patients after i.v. administration of 600 mg LZD (standard dose) [64], using a dynamic PD *in vitro* model. The PK characteristics of LZD were simplified imitated by a one compartment model, for a period of 12 h according to the dosing interval of the standard dosing regimen for LZD. Three different i.v. bolus injection profiles with $C_0 \approx 5, 10$ and $15 \mu\text{g/mL}$ were investigated referring to the unbound maximal concentrations observed in plasma ($\approx 10 - 15 \mu\text{g/mL}$) and in the interstitial (tissue) fluid ($\approx 5 - 8 \mu\text{g/mL}$), respectively, for critically ill, septic patients. The *in vivo* observed short resorption phase of the tissue profile, that took until about 1 h after end of infusion [64], was not considered by this *in vitro* approach. Nonetheless, the mono-exponentially declining phase of the LZD concentration-time course was very similar to the *in vivo* profiles in plasma and interstitial fluid [64].

Additionally, based on the descriptive results from the static *in vitro* model (see 4.2.2.3), a 6 h continuous i.v. infusion plus initial i.v. bolus injection with immediate (unbound) steady state LZD concentration of $C_{ss} \approx 17 \mu\text{g/mL}$ in plasma, was imitated *in vitro*. Due to the currently limited information about LZD exposure in human tissue fluid, the respective LZD concentration-time course in the interstitial fluid could not be investigated in this *in vitro* study.

4.2.2.4.1 Imitating the pharmacokinetics of linezolid *in vitro*

The calculated LZD concentration-time profiles and PK parameters (see 3.1.2.2.2, Fig. 14 and Tab. 7) were comparable to the intended theoretical PK profiles and

parameters (see 2.4.4, Fig. 7 and Tab. 1), respectively. However, LZD samples taken through the filter unit were biased, and thus have been mathematically corrected based on data with direct sampling obtained from preliminary investigations. A reasonable explanation for the biased 'filter' sampling is the dead volume inside the utilised cannula and filter unit. In a similar way, the dead volume caused the slightly prolonged half-life, i.e. $t_{1/2} \approx 5.5$ h instead of $t_{1/2} = 4$ h. The intended half-life value of 4 h was chosen to imitate the 'worst case scenario' for critically ill patients suffering from sepsis. Nevertheless, the measured *in vitro* half-life of LZD was approximately equal to the average *in vivo* half-life observed in septic patients (i.e. $t_{1/2} \approx 5.1$ h) after single dose administration [64].

Future investigations with the utilised dynamic *in vitro* model should account for the respective dead volume of the cannula and filter unit (here ≈ 0.3 mL), e.g. by means of carefully mixing via additional cycles of withdrawing and adding of the same volume of medium. However, it might be more practical to validate the respective *in vitro* PK profile via preliminary investigations as done for this work, and thus omitting LZD sampling for the main experiments. The present results indicate that this is possible for LZD.

4.2.2.4.2 Constant versus changing linezolid exposure

The performed time-kill studies with changing LZD exposures generally provided similar observations as found for the investigations with constant LZD exposures (see 4.2.2.3), e.g. a time-limited killing phase followed by a persisting phase (see 3.2.3.1, Fig. 19). Moreover, the appearance of the SCV phenotype under high LZD exposures (here $C_0 \geq 9.5$ $\mu\text{g/mL}$) was confirmed. However, in case of the imitated 6 h continuous infusion the SCV phenotype suddenly disappeared completely after starting the stepwise dilution of medium, and subsequently an unexpected tendency for (re-)growth was found. Based on the previous discussion on the SCV phenotype (see 4.2.2.3.1) it is reasonable that the added fresh broth has reactivated 'persisters' of *S. aureus* and thus induced the observed (re-)growth. However, this unexpected tendency of (re-)growth affected only 2 – 3 of all data points (i.e. $\approx 2\%$) and the deviations were of small magnitude (i.e. $< \text{one log unit}$).

For future investigations using the dynamic *in vitro* model, the substitution of broth should be performed continuously throughout the experiment. In case of initially imitating a constant steady state drug concentration, this can be accomplished by

continuously adding fresh broth containing the respective same (steady state) drug concentration as inside the *in vitro* system.

4.2.2.4.3 Plasma versus tissue exposure of linezolid for standard dosing

Comparing the investigated *in vitro* LZD exposure profiles imitating *in vivo* LZD exposure profiles in plasma and in the interstitial (tissue) fluid for standard dosing, relevant differences were found concerning the antibacterial activity: The two *in vitro* LZD profiles (with $C_0 \approx 10$ and $15 \mu\text{g/mL}$) referring to the *in vivo* plasma profile, provided bacterial reduction of 1 – 2 log units after 12 h. In contrast, the *in vitro* LZD exposure profile (with $C_0 \approx 5 \mu\text{g/mL}$) referring to the *in vivo* tissue profile, just maintained the bacterial inoculum, and thus performed merely bacteriostatic against *S. aureus*. Hence, the present *in vitro* findings seem to indicate that the concentration-time profile in tissue of septic patients receiving the standard dosing of LZD, might be limited to a 'purely' bacteriostatic activity. However, the *in vivo* observed tissue profile was more complex, i.e. with resorption phase [64], than the *in vitro* imitated LZD profile. Moreover, the direct transfer of these *in vitro* results to the *in vivo* situation of the patient is difficult, because bacterial growth and killing might be different in the patient's tissue, and possible accumulation of LZD in tissue after multiple (standard) dosing might lead to increased LZD exposure in tissue fluid. Furthermore, the present *in vitro* approach did not account for effects of the immune system. Nevertheless, as stated in many PK/PD articles [104, 106, 177], the *in vitro* studied situation maybe of predictable value for immunocompromised patients who most frequently suffer from severe nosocomial gram-positive infections [5, 12].

To the author's knowledge, no comparable investigations have been published concerning the antibacterial activity of LZD concentration-time profiles similar to those observed in tissue of critically ill, septic patients. The antibacterial activity of the plasma concentration-time course for standard dosing of LZD, has been previously investigated using different strains of *S. aureus*. However, many of these *in vitro* approaches contained a confounder due to the lack of filter system, for preventing bacterial loss during antibiotic dilution, without using a mathematic correction [178, 179]. Thus, the respective results of these *in vitro* studies were relevantly biased in terms of overestimating the antibacterial activity of LZD. Nevertheless, Wang et al. used a reasonable *in vitro* approach with an appropriate filter system, for investigating the plasma PK profile of LZD (600 mg BID) against several clinical

isolates of *S. aureus* over 24 h [180]. They reported bacterial killing of ≈ 1.5 log units for *S. aureus* strains with MIC < 4 mg/L after 12 h, which is comparable to the findings of the present work. Moreover, in case of *S. aureus* strains with MIC = 4 mg/L the reported bacterial killing was little compared to the inoculum. Thus, they concluded that the standard dosing of LZD would not result in significant reduction of bacterial burdens when up against *S. aureus* strains with MIC = 4 mg/L [180].

4.2.2.4.4 Standard dosing versus continuous infusion of linezolid

Comparing different dosing regimens *in vitro* may allow the relative extrapolation to *in vivo* situation, as recommended by de la Pena et al. [106]. Regarding the present *in vitro* results from imitating the plasma LZD concentration-time profile for the continuous i.v. infusion plus initial i.v. bolus injection as loading dose, no relevant increase in bacterial killing was found in comparison to the LZD exposure profile in plasma for standard dosing. The modest benefit of a LZD loading dose agrees with the results of a previous *in silico* simulation from Zack et al. investigating clinical isolates of MRSA with MIC = 2 – 4 mg/L under *in vivo*-like LZD exposures [181].

The bacterial reduction in tissue might be more efficient for the investigated continuous infusion of LZD. However, the resulting LZD concentration-time course in tissue could not be investigated in this *in vitro* study, for reasons mentioned before (see 4.2.2.4). Furthermore, the question remains, if the huge LZD exposure associated with the *in vitro* imitated continuous i.v. infusion with (unbound) steady state LZD concentration of ≈ 17 $\mu\text{g/mL}$, would be tolerated by a patient.

Adembri et al. investigated 16 septic patients receiving LZD either as i.v. standard dosing (600 mg BID, i.e. 1200 mg/day) or as continuous infusion with an initial 300 mg i.v. loading dose plus continuous infusion of 900 mg/day, i.e. totally also 1200 mg/day [144, 182]. The continuous infusion provided unbound steady-state concentrations of ≈ 6 $\mu\text{g/mL}$, whereas the standard dosing regimen showed unbound peak and trough concentrations of about 12 $\mu\text{g/mL}$ and 1.5 $\mu\text{g/mL}$, respectively, at steady state. No significant differences concerning the therapeutic success were found between these groups, probably because of the small number of patients. They reported that no specific adverse effects were found associated with the route of administration. One case of severe thrombocytopenia associated with leukopenia occurred in a patient of the continuous infusion group after 12 days of treatment.

However, platelets and white blood cells returned to normal value after LZD suspension upon resolution of sepsis [144].

4.2.2.4.5 Pharmacokinetic/pharmacodynamic indices

Descriptive PK/PD analysis of the current *in vitro* results revealed an increasing log-linear correlation between the bacterial reduction and the three PK/PD indices, in the order AUC_{12h}/MIC , C_{max}/MIC and $t_{C \geq MIC}$, respectively. Recent *in vitro* investigations for *S. aureus* under *in vivo*-like LZD exposures reported a high (sigmoidal) relation between bacterial reduction and AUC_{24h}/MIC [180, 183]. A previous *in vivo* investigation from Andes et al. with *S. aureus* infected mice reported a similar extent of (nonlinear) correlation between bacterial reduction and AUC_{24h}/MIC ($r^2 = 0.75$) and $t_{C \geq MIC}$ ($r^2 = 0.74$), respectively, whereas the *in vivo* correlation for C_{max}/MIC was little less ($r^2 = 0.65$) [184]. The latter case might be due to the *in vivo* determination of C_{max} which often lacks precision [113], and thus results in lower correlation.

Rayner et al. performed a retrospective, non-blinded analysis from 288 seriously ill patients suffering from gram-positive infections [185], and found a good correlation between clinical efficiency and both AUC_{24h}/MIC and $t_{C \geq MIC}$. Moreover, clinical efficacy was reported as maximal, if $AUC_{24h}/MIC \geq 100$ h or $t_{C \geq MIC} \geq 85\%$ based on the total (unbound + bound) LZD concentration-time course at steady state. In a previous study at the Dept. of Clinical Pharmacy it was reported that healthy volunteers receiving standard dosing of LZD showed average AUC_{24h}/MIC values of 123 h and 61 h assuming $MIC = 2$ mg/L and 4 mg/L, respectively [63]. Adembri et al. reported that septic patients receiving standard dosing of LZD showed an average AUC_{24h}/MIC values of 92 h and 47 h assuming $MIC = 2$ mg/L and 4 mg/L, respectively [144].

When comparing these clinically obtained values of AUC_{24h}/MIC with the breakpoint suggested from Rayner et al. [185], diminished clinical efficacy may be expected using standard dosing of LZD against infections of *S. aureus* isolates showing $MIC = 4$ mg/L. As discussed in the previous subsection (see 4.2.1), MIC-based PK/PD approaches may lack of precision, and thus these results should be considered with caution when interpreting and predicting the clinical situation of patients. Nevertheless, Moise et al. substantiated the suspicion of suboptimal standard dosing of LZD, by showing that infections of *S. aureus* isolates with

MIC = 4 mg/L were associated with reduced clinical success rates and significant longer times to bacterial eradication, compared to isolates with MIC < 4 mg/L [90].

4.3 Pharmacokinetic/pharmacodynamic modelling

The developed mathematic PK/PD model successfully characterised the RBR of *S. aureus* for various *in vitro* investigated LZD exposure profiles, and thus provided the basis for predicting future LZD exposure profiles that were not experimentally investigated, as discussed in the section 4.4.

Curve fitting was applied via the Solver function in Excel, using an OBJ that was adjusted to the current problem. The utilised scaling factor of the OBJ was chosen to avoid premature abortion of the iteration process, referring to the recommendations of Frontline Systems [114]. The 'weighting' scheme of the OBJ was implemented for considering the differences between the two combined data sets. The data set obtained from the static *in vitro* model contained more LZD exposure profiles (7 vs. 4) which were observed over a longer period of time (24 h vs. 12 h), compared to the data set obtained from the dynamic *in vitro* model. Thus, for simultaneously modelling the combined data set, the number of data points (n = 88 vs. 40) served as 'weighting' factor for the OBJ, in order to 'stress' the more detailed (i.e. larger) data set.

Excel's Answer report was helpful in determining which of the defined constraints (see 2.5.1.4) limited the minimisation of the OBJ. Furthermore, for each model parameter the CI_{95%} has been estimated via BS, a reasonable numeric approach to estimate the CI_{95%} [109, 161], using a logic combination of standard spreadsheet functions and a simple VBA sub procedure (see 7.5.1). In addition, the applied correlation matrix revealed helpful information for avoiding over-parameterisation [117].

Overall, curve fitting via the Solver function in Excel was applicable for the current PK/PD data (run time ≈ 18 min, with *Aspire 5110* from Acer), and allowed the use of several customised methods and functions. However, in case of very large data sets using Solver might take a long time for PK/PD modelling to estimate appropriate model parameter values with CI_{95%}. Thus, future investigations should compare Solver to specialised PK/PD software programs, e.g. in terms of run time and parameter estimates.

4.3.1 Model development

The basic relation between LZD exposure and the RBR was described by the 'sigmoidal' E_{\max} model as structural model. This model was chosen due to its clearness and wide applicability. The mathematic equation was first noted by Archibald V. Hill studying the association between haemoglobin and oxygen [186]. Today, this model is widely used for various PD aspects, in particular to describe the equilibrium relationship between the measured drug concentration and the drug effect. Originally, the parameter value of the Hill coefficient (H) was related to the mechanism of action. However, more often this model is considered as an 'empirical' model, without any specific relation to the underlying mechanisms [1, 47, 50, 57, 119], as utilised here.

During model development, the chosen structural model was empirically modified to account for the initially observed time-dependency of the RBR. Thus, the intrinsic activity (E_{\max}), potency (EC_{50}) and steepness (H) of the effect-time course were adjusted via a simple 'time-delay' term, frequently used in PK/PD modelling of time-kill curves [104, 137-141].

Moreover, a hypothetical effect CMT was implemented, referring to the assumed LZD concentration-time course at the 'effect site', i.e. inside the bacterial cell. The assumption of an indirect link between the extracellular LZD concentration measured in broth and the LZD concentration inside the bacterial cell, agreed with previous finding from Barcia-Macay et al. investigating the intracellular activity of LZD in macrophages [187]. They found only modest intracellular accumulation of LZD. Thus, it might be assumed that the accumulation inside bacterial cells is also less than the extracellular LZD concentration.

4.3.2 Final model

For the *indirect link* model, the probabilistic 'superiority' was estimated as 100%, compared to both the structural model and the modified 'sigmoidal' E_{\max} model. Hence, the indirect link model was selected as *final* PK/PD model. Moreover, the final PK/PD model successfully described the RBR of *S. aureus* for various *in vitro* LZD exposure profiles. However, the observed slight U-pattern of two residual plots revealed a little trend of underestimation at $t = 0$ h and 4 h, combined with a slight overestimation in-between (see 7.2, Fig. 38 b and c): At $t = 0$ h the predicted RBR

was always zero, whereas the observed RBR partly showed values $> 0\%$ due to differences between the bacterial inocula. From $t = 40$ min to 3 h, the predicted effect-time courses for the 'dynamic' LZD exposures were slightly overestimated, whereas at $t = 4$ h the predicted effect-time courses for the constant LZD exposures demonstrated little underestimation for most LZD concentrations. Nevertheless, these deviations were of acceptable magnitudes (i.e. $\leq 9.2\%$) and were limited to the first 4 h. Furthermore, the residual-time plot (see 7.2, Fig. 38 c) showed two single data points between $t = 10$ h and 12 h, that were moderately overestimated. These two data points were related to the LZD exposure profile imitating a continuous infusion, which showed an unexpected tendency for (re-)growth (see 3.2.3.2) that might be caused by the unintentional reactivation of 'persisters' (see 4.2.2.4.2). Thus, these two data points were accepted as 'outliers', but were not removed from the data set. Overall, the calculated 5% and 95% percentiles revealed that the majority of residuals showed magnitudes below $\pm 7\%$, which was judged as successful for mathematic modelling.

The estimated (final) model parameter values showed reasonable magnitudes with close $CI_{95\%}$. As expected from the predominantly observed bacteriostatic activity of LZD (see 4.2.2.3), the estimated value of E_{\max} ($\approx 74\%$) was below 100%, indicating that total bacterial eradication was not achieved. In addition, the time course of $EC_{50}(t)$ (see 7.2, Fig. 36) reached the observed MIC range ($= 2 - 4$ mg/L, see 4.2.1) between $t \approx 16$ h and ≈ 42 h. Thus, the estimated values of the two main PD parameters for the intrinsic activity (E_{\max}) and potency (EC_{50}) of LZD were comparable with the results from the descriptive data analysis and previous *in vitro* studies.

4.3.3 Future model development

A potential limitation of the final PK/PD model might be its predominately empirical character. Some previously introduced mathematic models for describing bacterial growth and killing under antibiotic exposure, utilised a mechanism-based approach with the assumption of a persisting or resistant subpopulation [169, 188, 189]. The assumption of a persisting subpopulation would be surely reasonable for *S. aureus* under LZD exposure, as shown from the present time-kill studies where 'persisters' were identified (see 4.2.2.3.1). However, the two-subpopulation model approach was not selected for the present work, because 'persisters' could not reliably be quantified

due to their phenotypic instability during the sample purification process. Using a mechanistic subpopulation model to describing the measured total amount of bacteria from both subpopulations, is possible, but may cause serious bias when using the model for extrapolation via *in silico* simulation, as applied for this work. Future time-kill studies should try to quantify 'persisters' to reliably apply mechanism-based model approaches.

4.4 *In silico* simulation and analysis

Thirteen dosing regimens, including twelve hypothetical dosing regimens and the standard dosing regimen of LZD (see 2.6.3, Tab. 3), have been successfully investigated *in silico* via deterministic and stochastic simulations, imitating LZD treatment for 14 days. The *in silico* simulations were accomplished by mathematically combining the developed *in vitro* PK/PD model for LZD with the previously developed *in vivo* (population) PK model of LZD (see 3.4, Fig. 25). Here, the effect CMT was linked to the central CMT as the LZD concentration-time course in this CMT referred to (unbound) LZD concentrations measured in plasma. In contrast, the concentration-time course in the peripheral CMT was only modelled as auxiliary construction, and thus was purely hypothetical. As mentioned by Derendorf et al., if additional information about the drug concentration-time course in tissue fluid is available, the link to the peripheral CMT might be also reasonable [50]. However, due to the currently limited information about LZD exposure in human tissue fluid, this data was not implemented in the utilised (population) PK model of LZD [66]. Future *in silico* simulations should additionally investigate the effect of the (unbound) LZD concentration-time course in tissue fluid of critically ill, septic patients, based on an extended (population) PK model.

4.4.1 Deterministic simulation

The deterministic *in silico* simulation revealed detailed information about the fluctuation of the average (unbound) LZD concentration-time courses in plasma and at the assumed 'effect site', and the resulting effect-time courses (see 7.2, Fig. 39 - Fig. 42). Regarding the latter, it took about five to six days until the PD steady state was reached, whereas the LZD concentration-time course in plasma and at the 'effect site' reached (PK) steady state already after two days. The time to reach the PD steady state was determined by the hyperbolic time course of $EC_{50}(t)$ (see 7.2,

Fig. 36), which took about 5.6 days until the plateau was reached. Thus, time-dependent PD processes affected the effect-time course at PK steady state. As a result, the initially increasing effect subsequently decreased to different extent, depending on the ‘administered’ daily dose of LZD: Lower doses, e.g. 600 mg/day, provided a relevant decrease of the maximal observed effect, whereas very high doses, e.g. 2400 mg/day, showed only a little decrease of the effect before reaching PD steady state. Despite different time scales, this observation agrees with the results from the (static) *in vitro* time-kill studies where for low LZD exposures (< 3.5 µg/mL) the antibacterial effect initially increased, but subsequently decreased due to bacterial (re-)growth (see 3.2.2.2, Fig. 16 b and Fig. 17).

For a ‘typical patient’ (i.e. without IIV), the different ‘administered’ fractions of the daily LZD dose revealed relevant differences in the resulting LZD exposure profiles: As shown in Tab. 10 (see 3.4.1), QD dosing using 1200 – 2400 mg/day resulted in quite high maximal (unbound) LZD concentration at (PK) steady state (i.e. $C_{p,ss,max} \approx 27 - 45 \mu\text{g/mL}$), which might lead to relevant acute toxicity as adverse drug effect. Thus, QD dosing of LZD might be inappropriate for therapy. In case of BID, TID and QID dosing regimens, the observed fluctuations of the LZD concentration-time courses were less pronounced compared to QD dosing using the respectively same daily dose of LZD. Moreover, TID and QID dosing regimens provided minimal fluctuation of the effect-time course at (PD) steady state (with $ERI_{ss} < 5\%$), which might be beneficial for an effective antibiotic therapy.

Furthermore, the relation between the ‘administered’ daily dose of LZD and the observed ‘response’ (measured as $AUC_{E(14 \text{ days})}$) revealed that for doses ≤ 1800 mg/day an almost linear relation can be assumed. In contrast, for 2400 mg/day a reduced increase in the ‘response’ was observed. Thus, 1800 mg/day might be optimal for just obtaining maximal efficacy. Overall, the results from the deterministic *in silico* simulation indicated that 1800 mg/day administered as 600 mg TID represents a highly rational dosing regimen of LZD for critically ill patients suffering from infections of *S. aureus* with MIC = 4 mg/L, as further discussed in the next section.

4.4.2 Stochastic simulation

13,000 virtual ‘*in silico* patients’ were successfully simulated and analysed in Excel, taking into account the IIV of the patient population. Each dosing regimen was

investigated using a population of 1,000 '*in silico* patients'. In comparison, previous stochastic *in silico* simulations in Excel analysed 10,000 individuals per question [113, 190]. However, for the current PK/PD problem only 1,000 individuals were simulated, due to the complexity of the underlying mathematic models and the resulting calculation time. The stochastic simulation of 1,000 '*in silico* patients' took about 4 – 12 h (with *Aspire 5110* from Acer), depending on the respective dosing regimen. Thus, simulating 10,000 individuals per dosing regimen in Excel was impractical. However, descriptive ($RE \leq \pm 4.2\%$) and inferential ($p \geq 0.076$) statistics of the monitored PK parameter (CL , V_2 and V_3) distributions, provided evidence that 1,000 individuals were sufficient to reproducibly describe the patient population.

Distributions of individual $AUC_{E(14 \text{ days})}$ values were graphically analysed via box plots, a frequently utilised technique for the visual comparison of the medians and the 5%, 25%, 75% and 95% percentiles [134, 191]. A further benefit of the box plots technique is that it can be used for not normally distributed continuous data, as present here: Regarding the box plots for $AUC_{E(14 \text{ days})}$ (see 3.4.2, Fig. 27 and 7.2, Fig. 45) differently shaped distributions were observed. For the lowest dose of LZD, i.e. 600 mg/day, the distribution was skewed towards higher values of $AUC_{E(14 \text{ days})}$, due to its location relative near to zero and the underlying exponential variability model. In contrast, 1200 mg/day provided distributions of $AUC_{E(14 \text{ days})}$ that looked symmetrically. For higher doses, e.g. 1800 – 2400 mg/day, the respective distributions were (partially) skewed towards lower values of $AUC_{E(14 \text{ days})}$, resulting from the model parameter value for the maximal effect (E_{\max}) that served as 'threshold' for the effect. Thus, the shape of the $AUC_{E(14 \text{ days})}$ box plots for ≥ 1800 mg/day were (partially) affected by the value of E_{\max} . The highly skewed distribution for dosing regimens with 2400 mg/day revealed that this high dose of LZD often reached the maximal effect. However, on the other hand adverse drug effects might also occur more frequently when using this high amount of LZD. Hence, using 2400 mg/day LZD might be intolerable for therapy.

For quantifying the differences between the distributions of $AUC_{E(14 \text{ days})}$ resulting from different daily doses of LZD, the methodology of ES was applied due to the following consideration: Evaluating differences between measured data sets via inferential statistics often do not provide enough information whether the observed difference is of practical relevance. In contrast, calculating the ES is known to be helpful for estimating whether the found difference matters or not. Moreover, unlike

statistical tests of significance, ES measures are less affected by sample size [192]. The measure of ES expresses score differences in units of variability, e.g. SD. One frequently used measure of ES is *cohen's d*, referring to the differences of two means which is normalised by the pooled SD. For normal distributions with equal variability, Cohen provided conventional definitions of ES which have been found great practical acceptance [192], e.g. $ES \geq 0.8$ SD refers to a *large effect* which indicates a non-overlap of $\geq 47.4\%$ in the two considered distributions [142].

For the present work, ES was calculated using analogous parameters from the box plot statistics, i.e. using the median and IQR instead of mean and SD, as the data was not exactly normally distributed. Due to the modification of (cohen's d) ES, the ES breakpoint for practical relevance (i.e. $ES \geq 0.8$ SD) has been adjusted, too: Assuming a Gaussian distribution with large sample size ($n = 1,000$), the mean can be set equal to the sample median. Furthermore, the IQR can be expressed as $x \cdot SD$, where x refers to a dimensionless constant that can be numerically estimated as $x \approx 1.35$. As a result, the analogous ES breakpoint for practical relevance was calculated as ≥ 0.6 IQR. However, it should be recognised that the calculated ES breakpoint is still based on a Gaussian distribution which did not exactly fit to the present data. Nevertheless, it was assumed that the (two-sided) IQR is less affected from non-normality, compared to the (one-sided) SD.

The calculated ES revealed that 1800 mg/day might be the optimal daily dose of LZD, which is in accordance with the results from the deterministic *in silico* simulation, i.e. 1800 mg/day administered as 600 mg TID. This hypothesis agrees with the conclusion of a clinical investigation from Buerger et al. with critically ill, septic patients [64]. They recommended using 600 mg TID to avoid sub-inhibitory LZD concentrations in the infected tissue interstitium, and thus to circumvent therapeutic failure and the development of bacterial resistance. Furthermore, the same dosing recommendation was developed by Zack et al., based on a PK/PD *in silico* simulation of LZD against MRSA [181]. They concluded that if tolerable, 600 mg TID may offer a substantial benefit over 600 mg BID for the treatment of MRSA infections with $MIC = 4$ mg/L.

4.4.3 Potential limitations and future investigations

The current PK/PD *in silico* approach determined the potential antibacterial effect of LZD, whereas the occurrence of adverse drug effects was not considered. However,

it should be recognised that the use of an increased daily dose, as discussed here, might lead to so far unknown adverse drug effects in the patient. Thus, if using LZD as 600 mg TID, the tolerability has to be monitored carefully. On the other hand, known severe adverse effects of LZD, e.g. thrombocytopenia, were predominately associated with long-term use of LZD for \geq two weeks [60, 62, 91]. Hence, the use of LZD administered as 600 mg TID might allow shortening the duration of therapy, which might help to avoid the occurrence of severe changes in the haemogram. However, to the author's best knowledge, the tolerability of 1800 mg/day LZD, administered as 600 mg TID, has not yet been investigated in human.

Another potential limitation of the performed simulations is the extrapolation of observed (*in vivo*) PK and (*in vitro*) PD characteristics of LZD, up to 14 days. The underlying experimental PK and PD data were limited to four days and one day, respectively. In addition, whereas the (population) PK model can surely be used for predicting *in vivo* scenarios, the developed PK/PD model might be limited to the *in vitro* situation. However, as discussed before (see 4.2.2.4.3) the *in vitro* PD of LZD maybe of predictable value for immunocompromised patients who most frequently suffer from severe nosocomial gram-positive infections [5, 12]. Furthermore, the implemented PD data were related to the antibacterial activity against *S. aureus*, one of the most frequently reported pathogens for nosocomial infections (see 1.1.1). However, other gram-positive bacteria, e.g. enterococci, might show a different behaviour under LZD exposure. Thus, further investigations should include PD data that cover 48 h of LZD exposure against different types of bacteria.

Overall, the present PK/PD *in silico* approach revealed detailed information about the complex interactions between the critically ill, septic patient population, LZD and *S. aureus*. As stated by the EMEA, theoretical PK/PD approaches, as utilised here, cannot replace clinical trials of efficacy and tolerability, but rather complement them to more quickly develop better dosing recommendations [157]. As reported from Bonate, PK/PD modelling and *in silico* simulation might help saving about 10% of costs in clinical drug development, via explorative 'virtual' (clinical) trials on a computer [131]. In this context, the hypothetical dosing recommendation of the present work might provide a rational basis for conducting a prospective clinical trial with critically ill patients using 600 mg LZD administered TID, to compare the clinical efficacy and tolerability towards its standard dosing regimen.

5 Conclusion and perspectives

This thesis aimed to develop a rational hypothesis for an optimised dosing regimen of LZD for critically ill patients suffering from severe infections of *S. aureus*, based on PK/PD modelling, *in silico* simulation and analysis.

Firstly, an HPLC assay for the quantitative determination of LZD in MHB was developed and successfully validated according to the FDA guideline. Pre- and in-study validation parameters revealed high linearity, analytical recovery, accuracy and precision. Thus, the HPLC assay allowed the reliable and accurate determination of LZD samples obtained from the PD *in vitro* models. However, before its application for LZD samples which additionally contain other antibiotics, the specificity for LZD should be determined. Overall, the validated HPLC method established the basis for investigating various LZD concentration-time profiles *in vitro*.

Secondly, an economic PD *in vitro* approach was established to characterise the antibacterial activity of LZD towards a penicillin-resistant strain of *S. aureus* under various constant (via static model) and *in vivo*-like (via dynamic model) LZD exposures. In the static *in vitro* model, the MIC and time-kill curves were successfully determined. The MIC (= 2 - 4 mg/L) provided a relative imprecise estimation of the bacteriostatic acting LZD concentration. In contrast, the time-kill curve approach allowed characterising the antibacterial activity of LZD in dependency of time and LZD concentration: $\geq 3.5 \mu\text{g/mL}$ prevented bacterial (re-)growth for 24 h, and $\approx 17 \mu\text{g/mL}$ were sufficient to approximately reach the maximal effect after 6 h. Nevertheless, bacterial eradication of *S. aureus* was not achieved due to the occurrence of bacterial persistence. In the persisting phase, the SCV phenotype was identified indicating the development of phenotypic tolerance/resistance towards LZD. Further *in vitro* investigations should quantify phenotypic switching of *S. aureus* under antibiotic exposure, in order to develop an 'anti-persister' therapy.

Moreover, imitating *in vivo*-like LZD exposure in tissue fluid of septic patients receiving standard dosing of LZD, revealed a merely bacteriostatic activity against *S. aureus*. Further *in vitro* experiments should imitate multiple (standard) dosing of LZD, to capture the influence of LZD accumulation in tissue fluid. The explorative *in vitro* investigation of a 6 h continuous i.v. infusion with initial i.v. bolus injection as loading dose provided no relevant benefit compared to the standard dosing of LZD.

Thirdly, the descriptive PK/PD analysis identified the highest correlation between the antibacterial effect and the 'time above the MIC' ($t_{C \geq MIC}$). However, as the MIC generally lacks precision, such MIC-based PK/PD approach should be interpreted with caution when evaluating dosing regimens of antibiotics. Thus, as an alternative PD measure, the RBR, which quantifies bacterial killing in relation to bacterial growth without antibiotic, was introduced as the net estimate of the antibacterial effect. The RBR of *S. aureus* under various LZD exposures was successfully analysed via PK/PD modelling with Excel using an indirect link model approach. Based on a modified 'sigmoidal' E_{max} model, a hypothetical effect CMT was implemented in the PK model, referring to the assumed LZD concentration-time course at the 'effect site', i.e. inside the bacterial cell. The existence of the kinetic effect CMT is in accordance with previous findings, indicating differences between intra- and extracellular LZD concentrations. Nevertheless, the developed PK/PD model is mainly empirical, and thus does not specifically reflect the underlying physiologic mechanisms of bacterial growth and killing. Further PK/PD modelling approaches might try to account for physiologic mechanisms, e.g. the occurrence of SCV.

In a subsequent step, the developed *in vitro* PK/PD model was combined with a previously developed *in vivo* (population) PK model of LZD, to investigate and evaluate the potential efficacy of twelve hypothetical dosing regimens for LZD vs. its standard dosing regimen. Here, deterministic (without IIV) and stochastic (with IIV) *in silico* simulations were successfully performed in Excel, imitating 14 days of LZD therapy. The results from both simulation approaches proposed that 600 mg LZD administered TID might be more efficient than standard dosing (i.e. 600 mg BID), for critically ill, septic patients suffering from severe infections of *S. aureus* barely susceptible to LZD, i.e. MIC = 4 mg/L. These results are supported by previous studies from the literature.

In a further step, the developed (hypothetical) dosing recommendation for LZD should be prospectively investigated *in vivo*, e.g. in a clinical trial with critically ill, septic patients suffering from *S. aureus* with MIC = 4 mg/L. However, if using LZD as 600 mg TID in humans, the tolerability should be monitored carefully.

6 Bibliography

- [1] B. Meibohm, H. Derendorf. Basic concepts of pharmacokinetic/pharmacodynamic (PK/PD) modelling. *Int. J. Clin. Pharmacol. Ther.*, 35: 401-413 (1997).
- [2] WHO. The global burden of disease: 2004 update. World Health Organization, 2008. (Accessed 05 April, 2009, at http://www.who.int/healthinfo/global_burden_disease/GBD_report_2004update_full.pdf.)
- [3] Brunkhorst. Newsletter Nr. 17 - Sepsis fordert viel mehr Todesopfer als gedacht. Bundesministerium fuer Bildung und Forschung, 2005. (Accessed 05 April, 2009, at http://www.gesundheitsforschung-bmbf.de/_media/NL_17.pdf.)
- [4] R.P. Wenzel. Treating sepsis. *N. Engl. J. Med.*, 347: 966-967 (2002).
- [5] T. Yoshida, K. Tsushima, A. Tsuchiya, N. Nishikawa, K. Shirahata, K. Kaneko, K. Ito, H. Kawakami, S. Nakagawa, T. Suzuki, K. Kubo, S. Ikeda. Risk factors for hospital-acquired bacteremia. *Intern. Med.*, 44: 1157-1162 (2005).
- [6] G.M. Bearman, R.P. Wenzel. Bacteremias: a leading cause of death. *Arch. Med. Res.*, 36: 646-659 (2005).
- [7] J.L. Vincent. EPIC II: sepsis around the world. *Minerva Anesthesiol.*, 74: 293-296 (2008).
- [8] F.H. Kayser, K.A. Bienz, J. Eckert, R.M. Zinkernagel. *Medizinische Mikrobiologie*, Stuttgart, Thieme Verlag (2005).
- [9] H. Schöfer, N. Brockmeyer, J. Dissemond, I. Effendy, S. Esser, H.K. Geiss, S. Harder, M. Hartmann, U. Jappe, A. Plettenberg, H. Reinmann, P. Shah, E. Tschachler, T. Wichelhaus. Staphylokokken-Infektionen der Haut und Schleimhäute - Leitlinie der Deutschen Dermatologischen Gesellschaft (DDG), Arbeitsgemeinschaft für Dermatologische Infektiologie (ADI). *Chemother. J.*, 14: 67-73 (2005).
- [10] W. Witte. Epidemiologie von Staphylokokkus aureus. *Chemother. J.*, 17: 274-281 (2008).
- [11] WHO. The world health report. World Health Organization, 2007. (Accessed 05 April, 2009, at http://www.who.int/whr/2007/whr07_en.pdf.)
- [12] L.B. Rice. Federal funding for the study of antimicrobial resistance in nosocomial pathogens: no ESKAPE. *J. Infect. Dis.*, 197: 1079-1081 (2008).
- [13] B. Spellberg, R. Guidos, D. Gilbert, J. Bradley, H.W. Boucher, W.M. Scheld, J.G. Bartlett, J. Edwards, Jr. The epidemic of antibiotic-resistant infections: a call to action for the medical community from the Infectious Diseases Society of America. *Clin. Infect. Dis.*, 46: 155-164 (2008).
- [14] W. Stille, H.R. Brodt, A.H. Groll, G. Just-Nuebling. *Antibiotika-Therapie*, Stuttgart, Schattauer Verlag (2004).
- [15] P. Gastmeier, C. Geffers. Nosocomial infections in Germany. What are the numbers, based on the estimates for 2006? *Dtsch. Med. Wochenschr.*, 133: 1111-1115 (2008).
- [16] J.L. Vincent, D.J. Bihari, P.M. Suter, H.A. Bruining, J. White, M.H. Nicolas-Chanoin, M. Wolff, R.C. Spencer, M. Hemmer. The prevalence of nosocomial infection in intensive care units in Europe. Results of the European Prevalence of Infection in Intensive Care (EPIC) Study. EPIC International Advisory Committee. *JAMA*, 274: 639-644 (1995).
- [17] H.W. Boucher, G.H. Talbot, J.S. Bradley, J.E. Edwards, D. Gilbert, L.B. Rice, M. Scheld, B. Spellberg, J. Bartlett. Bad bugs, no drugs: no ESKAPE! An update from the Infectious Diseases Society of America. *Clin. Infect. Dis.*, 48: 1-12 (2009).

- [18] G.H. Talbot, J. Bradley, J.E. Edwards, Jr., D. Gilbert, M. Scheld, J.G. Bartlett. Bad bugs need drugs: an update on the development pipeline from the Antimicrobial Availability Task Force of the Infectious Diseases Society of America. *Clin. Infect. Dis.*, 42: 657-668 (2006).
- [19] D.M. Livermore. Antibiotic resistance in staphylococci. *Int. J. Antimicrob. Agents*, 16 Suppl 1: S3-10 (2000).
- [20] B.A. Freeman. *Burrow's textbook of microbiology*, Philadelphia, W.B. Saunders Company (1985).
- [21] U. Theuretzbacher. β -Lactamasen. *Pharm. Unserer Zeit*, 35: 416-421 (2006).
- [22] H.W. Boucher, G.R. Corey. Epidemiology of methicillin-resistant *Staphylococcus aureus*. *Clin. Infect. Dis.*, 46 Suppl 5: S344-349 (2008).
- [23] R.M. Klevens, J.R. Edwards, F.C. Tenover, L.C. McDonald, T. Horan, R. Gaynes. Changes in the epidemiology of methicillin-resistant *Staphylococcus aureus* in intensive care units in US hospitals, 1992-2003. *Clin. Infect. Dis.*, 42: 389-391 (2006).
- [24] PEG. Arbeitsgemeinschaft "Empfindlichkeitsprüfungen & Resistenz" - PEG-Resistenzstudie. Paul Ehrlich Gesellschaft, 2004. (Accessed 18 December, 2007, at http://www.p-e-g.org/ag_resistenz/main.htm.)
- [25] PEG. Arbeitsgemeinschaft "Empfindlichkeitsprüfungen & Resistenz" - PEG-Resistenzstudie. Paul Ehrlich Gesellschaft, 2007. (Accessed 07 April, 2009, at http://www.p-e-g.org/ag_resistenz/main.htm.)
- [26] H.J. Linde, N. Lehn. Methicillin-resistenter *Staphylokokkus aureus*. *Pharm. Unserer Zeit*, 35: 422-425 (2006).
- [27] M.H. Beers, R.S. Porter, T.V. Jones. *The Merck manual of diagnosis and therapy*, New York, Merck Research Laboratories (2006).
- [28] F. Vogel, C. Lebert. *Infektionen in Klinik und Praxis*, Stuttgart, Wissenschaftliche Verlagsgesellschaft mbH (2004).
- [29] SepNet. Kompetenznetz Sepsis - Deutsche Sepsis-Gesellschaft e.V. (Accessed 05 April, 2009, at <http://www.sepsis-gesellschaft.de/DSG/Deutsch/SepNet/Hintergrund?sid=xXcVRm2vSdtn4M16nt2qwx&iid=1>.)
- [30] K. Reinhart, F.M. Brunkhorst, H.G. Bone, H. Gerlach, M. Grundling, G. Kreymann, P. Kujath, G. Marggraf, K. Mayer, A. Meier-Hellmann, C. Peckelsen, C. Putensen, F. Stuber, M. Quintel, M. Ragaller, R. Rossaint, N. Weiler, T. Welte, K. Werdan. Diagnosis and therapy of sepsis. *Clin. Res. Cardiol.*, 95: 429-454 (2006).
- [31] F.M. Brunkhorst, K. Reinhart. Sepsis therapy: present guidelines and their application. *Chirurg*, 79: 306-314 (2008).
- [32] B. Berger-Bachi, N. McCallum. State of the knowledge of bacterial resistance. *Injury*, 37 Suppl 2: S20-25 (2006).
- [33] M. Mueller, A. de la Pena, H. Derendorf. Issues in pharmacokinetics and pharmacodynamics of anti-infective agents: kill curves versus MIC. *Antimicrob. Agents Chemother.*, 48: 369-377 (2004).
- [34] R.C. Owens, Jr., P.G. Ambrose. Antimicrobial stewardship and the role of pharmacokinetics-pharmacodynamics in the modern antibiotic era. *Diagn. Microbiol. Infect. Dis.*, 57: 77S-83S (2007).
- [35] F. Scaglione. Can PK/PD be used in everyday clinical practice. *Int. J. Antimicrob. Agents*, 19: 349-353 (2002).
- [36] S. Heinzl. Multiresistenz und neue Antibiotika. *Krankenhauspharmazie*, 28: 101-102 (2007).

- [37] T.R. Fritsche, H.S. Sander, R.N. Jones. Epidemiology of antimicrobial resistance, susceptibility profiles and resistance trends. In: V. Lorian (Eds.) *Antibiotics in laboratory medicine*. 5th ed., Philadelphia, Lippincott Williams & Wilkins 815-850 (2005).
- [38] F.J. Schmitz. Rationale Antibiotika-Therapie unter Berücksichtigung ökologischer Aspekte. *Chemother. J.*, 17: 267-273 (2008).
- [39] L.R. Merz, D.K. Warren, M.H. Kollef, V.J. Fraser. Effects of an antibiotic cycling program on antibiotic prescribing practices in an intensive care unit. *Antimicrob. Agents Chemother.*, 48: 2861-2865 (2004).
- [40] C.T. Bergstrom, M. Lo, M. Lipsitch. Ecological theory suggests that antimicrobial cycling will not reduce antimicrobial resistance in hospitals. *Proc. Natl. Acad. Sci. U. S. A.*, 101: 13285-13290 (2004).
- [41] L.R. Merz, D.K. Warren, M.H. Kollef, S.K. Fridkin, V.J. Fraser. The impact of an antibiotic cycling program on empirical therapy for gram-negative infections. *Chest*, 130: 1672-1678 (2006).
- [42] B.R. Levin, M.J. Bonten. Cycling antibiotics may not be good for your health. *Proc. Natl. Acad. Sci. U. S. A.*, 101: 13101-13102 (2004).
- [43] T.C. Bailey, J.R. Little, B. Littenberg, R.M. Reichley, W.C. Dunagan. A meta-analysis of extended-interval dosing versus multiple daily dosing of aminoglycosides. *Clin. Infect. Dis.*, 24: 786-795 (1997).
- [44] M. Gibaldi, D. Perrier. *Pharmacokinetics*, New York, Marcel Dekker, Inc. (1982).
- [45] P.K. Narang, R.C. Li. Factors influencing variability in kinetics and dynamics. In: N.R. Cuttler, J.J. Sramek, P.K. Narang (Eds.) *Pharmacodynamics and drug development: Perspectives in clinical pharmacology*. 1st ed., Chichester, John Wiley & Sons 45-72 (1994).
- [46] H.P. Rang, M.M. Dale, J.M. Ritter. *Pharmacology*, Oxford, Elsevier LTD (2007).
- [47] N.H.G. Holford, T.M. Ludden. Time course of drug effect. In: P.G. Welling, L.P. Balant (Eds.) *Pharmacokinetics of drugs*. 1st ed., Berlin, Springer Verlag 333-352 (1994).
- [48] R.J. Wills. Basic pharmacodynamic concepts and models. In: N.R. Cuttler, J.J. Sramek, P.K. Narang (Eds.) *Pharmacodynamics and drug development: Perspectives in clinical pharmacology*. 1st ed., Chichester, John Wiley & Sons 3-17 (1994).
- [49] F. Pea, P. Viale, M. Furlanut. Antimicrobial therapy in critically ill patients: a review of pathophysiological conditions responsible for altered disposition and pharmacokinetic variability. *Clin. Pharmacokinet.*, 44: 1009-1034 (2005).
- [50] H. Derendorf, B. Meibohm. Modeling of pharmacokinetic/pharmacodynamic (PK/PD) relationships: concepts and perspectives. *Pharm. Res.*, 16: 176-185 (1999).
- [51] BDWG. Biomarkers and surrogate endpoints: preferred definitions and conceptual framework - (Biomarkers Definitions Working Group). *Clin. Pharmacol. Ther.*, 69: 89-95 (2001).
- [52] H. Derendorf, T. Gramatté, H.G. Schäfer. *Pharmakokinetik - Einführung in die Theorie und Relevanz für die Arzneimitteltherapie*, Stuttgart, Wissenschaftliche Verlagsgesellschaft mbH (2002).
- [53] G. Schmitz, S. Endres, D. Goette. *Biomarker - Bedeutung für medizinischen Fortschritt und Nutzenbewertung*, Stuttgart, Schattauer Verlag (2008).

- [54] P.J. Williams, E.I. Ette. Pharmacometrics: Impacting drug development and pharmacotherapy. In: E.I. Ette , P.J. Williams (Eds.) *Pharmacometrics: The science of quantitative pharmacology*. 1st ed., New Jersey, John Wiley & Sons, Inc. 1-24 (2007).
- [55] FDA. Guidance for industry - Exposure-response relationships - Study design, data Analysis, and regulatory applications. Food and Drug Administration, 2003. (Accessed 05 April, 2009, at <http://www.fda.gov/cder/guidance/5341fnl.htm>.)
- [56] W.A. Colburn, M. Eldon. Simultaneous pharmacokinetic/pharmacodynamic modeling. In: N.R. Cuttler, J.J. Sramek , P.K. Narang (Eds.) *Pharmacodynamics and drug development: Perspectives in clinical pharmacology*. 1st ed., Chichester, John Wiley & Sons 19-44 (1994).
- [57] G. Hochhaus, H. Derendorf. Dose optimisation based on pharmacokinetic-pharmacodynamic modeling. In: G. Hochhaus , H. Derendorf (Eds.) *Handbook of pharmacokinetic/pharmacodynamic correlations* 1st ed., Boca Raton, CRC-Press 79-120 (1995).
- [58] Pharmacia. Linezolid (PNU-100766) investigator brochure (2002).
- [59] Pharmacia. Linezolid technical information (1998).
- [60] Pfizer. Zyvoxid - German summary of product characteristics. 2008. (Accessed at <http://www.pfizer.de/produkte/gisuche.htm>.)
- [61] F. Islinger, P. Dehghanyar, R. Sauermann, C. Burger, C. Kloft, M. Muller, C. Joukhadar. The effect of food on plasma and tissue concentrations of linezolid after multiple doses. *Int. J. Antimicrob. Agents*, 27: 108-112 (2006).
- [62] C.M. Perry, B. Jarvis. Linezolid: a review of its use in the management of serious gram-positive infections. *Drugs*, 61: 525-551 (2001).
- [63] P. Dehghanyar, C. Buerger, M. Zeitlinger, F. Islinger, F. Kovar, M. Muller, C. Kloft, C. Joukhadar. Penetration of linezolid into soft tissues of healthy volunteers after single and multiple doses. *Antimicrob. Agents Chemother.*, 49: 2367-2371 (2005).
- [64] C. Buerger, N. Plock, P. Dehghanyar, C. Joukhadar, C. Kloft. Pharmacokinetics of unbound linezolid in plasma and tissue interstitium of critically ill patients after multiple dosing using microdialysis. *Antimicrob. Agents Chemother.*, 50: 2455-2463 (2006).
- [65] C. Thallinger, C. Buerger, N. Plock, S. Kljucar, S. Wuenscher, R. Sauermann, C. Kloft, C. Joukhadar. Effect of severity of sepsis on tissue concentrations of linezolid. *J. Antimicrob. Chemother.*, 61: 173-176 (2008).
- [66] N. Plock, C. Buerger, C. Joukhadar, S. Kljucar, C. Kloft. Does linezolid inhibit its own metabolism? Population pharmacokinetics as a tool to explain the observed nonlinearity in both healthy volunteers and septic patients. *Drug Metab. Dispos.*, 35: 1816-1823 (2007).
- [67] M.A. Wynalda, M.J. Hauer, L.C. Wienkers. Oxidation of the novel oxazolidinone antibiotic linezolid in human liver microsomes. *Drug Metab. Dispos.*, 28: 1014-1017 (2000).
- [68] D.M. Livermore. Linezolid in vitro: mechanism and antibacterial spectrum. *J. Antimicrob. Chemother.*, 51 Suppl 2: ii9-16 (2003).
- [69] S.M. Swaney, H. Aoki, M.C. Ganoza, D.L. Shinabarger. The oxazolidinone linezolid inhibits initiation of protein synthesis in bacteria. *Antimicrob. Agents Chemother.*, 42: 3251-3255 (1998).
- [70] P. Kloss, L. Xiong, D.L. Shinabarger, A.S. Mankin. Resistance mutations in 23 S rRNA identify the site of action of the protein synthesis inhibitor linezolid in the ribosomal peptidyl transferase center. *J. Mol. Biol.*, 294: 93-101 (1999).

- [71] L. Xiong, P. Kloss, S. Douthwaite, N.M. Andersen, S. Swaney, D.L. Shinabarger, A.S. Mankin. Oxazolidinone resistance mutations in 23S rRNA of *Escherichia coli* reveal the central region of domain V as the primary site of drug action. *J. Bacteriol.*, 182: 5325-5331 (2000).
- [72] S.K. Pillai, G. Sakoulas, C. Wennersten, G.M. Eliopoulos, R.C. Moellering, Jr., M.J. Ferraro, H.S. Gold. Linezolid resistance in *Staphylococcus aureus*: characterization and stability of resistant phenotype. *J. Infect. Dis.*, 186: 1603-1607 (2002).
- [73] S. Besier, A. Ludwig, J. Zander, V. Brade, T.A. Wichelhaus. Linezolid resistance in *Staphylococcus aureus*: gene dosage effect, stability, fitness costs, and cross-resistances. *Antimicrob. Agents Chemother.*, 52: 1570-1572 (2008).
- [74] N. Bourgeois-Nicolaos, L. Massias, B. Couson, M.J. Butel, A. Andremont, F. Doucet-Populaire. Dose dependence of emergence of resistance to linezolid in *Enterococcus faecalis* in vivo. *J. Infect. Dis.*, 195: 1480-1488 (2007).
- [75] P. Heisig. Was ist neu an Ketoliden und Oxazolidinonen? - Wirkungs- und Resistenzmechanismen. *Pharm. Unserer Zeit*, 33: 10-19 (2004).
- [76] K.A. Ruggero, L.K. Schroeder, P.C. Schreckenberger, A.S. Mankin, J.P. Quinn. Nosocomial superinfections due to linezolid-resistant *Enterococcus faecalis*: evidence for a gene dosage effect on linezolid MICs. *Diagn. Microbiol. Infect. Dis.*, 47: 511-513 (2003).
- [77] G.E. Zurenko, B.H. Yagi, R.D. Schaadt, J.W. Allison, J.O. Kilburn, S.E. Glickman, D.K. Hutchinson, M.R. Barbachyn, S.J. Brickner. In vitro activities of U-100592 and U-100766, novel oxazolidinone antibacterial agents. *Antimicrob. Agents Chemother.*, 40: 839-845 (1996).
- [78] Z. Bersos, M. Maniati, F. Kontos, E. Petinaki, A.N. Maniatis. First report of a linezolid-resistant vancomycin-resistant *Enterococcus faecium* strain in Greece. *J. Antimicrob. Chemother.*, 53: 685-686 (2004).
- [79] R.D. Gonzales, P.C. Schreckenberger, M.B. Graham, S. Kelkar, K. DenBesten, J.P. Quinn. Infections due to vancomycin-resistant *Enterococcus faecium* resistant to linezolid. *Lancet*, 357: 1179 (2001).
- [80] C. Auckland, L. Teare, F. Cooke, M.E. Kaufmann, M. Warner, G. Jones, K. Bamford, H. Ayles, A.P. Johnson. Linezolid-resistant enterococci: report of the first isolates in the United Kingdom. *J. Antimicrob. Chemother.*, 50: 743-746 (2002).
- [81] A.P. Johnson, L. Tysall, M.V. Stockdale, N. Woodford, M.E. Kaufmann, M. Warner, D.M. Livermore, F. Asboth, F.J. Allerberger. Emerging linezolid-resistant *Enterococcus faecalis* and *Enterococcus faecium* isolated from two Austrian patients in the same intensive care unit. *Eur. J. Clin. Microbiol. Infect. Dis.*, 21: 751-754 (2002).
- [82] M. Bassetti, P.A. Farrel, D.A. Callan, J.E. Topal, L.M. Dembry. Emergence of linezolid-resistant *Enterococcus faecium* during treatment of enterococcal infections. *Int. J. Antimicrob. Agents*, 21: 593-594 (2003).
- [83] S. Tsiodras, H.S. Gold, G. Sakoulas, G.M. Eliopoulos, C. Wennersten, L. Venkataraman, R.C. Moellering, M.J. Ferraro. Linezolid resistance in a clinical isolate of *Staphylococcus aureus*. *Lancet*, 358: 207-208 (2001).
- [84] RKI. MRSA: Sekundäre Linezolidresistenz bei einem Patienten mit Beatmungspneumonie. Robert Koch Institut, 2008. (Accessed 13 April, 2009, at http://www.rki.de/cln_100/nn_969736/DE/Content/Infekt/EpidBull/Archiv/2008/09__08,templateId=raw,property=publicationFile.pdf/09_08.pdf.)

- [85] H. Nikaido, Y. Takatsuka. Mechanisms of RND multidrug efflux pumps. *Biochim. Biophys. Acta*, 1794: 769-781 (2009).
- [86] A. Schumacher, R. Trittler, J.A. Bohnert, K. Kummerer, J.M. Pages, W.V. Kern. Intracellular accumulation of linezolid in *Escherichia coli*, *Citrobacter freundii* and *Enterobacter aerogenes*: role of enhanced efflux pump activity and inactivation. *J. Antimicrob. Chemother.*, 59: 1261-1264 (2007).
- [87] J.M. Pages, L. Amaral. Mechanisms of drug efflux and strategies to combat them: Challenging the efflux pump of Gram-negative bacteria. *Biochim. Biophys. Acta*, 1794: 826-833 (2009).
- [88] EUCAST. Linezolid breakpoints. *Clin. Microbiol. Infect.*, 7: 283-284 (2001).
- [89] EUCAST. EUCAST Technical Note on linezolid. *Clin. Microbiol. Infect.*, 12: 1243-1245 (2006).
- [90] P.A. Moise, R.S. Castro, C. Sul, A. Forrest, G. Sakoulas. Relationship of linezolid minimum inhibitory concentration and time to bacterial eradication in treatment for methicillin-resistant *Staphylococcus aureus* infection. *Ann. Pharmacother.*, 42: 592-593 (2008).
- [91] G. French. Safety and tolerability of linezolid. *J. Antimicrob. Chemother.*, 51 Suppl 2: ii45-53 (2003).
- [92] K.L. Leach, S.M. Swaney, J.R. Colca, W.G. McDonald, J.R. Blinn, L.M. Thomasco, R.C. Gadwood, D. Shinabarger, L. Xiong, A.S. Mankin. The site of action of oxazolidinone antibiotics in living bacteria and in human mitochondria. *Mol. Cell*, 26: 393-402 (2007).
- [93] M.C. Birmingham, C.R. Rayner, A.K. Meagher, S.M. Flavin, D.H. Batts, J.J. Schentag. Linezolid for the treatment of multidrug-resistant, gram-positive infections: experience from a compassionate-use program. *Clin. Infect. Dis.*, 36: 159-168 (2003).
- [94] P.A. Moise, A. Forrest, M.C. Birmingham, J.J. Schentag. The efficacy and safety of linezolid as treatment for *Staphylococcus aureus* infections in compassionate use patients who are intolerant of, or who have failed to respond to, vancomycin. *J. Antimicrob. Chemother.*, 50: 1017-1026 (2002).
- [95] P. Munoz, M. Rodriguez-Creixems, M. Moreno, M. Marin, V. Ramallo, E. Bouza. Linezolid therapy for infective endocarditis. *Clin. Microbiol. Infect.*, 13: 211-215 (2007).
- [96] H. Lode, R. Stahlmann, H. Skopnik. Rationaler Einsatz oraler Antibiotika bei Erwachsenen und Schulkindern (Lebensalter ab 6 Jahre). *Chemother. J.*, 15: 129-144 (2006).
- [97] M.D. Johnson, C.F. Decker. Antimicrobial agents in treatment of MRSA infections. *Dis. Mon.*, 54: 793-800 (2008).
- [98] C. Buerger, C. Joukhadar, M. Muller, C. Kloft. Development of a liquid chromatography method for the determination of linezolid and its application to in vitro and human microdialysis samples. *J. Chromatogr. B Analyt. Technol. Biomed. Life. Sci.*, 796: 155-164 (2003).
- [99] G. Aced, H.J. Moeckel. *Liquidchromatographie - Apparative, theoretische und methodische Grundlagen der HPLC*, Weinheim, VCH (1991).
- [100] FDA. Guidance for industry - Bioanalytical method validation. Food and Drug Administration, 2001. (Accessed 13 March, 2007, at <http://www.fda.gov/cder/guidance/4252fnl.htm>.)
- [101] A.M. Almeida, M.M. Castel-Branco, A.C. Falcao. Linear regression for calibration lines revisited: weighting schemes for bioanalytical methods. *J. Chromatogr. B Analyt. Technol. Biomed. Life. Sci.*, 774: 215-222 (2002).

- [102] J.D. Turnidge, J.M. Bell. Antimicrobial susceptibility on solid media. In: V. Lorian (Eds.) *Antibiotics in laboratory medicine*. 5th ed., Philadelphia, Lippincott Williams & Wilkins 8-60 (2005).
- [103] D. Amsterdam. Susceptibility testing of antimicrobials in liquid media. In: V. Lorian (Eds.) *Antibiotics in laboratory medicine*. 5th ed., Philadelphia, Lippincott Williams & Wilkins 61-143 (2005).
- [104] A. Nolting, T. Dalla Costa, K.H. Rand, H. Derendorf. Pharmacokinetic-pharmacodynamic modeling of the antibiotic effect of piperacillin in vitro. *Pharm. Res.*, 13: 91-96 (1996).
- [105] Karbachsch. Prüfmethode für integrierte Filtersysteme. *Pharm. Ind.*, 45: 540-544 (1983).
- [106] A. de la Pena, A. Grabe, K.H. Rand, E. Rehak, J. Gross, U. Thyroff-Friesinger, M. Muller, H. Derendorf. PK-PD modelling of the effect of cefaclor on four different bacterial strains. *Int. J. Antimicrob. Agents*, 23: 218-225 (2004).
- [107] A.L. Koch. Growth measurement. In: P. Gerhardt, R.G.E. Murray, W.A. Wood, N.R. Krieg (Eds.) *Methods for general and molecular bacteriology*. 1st ed., Washington, American Society for Microbiology 248-277 (1994).
- [108] Oxoid. Product detail - Diagnostic reagents - Staphytest Plus. 2007. (Accessed 15 May, 2007, at http://www.oxoid.com/UK/blue/prod_detail/prod_detail.asp?pr=DR0850&org=153&c=UK&lang=EN.)
- [109] B. Efron, R. Tibshirani. Bootstrap method for standard errors, confidence intervals, and other measures of statistical accuracy. *Stat. Sci.*, 1: 54-77 (1986).
- [110] R.W. Johnson. An Introduction to the Bootstrap. *Teach. Stat.*, 23: 49-54 (2001).
- [111] B. Efron, R. Tibshirani. Statistical data analysis in the computer age. *Science*, 253: 390-395 (1991).
- [112] K. Teknomo. Bootstrapping sampling tutorial. (Accessed 22 March, 2007, at <http://people.revoledu.com/kardi/tutorial/Bootstrap/examples.htm>.)
- [113] C. Scheerans, H. Derendorf, C. Kloft. Proposal for a standardised identification of the mono-exponential terminal phase for orally administered drugs. *Biopharm. Drug Dispos.*, 29: 145-157 (2007).
- [114] E.J. Billo. *Excel for scientists and engineers - Numerical methods*, Hoboken, John Wiley & Sons, Inc. (2007).
- [115] D.M. Bourg. *Excel scientific and engineering cookbook*, Sebastopol, O'Reilly (2006).
- [116] D. Christie. Resampling with Excel. *Teach. Stat.*, 26: 9-14 (2004).
- [117] H. Motulsky, A. Christopoulos. *Fitting models to biological data using linear and nonlinear regression - A practical guide to curve fitting*, New York, Oxford University Press (2004).
- [118] T.L. Schwinghammer, P.D. Kroboth. Basic concepts in pharmacodynamic modeling. *J. Clin. Pharmacol.*, 28: 388-394 (1988).
- [119] N.H. Holford, L.B. Sheiner. Understanding the dose-effect relationship: clinical application of pharmacokinetic-pharmacodynamic models. *Clin. Pharmacokinet.*, 6: 429-453 (1981).
- [120] A.A. Firsov, V.M. Chernykh, S.M. Navashin. Quantitative analysis of antimicrobial effect kinetics in an in vitro dynamic model. *Antimicrob. Agents Chemother.*, 34: 1312-1317 (1990).
- [121] J.W. Mouton, M.N. Dudley, O. Cars, H. Derendorf, G.L. Drusano. Standardization of pharmacokinetic/pharmacodynamic (PK/PD) terminology for anti-infective drugs. *Int. J. Antimicrob. Agents*, 19: 355-358 (2002).

- [122] J.W. Mouton, M.N. Dudley, O. Cars, H. Derendorf, G.L. Drusano. Standardization of pharmacokinetic/pharmacodynamic (PK/PD) terminology for anti-infective drugs: an update. *J. Antimicrob. Chemother.*, 55: 601-607 (2005).
- [123] D. Fylstra, L. Lasdon, J. Watson, A. Waren. Design and use of Microsoft Excel Solver. *Interfaces*, 28: 29-55 (1998).
- [124] Microsoft. How to create Visual Basic macros by using Excel Solver in Excel 97 - (Article ID 843304). 2006. (Accessed 02 July, 2008, at <http://support.microsoft.com>.)
- [125] D.W.A. Bourne. *Mathematical modeling of pharmacokinetic data*, Lancaster, Technomic Publishing Company, Inc. (1995).
- [126] H. Akaike. A new look at the statistical model identification. *IEEE Trans. Automat. Contr.*, 19: 716-722 (1974).
- [127] N. Sugiura. Further analysis of the data by Akaike's information criterion and the finite corrections. *Commun. Stat. Theory Methods*, A7: 13-26 (1978).
- [128] K.P. Burnham, D.R. Anderson. *Model selection and multimodel interface - A practical information-Theoretic approach*, Berlin, Springer Verlag (2002).
- [129] P.L. Bonate. *Pharmacokinetic-pharmacodynamic modeling and simulation*, New York, Springer Science+Business Media, Inc. (2006).
- [130] E.I. Ette, P.J. Williams, A. Ahmad. Population pharmacokinetic estimation methods. In: E.I. Ette, P.J. Williams (Eds.) *Pharmacometrics: The science of quantitative pharmacology*. 1st ed., Hoboken, John Wiley & Sons, Inc. 265-286 (2007).
- [131] P.L. Bonate. Clinical trial simulation: Theory. In: E.I. Ette, P.J. Williams (Eds.) *Pharmacometrics: the science of quantitative pharmacology*. 1st ed., New Jersey, John Wiley & Sons, Inc. 851-872 (2007).
- [132] F.H. Dost. *Grundlagen der Pharmakokinetik*, Stuttgart, Georg Thieme Verlag (1968).
- [133] C.D. Thron. Linearity and superposition in pharmacokinetics. *Pharmacol. Rev.*, 26: 3-31 (1974).
- [134] R.R. Wilcox, J. Muska. Measuring effect size: a non-parametric analogue of omega 2. *Br. J. Math. Stat. Psychol.*, 52 (Pt 1): 93-110 (1999).
- [135] P. Girard, J.P. Boissel. Clockwise hysteresis or proteresis. *J. Pharmacokinet. Biopharm.*, 17: 401-402 (1989).
- [136] D.B. Campbell. The use of kinetic-dynamic interactions in the evaluation of drugs. *Psychopharmacology (Berl.)*, 100: 433-450 (1990).
- [137] R.C. Li. Simultaneous pharmacodynamic analysis of the lag and bactericidal phases exhibited by beta-lactams against *Escherichia coli*. *Antimicrob. Agents Chemother.*, 40: 2306-2310 (1996).
- [138] P. Liu, K.H. Rand, B. Obermann, H. Derendorf. Pharmacokinetic-pharmacodynamic modelling of antibacterial activity of cefpodoxime and cefixime in in vitro kinetic models. *Int. J. Antimicrob. Agents*, 25: 120-129 (2005).
- [139] J.W. Mouton, A.A. Vinks, N.C. Punt. Pharmacokinetic-pharmacodynamic modeling of activity of ceftazidime during continuous and intermittent infusion. *Antimicrob. Agents Chemother.*, 41: 733-738 (1997).
- [140] E.L. Schuck, A. Dalhoff, H. Stass, H. Derendorf. Pharmacokinetic/pharmacodynamic (PK/PD) evaluation of a once-daily treatment using ciprofloxacin in an extended-release dosage form. *Infection*, 33 Suppl 2: 22-28 (2005).

- [141] V.H. Tam, A.N. Schilling, M. Nikolaou. Modelling time-kill studies to discern the pharmacodynamics of meropenem. *J. Antimicrob. Chemother.*, 55: 699-706 (2005).
- [142] J. Cohen. *Statistical power analysis for the behavioral sciences*, Hillsdale, Lawrence Erlbaum Assoc Inc (1988).
- [143] C. Buerger. Pharmakokinetik von Linezolid in der Biophase bei gesunden Probanden und Intensivpatienten. Berlin: Freie Universitaet (2006).
- [144] C. Adembri, S. Fallani, M.I. Cassetta, S. Arrigucci, A. Ottaviano, P. Pecile, T. Mazzei, R. De Gaudio, A. Novelli. Linezolid pharmacokinetic/pharmacodynamic profile in critically ill septic patients: intermittent versus continuous infusion. *Int. J. Antimicrob. Agents*, 31: 122-129 (2008).
- [145] R. Cha, R.L. Akins, M.J. Rybak. Linezolid, levofloxacin, and vancomycin against vancomycin-tolerant and fluoroquinolone-resistant *Streptococcus pneumoniae* in an in vitro pharmacodynamic model. *Pharmacotherapy*, 23: 1531-1537 (2003).
- [146] B.W. Gunderson, K.H. Ibrahim, C.A. Peloquin, L.B. Hovde, J.C. Rotschafer. Comparison of linezolid activities under aerobic and anaerobic conditions against methicillin-resistant *Staphylococcus aureus* and vancomycin-resistant *Enterococcus faecium*. *Antimicrob. Agents Chemother.*, 47: 398-399 (2003).
- [147] B.B. Ba, B.B. Nso, C. Quentin, M.C. Saux. Determination of linezolid in growth media by high-performance liquid chromatography with on-line extraction. *J. Chromatogr. B Analyt. Technol. Biomed. Life. Sci.*, 854: 104-108 (2007).
- [148] J.H. Song. Introduction: the goals of antimicrobial therapy. *Int. J. Infect. Dis.*, 7 Suppl 1: S1-4 (2003).
- [149] E.L. Schuck, H. Derendorf. Pharmacokinetic/pharmacodynamic evaluation of anti-infective agents. *Expert Rev. Anti Infect. Ther.*, 3: 361-373 (2005).
- [150] F. Burkhardt. *Mikrobiologische Diagnostik*, Stuttgart, Thieme Verlag (1992).
- [151] H.K. Geiss, D. Mack, H. Seifert. Identifizierung von speziellen Resistenzmechanismen und Interpretation von Ergebnissen der Antibiotika-Empfindlichkeitstestung bei grampositiven und gramnegativen Erregern. *Chemother. J.*, 13: 1-16 (2004).
- [152] S.J. Brickner, D.K. Hutchinson, M.R. Barbachyn, P.R. Manninen, D.A. Ulanowicz, S.A. Garmon, K.C. Grega, S.K. Hendges, D.S. Toops, C.W. Ford, G.E. Zurenko. Synthesis and antibacterial activity of U-100592 and U-100766, two oxazolidinone antibacterial agents for the potential treatment of multidrug-resistant gram-positive bacterial infections. *J. Med. Chem.*, 39: 673-679 (1996).
- [153] R. Wise, J.M. Andrews, F.J. Boswell, J.P. Ashby. The in-vitro activity of linezolid (U-100766) and tentative breakpoints. *J. Antimicrob. Chemother.*, 42: 721-728 (1998).
- [154] C. Jacqueline, D. Navas, E. Batard, A.F. Miegerville, V. Le Mabecque, M.F. Kergueris, D. Bugnon, G. Potel, J. Caillon. In vitro and in vivo synergistic activities of linezolid combined with subinhibitory concentrations of imipenem against methicillin-resistant *Staphylococcus aureus*. *Antimicrob. Agents Chemother.*, 49: 45-51 (2005).
- [155] G. Kahlmeter, D.F. Brown, F.W. Goldstein, A.P. MacGowan, J.W. Mouton, I. Odenholt, A. Rodloff, C.J. Soussy, M. Steinbakk, F. Soriano, O. Stetsiouk. European Committee on Antimicrobial Susceptibility Testing (EUCAST) Technical Notes on antimicrobial susceptibility testing. *Clin. Microbiol. Infect.*, 12: 501-503 (2006).

- [156] A. Nolting, H. Derendorf. Pharmacokinetic/pharmacodynamic modeling of antibiotics. In: H. Derendorf, G. Hochhaus (Eds.) *Handbook of pharmacokinetic/pharmacodynamic correlations* 1st ed., Boca Raton, CRC Press 363-388 (1995).
- [157] EMEA. Points to consider on pharmacokinetics and pharmacodynamics in the development of antibacterial medical products. European Medicines Agency, 2000. (Accessed 05 April, 2009, at <http://www.tga.health.gov.au/docs/pdf/euguide/ewp/265599en.pdf>.)
- [158] J. Aitchison, J.A.C. Brown. *The lognormal distribution*, Cambridge, Cambridge University Press (1963).
- [159] C.H. Olsen. Review of the use of statistics in infection and immunity. *Infect. Immun.*, 71: 6689-6692 (2003).
- [160] B. Efron. Bootstrap Methods: Another Look at the Jackknife. *Ann. Stat.*, 7: 1-26 (1977).
- [161] M.R. Chernick. *Bootstrap methods: A guide for practitioners and researchers*, Hoboken, John Wiley & Sons (2008).
- [162] R.N. Jones, D.M. Johnson, M.E. Erwin. In vitro antimicrobial activities and spectra of U-100592 and U-100766, two novel fluorinated oxazolidinones. *Antimicrob. Agents Chemother.*, 40: 720-726 (1996).
- [163] J.H. Jorgensen, M.L. McElmeel, C.W. Trippy. In vitro activities of the oxazolidinone antibiotics U-100592 and U-100766 against *Staphylococcus aureus* and coagulase-negative *Staphylococcus* species. *Antimicrob. Agents Chemother.*, 41: 465-467 (1997).
- [164] G.W. Kaatz, S.M. Seo. In vitro activities of oxazolidinone compounds U100592 and U100766 against *Staphylococcus aureus* and *Staphylococcus epidermidis*. *Antimicrob. Agents Chemother.*, 40: 799-801 (1996).
- [165] P.F. Smith, B.M. Booker, A.B. Ogundele, P. Kelchin. Comparative in vitro activities of daptomycin, linezolid, and quinupristin/dalfopristin against Gram-positive bacterial isolates from a large cancer center. *Diagn. Microbiol. Infect. Dis.*, 52: 255-259 (2005).
- [166] K. Lewis. Persister cells, dormancy and infectious disease. *Nat. Rev. Microbiol.*, 5: 48-56 (2007).
- [167] E. Tuomanen. Phenotypic tolerance: the search for beta-lactam antibiotics that kill nongrowing bacteria. *Rev. Infect. Dis.*, 8 Suppl 3: S279-291 (1986).
- [168] I. Keren, N. Kaldalu, A. Spoering, Y. Wang, K. Lewis. Persister cells and tolerance to antimicrobials. *FEMS Microbiol. Lett.*, 230: 13-18 (2004).
- [169] B.R. Levin, D.E. Rozen. Non-inherited antibiotic resistance. *Nat. Rev. Microbiol.*, 4: 556-562 (2006).
- [170] O. Krut, H. Sommer, M. Kronke. Antibiotic-induced persistence of cytotoxic *Staphylococcus aureus* in non-phagocytic cells. *J. Antimicrob. Chemother.*, 53: 167-173 (2004).
- [171] N. Baumert, C. von Eiff, F. Schaaff, G. Peters, R.A. Proctor, H.G. Sahl. Physiology and antibiotic susceptibility of *Staphylococcus aureus* small colony variants. *Microb. Drug Resist.*, 8: 253-260 (2002).
- [172] R.A. Proctor, C. von Eiff, B.C. Kahl, K. Becker, P. McNamara, M. Herrmann, G. Peters. Small colony variants: a pathogenic form of bacteria that facilitates persistent and recurrent infections. *Nat. Rev. Microbiol.*, 4: 295-305 (2006).
- [173] R.A. Proctor, B. Kahl, C. von Eiff, P.E. Vaudaux, D.P. Lew, G. Peters. *Staphylococcal* small colony variants have novel mechanisms for antibiotic resistance. *Clin. Infect. Dis.*, 27 Suppl 1: S68-74 (1998).

- [174] R.A. Proctor, J.M. Balwit, O. Vesga. Variant subpopulations of *Staphylococcus aureus* as cause of persistent and recurrent infections. *Infect. Agents Dis.*, 3: 302-312 (1994).
- [175] R.A. Proctor, G. Peters. Small colony variants in *staphylococcal* infections: diagnostic and therapeutic implications. *Clin. Infect. Dis.*, 27: 419-422 (1998).
- [176] R.C. Massey, A. Buckling, S.J. Peacock. Phenotypic switching of antibiotic resistance circumvents permanent costs in *Staphylococcus aureus*. *Curr. Biol.*, 11: 1810-1814 (2001).
- [177] S. Delacher, H. Derendorf, U. Hollenstein, M. Brunner, C. Joukhadar, S. Hofmann, A. Georgopoulos, H.G. Eichler, M. Muller. A combined in vivo pharmacokinetic-in vitro pharmacodynamic approach to simulate target site pharmacodynamics of antibiotics in humans. *J. Antimicrob. Chemother.*, 46: 733-739 (2000).
- [178] L.M. Boak, J. Li, C.R. Rayner, R.L. Nation. Pharmacokinetic/pharmacodynamic factors influencing emergence of resistance to linezolid in an in vitro model. *Antimicrob. Agents Chemother.*, 51: 1287-1292 (2007).
- [179] R. Cha, W.J. Brown, M.J. Rybak. Bactericidal activities of daptomycin, quinupristin-dalfopristin, and linezolid against vancomycin-resistant *Staphylococcus aureus* in an in vitro pharmacodynamic model with simulated endocardial vegetations. *Antimicrob. Agents Chemother.*, 47: 3960-3963 (2003).
- [180] L. Wang, M.K. Wismer, F. Racine, D. Conway, R.A. Jacobbe, O. Berejnaia, G.S. Kath. Development of an integrated semi-automated system for in vitro pharmacodynamic modelling. *J. Antimicrob. Chemother.*, 62: 1070-1077 (2008).
- [181] J.Z. Zack, A. Forrest, S. Bilic, P. Kelchlin, P.F. Smith. PK/PD in silico simulations of linezolid activity against methicillin-resistant *Staphylococcus aureus*. In: 45th Interscience Conference on Antimicrobial Agents and Chemotherapy (ICAAC), Washington, DC (2005).
- [182] C. Adembri, M.I. Cassetta, G. Baldini, S. Fallani, A.R. de Gaudio, T. Mazzei, A. Novelli. Linezolid disposition in critically ill patients: intermittent vs continuous infusion. In: 45th Interscience Conference on Antimicrobial Agents and Chemotherapy (ICAAC), Washington, DC (2005).
- [183] E.N. Strukova, M.V. Smirnova, S.N. Vostrov, I.Y. Lubenko, A.A. Firsov, S.H. Zinner, Y.A. Portnoy. Linezolid pharmacodynamics with *Staphylococcus aureus* in an in vitro dynamic model. *Int. J. Antimicrob. Agents*, 33: 251-254 (2009).
- [184] D. Andes, M.L. van Ogtrop, J. Peng, W.A. Craig. In vivo pharmacodynamics of a new oxazolidinone (linezolid). *Antimicrob. Agents Chemother.*, 46: 3484-3489 (2002).
- [185] C.R. Rayner, A. Forrest, A.K. Meagher, M.C. Birmingham, J.J. Schentag. Clinical pharmacodynamics of linezolid in seriously ill patients treated in a compassionate use programme. *Clin. Pharmacokinet.*, 42: 1411-1423 (2003).
- [186] A.V. Hill. The possible effects of the aggregation of the molecules of haemoglobin on its dissociation curves. *J. Physiol.*, 40 (Suppl): 4-7 (1910).
- [187] M. Barcia-Macay, C. Seral, M.P. Mingeot-Leclercq, P.M. Tulkens, F. Van Bambeke. Pharmacodynamic evaluation of the intracellular activities of antibiotics against *Staphylococcus aureus* in a model of THP-1 macrophages. *Antimicrob. Agents Chemother.*, 50: 841-851 (2006).
- [188] N.Q. Balaban, J. Merrin, R. Chait, L. Kowalik, S. Leibler. Bacterial persistence as a phenotypic switch. *Science*, 305: 1622-1625 (2004).

- [189] E.I. Nielsen, A. Viberg, E. Lowdin, O. Cars, M.O. Karlsson, M. Sandstrom. Semimechanistic pharmacokinetic/pharmacodynamic model for assessment of activity of antibacterial agents from time-kill curve experiments. *Antimicrob. Agents Chemother.*, 51: 128-136 (2007).
- [190] K.M. Thompson, D.E. Burmaster, E.A. Crouch. Monte Carlo techniques for quantitative uncertainty analysis in public health risk assessments. *Risk Anal.*, 12: 53-63 (1992).
- [191] M. Pfannkuck. Comparing box plot distributions: A teacher's reasoning. *Stat. Educ. Res. J.*, 5: 27-45 (2006).
- [192] G.R. Norman, G.L. Streiner. *Biostatistics: The bare essentials*, Hamilton, B.C. Decker Inc (2007).
- [193] M.L. Gaddis, G.M. Gaddis. Introduction to biostatistics: Part 1, Basic concepts. *Ann. Emerg. Med.*, 19: 86-89 (1990).
- [194] S. Bolton. *Pharmaceutical statistics - Practical and clinical applications*, New York, Marcel Dekker, INC. (1990).
- [195] G.M. Gaddis, M.L. Gaddis. Introduction to biostatistics: Part 4, statistical inference techniques in hypothesis testing. *Ann. Emerg. Med.*, 19: 820-825 (1990).
- [196] G.M. Gaddis, M.L. Gaddis. Introduction to biostatistics: Part 2, Descriptive statistics. *Ann. Emerg. Med.*, 19: 309-315 (1990).
- [197] G.M. Gaddis, M.L. Gaddis. Introduction to biostatistics: Part 5, Statistical inference techniques for hypothesis testing with nonparametric data. *Ann. Emerg. Med.*, 19: 1054-1059 (1990).
- [198] G.M. Gaddis, M.L. Gaddis. Introduction to biostatistics: Part 3, Sensitivity, specificity, predictive value, and hypothesis testing. *Ann. Emerg. Med.*, 19: 591-597 (1990).
- [199] S. McKillup. *Statistics explained - An introductory guide for life scientists*, Cambridge, Cambridge University Press (2006).
- [200] F. Brosius. *SPSS 12*, Bonn, Mitp-Verlag (2004).
- [201] M.L. Gaddis, G.M. Gaddis. Introduction to biostatistics: Part 6, Correlation and regression. *Ann. Emerg. Med.*, 19: 1462-1468 (1990).
- [202] J. Gabrielsson, D. Weiner. *Pharmacokinetic and pharmacodynamic data analysis: Concepts & applications*, Stockholm, Swedish Pharmaceutical Press (2000).
- [203] R. de Levie. *Advanced Excel for scientific data analysis*, New York, Oxford University Press (2008).
- [204] W.H. Press, S.A. Teukolsky, W.T. Vetterling, B.P. Flannery. *Numerical recipes* Cambridge, Cambridge University Press (2007).
- [205] L.S. Lasdon, A.D. Waren, A. Jain, M. Ratner. Design and Testing of a Generalized Reduced Gradient Code for Nonlinear Programming. *ACM Trans. Math. Soft.*, 4: 3450 (1978).
- [206] M. Mayersohn, M. Gibaldi. Mathematical methods in pharmacokinetics. I. Use of the Laplace transformation for solving differential rate equations. *Am. J. Pharm. Educ.*, 34: 608-614 (1970).
- [207] L. Papula. *Mathematik für Ingenieure und Naturwissenschaftler - Band 2*, Braunschweig/ Wiesbaden, Vieweg & Sohn Verlagsgesellschaft mbH (2001).
- [208] L.Z. Benet, J.S. Turi. Use of general partial fraction theorem for obtaining inverse Laplace transforms in pharmacokinetic analysis. *J. Pharm. Sci.*, 60: 1593-1594 (1971).
- [209] A.M. Law. *Simulation modeling and analysis*, Boston, McGraw-Hill (2007).

- [210] R.Y. Rubinstein. *Simulation and the Monte Carlo method*, New York, John Wiley & Sons (1982).
- [211] N. Metropolis, S. Ulam. The Monte Carlo method. *J. Am. Stat. Assoc.*, 44: 335-341 (1949).
- [212] D.E. Popescu, C. Popescu, G. Gabor. Monte Carlo simulation using Excel for predicting reliability of a geothermal plant, International Geothermal Conference, Reykjavik. 2003. (Accessed 05 April, 2009, at http://jardhitafelag.is/papers/PDF_Session_07/S07Paper047.pdf.)
- [213] B.A. Wichman, I.D. Hill. Building a random-number generator. *BYTE*: 127-128 (1987).
- [214] B.A. Wichmann, I.D. Hill. Algorithm AS 183: An efficient and portable pseudo-random number generator. *Appl. Stat.*, 31: 188-190 (1982).
- [215] Microsoft. Description of the RAND function in Excel 2007 and in Excel 2003 - (Article ID: 828795). 2006. (Accessed 21 January 2009, at <http://support.microsoft.com/?scid=kb%3Ben-us%3B828795&x=11&y=10>.)

7 Appendix

7.1 Tables

Tab. 13 Composition of phosphate-buffered saline with peptone (PBSP) that served as diluent of bacterial suspensions [107].

Ingredients	Amount (mass or volume)
Sodium chloride (NaCl)	8.5 g
Potassium dihydrogen phosphate (KH ₂ PO ₄)	0.3 g
Disodium hydrogen phosphate (Na ₂ HPO ₄)	0.6 g
Peptone from meat, peptic	1.0 g
Distilled water (pH = 7.0)	1.0 L

Tab. 14 Parametric model comparison of the three nested models for pharmacokinetic/ pharmacodynamic modelling of data set I (with $n = 88$), showing the respective amount of model parameters ($K - 1$), the AIC_C values, the probabilities (P_i) of being the relative 'best' model and the respective probabilistic 'superiority' ($1 - P_i$) in favour of the model with the lowest AIC_C value (*).

Pharmacokinetic/ pharmacodynamic models	$K - 1$	Data set	AIC_C	P_i , %	$1 - P_i$, %
'Sigmoidal' E_{max} model	3	I	500.578	0.0	100.0
Modified 'sigmoidal' E_{max} model	6	I	205.649	2.9	97.1
Indirect link model	7	I	198.598*	50.0	50.0

Tab. 15 Parametric model comparison of the three nested models for pharmacokinetic/ pharmacodynamic modelling of data set I+II (with $n = 128$), showing the respective amount of model parameters ($K - 1$), the AIC_C values, the probabilities (P_i) of being the relative 'best' model and the respective probabilistic 'superiority' ($1 - P_i$) in favour of the model with the lowest AIC_C value (*).

Pharmacokinetic/ pharmacodynamic models	Data set	$K - 1$	AIC_C	P_i , %	$1 - P_i$, %
'Sigmoidal' E_{max} model	I+II	3	880.057	0.0	100.0
Modified 'sigmoidal' E_{max} model	I+II	6	444.950	0.0	100.0
Indirect link model	I+II	7	351.739*	50.0	50.0

Tab. 16 Correlation matrix for the final pharmacokinetic/pharmacodynamic model, showing the calculated correlation coefficients (r) for modelling the combined data set (I+II), the model parameters are described in 3.3.2.2.

Model parameter	E_{\max} , %	EC_{50} [$\mu\text{g/mL}$]	H [-]	k_{eo} [h^{-1}]	a_e [h^{-1}]	b_e [h^{-1}]	z_e [h^{-1}]
E_{\max} , %	1.000	-	-	-	-	-	-
EC_{50} [$\mu\text{g/mL}$]	-0.153	1.000	-	-	-	-	-
H [-]	-0.663	0.339	1.000	-	-	-	-
k_{eo} [h^{-1}]	-0.136	-0.035	-0.164	1.000	-	-	-
a_e [h^{-1}]	-0.217	-0.032	0.057	-0.476	1.000	-	-
b_e [h^{-1}]	0.504	-0.663	-0.646	0.436	-0.187	1.000	-
z_e [h^{-1}]	0.222	-0.195	-0.576	0.725	-0.538	0.617	1.000

7.2 Figures

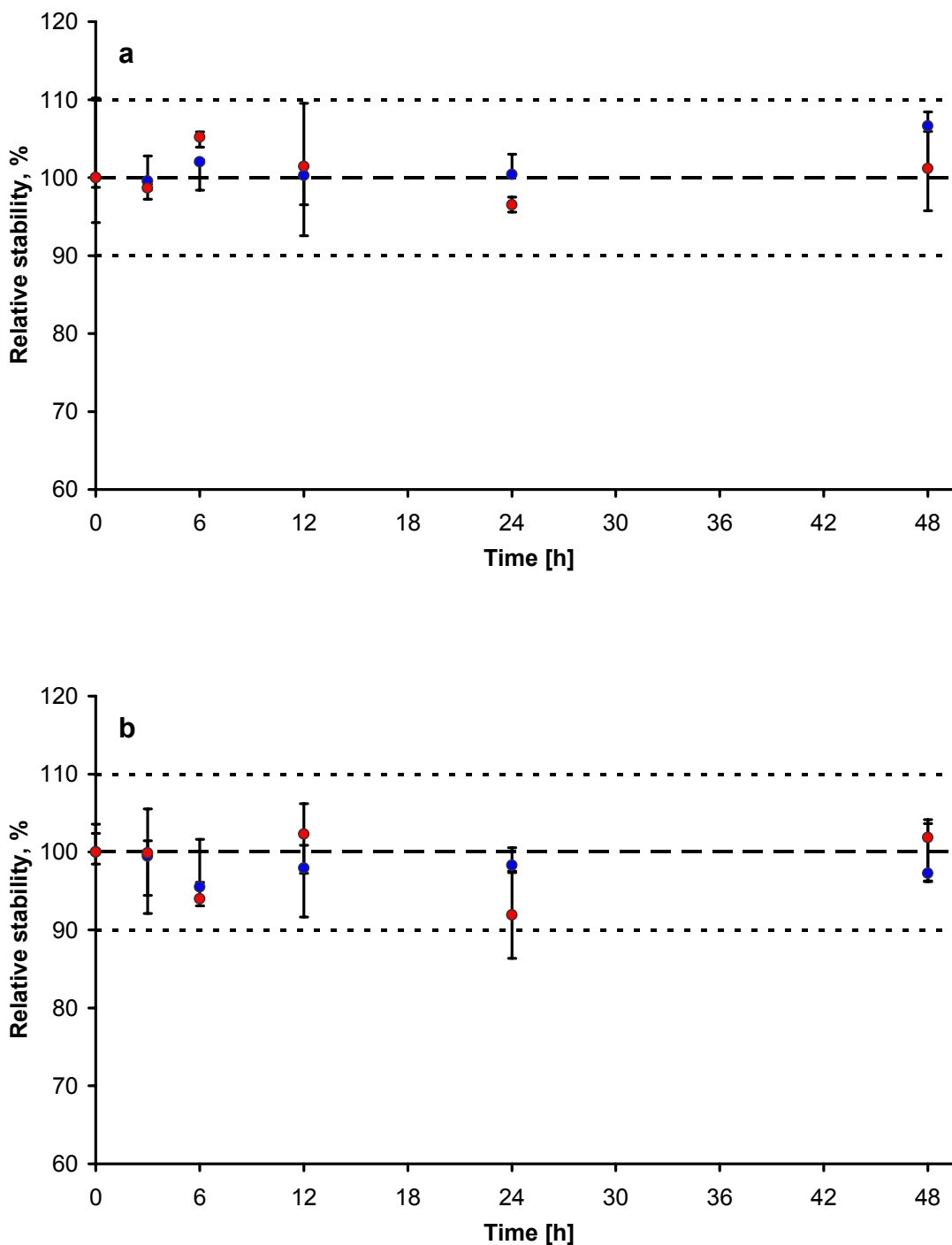


Fig. 28 In vitro stability investigation of linezolid (LZD) inside the static in vitro model, using nominal LZD concentrations of $C_{LZD} = 0.5 \mu\text{g/mL}$ (red data points) and $10.0 \mu\text{g/mL}$ (blue data points) in Mueller-Hinton broth at 36°C with (a) and without (b) bacteria, showing the relative stability as medians and ranges of three aliquots vs. time; dashed line: 100% relative stability; dotted lines: 90% and 110% relative stability, respectively.

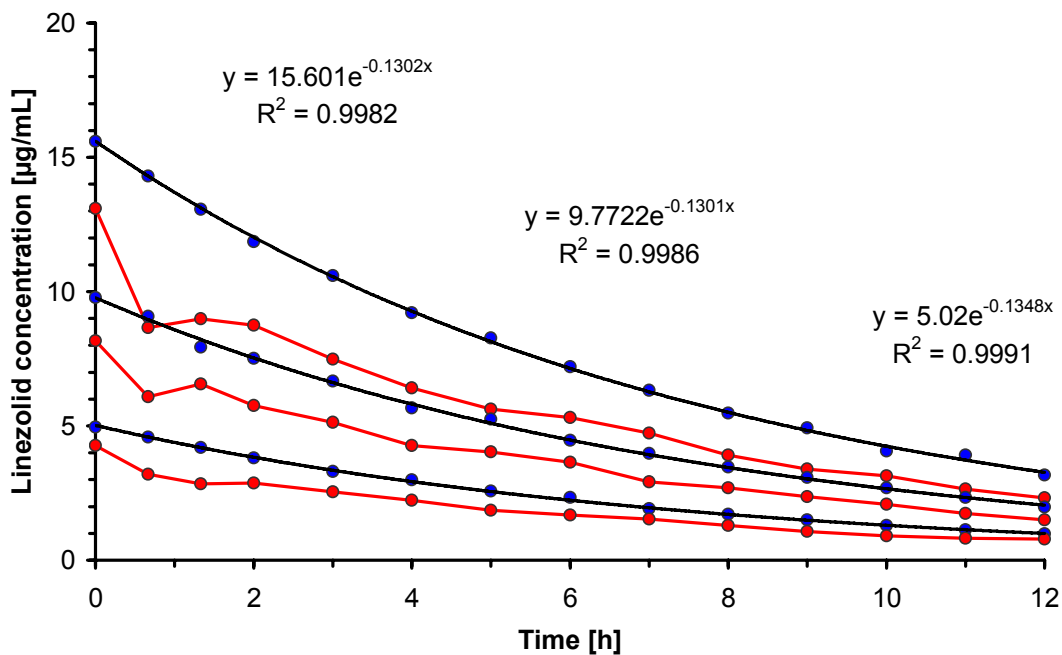


Fig. 29 Linezolid (LZD) concentration-time courses obtained from the preliminary investigations using the dynamic *in vitro* model, for samples taken directly through the flask neck (red data points) and the respective samples taken through the membrane filter unit (blue data points), using log-linear regression (black solid lines) for the latter type of samples, showing the respective model equations with y = LZD concentration, x = time, and R^2 = coefficient of determination.

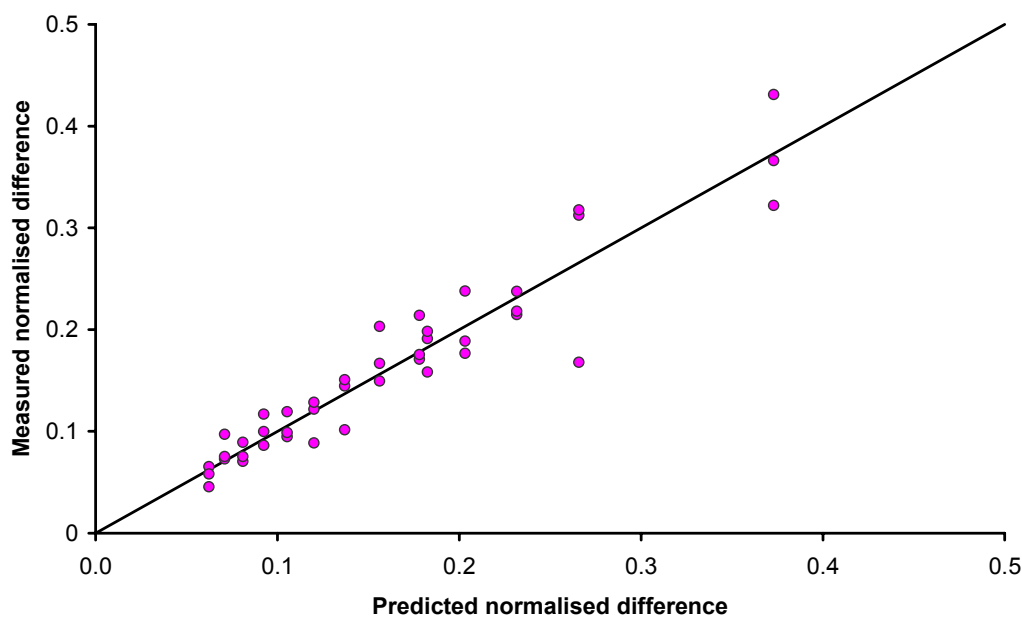


Fig. 30 Goodness of fit plot of the correction factors/function for linezolid concentrations obtained from preliminary investigations using the dynamic *in vitro* model (without bacteria): measured vs. predicted normalised differences, showing symmetrically distributed data points around the line of identity (black solid line).

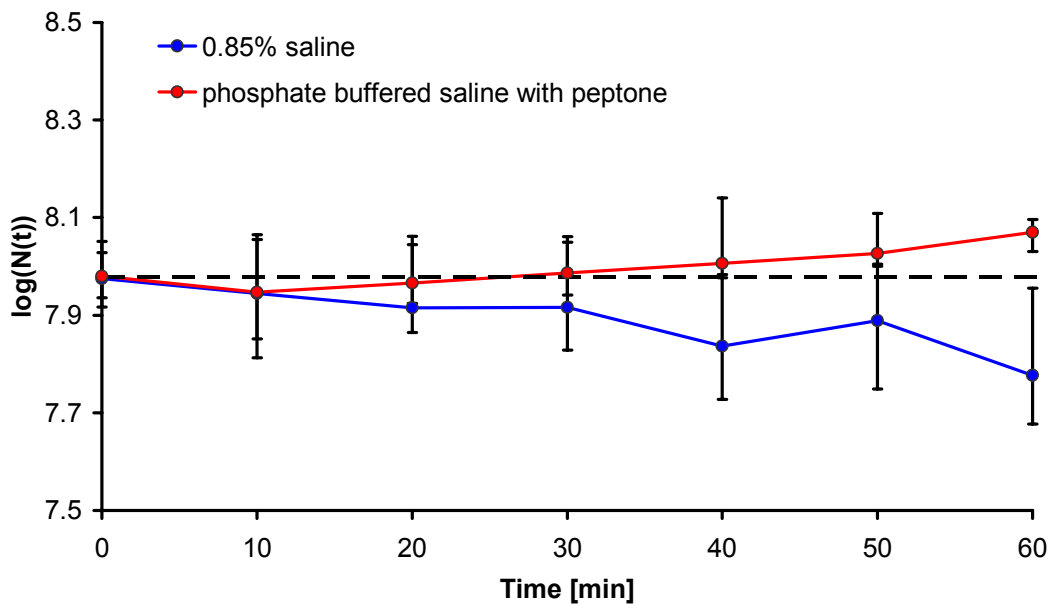


Fig. 31 Semi-logarithmic bacterial concentration- $N(t)$ -time courses for investigating the bacterial survival of *S. aureus* (ATCC 29213) in 0.85% saline (blue data points) and in phosphate buffered saline with peptone (red data points), showing the medians with 5% and 95% percentiles as error bars calculated from eight aliquots; the dashed line refers to the median initial bacterial concentration at $t = 0$ min.

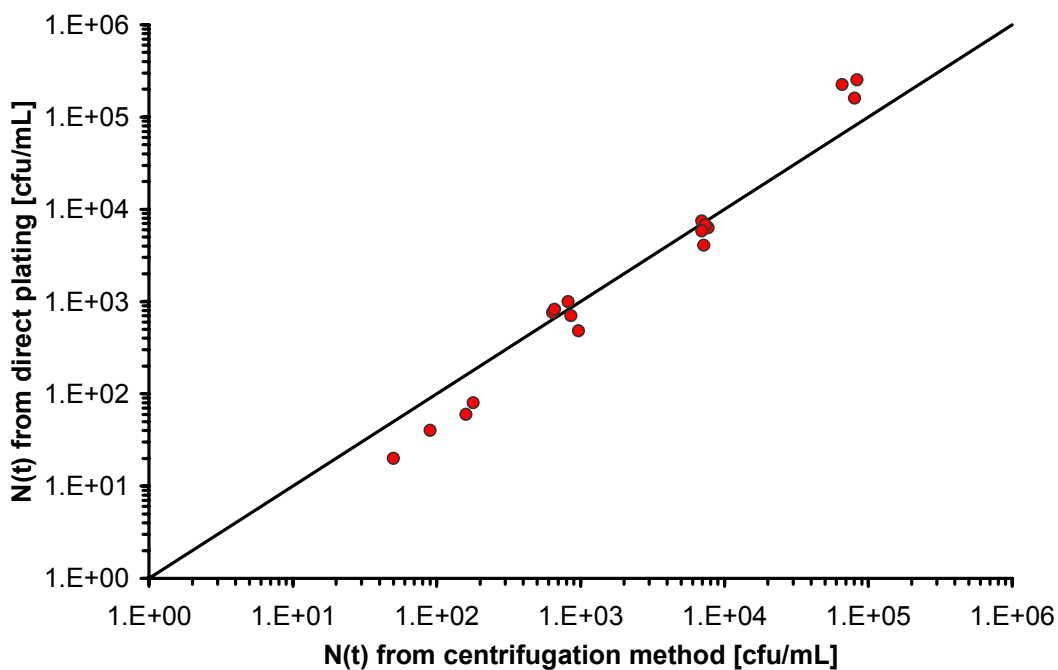


Fig. 32 Bacterial concentrations ($N(t)$) of *S. aureus* (ATCC 29213) using direct plating vs. the centrifugation method (red data points), with the line of identity (black solid line).

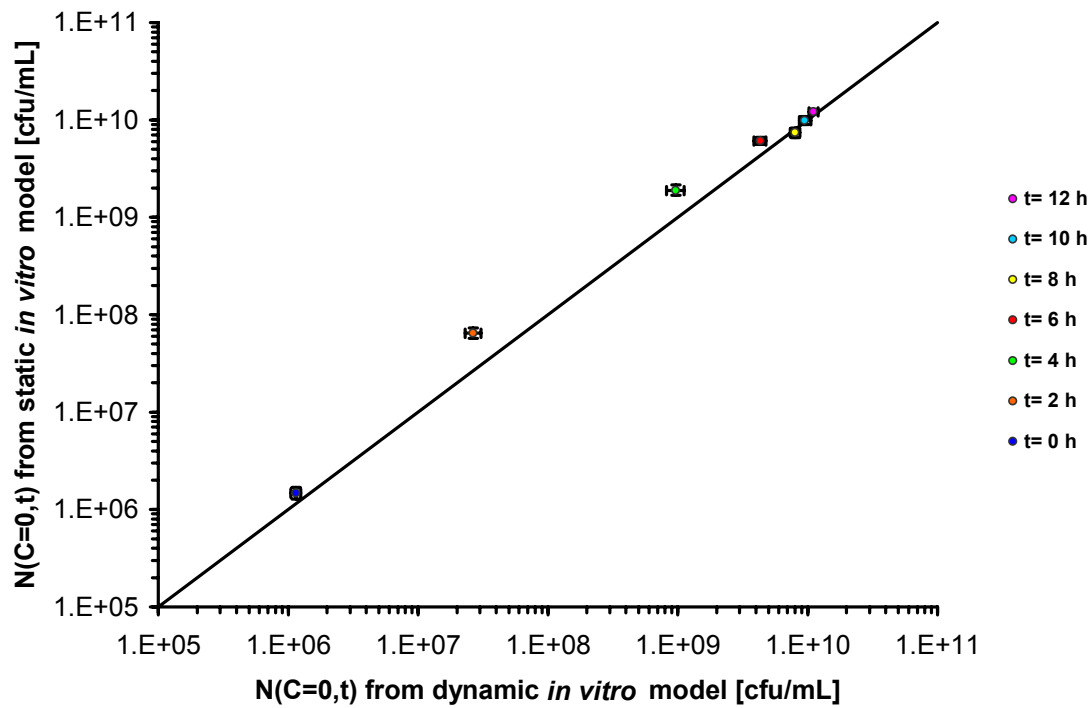


Fig. 33 Comparison of bacterial growth of *S. aureus* (ATCC 29213) in the static and dynamic *in vitro* model, showing the respective geometric means of the bacterial concentrations measured without linezolid exposure ($N(C=0, t)$) at different time points (coloured data points), error bars referring to the corresponding confidence intervals ($CI_{95\%}$), and the line of identity (black solid line).

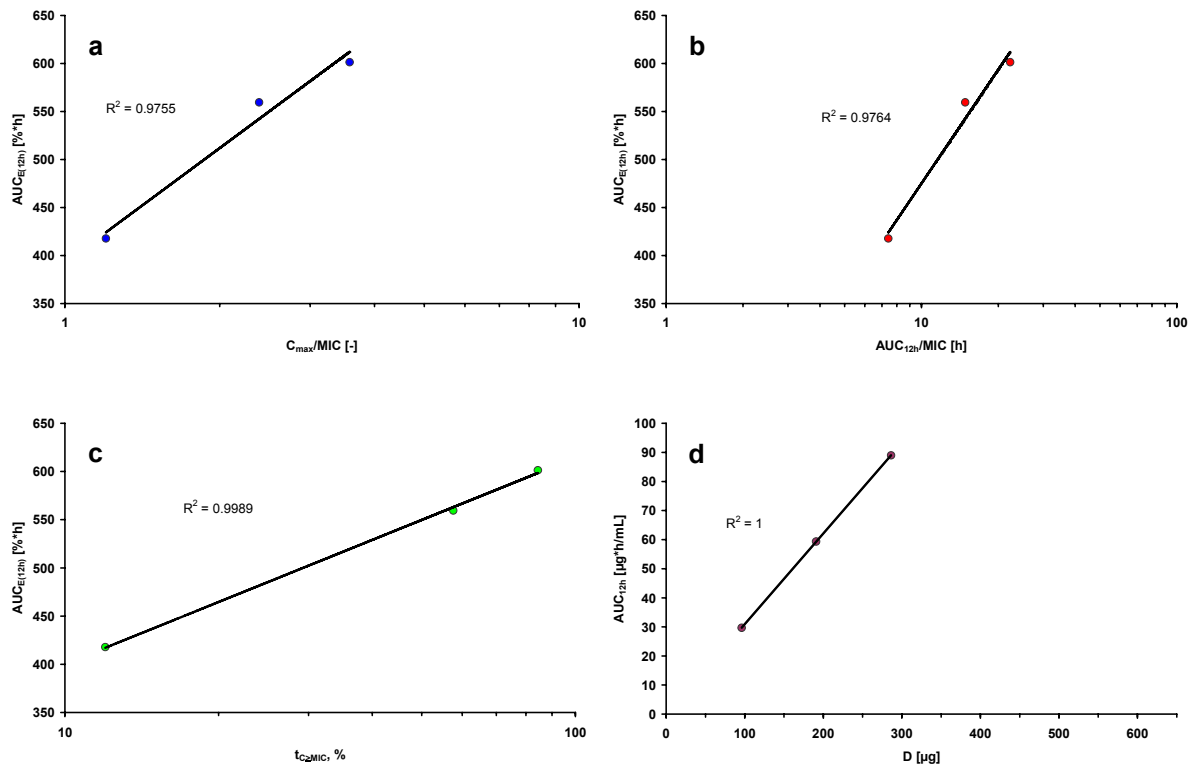


Fig. 34 Correlation analysis for data obtained from the three imitated i.v. bolus injections of linezolid (LZD), showing the *in vitro* pharmacodynamic outcome, $AUC_{E(12h)}$ = area under the effect-time curve after 12 h, vs. the three pharmacokinetic/pharmacodynamic indices: (a) C_{max}/MIC , (b) AUC_{12h}/MIC and (c) $t_{C>MIC}$, and vs. (d) the administered dose (D), with C_{max} = maximal LZD concentration, MIC = minimum inhibitory concentration (at 24 h), AUC_{12h} = area under the LZD concentration-time curve after 12 h, $t_{C>MIC}$ = time with the LZD concentration $\geq MIC$, and R^2 = coefficient of determination.

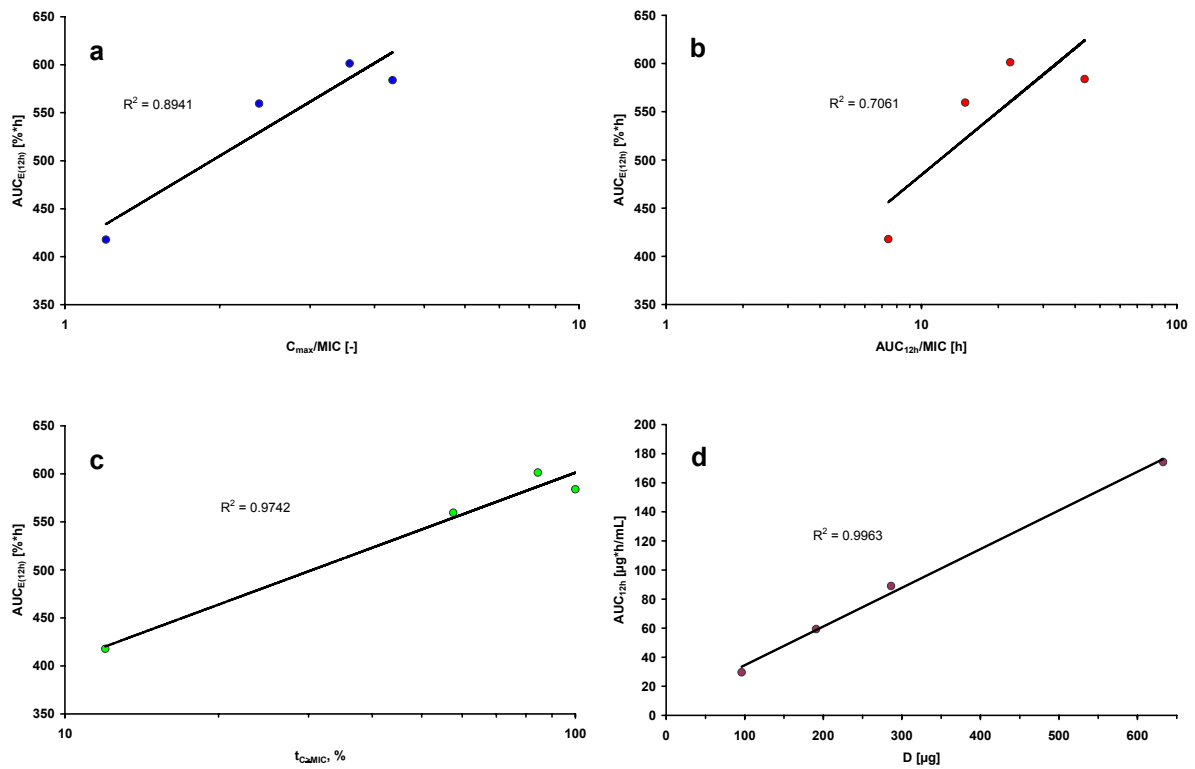


Fig. 35 Correlation analysis for data obtained from all four imitated i.v. linezolid (LZD) exposure profiles, showing the in vitro pharmacodynamic outcome, $AUC_{E(12h)}$ = area under the effect-time curve after 12 h, vs. the three pharmacokinetic/pharmacodynamic indices (a) C_{max}/MIC , (b) AUC_{12h}/MIC and (c) $t_{C \geq MIC}$, and vs. (d) the administered dose (D), with C_{max} = maximal LZD concentration, MIC = minimum inhibitory concentration (at 24 h), AUC_{12h} = area under the LZD concentration-time curve after 12 h, $t_{C \geq MIC}$ = time with the LZD concentration $\geq MIC$, and R^2 = coefficient of determination.

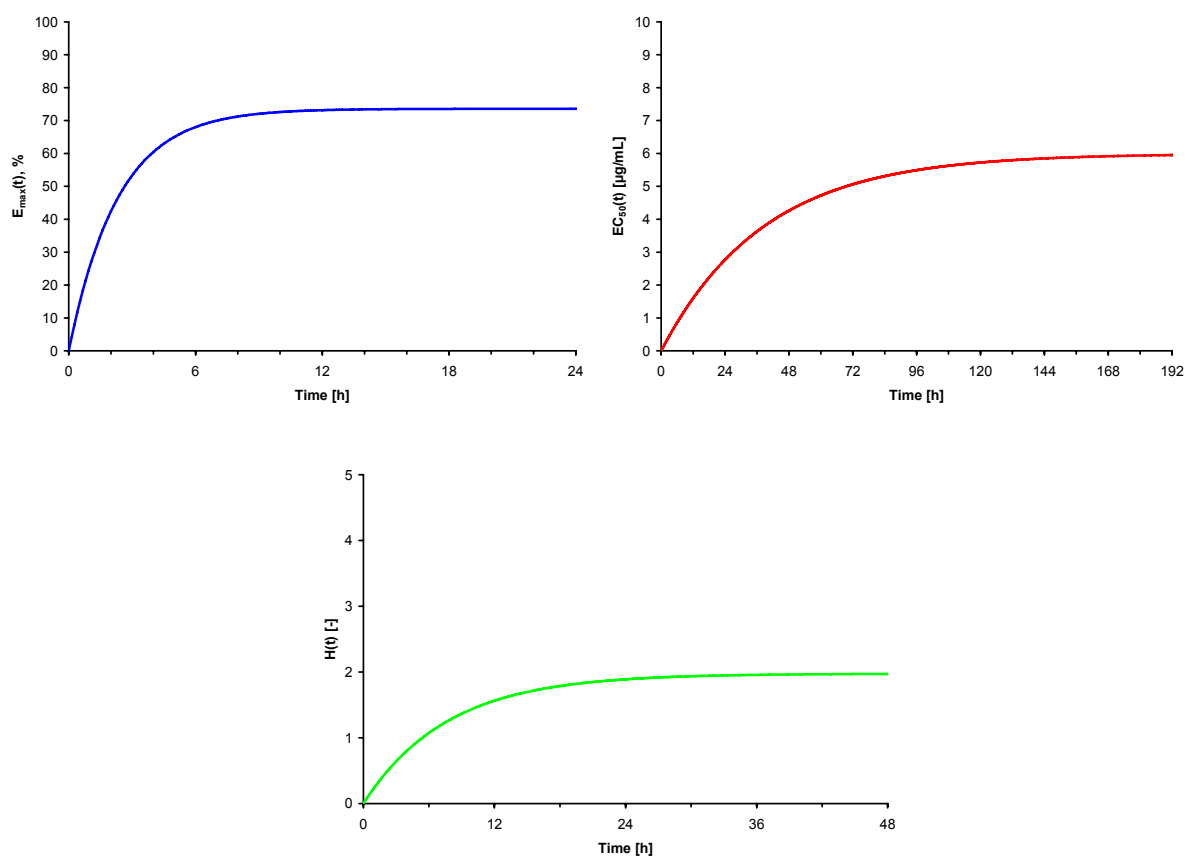


Fig. 36 Time courses of the three sub functions $E_{max}(t)$ (blue curve), $EC_{50}(t)$ (red curve) and $H(t)$ (green curve) of the final pharmacokinetic/pharmacodynamic model (see 3.3.4), using the model parameter estimates from modelling the combined data set (I+II).

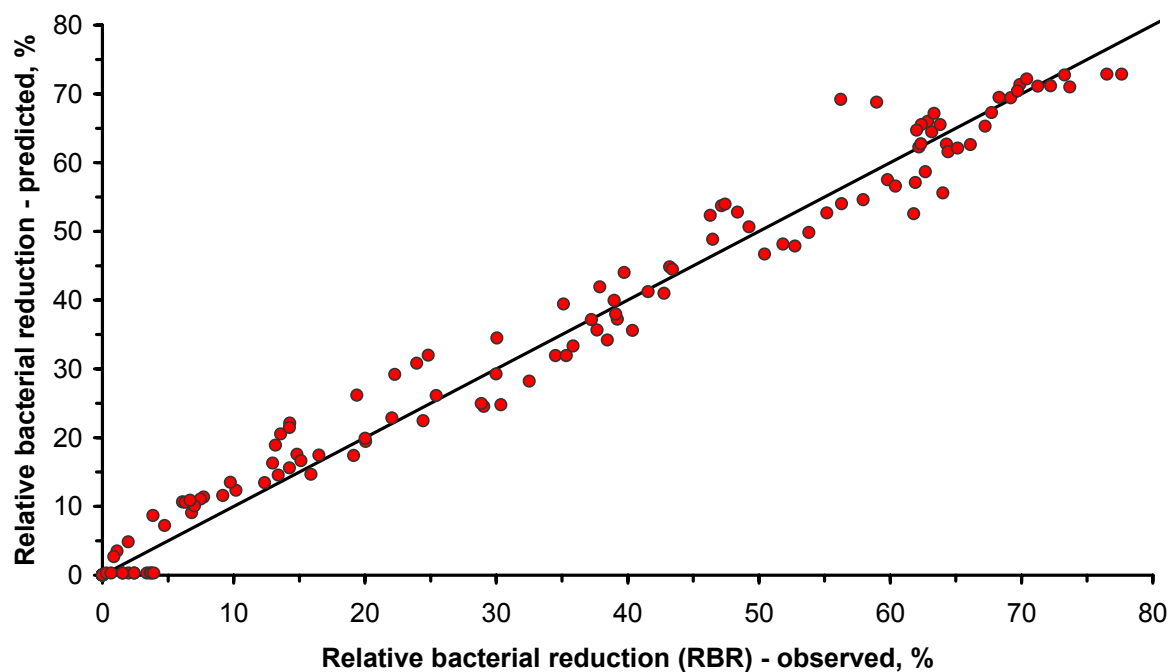


Fig. 37 Goodness of fit plot for the final pharmacokinetic/pharmacodynamic model (see 3.3.4): Relative bacterial reduction (RBR) predicted vs. RBR observed in the static and dynamic *in vitro* model, additionally showing the line of identity (black solid line).

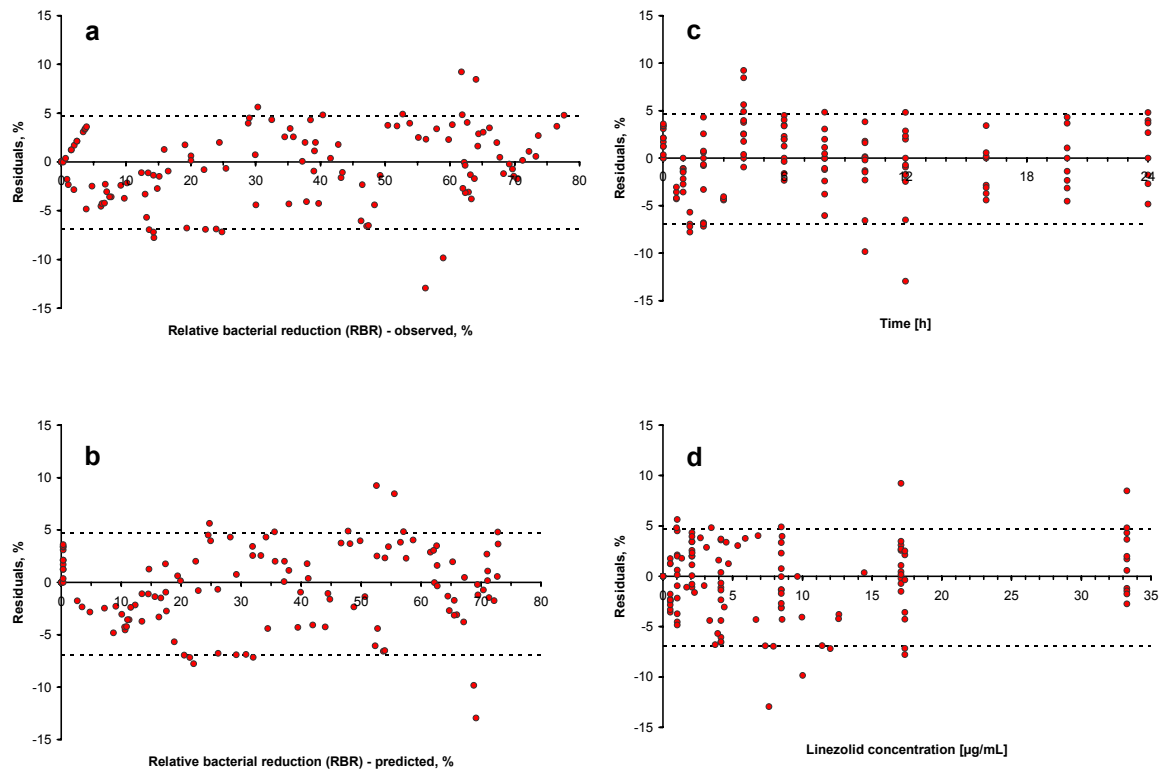


Fig. 38 Goodness of fit plots for the final pharmacokinetic/pharmacodynamic model (see 3.3.4): Residuals (= RBR observed – RBR predicted) vs. (a) the relative bacterial reduction (RBR) observed in the static and dynamic *in vitro* model, vs. (b) the RBR predicted by the final model, vs. (c) the linezolid (LZD) exposure time, and vs. (d) the LZD concentration investigated in the static and dynamic *in vitro* model, additionally showing the respective 5% and 95% percentiles (dashed lines).

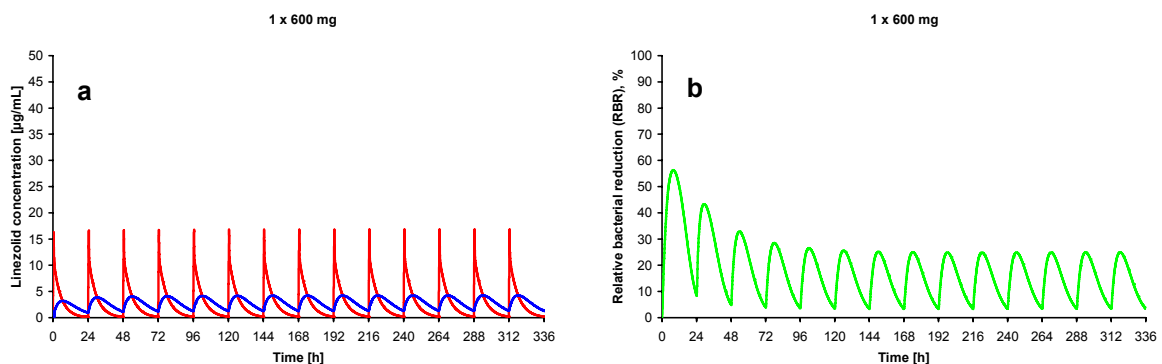


Fig. 39 Deterministic *in silico* simulation for linezolid (LZD) imitating the dosing regimen of 600 mg once daily, showing (a) the LZD concentration-time courses in plasma (red curve) and at the 'effect site' (blue curve), and (b) the respective effect-time course (green curve).

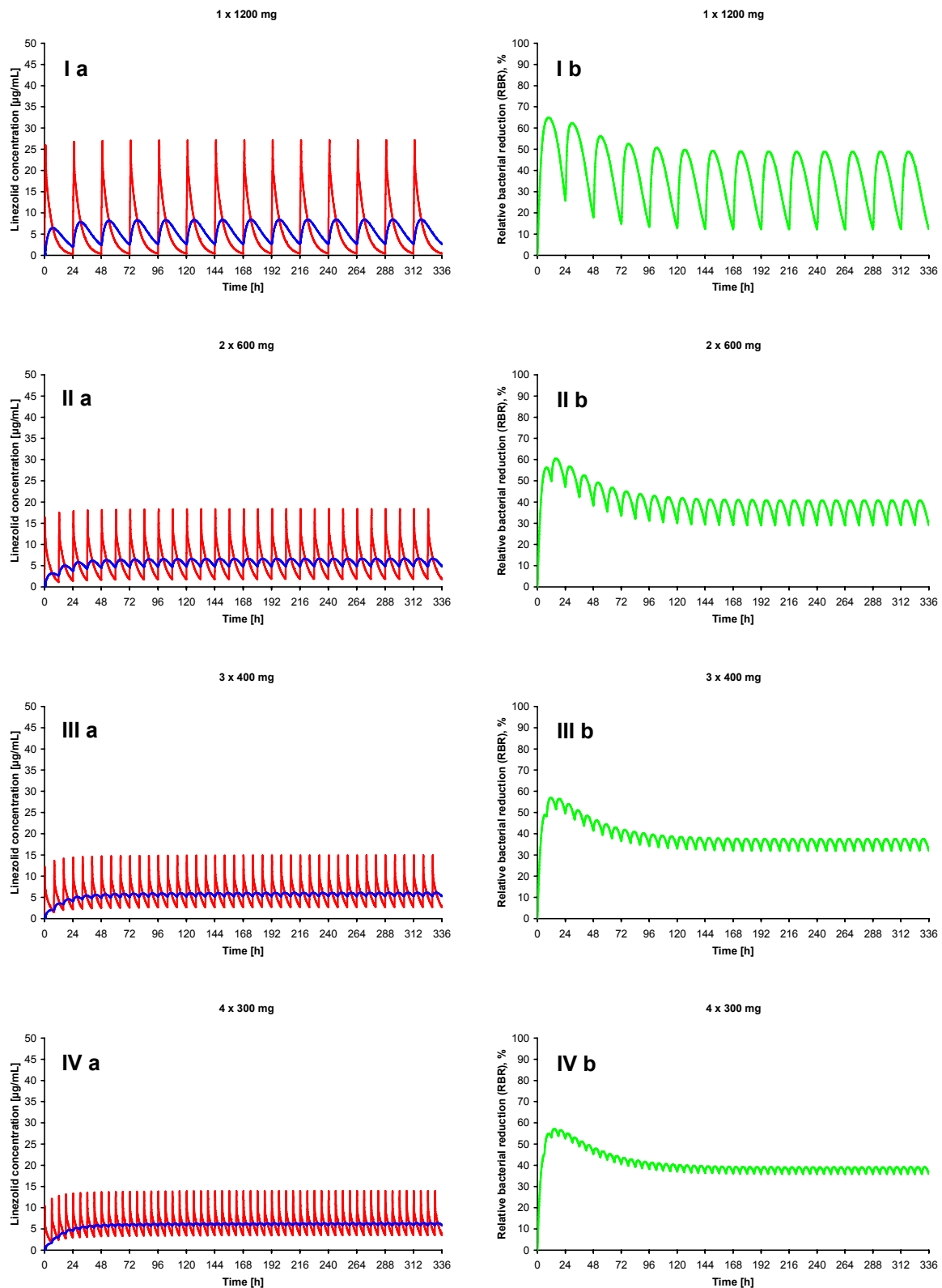


Fig. 40 Deterministic *in silico* simulation for 1200 mg/day linezolid (LZD), imitating dosing regimens of (I) 1200 mg once daily, (II) 600 mg twice daily, (III) 400 mg three times a day, and (IV) 300 mg four times a day, showing (a) the LZD concentration-time courses in plasma (red curves) and at the 'effect site' (blue curves), and (b) the respective effect-time course (green curves).

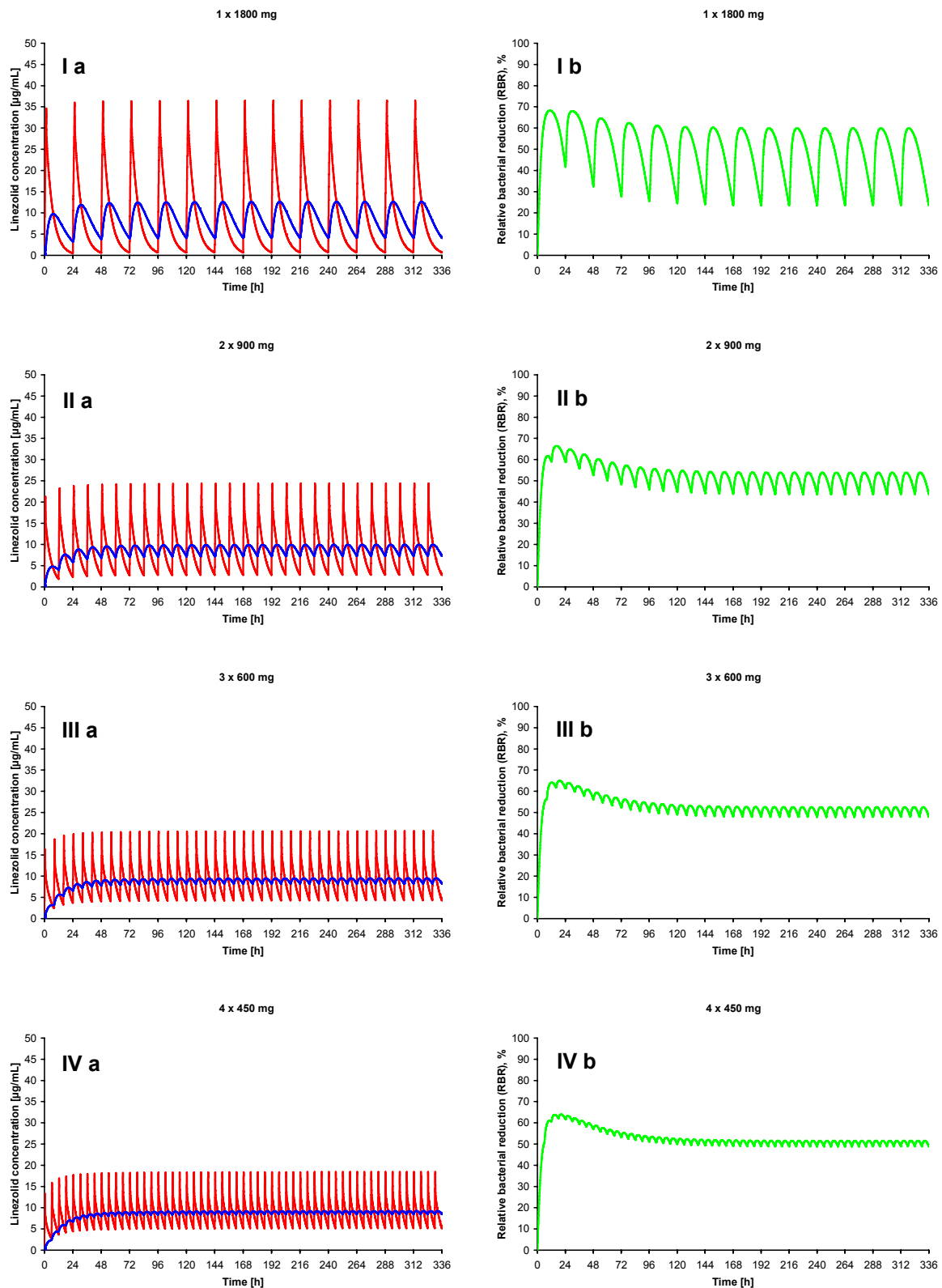


Fig. 41 Deterministic in silico simulation for 1800 mg/day linezolid (LZD), imitating dosing regimens of (I) 1800 mg once daily, (II) 900 mg twice daily, (III) 600 mg three times a day, and (IV) 450 mg four times a day, showing (a) the LZD concentration-time courses in plasma (red curves) and at the 'effect site' (blue curves), and (b) the respective effect-time course (green curves).

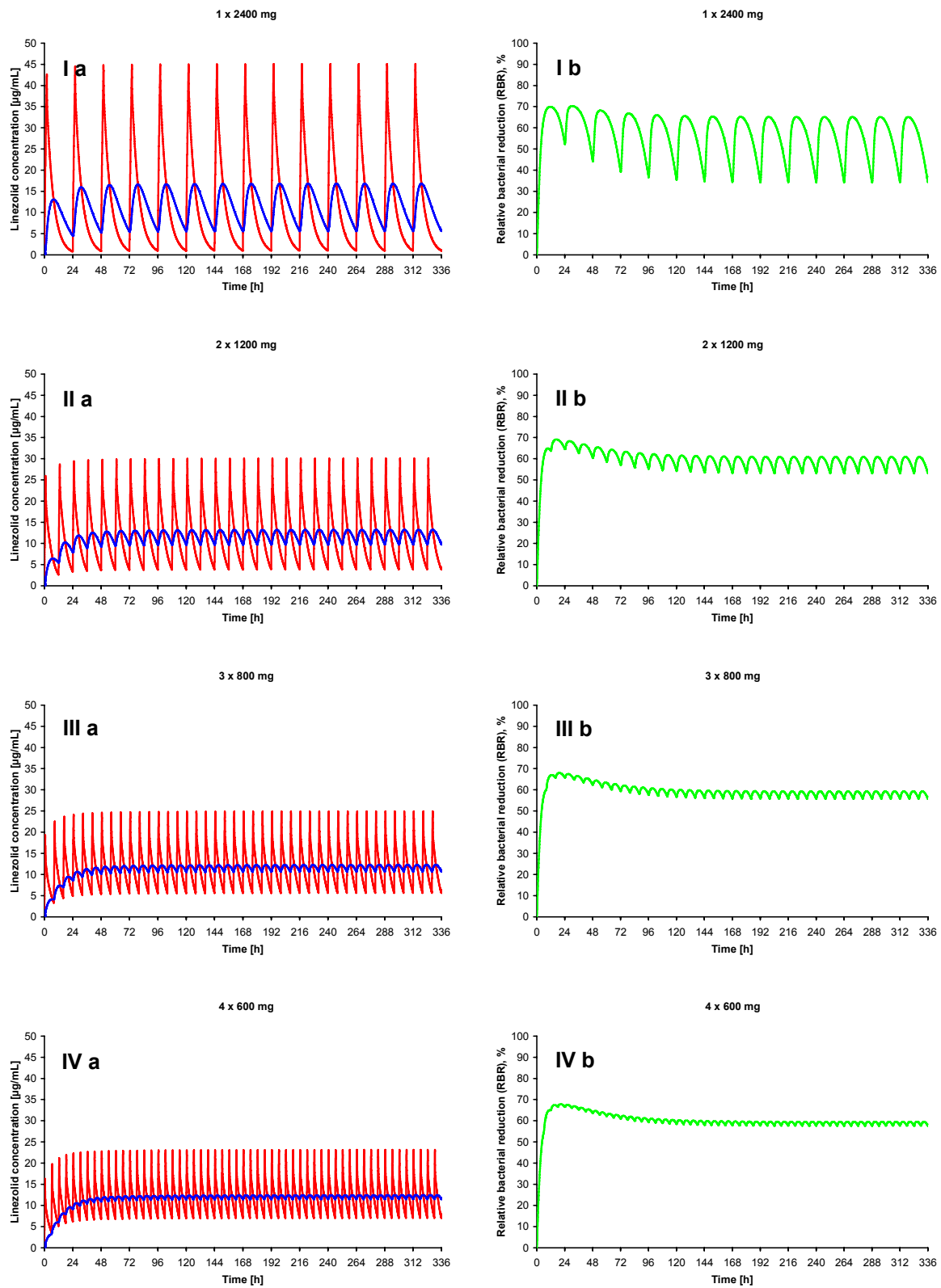


Fig. 42 Deterministic *in silico* simulation for 2400 mg/day linezolid (LZD), imitating dosing regimens of (I) 2400 mg once daily, (II) 1200 mg twice daily, (III) 800 mg three times a day, and (IV) 600 mg four times a day, showing (a) the LZD concentration-time courses in plasma (red curves) and at the 'effect site' (blue curves), and (b) the respective effect-time course (green curves).

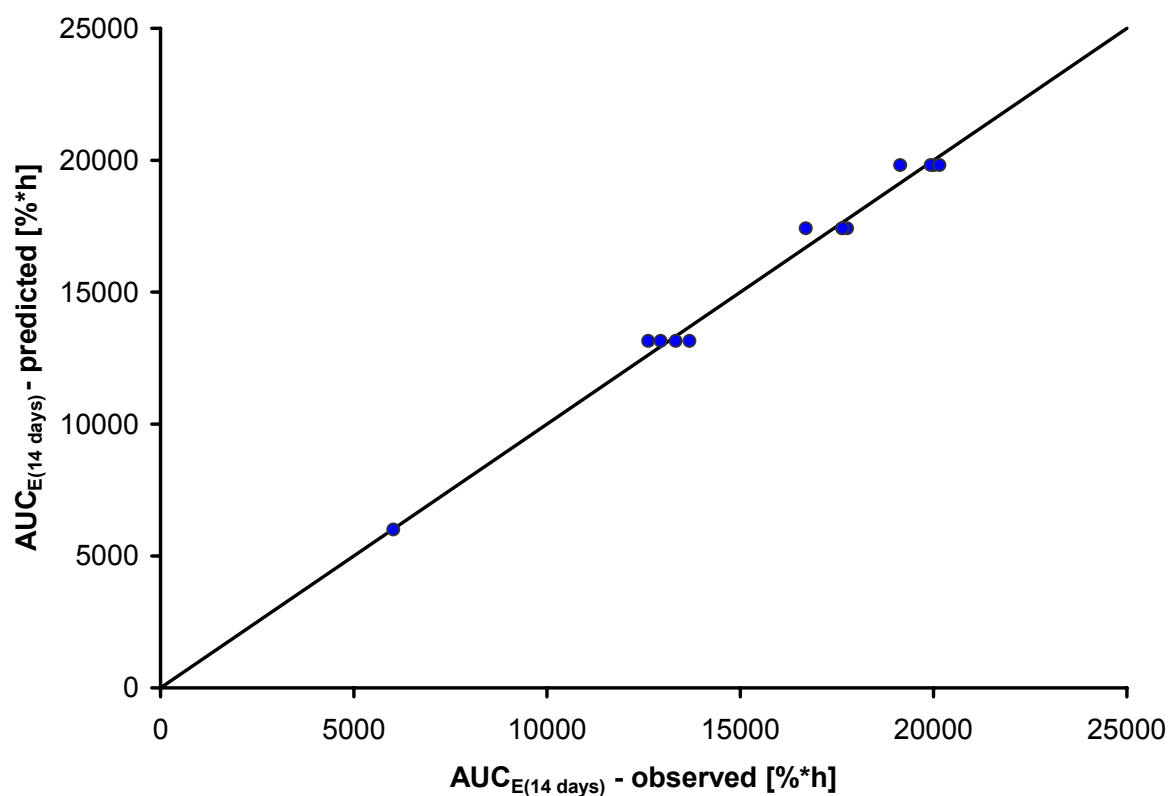


Fig. 43 Goodness of fit plot for modelling the dose-‘response’ relation of the deterministic in silico simulation, showing the model-predicted area under the effect-time course after 14 days of linezolid therapy ($AUC_{E(14 \text{ days})}$) vs. the observed $AUC_{E(14 \text{ days})}$, additionally showing the line of identity (black solid line).

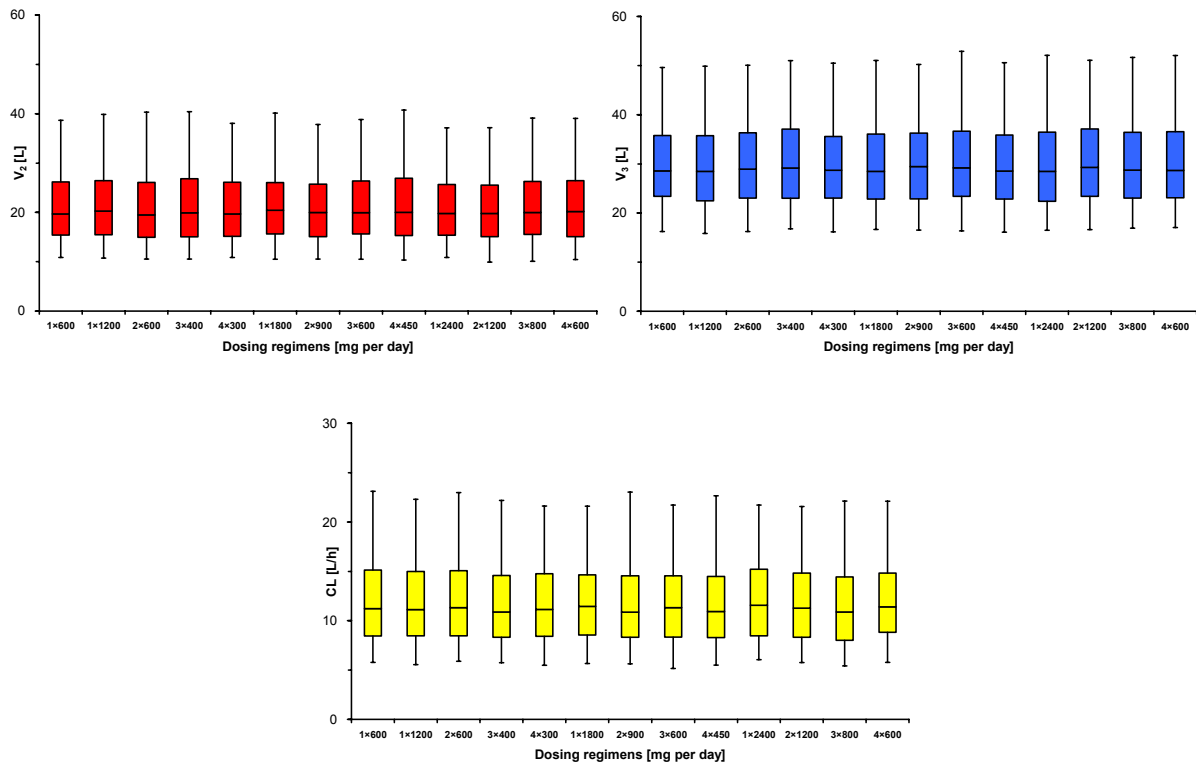


Fig. 44 Box-and-whisker plots of the Monte Carlo simulation, showing the pharmacokinetic parameters clearance (CL, yellow boxes) and volume of distribution in the central (V_2 , red boxes) and peripheral (V_3 , blue boxes) compartments of one thousand virtual 'in silico patients', for each simulated dosing regimen, the respective box refers to the 25% and 75% percentiles, the bisecting line of the box is equal to the median, and the whiskers represent the 5% and 95% percentiles.

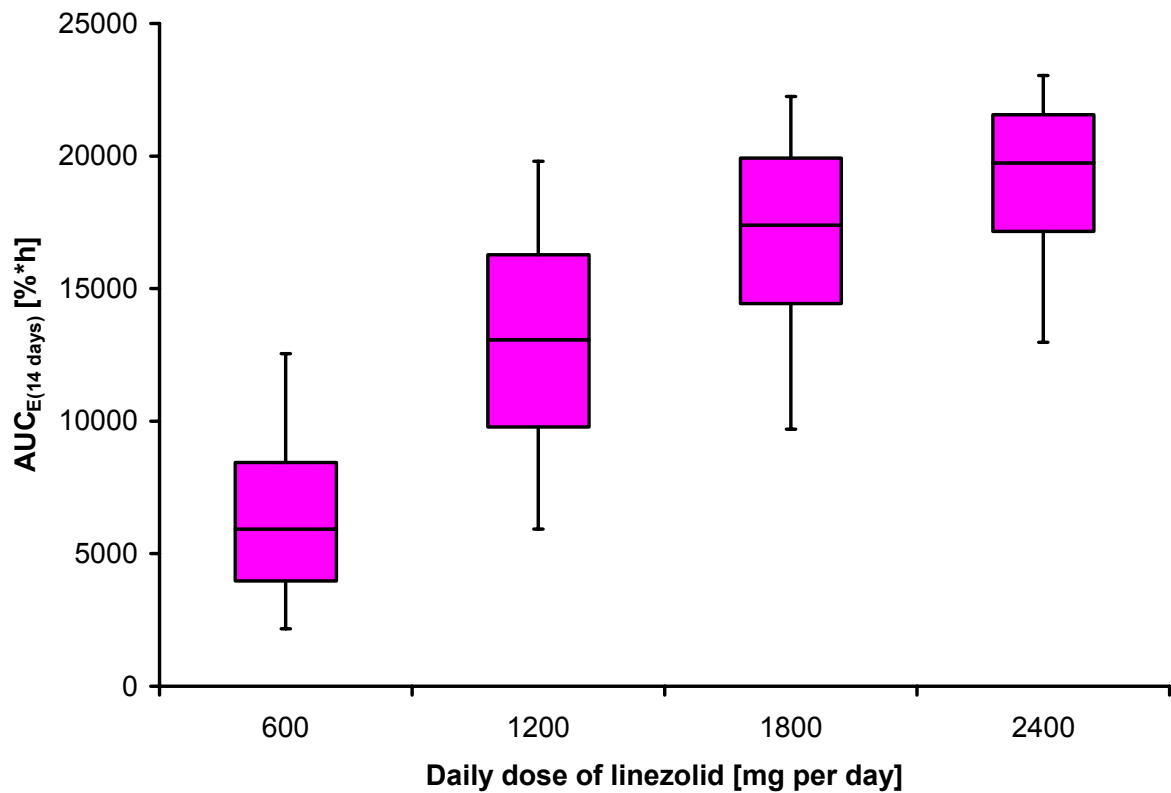


Fig. 45 Box-and-whisker plots for the Monte Carlo simulation, showing the observed area under the effect-time course after 14 days of linezolid therapy ($AUC_{E(14 \text{ days})}$) of thirteen thousand virtual 'in silico patients' with four different daily doses of linezolid, the box refers to the 25% and 75% percentiles, the bisecting line of the box is equal to the median, and the whiskers represent the 5% and 95% percentiles.

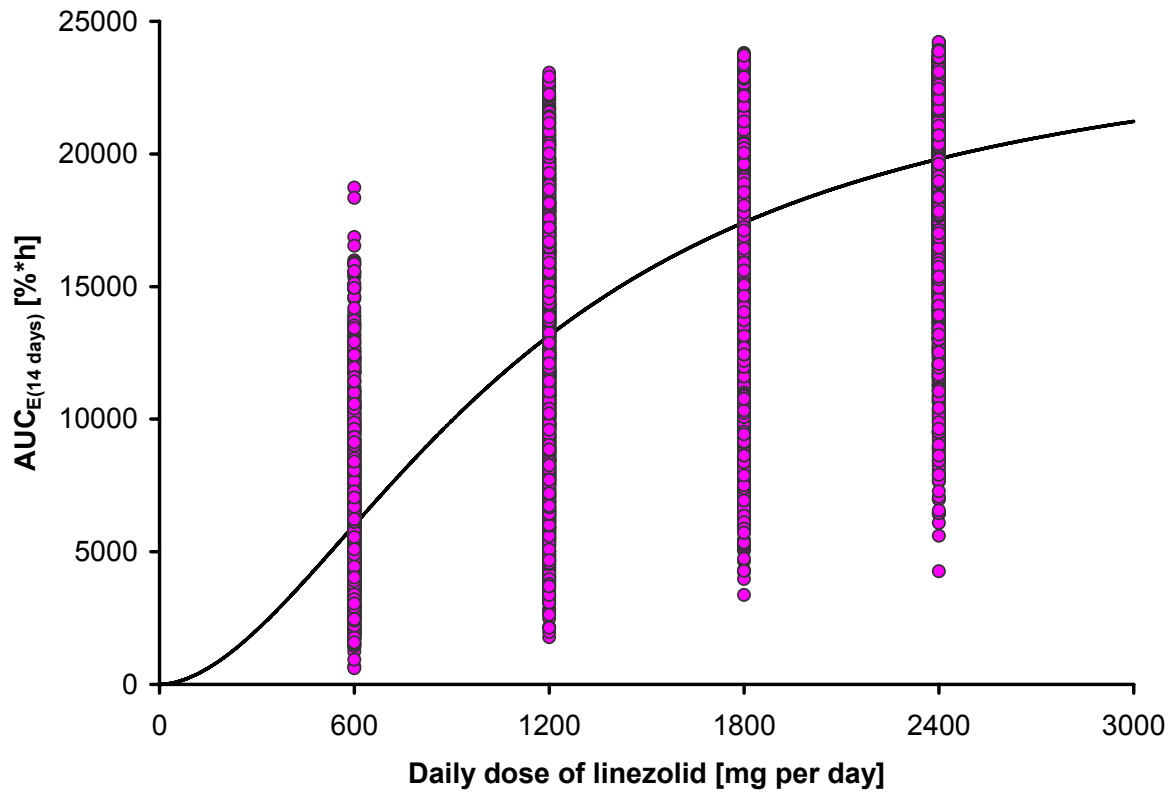


Fig. 46 Dose-'response' relation for the Monte Carlo simulation, showing the observed values for the area under the effect-time course after 14 days of linezolid therapy ($AUC_{E(14 \text{ days})}$, pink data points) of thirteen thousand virtual 'in silico patients' with four different daily doses of linezolid, and the model-predicted dose-'response' curve for the deterministic in silico simulation (black solid line, see 3.4.1).

7.3 Fundamental mathematic methods

The fundamental mathematic methods utilised in this thesis are mentioned in the respective sections and explained in the following text.

7.3.1 Descriptive statistics

For descriptive statistics of the experimental data, different statistical measures of central tendency, variability, precision and accuracy were calculated, according to the attributes of the respective data variable [193]. The descriptive data analyses were performed via Excel.

7.3.1.1 Measures of central tendency

- *Arithmetic average (or mean)*: Sum of the observations divided by the number of observations [194], which describes a normally distributed population [195].
- *Geometric mean*: The n^{th} root of the product of n observations, meaningful as measurement of population growth [194].
- *Median*: Value which divides the data ranked in order in half, a half being less and a half being greater than the median [194]. The median is unaffected by outliers and useful when continuous data are not normally distributed [196].

7.3.1.2 Measures of variability, precision and accuracy

- *Range (R)*: Difference between the smallest and the largest value in the data set [194].
- *Quantiles (or percentiles, %)*: The n^{th} quantile denotes a value below which n percent of the data, ranked in order, are found [194].
- *Interquartile range (IQR)*: Interval between the 25th and 75th quantiles, a measure of variability directly related to the median [196].
- *Standard deviation (SD)*: Estimate of the degree of scatter of individual sample data points about the sample mean [196], for a normally distributed population [195].
- *Coefficient of variation (CV), %*: Percentaged ratio of the SD to the mean [194].

- *Relative error* (RE), %: Percentaged ratio of the difference between the estimated value and the nominal value, to the nominal value [113].

7.3.2 Inferential statistics

Inferential statistics imply the use of statistical methods to make inferences concerning certain unknown aspects of a population. Two main aspects of inferential statistics are *estimation* and hypothesis *testing* which are both briefly explained in the following text.

7.3.2.1 Estimation

Statistical parameters derived from samples, so called point estimates, are often utilised to estimate the true population parameters. These estimates are more or less acceptable surrogates for the unknown true values. Thus, it is useful to calculate an interval that is apt to contain the true parameter value, to clearly evaluate the quality of these estimates. These intervals are known as *confidence intervals* [194, 196]:

7.3.2.1.1 Confidence interval

The confidence interval (CI) of an estimated statistical parameter, e.g. the mean of a sample set, is equal to the range of values likely to be representative of the respective true population parameter. The degree of confidence can be arbitrarily chosen, but most frequently expressed as the 95% CI (CI_{95%}) [196]. In this thesis, the CI_{95%} was numerically estimated via bootstrapping (see 2.4.6.1 and 2.5.1.5.2).

7.3.2.2 Hypothesis testing

Statistical hypothesis testing contains methods of making statistical decisions (test of significance) using experimental data, to choose between the alternatives to accept or reject the previously made hypothesis, which is generally useful to minimise certain risks. The selection of an appropriate test of significance is dependent on the type of data to be analysed [193], and the number of groups to be compared. *Parametric* tests of statistical significance are based on statistical parameters, e.g. mean or SD, and thus appropriately used for most (normally distributed) continuous variables [195]. For continuous data that are not normally distributed, *nonparametric* tests should be preferred [197]. For hypothesis testing of the experimental data, the following two tests of significance were used.

7.3.2.2.1 Analysis of variance

The analysis of variance (ANOVA) is a parametric test of significance, assuming *normality* of the population from which the samples were drawn, *homogeneity* of the variances of the population and *independence* of the data points within the sample group. ANOVA is an accepted method of comparing two or more groups from one experiment, whereas the α -level, i.e. the probability of making a type one error [198], is held constant at the preset level [195]. In the present work (see 3.1.1, 3.2.1 and 3.2.3.1), the one-way ANOVA was performed via Excel with $\alpha = 0.05$ [115]. In case of log-normally distributed data, the respective log-transformed data set was used.

7.3.2.2.2 Kruskal-Wallis test

The Kruskal-Wallis one-way analysis of variance by ranks (Kruskal-Wallis test) is the nonparametric analogue of a one-way ANOVA [197, 199]. It is an extension of the rank sum test, that can be used when two or more groups are compared, by testing the equality of population medians among the groups [194]. The Kruskal-Wallis test was performed (see 3.4.2) via SPSS with $\alpha = 0.05$, in case of not normally or respectively unknown distributed data [200].

7.3.3 Correlation analysis

Correlation is an exploratory technique used to examine whether the values of two variables are significantly related, e.g. for linear correlation, to examine whether the values of both variables change in a consistent way. However, there is no expectation that the value of one variable can be predicted from the other, or that there is any causal relation between them. Furthermore, the correlation will be the same, if the two variables become interchanged [117, 199]. For the present work, the following measurements of correlation were applied via Excel [114].

7.3.3.1 Pearson correlation coefficient

The Pearson correlation coefficient (r) is used to quantify the strength of a *linear* relation between two continuous variables that are *normally* distributed. In case of unequal variances, an appropriate *weighting* scheme (see 7.3.4.3) can be implemented [101]. The value r can be of any value from -1 to +1, whereas the two extreme cases mean perfect (negative / positive) linear correlation, and a value of

zero shows the lack of a linear correlation between the two investigated variables [199, 201].

7.3.3.2 Coefficient of determination

The coefficient of determination (r^2) is defined as the squared Pearson correlation coefficient, and implies the fraction of variation that is shared by both variables [117].

7.3.4 Regression analysis

Regression analysis describes the functional relationship between two or more variables by fitting a mathematic model to the experimental data. In contrast to correlation analysis, an underlying relation is assumed, i.e. the variables cannot be interchanged. Thus, the value from one variable can be predicted by the other variable(s) [199]. Generally, two types of regression analysis exist, these are *linear* and *nonlinear* regression (see 7.3.4.4 and 7.3.4.5), which were both applied in the present work (see 2.3.2.4, 2.5, 3.1.2.2 and 3.4.1).

7.3.4.1 Models, variables, parameters and constants

The regression *model* is a mathematic equation that defines the outcome variable y (dependent variable) as a function of one or more other (independent) variable(s) x and one or more model parameter(s). Thus, y depends on the value of x , but not vice versa. The model *parameters* define the properties of the regression model. Beside parameters and variables, regression models often include one or more *constants*. At the beginning of the regression analysis, the values of the included constants are preset, whereas the values of the respective model parameters are unknown. The aim of the regression analysis is to find the best-fit values of the parameters that allow to describe the total experimental data and to predict y from x [125]. Regression analysis most commonly estimates the best-fit values of model parameters by using the least squares (LS) method, as utilised for the present work (see 2.5.1.5).

7.3.4.2 Least squares method

The LS method, first described by Carl F. Gauß, is a *maximum likelihood estimation* technique which assumes that y is normally distributed and x is error-free. Given this specific assumption, the LS method helps to decide which values of model parameter are the most likely ones to perform the best-fit to the experimental data. The LS

method calculates the sum of the squares of the vertical distances (*sum of squared residuals*, SSR) between the measured data points (y_{observed} , with amount n) and the regression line or curve ($y_{\text{predicted}}$), respectively (eq. A1).

$$SSR = \sum_{i=1}^{i=n} (y_{\text{observed},i} - y_{\text{predicted},i})^2 \quad \text{eq. A1}$$

The functional aim of the LS method is to minimise the SSR to obtain parameter values with the highest probability, i.e. the best-fit values [117].

7.3.4.3 Weighted least squares method

Regression analysis using the SSR is based on the assumption that the dependent variable y follows a Gaussian distribution (normally distributed) containing a *homoscedastic* error, i.e. the standard deviation is assumed to be the same for all measured data points. However, for real data this is often not true, i.e. data with a so called *heteroscedastic* error are present. In this case, the standard LS method may lead to biased regression curves and parameter values, respectively. Additional flexibility can be added to the regression analysis by means of *weighting*. The weighted SSR (WSS) is calculated (eq. A2) by multiplying each squared residual by a weighting factor (W_i) [101, 117, 125, 202].

$$WSS = \sum_{i=1}^{i=n} (y_{\text{observed},i} - y_{\text{predicted},i})^2 \cdot W_i \quad \text{eq. A2}$$

7.3.4.4 Simple linear regression

Simple linear regression describes the functional relationship between y and x as 'straight line' with $y = m_S \cdot x + b$ as regression model. The regression model contains only the two parameters m_S and b as slope and intercept, respectively. Here, an *algebraic* tool can be used to exactly calculate the best-fit values of the two parameters directly from the original data set [199]. For the current work (see 3.1.1), linear regression was applied via Excel [203]. In case of data containing a *heteroscedastic error*, linear regression was applied with an appropriate *weighting* scheme (see 2.3.2.4), according to Almeida et al. [101].

7.3.4.5 Nonlinear regression

Nonlinear regression is more complex than simple linear regression. As there is no algebraic tool available, best-fit values of the respective parameters cannot be calculated directly by the observed values of y and x . Instead, nonlinear regression uses *numeric iteration* for the parameter adjustment, which is frequently called mathematic *modelling*. The objective of the modelling process is to adjust the model parameters to obtain the 'optimal' fit (estimated best-fit) to the experimental data.

7.3.4.5.1 Numeric iteration approach

The iterative approximation approach of mathematic modelling first needs an *initial estimate* for each model parameter and possibly lower and upper limits as rational *constraints*. The 'roughly' estimated initial values can be obtained from graphical or other tools. Subsequently, the values of $y_{\text{predicted}}$ are obtained from the regression model for each x_{observed} , and the respective SSR (or WSS) is calculated. Then, the parameter values will be iteratively adjusted to minimise the SSR (or WSS) in order to fit the regression curve to the observed data points [117].

The process of iterative parameter adjustment for minimising the SSR (or WSS) can be very complex, and thus is generally performed via automated *optimisation algorithms*, as utilised in this thesis (see 2.5.1.5). These algorithms are numeric tools for optimising, i.e. minimising or maximising, a selected *objective function* (OBJ) of a mathematic 'problem'. The calculated value of the OBJ is dependent on the current parameter values which have to be adjusted for solving the considered mathematic 'problem'. The numerically found *extremum* (minimum or maximum value of the OBJ) can either be *global*, i.e. truly the highest or lowest function value, or just *local*, i.e. the highest or lowest value in a finite neighbourhood and not on the boundary of that neighbourhood. However, finding the global extremum is the ultimate aim of this approach. As there is no perfect optimisation algorithm available, different algorithms can be combined [204]. For nonlinear regression, generally the SSR (or WSS) serves as OBJ, which is supposed to be minimised by the chosen algorithm. In the present work, the *Generalized Reduced Gradient* (GRG2) algorithm has been used in Excel to minimise the OBJ (see 2.5.1.5). The GRG2 algorithm was developed by Leon Lasdon (University of Texas), and Allan Waren (Cleveland State University) [205].

7.3.5 Solving ordinary differential equations

A differential equation is a mathematic equation for an unknown function $f(x)$ of one or several variables that relates the values of the function itself and of its derivatives of various orders. Differential equations play an important role in pharmacometrics, e.g. for PK/PD modelling [1], which have to be integrated ('solved') for their practical application. An *ordinary differential equation* (ODE) is a differential equation in which the unknown function $f(x)$ is a function of a single independent variable (x), e.g. the first-order ODE $df(x)/dx$. The *order* of an ODE is the order of the highest derivatives of the dependent variable appearing in the equation. For this thesis, only first-order ODEs were solved (see 2.6.2 and 3.4).

7.3.5.1 Laplace transform

ODEs are frequently rate of change equations, $df(t)/dt$ with time (t) as independent variable, that describe one or more zero- or first-order process(es). These equations are called *linear* ODEs. For solving such linear equations, i.e. finding $f(t)$, a conventional *algebraic* technique called Laplace transform can be easily applied, as done in the present work (see 3.3.2.2.1 and 7.4).

Basically, Laplace transform replaces the time domain t of the considered time-dependent function $f(t)$ by the complex domain of the *Laplace operator* s , written as \bar{f} . The means by which $df(t)/dt$ is transformed into \bar{f} is given by the *Laplace integral* $L(df(t)/dt)$ calculated from time zero to time infinity (eq. A3) [44, 206, 207],

$$L\left(\frac{df(t)}{dt}\right) = \int_0^{\infty} e^{-s \cdot t} \cdot \left(\frac{df(t)}{dt}\right) \cdot dt = (s \cdot \bar{f}) - f(0) \quad \text{eq. A3}$$

where $f(0)$ refers to the initial conditions, i.e. the value of $f(t)$ at $t = 0$.

7.3.5.2 General partial fraction theorem

The inverse of the Laplace transform can be obtained via the use of the general partial fraction (GPF) theorem. Here, the Laplace transform is transposed in the form of the quotient of two polynomials $P(s)/Q(s)$, where the denominator has a higher degree and contains the factor $s-\lambda_i$, which is not repeated. λ_i 's are the *roots* of the denominator, with amount M . The inverse Laplace transform L^{-1} can be calculated via eq. A4,

$$L^{-1} \left\{ \frac{P(s)}{Q(s)} \right\} = \sum_{i=1}^M \frac{P(\lambda_i)}{Q_i(\lambda_i)} \cdot e^{-\lambda_i \cdot t} \quad \text{eq. A4}$$

where $Q_i(\lambda_i)$ is the value of the denominator when λ_i is substituted for all s terms except for the originally containing λ_i , this term being omitted. The $P(\lambda_i)$ term is obtained by substitution of the appropriate root for every value of s [44, 208]. For the present work, the GPF theorem was utilised for solving Laplace transforms (see 7.4).

7.3.5.3 Fourth-order Runge-Kutta method

For more complex (e.g. nonlinear) ODEs, these equations are often elementary not solvable or too complex to be solved. Then *numeric* integration approaches are needed to provide the ‘best’ estimation for the exact solution. The fourth-order Runge-Kutta (RK4) method is an *iterative* approach to numerically solve ODEs with a known *initial value*, developed by Carl D. T. Runge and Martin W. Kutta [207]. This method is based on the idea of the *polygonal curve* of the *Euler’s method* with improved accuracy, as described in the following.

For a considered first-order ODE $y' = f(x; y)$ with a given initial value problem $y(x_0) = y_0$, first the *tangent slope* $m_T = (y - y_0)/(x - x_0)$ is calculated for the interval $x_0 \leq x \leq x_1 = x_0 + h_{SS}$, where h_{SS} is the *step size* which essentially determines the accuracy of method. Subsequently, the solution for the considered interval is estimated by the straight line function $y = y_0 + h_{SS} \cdot m_T$.

In contrast to the Euler’s method, the tangent slope is calculated as ‘*averaged*’ slope (m_{av}) based on *four* single slopes (m_{T1-4}) obtained from the boundaries and the centre (i.e. at $h_{SS}/2$) of the considered interval h_{SS} , using different ‘*weights*’: $m_{av} = 1/6 \cdot (m_{T1} + 2 \cdot m_{T2} + 2 \cdot m_{T3} + m_{T4})$. Thus, the RK4 method uses the following calculation rule with $k_{1-4} = h_{SS} \cdot m_{T1-4}$ as auxiliary quantities [207]:

$$y(x_{n+1}) \approx y_{n+1} = y_n + 1/6 \cdot (k_1 + 2 \cdot k_2 + 2 \cdot k_3 + k_4)$$

$$k_1 = h_{SS} \cdot f(x_n; y_n)$$

$$k_2 = h_{SS} \cdot f(x_n + h_{SS}/2; y_n + k_1/2)$$

$$k_3 = h_{SS} \cdot f(x_n + h_{SS}/2; y_n + k_2/2)$$

$$k_4 = h_{SS} \cdot f(x_n + h_{SS}; y_n + k_3)$$

The RK4 method was applied for the *in silico* simulation (see 3.4) to solve the (nonlinear) system of coupled ODEs of the utilised (population) PK model for LZD (see 2.6.2) together with the developed final *in vitro* PK/PD model (see 3.4).

7.3.6 Simulation technique

7.3.6.1 Systems, models and simulations

A *simulation* represents certain key characteristics of a selected (physical or abstract) *system* that is extremely expensive or rare, laborious or resource-intensive to investigate, or not even available in reality, and is based on (e.g. mathematic) models. Mathematic *models* are classified in many ways, e.g. in *deterministic* and *stochastic* models. If a simulation model does not contain any probabilistic (i.e. random) components, it is called deterministic, whereas in a stochastic model at least one variable is random [131], e.g. clearance or volume of distribution as utilised in the present work (see 2.6.3).

Simulation enables the experimenter to replicate an ‘experiment’ as many times as needed, e.g. using different conditions, with minimal additional effort. If the relationships that compose the underlying model are ‘simple’ enough, it may be possible to use mathematic methods to obtain exact information on questions of interest, i.e. an *analytical* solution is available. However, most ‘real world’ systems are too complex to allow realistic models to be evaluated analytically. Thus, these problems must be studied *numerically* via *in silico* simulation to estimate the desired true characteristics of the model [209, 210].

7.3.6.2 *In silico* simulation

In silico simulation is a numeric technique for performing ‘experiments’ on a computer. It involves certain types of mathematic and logical models that describe the behaviour of a considered (economic, engineering or biological) system, to solve a specific ‘problem’. In more detail, *in silico* simulation is a technique of performing *sampling* experiments on the model of the considered system. The system is a set of related *elements* that contains the ‘problem’ to be solved. The simulation model is a representation and abstraction of the respective system that can have *input* and *output variables* and several *parameters*. For instance, *stochastic* simulations sample input variables from particular *distributions* and involve the use of randomness via the

Monte Carlo method (MCM), frequently called *Monte Carlo simulation* (MCS) [131, 210].

7.3.6.3 Monte Carlo method and simulation

The MCM was introduced by Nicholas C. Metropolis and Stanislaw M. Ulam during World War II for a 'realistic' solution of a model, using *randomness* [211], suggested by the gambling casinos at the city of Monte Carlo in Monaco. This method can be used not only for the solution of *stochastic* 'problems', but also for solving *deterministic* 'problems'. Using the MCM can be time-consuming and provides 'only' statistical estimates rather than exact results, but for many 'problems' it may be the only available way to obtain an answer [114, 210].

MCS is a very powerful tool to explore and conduct complex systems where experimental data is limited, e.g. simulating 'real life' scenarios. This frequently used simulation technique is based on repeated random sampling of (a) 'hypothetical' population(s), in order to simulate thousand(s) of different 'hypothetical' cases for the investigated system [113, 190, 209-212]. Randomness is generated on a computer by a *pseudo-random number generator*. Thus, the generated numbers were not truly random. However, in terms of the simulation issue randomness is sufficient, if the generated numbers are uniformly distributed, statistically independent and reproducible [210].

For the present thesis, MCS was applied via Excel for testing various hypothetical dosing regimens for LZD (see 2.6.3). The pseudo-random number generator in Excel (version 2003) is based on the *Wichmann-Hill algorithm* [213, 214], that has been tested for sufficiency [114, 209, 215].

7.4 Mathematic deviations

7.4.1 Derivation of Equation M1

The initial drug concentration (C_0) in the dynamic PD *in vitro* model can be expressed as

$$C_0 = \frac{D}{V}, \quad \text{eq. A5}$$

where V is the volume of broth and D is the initial amount of drug. After performing the first dilution step at time point $t_1 = \Delta t_{dil}$, the drug concentration $C(t_1)$ can be calculated as

$$C(t_1) = C_0 \cdot e^{-k_e \cdot \Delta t_{dil}}, \quad \text{eq. A6}$$

where k_e refers to the simulated elimination rate constant. Alternatively, $C(t_1)$ can also be expressed as

$$C(t_1) = \frac{(D - \Delta d)}{V} = \frac{D}{V} - \frac{\Delta d}{V}, \quad \text{eq. A6a}$$

where Δd is the amount of drug withdrawn. Thus, eq. A6 and A6a can be set equal:

$$C_0 \cdot e^{-k_e \cdot \Delta t_{dil}} = \frac{D}{V} - \frac{\Delta d}{V}. \quad \text{eq. A6b}$$

The substitution of C_0 in eq. A6b by eq. A5 results in

$$\frac{D}{V} \cdot e^{-k_e \cdot \Delta t_{dil}} = \frac{D}{V} - \frac{\Delta d}{V}. \quad \text{eq. A6c}$$

Transposing eq. A6c reveals

$$D \cdot (1 - e^{-k_e \cdot \Delta t_{dil}}) = \Delta d. \quad \text{eq. A6d}$$

D can be expressed by eq. A5 as $D = C_0 \cdot V$, and analogously Δd can be calculated as $\Delta d = C_0 \cdot V_{sub}$, where V_{sub} is the substituted volume of broth. Replacing D and Δd in eq. A6d by the expressions $C_0 \cdot V$ and $C_0 \cdot V_{sub}$, respectively, results in

$$V_{sub} = V \cdot (1 - e^{-k_e \cdot \Delta t_{dil}}). \quad \text{eq. A6e}$$

Moreover, k_e can be expressed as $k_e = \ln(2) / t_{1/2}$ [44], where $t_{1/2}$ refers to the half-life, in eq. A6e resulting in eq. M1 (see 2.4.4.2.2).

7.4.2 Derivation of Equation R2

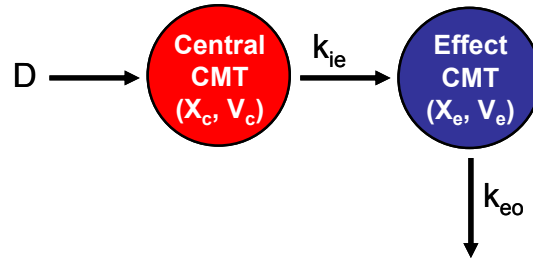


Fig. 47 Schematic depiction of the effect compartment (CMT) model, considering constant drug concentrations in the central CMT.

The drug concentration in the central CMT (referring to plasma, Fig. 47) is given by $C_p = X_c/V_c$, where X_c refers to the amount of drug in the central CMT and V_c is the volume of distribution of the considered CMT. Due to the lack of drug elimination from the central CMT, C_p is assumed to be constant and thus equals to the initial drug concentration C_0 , which is defined as

$$C_0 = \frac{D}{V_c}, \quad \text{eq. A7}$$

where D is the administered dose. In contrast, the drug concentration in the effect CMT ($C_e(t)$) is a function of time (t) that is calculated as

$$C_e(t) = \frac{X_e(t)}{V_e}. \quad \text{eq. A8}$$

Here, the function $X_e(t)$ describes the amount of drug in the effect CMT at time point t , and V_e is the volume of distribution of the effect CMT. The change of $X_e(t)$ over time ($dX_e(t)/dt$) can be derived from Fig. 47 as

$$\frac{dX_e(t)}{dt} = k_{ie} \cdot D - k_{eo} \cdot X_e(t), \quad \text{eq. A9}$$

where k_{ie} and k_{eo} are the first-order rate constants for the drug transfer into and from the effect CMT, respectively. At time point $t = 0$, $X_e(t)$ is zero, and thus using *Laplace transform* (see 7.3.5.1) on eq. A9 and transposing result in

$$\overline{X_e} = \frac{k_{ie} \cdot D}{s \cdot (s + k_{eo})}, \quad \text{eq. A9a}$$

with s equals the Laplace operator. The inverse of the Laplace transform is obtained via the use of the *GPF theorem* (see 7.3.5.2), and subsequent transposing reveals

$$X_e(t) = \frac{k_{ie} \cdot D}{k_{eo}} \cdot (1 - e^{-k_{eo} \cdot t}). \quad \text{eq. A9b}$$

Combining eq. A8 and A9b gives

$$C_e(t) = \frac{k_{ie} \cdot D}{k_{eo} \cdot V_e} \cdot (1 - e^{-k_{eo} \cdot t}). \quad \text{eq. A9c}$$

At steady state, the products $V_e \cdot k_{eo}$ and $k_{ie} \cdot V_c$ are equal [57], and thus V_e can be calculated as

$$V_e = \frac{k_{ie}}{k_{eo}} \cdot V_c. \quad \text{eq. A10}$$

Combining eq. A9c with A10 and subsequently inserting eq. A7, finally result in eq. R2 (see 3.3.2.2.1).

7.4.3 Derivation of Equation R2a

Firstly, the *half-life* of the drug in the effect CMT ($t_{e1/2}$) can be calculated based on eq. R2 (see 3.3.2.2.1), for $C_e(t_{e1/2}) = \frac{1}{2} \cdot C_0$, as

$$t_{e1/2} = \frac{\ln(2)}{k_{eo}}. \quad \text{eq. A11}$$

Moreover, the independent variable t in eq. R2 can be expressed as a certain fraction F_x of $t_{e1/2}$. Hence, using $t = F_x \cdot t_{e1/2} = F_x \cdot (\ln(2)/k_{eo})$ results in

$$\frac{C_e(t)}{C_0} = 1 - e^{-F_x \cdot \ln(2)}. \quad \text{eq. A12}$$

The *equilibrium time* (t_{eq}) determines how long it takes until the time course of $C_e(t)$ reaches $C_p(t)$, i.e. in the present case C_0 . For numerically estimating t_{eq} , different values for F_x can be used in eq. A12, as done in Tab. 17, to find the value of F_x that leads to $C_e(t)/C_0 \approx 1$. For $F_x = 5$, i.e. at $t = 5 \cdot t_{e1/2}$, the equilibrium of $C_e(t)$ is almost reached. Thus, for $t_{eq} \approx 5 \cdot t_{e1/2}$, inserting eq. A11 reveals eq. R2a (see 3.3.2.2.1).

Tab. 17 Results from eq. A12 using different values for the fraction F_x of $t_{e1/2}$.

F_x	$e^{-F_x \cdot \ln(2)}$	$1 - e^{-F_x \cdot \ln(2)}$	$C_e(t)/C_0, \%$
1	1/2	0.500	50.0
2	1/4	0.750	75.0
3	1/8	0.875	87.5
4	1/16	0.938	93.8
5	1/32	0.969	96.9
6	1/64	0.984	98.4
7	1/128	0.992	99.2

7.4.4 Derivation of Equation R3

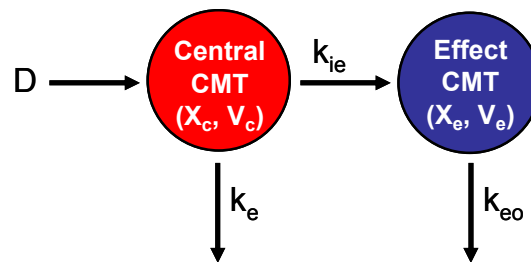


Fig. 48 Schematic depiction of the effect compartment (CMT) model, considering an intravenous bolus injection with first-order drug elimination from the central CMT.

The change of drug amount in the central CMT over time ($dX_c(t)/dt$) can be derived from Fig. 48 as

$$\frac{dX_c(t)}{dt} = -(k_e + k_{ie}) \cdot X_c(t). \quad \text{eq. A13}$$

Here, k_e refers to the first-order elimination rate constant from the central CMT, and k_{ie} and k_{eo} are the first-order rate constants for the drug transfer into and from the effect CMT. At time point $t = 0$, $X_c(t)$ is equal to the administered dose D . Thus, using *Laplace transform* (see 7.3.5.1) on eq. A13 and transposing result in

$$\overline{X_c} = \frac{D}{(s + k_e + k_{ie})}. \quad \text{eq. A13a}$$

The change of drug amount in the effect CMT over time ($dX_e(t)/dt$) can also be derived from Fig. 48 as

$$\frac{dX_e(t)}{dt} = k_{ie} \cdot X_c(t) - k_{eo} \cdot X_e(t), \quad \text{eq. A14}$$

At $t = 0$, the function $X_e(t)$ is zero. Using *Laplace transform* on eq. A14, subsequently inserting eq. A13a, and transposing result in

$$\overline{X_e} = \frac{k_{ie} \cdot D}{(s + k_e + k_{ie}) \cdot (s + k_{eo})}. \quad \text{eq. A14a}$$

Assuming $k_{ie} \ll k_e$ [57], eq. A14a can be simplified to

$$\overline{X_e} = \frac{k_{ie} \cdot D}{(s + k_e) \cdot (s + k_{eo})}. \quad \text{eq. A14b}$$

The inverse of the Laplace transform is obtained by using the *GPF theorem* (see 7.3.5.2) and transposing as

$$X_e(t) = \frac{k_{ie} \cdot D}{(k_{eo} - k_e)} \cdot (e^{-k_e \cdot t} - e^{-k_{eo} \cdot t}). \quad \text{eq. A14c}$$

Combining eq. A8 with A14c and subsequently inserting eq. A10 and A7, reveal eq. R3 (see 3.3.2.2.1).

7.4.5 Derivation of Equation R3a

At the maximum of $C_e(t)$, the first derivative of eq. R3 is equal zero:

$$\frac{dC_e(t_{e,\max})}{dt} = 0 = \frac{C_0 \cdot k_{eo}^2}{(k_{eo} - k_e)} \cdot e^{-k_{eo} \cdot t_{e,\max}} - \frac{C_0 \cdot k_{eo} \cdot k_e}{(k_{eo} - k_e)} \cdot e^{-k_e \cdot t_{e,\max}}, \quad \text{eq. A15}$$

and subsequently transposing of eq. A15 reveals eq. R3a (see 3.3.2.2.1).

7.4.6 Derivation of Equation R4

The change of drug amount in the central CMT over time ($dX_c(t)/dt$) can be derived from Fig. 49 as

$$\frac{dX_c(t)}{dt} = k_0 - (k_e + k_{ie}) \cdot X_c(t), \quad \text{eq. A16}$$

where k_0 refers to the zero-order infusion rate constant, k_e is to the first-order elimination rate constant from the central CMT, and k_{ie} and k_{eo} are the first-order rate constants for the drug transfer into and from the effect CMT. To account for a defined duration of infusion T_i , the *Laplace transform* (see 7.3.5.1) of eq. A16 can be

accomplished via the use of *general input and disposition functions* [44]: For a zero-order absorption, the input function is $in(s) = k_0 \cdot (1 - e^{-T_i \cdot s})/s$, whereas for a first-order elimination the respective disposition function is $d(s) = (s + k_e + k_{ie})^{-1}$. Assuming $k_{ie} \ll k_e$ [57], the disposition function can be simplified to $d(s) = (s + k_e)^{-1}$. The product $a(s) = in(s) \cdot d(s)$ yields the *Laplace transform* for eq. A16 as

$$\overline{X_c} = \frac{k_0 \cdot (1 - e^{-T_i \cdot s})}{s \cdot (s + k_e)}. \quad \text{eq. A16a}$$

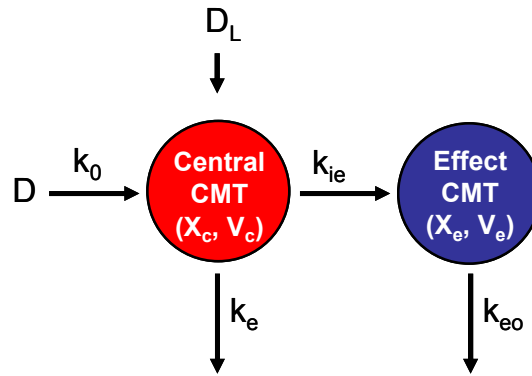


Fig. 49 Schematic depiction of the effect compartment (CMT) model, considering an intravenous bolus injection plus continuous infusion with first-order drug elimination from the central CMT.

The change of drug amount in the effect CMT over time ($dX_e(t)/dt$), is again given by eq. A14. At $t = 0$, the function $X_e(t)$ is zero. Using Laplace transform on Eq. A14, subsequently inserting eq. 16a, and transposing result in

$$\overline{X_e} = \frac{k_{ie} \cdot k_0 \cdot (1 - e^{-T_i \cdot s})}{s \cdot (s + k_e) \cdot (s + k_{eo})}. \quad \text{eq. A17}$$

The inverse of the Laplace transform is obtained by using the *GPF theorem* (see 7.3.5.2) and transposing as

$$X_e(t) = \frac{k_{ie} \cdot k_0}{k_e \cdot k_{eo} \cdot (k_{eo} - k_e)} \cdot [k_{eo} \cdot (e^{k_e \cdot T_i} - 1) \cdot e^{-k_e \cdot t} - k_e \cdot (e^{k_{eo} \cdot T_i} - 1) \cdot e^{-k_{eo} \cdot t}]. \quad \text{eq. A17a}$$

Combining eq. A8 with A17a and subsequently inserting eq. A10, reveal the function for $C_e(t)$ as

$$C_e(t) = \frac{k_0}{k_e \cdot V_c \cdot (k_{eo} - k_e)} \cdot [k_{eo} \cdot (e^{k_e \cdot T_i} - 1) \cdot e^{-k_e \cdot t} - k_e \cdot (e^{k_{eo} \cdot T_i} - 1) \cdot e^{-k_{eo} \cdot t}] \quad [57]. \quad \text{eq. A17b}$$

For $t = \infty$, the drug concentration in the central CMT at steady state (C_{ss}) can be calculated as $C_{ss} = k_0/(V_c \cdot k_e)$ [44]. Thus, eq. A17b can also be written as

$$C_e(t) = \frac{C_{ss}}{(k_{eo} - k_e)} \cdot [k_{eo} \cdot (e^{k_e \cdot T_i} - 1) \cdot e^{-k_e \cdot t} - k_e \cdot (e^{k_{eo} \cdot T_i} - 1) \cdot e^{-k_{eo} \cdot t}] \quad \text{eq. A17c}$$

For immediately reaching C_{ss} , a loading dose (D_L) with $D_L = k_0/k_e$ [44] can be given simultaneously as i.v. bolus injection, at $t = 0$. The respective function for $C_e(t)$ can be derived via the *principle of superposition* [44, 132, 133]: The sum of eq. R3 and A17c, with $C_0 = C_{ss}$, i.e. using

$$C_0 = \frac{D_L}{V_c} = C_{ss} = \frac{k_0}{k_e \cdot V_c}, \quad \text{eq. A18}$$

reveals eq. R4 (see 3.3.2.2.1).

7.4.7 Derivation of Equation R4a

At the maximum of $C_e(t)$, the first derivative of eq. R4 is equal zero, and subsequently transposing reveals eq. R4a (see 3.3.2.2.1).

7.4.8 Derivation of Equation R6

The change of drug amount in the effect CMT over time ($dX_e(t)/dt$) can be derived from Fig. 50 as

$$\frac{dX_e(t)}{dt} = k_{ie} \cdot X_2(t) - k_{eo} \cdot X_e(t), \quad \text{eq. A19}$$

where k_{ie} and k_{eo} are the first-order rate constants for the drug transfer into and from the effect CMT, and $X_2(t)$ refers to the drug amount in the central CMT. The drug concentration in the central CMT, i.e. in plasma, ($C_p(t)$) is calculated as

$$C_p(t) = \frac{X_2(t)}{V_2}, \quad \text{eq. A20}$$

whereas the drug concentration in the effect CMT ($C_e(t)$) is calculated as

$$C_e(t) = \frac{X_e(t)}{V_e}, \quad \text{eq. A21}$$

where V_2 and V_e refer to the volume of distribution of the central CMT and the effect CMT, respectively. Thus, multiplying eq. A19 on both sides with $1/V_e$ results in

$$\frac{dC_e(t)}{dt} = k_{ie} \cdot \frac{X_2(t)}{V_e} - k_{eo} \cdot C_e(t). \quad \text{eq. A22}$$

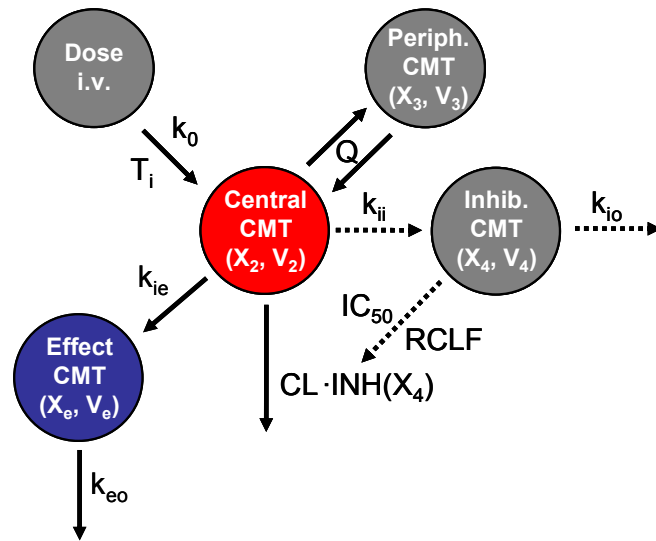


Fig. 50 Schematic depiction of the pharmacokinetic/pharmacodynamic model utilised for the *in silico* simulation, parameters are explained in the text.

At steady state, the products $V_e \cdot k_{eo}$ and $k_{ie} \cdot V_2$ are equal [57], and thus k_{ie} can be calculated as

$$k_{ie} = \frac{V_e}{V_2} \cdot k_{eo}. \quad \text{eq. A23}$$

Combining eq. A22 with A23 and subsequently inserting eq. A20, reveal eq. R6 (see 3.4).

7.5 VBA scripts

The original VBA scripts for the PK/PD modelling and stochastic *in silico* simulation part of this thesis are printed below. Explaining comments are highlighted in red. However, these two scripts are related to customised Excel spreadsheets, and thus will not run alone. Due to re-formatting in Word, the VBA code might also not work when copying directly in Excel's VBA editor. Moreover, the notation in the original VBA scripts partially differs from the previous notation of this work, as follows:

- $A_{2-4} = X_{2-4}$
- $TI = T_i$
- $R0 = k_0$
- $KIC = k_{i0}$
- $a_ = a_e$
- $b_ = b_e$
- $z_ = z_e$
- $n_ = H$

7.5.1 Pharmacokinetic/pharmacodynamic modelling

```
Sub Solver_BS()  
  
'Solver with automated BS for estimating the CI95% of each model  
'parameter:  
  
Answer = MsgBox("Bootstrapping for Solver function", vbYesNo)  
If Answer <> vbYes Then Exit Sub  
Num = InputBox("Please enter the number of bootstraps you want to  
perform")  
  
'For-next-loop:  
For N = 1 To Num  
  
'To automatically create a new bootstrap in the spreadsheet:  
Calculate  
  
'For controlling Solver via VBA:  
  
'Reset SolverOptions:  
SolverReset  
  
'default settings:
```



```

'SolverOptions
'SolverOptions MaxTime:=100, Iterations:=100, _
'Precision:=0.000001, 'AssumeLinear:=False, _
'StepThru:=False, Estimates:=1, Derivatives:=1, _
'SearchOption:=1, Scaling:=False, Convergence:=0.0001, _
'AssumeNonNeg:=False

'Utilised settings:

SolverOptions MaxTime:=100, Iterations:=100, Precision:=0.000001,
AssumeLinear:=False, _
StepThru:=False, Estimates:=2, Derivatives:=1, SearchOption:=2,
Scaling:=True, Convergence:=0.0001, _
AssumeNonNeg:=False

'Instruction to minimise the chosen OBJ by adjusting the defined
'parameters:
SolverOK setCell:="$L$13", maxMinVal:=2, ValueOf:="0", _
byChange:="$D$11:$J$11"

'Chosen constraints for model parameters:
'=[SolverAdd: relation 1 for <=(max)and 3 for >=(min)]

'For parameter Emax:
SolverAdd cellRef:=Range("D11"), relation:=3,
formulaText:=Range("D12")
SolverAdd cellRef:=Range("D11"), relation:=1,
formulaText:=Range("D13")
'For parameter EC50:
SolverAdd cellRef:=Range("E11"), relation:=3,
formulaText:=Range("E12")
SolverAdd cellRef:=Range("E11"), relation:=1,
formulaText:=Range("E13")
For parameter n_:
SolverAdd cellRef:=Range("F11"), relation:=3,
formulaText:=Range("F12")
SolverAdd cellRef:=Range("F11"), relation:=1,
formulaText:=Range("F13")
'For parameter keo:
SolverAdd cellRef:=Range("G11"), relation:=3,
formulaText:=Range("G12")
SolverAdd cellRef:=Range("G11"), relation:=1,
formulaText:=Range("G13")
'For parameter a_:
SolverAdd cellRef:=Range("H11"), relation:=3,
formulaText:=Range("H12")
SolverAdd cellRef:=Range("H11"), relation:=1,
formulaText:=Range("H13")
'For parameter b_:
SolverAdd cellRef:=Range("I11"), relation:=3,
formulaText:=Range("I12")
SolverAdd cellRef:=Range("I11"), relation:=1,
formulaText:=Range("I13")
'For parameter z_:
SolverAdd cellRef:=Range("J11"), relation:=3,
formulaText:=Range("J12")

```

```
SolverAdd cellRef:=Range("J11"), relation:=1,
formulaText:=Range("J13")

'Starts solving the problem directly (without dialog window):
SolverSolve UserFinish:=True

'(Re-)writes the currently found solution in the spreadsheet:
SolverFinish KeepFinal:=1

'Copies the new solution and pastes the respective values to another
'place in the spreadsheet where it cannot be overwritten:

Range("D11:O11").Select
Selection.Copy
ActiveCell(N, 16).Select
Selection.PasteSpecial _
Paste:=xlValues, Operation:=xlNone, SkipBlanks:=False,
Transpose:=False
Application.CutCopyMode = False

Next N

End Sub

Sub CopySummary()

'For automatically saving the summary parameters of the solution in
'the run summary spreadsheet:

Answer = MsgBox("You want to copy the parameter summary to worksheet
parameter?", vbYesNo)
If Answer <> vbYes Then Exit Sub
Range("R1:AL9").Select
Selection.Copy
Sheets("run summary 3").Select
Range("A1").Select
Selection.PasteSpecial _
Paste:=xlValues, Operation:=xlNone, SkipBlanks:=False,
Transpose:=False
Application.CutCopyMode = False
End Sub

Sub ResetInitials()
'For resetting the previously defined initial values:
Answer = MsgBox("You want to reset initials?", vbYesNo)
If Answer <> vbYes Then Exit Sub
Sheets("Solver data").Select
Range("D8:J8").Select
Selection.Copy
Sheets("Solver data").Select
Range("D11").Select
Selection.PasteSpecial _
Paste:=xlValues, Operation:=xlNone, SkipBlanks:=False,
Transpose:=False
Application.CutCopyMode = False
End Sub
```

7.5.2 Stochastic *in silico* simulation

```

Function dA2dt(A2_x, A3_x, A4_x, RX, Q, V2, V3, Cl, INH)
'Drug amount in the central CMT, i.v. infusion:
dA2dt = RX - ((Q / V2) * A2_x) + ((Q / V3) * A3_x) - ((Cl * INH) /
V2) * A2_x)
End Function

Function dA3dt(A2_x, A3_x, A4_x, Q, V2, V3)
'Drug amount in the peripheral CMT, i.v. infusion:
dA3dt = ((Q / V2) * A2_x) - ((Q / V3) * A3_x)
End Function

Function dA4dt(A2_x, A3_x, A4_x, KIC, V2)
'Drug amount in the inhibition CMT, i.v. infusion:
dA4dt = KIC * ((A2_x / V2) - A4_x)
End Function

Function INH_(RCLF, A4, IC50)
'Inhibition factor on clearance:
INH_ = RCLF + (1 - RCLF) * (1 - (A4 / (IC50 + A4)))
End Function

Function dCedt(A2_x, A3_x, A4_x, Ce_x, keo, V2)
'Drug concentration in the effect CMT:
dCedt = keo * ((A2_x / V2) - Ce_x)
End Function

Sub PopPK_Sim_LZD_MD()

'Defined data types to save calculation time and avoid rounding
'errors:
Dim t_PMs, t, t_s, t0, dt, t_(1 To 56), n, n0, Ntotal, Numpoints,
NumPoints_1, y, w, l, p, J, I, CpIND, tau As Long

Dim A2, A3, A4, A2_(1 To 56), A3_(1 To 56), A4_(1 To 56), Cp, Cl,
V2, Q, V3, KIC, IC50, INH_, R0, RX, R(1 To 56), TI, Ce, _
Ce_(1 To 56), keo, _
E, E_1, E_2, Emax, Emax_t, Emax_t_2, EC50, EC50_t, EC50_t_2, _
n_, n_t, n_t_2, a_, b_, z_, _
kA2_1_x, kA3_1_x, kA4_1_x, kCe_1_x, _
kA2_2_x, kA3_2_x, kA4_2_x, kCe_2_x, _
kA2_3_x, kA3_3_x, kA4_3_x, kCe_3_x, _
kA2_4_x, kA3_4_x, kA4_4_x, kCe_4_x, AUCE As Single

'Writes column names in the spreadsheet:
Range("A4").Value = "J"
Range("A4").Offset(0, 1).Value = "n"
Range("A4").Offset(0, 2).Value = "AUCE"
Range("A4").Offset(0, 3).Value = "CL"
Range("A4").Offset(0, 4).Value = "V2"
Range("A4").Offset(0, 5).Value = "V3"
Range("A4").Offset(0, 6).Value = "CpIND"

'For-next-loop - In-silico patients:
NumPoints_1 = 1000

```

```

For J = 1 To NumPoints_1

'To automatically create new individual values for the parameters
'CL, V2 and V3 in the spreadsheet:

Calculate

'Parameter values:

'(Population) PK parameters, i.e. individual PK parameter values
'calculated in the spreadsheet via an exponential variability model:

C1 = Worksheets("Sim data").Range("K5").Value 'variability
V2 = Worksheets("Sim data").Range("K6").Value 'variability
V3 = Worksheets("Sim data").Range("K7").Value 'variability

'fixed parameter values (population estimates):

Q = 75# / 3600 '[L/s]
KIC = 0.0019 / 3600 '[1/s]
IC50 = 0.1 '[mg/L]
RCLF = 0.764
n0 = 1

'(Standard) Dosing regimen:

R0 = 1200# / 3600 '[mg/s]
TI = 0.5 * 3600 '[s]
tau = 12# * 3600 'Dosing interval [s]

'PD parameters:

keo = 0.113 / 3600 '[1/s]
Emax = 73.586 ',%
EC50 = 5.994 '[µg/mL]
n_ = 1.975
a_ = 0.430 / 3600 '[1/s]
b_ = 0.026 / 3600 '[1/s]
z_ = 0.131 / 3600 '[1/s]

'Time parameters:

t0 = 0 '[s, h]
dt = 60 '[s]= 0.0167 '[h]

'Number of iterations (shown for the standard dosing regimen):

Ntotal = 28
Numpoints = Ntotal * (tau / dt) + 1

'Initial values:

n = n0
t_s = t0
t = t0
t_h_ = t0
t_PMs = t0

```

```

RX = R0

'Nested Loop - Reset values:

For l = 1 To Ntotal
R(l) = R0
A2_(l) = 0 '[mg]
A3_(l) = 0 '[mg]
A4_(l) = 0 '[mg]
Next l

E = 0 ',%
AUCE = 0 '[%*h]
E_1 = 0 ',%
E_2 = 0 ',%
CpIND = 0 'Artefact indicator

'Nested Loop 1 - Time:

For I = 1 To Numpoints
A2 = 0 '[mg]
A3 = 0 '[mg]
A4 = 0 '[mg]
Ce = 0 '[µg/mL]

'Nested Loop 1a - Sums-up drug amounts from all doses (principle of
'superposition):

For p = 1 To Ntotal
A2 = A2 + A2_(p)
A3 = A3 + A3_(p)
A4 = A4 + A4_(p)
Ce = Ce + Ce_(p)
Next p

'Drug concentrations in the central and peripheral CMTs:

Cp = A2 / V2

'Artefact indicator:

If Cp < 0 Then CpIND = 1
C_3 = A3 / V3

'PK/PD model:

Emax_t = Emax * (1 - Exp(-a_ * t))
EC50_t = EC50 * (1 - Exp(-b_ * t))
n_t = n_ * (1 - Exp(-z_ * t))
E = (Emax_t * (Ce ^ n_t)) / ((EC50_t ^ n_t) + (Ce ^ n_t))
E_1 = E

'Area under the effect-time course:

AUCE = AUCE + ((E_1 + E_2) / 2) * (dt / 3600)

'Simulation time:

```

```

t_s = t_s + dt
t = t_s

'Pace maker time:

t_PMs = t_PMs + dt
If t_PMs >= tau Then
t_PMs = 0
n = n + 1
End If

'Nested loop 2 - Dose:

For y = 1 To Ntotal
t_(y) = t - ((y - 1) * tau)
If (y - 1) * tau >= t Then t_(y) = 0

A2_x = A2_(y)
A3_x = A3_(y)
A4_x = A4_(y)
RX = R(y)
R(y) = R0
Ce_x = Ce_(y)

If t_(y) > TI Then R(y) = 0

'RK4 method for solving the system of coupled ODEs of the
'(population) PK/PD model:

kA2_1_x = dt * dA2dt(A2_x, A3_x, A4_x, RX, Q, V2, V3, C1, INH_(RCLF,
A4, IC50))
kA3_1_x = dt * dA3dt(A2_x, A3_x, A4_x, Q, V2, V3)
kA4_1_x = dt * dA4dt(A2_x, A3_x, A4_x, KIC, V2)
kCe_1_x = dt * dCedt(A2_x, A3_x, A4_x, Ce_x, keo, V2)

kA2_2_x = dt * dA2dt(A2_x + kA2_1_x / 2#, A3_x + kA3_1_x / 2#, A4_x
+ kA4_1_x / 2#, RX, Q, V2, V3, C1, INH_(RCLF, A4, IC50))
kA3_2_x = dt * dA3dt(A2_x + kA2_1_x / 2#, A3_x + kA3_1_x / 2#, A4_x
+ kA4_1_x / 2#, Q, V2, V3)
kA4_2_x = dt * dA4dt(A2_x + kA2_1_x / 2#, A3_x + kA3_1_x / 2#, A4_x
+ kA4_1_x / 2#, KIC, V2)
kCe_2_x = dt * dCedt(A2_x + kA2_1_x / 2#, A3_x + kA3_1_x / 2#, A4_x
+ kA4_1_x / 2#, Ce_x + kCe_1_x / 2#, keo, V2)

kA2_3_x = dt * dA2dt(A2_x + kA2_2_x / 2#, A3_x + kA3_2_x / 2#, A4_x
+ kA4_2_x / 2#, RX, Q, V2, V3, C1, INH_(RCLF, A4, IC50))
kA3_3_x = dt * dA3dt(A2_x + kA2_2_x / 2#, A3_x + kA3_2_x / 2#, A4_x
+ kA4_2_x / 2#, Q, V2, V3)
kA4_3_x = dt * dA4dt(A2_x + kA2_2_x / 2#, A3_x + kA3_2_x / 2#, A4_x
+ kA4_2_x / 2#, KIC, V2)
kCe_3_x = dt * dCedt(A2_x + kA2_2_x / 2#, A3_x + kA3_2_x / 2#, A4_x
+ kA4_2_x / 2#, Ce_x + kCe_2_x / 2#, keo, V2)

kA2_4_x = dt * dA2dt(A2_x + kA2_3_x, A3_x + kA3_3_x, A4_x + kA4_3_x,
RX, Q, V2, V3, C1, INH_(RCLF, A4, IC50))

```

```

kA3_4_x = dt * dA3dt(A2_x + kA2_3_x, A3_x + kA3_3_x, A4_x + kA4_3_x,
Q, V2, V3)
kA4_4_x = dt * dA4dt(A2_x + kA2_3_x, A3_x + kA3_3_x, A4_x + kA4_3_x,
KIC, V2)
kCe_4_x = dt * dCedt(A2_x + kA2_3_x, A3_x + kA3_3_x, A4_x + kA4_3_x,
Ce_x + kCe_3_x, keo, V2)

A2_(y) = A2_x + (kA2_1_x + 2 * (kA2_2_x + kA2_3_x) + kA2_4_x) / 6
A3_(y) = A3_x + (kA3_1_x + 2 * (kA3_2_x + kA3_3_x) + kA3_4_x) / 6
A4_(y) = A4_x + (kA4_1_x + 2 * (kA4_2_x + kA4_3_x) + kA4_4_x) / 6
Ce_(y) = Ce_x + (kCe_1_x + 2 * (kCe_2_x + kCe_3_x) + kCe_4_x) / 6

If (y - 1) * tau >= t Then
A2_(y) = 0 '[mg]
A3_(y) = 0 '[mg]
A4_(y) = 0 '[mg]
Ce_(y) = 0 '[µg/mL]
End If

Next y

E_max_t_2 = E_max * (1 - Exp(-a_ * (t - dt)))
EC50_t_2 = EC50 * (1 - Exp(-b_ * (t - dt)))
n_t_2 = n_ * (1 - Exp(-z_ * (t - dt)))
E_2 = (E_max_t_2 * (Ce ^ n_t_2)) / ((EC50_t_2 ^ n_t_2) + (Ce ^
n_t_2))

Next I

'Records selected parameter values in the spreadsheet:

Range("A4").Offset(J, 0).Value = J
Range("A4").Offset(J, 1).Value = n
Range("A4").Offset(J, 2).Value = AUCE
Range("A4").Offset(J, 3).Value = C1
Range("A4").Offset(J, 4).Value = V2
Range("A4").Offset(J, 5).Value = V3
Range("A4").Offset(J, 6).Value = CpIND

'Nested Loop 2a - Reset

For w = 1 To Ntotal
A2_(w) = 0 '[mg]
A3_(w) = 0 '[mg]
A4_(w) = 0 '[mg]
Ce_(w) = 0 '[µg/mL]
Next w

Next J

End Sub

```

8 Publications

8.1 Original papers, review article and book chapter

- C. Scheerans, H. Derendorf, C. Kloft.
Proposal for a standardised identification of the mono-exponential terminal phase for orally administered drugs.
Biopharm. Drug Dispos., 29:145-157 (2008).
- C. Kloft, C. Scheerans.
Prinzipien der Arzneistoffwirkung: PK/PD.
In: T. Dingermann/M. Schubert-Zsilavec (Eds.): *Individualisierte und optimierte Arzneimitteltherapie: Wirksamkeit und Vertraeglichkeit*, Govi-Verlag, Eschborn, *accepted* (2008).
- J. Gloede, C. Scheerans, H. Derendorf, C. Kloft.
In vitro pharmacodynamic models to determine the effect of antibacterial drugs.
J. Antimicrob. Chemother., *accepted* (2009).
- O. Schwalbe, C. Scheerans, I. Freiberg, A. Schmidt-Pokrzywniak, A. Stang, C. Kloft.
Compliance assessment of ambulatory Alzheimer patients to aid therapeutic decisions by healthcare professionals.
BMC Health Serv. Res., *submitted* (2009, *equally contributed*).
- C. Scheerans, J. Wagner, H. Derendorf, U. B. Goebel, C. Kloft.
Modelling *in vitro* pharmacodynamics of linezolid against *Staphylococcus aureus*.
In preparation.
- C. Scheerans, J. Wagner, H. Derendorf, U. B. Goebel, C. Kloft.
Pharmacokinetic/pharmacodynamic *in silico* simulation and analysis for dosing regimen evaluation of linezolid for critically ill patients.
In preparation.

8.2 Oral and poster presentations

- O. Schwalbe, C. Buerger, N. Plock, C. Scheerans, C. Kloft.
Human microdialysis: Urea as an endogenous reference compound to determine relative recovery of drugs.

World Conference on Dosing of Antiinfectives 2004. Nuernberg, 06-11 September 2004. Abstract book, A-122 (2004).

- C. Scheerans, J. Wagner, U.B. Goebel, C. Kloft.
Development of a pharmacokinetic/pharmacodynamic approach for linezolid.
Annual Meeting of the German Pharmaceutical Society (DPhG) 2005, Mainz, 05-08 October 2005. Abstract book, 95 (2005).
- C. Scheerans
Development of an innovative pharmacokinetic/pharmacodynamic model for linezolid.
University of Florida, Gainesville, USA, 13 January 2006
- C. Scheerans, J. Wagner, U.B. Goebel, C. Kloft, H. Derendorf.
Development of a semi-mechanistic pharmacokinetic/pharmacodynamic approach for linezolid.
19th Annual Research Showcase and Awards Recognition Day, College of Pharmacy, University of Florida, Gainesville, USA, 23 February 2006.
- J. Gloede, C. Scheerans, C. Kloft.
In vitro investigations to quantify the effects of antibiotics using linezolid as model drug.
Annual Meeting of the German Pharmaceutical Society (DPhG) 2007, Erlangen, 10-13 October 2007. Abstract book, 138 (2007).
- C. Scheerans.
Pharmakodynamische *In-vitro*-Untersuchungen zur rationalen Dosierung von Antibiotika: Am Beispiel von Linezolid gegen *Staphylokokkus aureus*.
In-house training Charité, Berlin, 12 February 2008.
- J. Gloede, C. Scheerans, C. Kloft.
Vancomycin resistant *Enterococcus faecium* under constant linezolid exposure.
Ehrlich II – 2nd World Conference on Magic Bullets, Nuernberg, 03-05 October 2008. Abstract book online www.ehrlich-2008.org/scientificprogram.htm, A-106 (2008).
- J. Gloede, C. Scheerans, C. Kloft.
PK/PD modelling of vancomycin resistant *Enterococcus* growing under constant linezolid exposure.

Annual Meeting of the German Pharmaceutical Society (DPhG) 2008, Bonn, 08-11 October 2008. Abstract book, 275 (2008).

- J. Gloede, C. Scheerans, C. Kloft.

PK/PD modelling of vancomycin resistant *Enterococcus faecium* growing under constant linezolid exposure.

Paul Ehrlich Society (PEG) Bad Honnef-Symposium 2009, Koenigswinter, 06-07 April 2009. *Chemother. J.*, 18: 70 (2009).

9 Acknowledgements

I would like to specially thank Professor Dr. Charlotte Kloft who gave me the opportunity to write my doctor thesis on such an interesting and challenging topic at the Freie Universitaet Berlin and the Martin-Luther-Universitaet Halle-Wittenberg. The professional discussions with her have always been an inspiration for my work. I thank her deeply for the freedom she allowed me in my research activities.

Furthermore, I want to thank:

- Professor Dr. Hartmut Derendorf who offered me the possibility to obtain methodical expertises from his lab (during my four month research trip) at the University of Florida, Gainesville, USA
- Professor Dr. Dr. Ulf B. Goebel for providing me a laboratory workplace at the Institute of Microbiology und Hygiene, Charité Campus Benjamin Franklin, Berlin
- Dr. Jutta Wagner and Jutta Imlau for their significant contribution to the microbiological part of my work
- Mike Nuernberg for the inspiring discussions and technical support
- Dr. Oliver Schwalbe, Dr. Wolfgang Mehnert for deeply discussing the clinical relevance of the overall results of my work
- Dr. Rolf Burghaus and Dr. Martin Blunck for discussing the mathematic derivations of eq. R4 and R4a, the utilised OBJ and the adjusted ES breakpoint
- Sebastian Scheerans, Marcus Scholz, Julia Gloede, Monika Frank and Franziska Simmel for reviewing different sections of the current work and providing the reference style
- Dr. Katharina Kuester for exchanging experiences in modelling and simulation
- Dr. Cornelia Buerger, Dr. Nele Plock and Sven Andrasch for supporting the analytical part of this work
- Pharmacia/Pfizer (Kalamazoo/New York, USA) for kindly providing LZD

The financial support of this work was provided by the Freie Universitaet Berlin, the Forschungskommission of the Freie Universitaet Berlin, the Deutsche Akademische Austauschdienst, and the Martin-Luther-Universitaet Halle-Wittenberg.

Curriculum vitae

Name	Christian Scheerans
Date of birth	17 December 1978
Place of birth	Hamburg
Nationality	German

Education and qualifications

Since October 2004	Doctoral thesis under the supervision of Prof. Dr. Charlotte Kloft Dept. of Clinical Pharmacy, Freie Universitaet Berlin and Martin-Luther-Universitaet Halle-Wittenberg
June 2004	Registration as pharmacist Hamburg, Germany
April 2003	Degree in Pharmacy (2. Staatsexamen) Universitaet Hamburg, Hamburg, Germany
June 1998	High school degree (Allgemeine Hochschulreife) Carl-von-Ossietzky-Gymnasium, Hamburg, Germany

Working Experience

Since May 2009	Clinical Pharmacokineticist Bayer Schering Pharma AG, Wuppertal, Germany
October 2004 – April 2009	Scientific assistant Dept. of Clinical Pharmacy, Freie Universitaet Berlin and Martin-Luther-Universitaet Halle-Wittenberg
November 2003 – April 2004	Pre-registration pharmacist Hubertus-Apotheke, Norderstedt, Germany
May 2003 – October 2003	Pre-registration pharmacist University of Florida, Gainesville, USA

Awards

January 2006 – April 2006	Travel scholarship (Deutscher Akademischer Austauschdienst) Research trip at the University of Florida, Gainesville, USA
October 2005	Poster award (Lesmueller Stiftung)

Erklärung

Hiermit erkläre ich, dass ich mich mit der vorliegenden Dissertation erstmals um die Erlangung eines Doktorgrades bewerbe.

Ferner erkläre ich, dass ich die vorliegende Arbeit selbständig und ohne fremde Hilfe angefertigt, andere als die von mir angegebenen Quellen und Hilfsmittel nicht benutzt und die den verwendeten Werken wörtlich oder inhaltlich entnommenen Stellen als solche kenntlich gemacht habe.

Halle (Saale), 29. März 2010



Christian Schwarz